(2)

AFWAL-TR-88-3026
VOLUME I

DURABILITY AND DAMAGE TOLERANCE OF BISMALEIMIDE COMPOSITES

VOLUME I: TECHNICAL REPORT

S.T. TYAHLA AND P.S. MCCLELLAN JR.

McDonnell Aircraft Company
McDonnell Douglas Corporation
P.O. Box 516
St. Louis, Missouri 63166

JUNE 1988

Final Report for Period 13 September 1985 - 15 January 1988

Approved for public release, distribution is unlimited

FLIGHT DYNAMICS LABORATORY
AIR FORCE WRIGHT AERONAUTICAL LABORATORIES
AIR FORCE SYSTEMS COMMAND
WRIGHT-PATTERSON AIR FORCE BASE, OHIO 45433-6553

NOTICE

When Government drawings, specifications, or other data are used for any purpose other than in connection with a definitely related Government procurement operation, the United States Government thereby incurs no responsibility nor any obligation whatsoever; and the fact that the government may have formulated, furnished, or in any way supplied the said drawings, specifications, or other data, is not to be regarded by implication or otherwise as in any manner licensing the holder or any other person or corporation, or conveying any rights or permission to manufacture use, or sell any patented invention that may in any way be related thereto.

This report has been reviewed by the Office of Public Affairs (ASD/PA) and is releasable to the National Technical Information Service (NTIS). At NTIS, it will be available to the general public, including foreign nations.

This technical report has been reviewed and is approved for publication.

Howard J. Storr

HOWARD J. STORR, JR, 2nd Lt, USAF
Project Engineer

Tony Gerardi

TONY G. GERARDI, ACTING CHIEF
Structural Integrity Branch
Structures Division

FOR THE COMMANDER

F L Dietrich

FREDERICK L. DIETRICH, Colonel, USAF
Chief, Structures Division

If your address has changed, if you wish to be removed from our mailing list, or if the addressee is no longer employed by your organization please notify AFWAL/FIBEC *W-PAFB, OH 45433 to help us maintain a current mailing list.*

Copies of this report should not be returned unless return is required by security considerations, contractual obligations, or notice on a specific document.

UNCLASSIFIED

SECURITY CLASSIFICATION OF THIS PAGE

REPORT DOCUMENTATION PAGE

1a. REPORT SECURITY CLASSIFICATION: UNCLASSIFIED

1b. RESTRICTIVE MARKINGS:

2a. SECURITY CLASSIFICATION AUTHORITY:

2b. DECLASSIFICATION / DOWNGRADING SCHEDULE:

3. DISTRIBUTION / AVAILABILITY OF REPORT: Approved for public release; distribution is unlimited.

4. PERFORMING ORGANIZATION REPORT NUMBER(S):

5. MONITORING ORGANIZATION REPORT NUMBER(S): AFWAL-TR-88-3026, Vol I

6a. NAME OF PERFORMING ORGANIZATION: McDonnell Aircraft Company, McDonnell Douglas Corporation

6b. OFFICE SYMBOL (If applicable):

7a. NAME OF MONITORING ORGANIZATION: Air Force Wright Aeronautical Laboratories, Flight Dynamic Laboratory (AFWAL/FIBEC)

6c. ADDRESS (City, State, and ZIP Code): P.O. Box 516, St. Louis, Missouri 63166

7b. ADDRESS (City, State, and ZIP Code): Wright-Patterson AFB OH 45433-6553

8a. NAME OF FUNDING/SPONSORING ORGANIZATION:

8b. OFFICE SYMBOL (If applicable):

9. PROCUREMENT INSTRUMENT IDENTIFICATION NUMBER: Contract F33615-85-C-3212

8c. ADDRESS (City, State, and ZIP Code):

10. SOURCE OF FUNDING NUMBERS

PROGRAM ELEMENT NO.	PROJECT NO.	TASK NO.	WORK UNIT ACCESSION NO.
62201F	2401	01	94

11. TITLE (Include Security Classification): Durability and Damage Tolerance of Bismaleimide Composites Volume I: Technical Report

12. PERSONAL AUTHOR(S): S. Timothy Tyahla and Paul S. McClellan, Jr.

13a. TYPE OF REPORT	13b. TIME COVERED	14. DATE OF REPORT (Year, Month, Day)	15. PAGE COUNT
Final	FROM Sep 85 TO Jan 88	88 Jun	172

16. SUPPLEMENTARY NOTATION:

17. COSATI CODES

FIELD	GROUP	SUB-GROUP
11	04	
13	13	

18. SUBJECT TERMS (Continue on reverse if necessary and identify by block number): Composite Materials, Bismaleimide, Fracture Toughness, Tough Resins, Stress Analysis, Static Strength, ~~Low-Energy~~ Impact Damage Tolerance

19. ABSTRACT (Continue on reverse if necessary and identify by block number)

This program was the evaluation of durability and damage tolerance of bismaleimide (BMI) composites. BMI resins have been developed for structural applications in 350°F to 450°F environments. This represents an improvement over epoxy resin capability of approximately 100°F.

In Task I of this program, we experimentally evaluated two second generation BMI systems (IM6/3100 and IM6/F650) and compared their performances with those of the baseline systems AS1/3501-6 and T300/V378A. The intermediate modulus fiber IM6 was chosen as the common fiber for both material systems because its high strength and stiffness are properties that are important for future fighter design.

In Task II, basic material properties were determined. The data included moisture absorption, glass transition temperature, thermal spike susceptibility, lamina properties, and interlaminar fracture toughness test results. Lamina properties and fracture toughness test data were used to correlate laminate behavior exhibited in Task III. (cont.)

20. DISTRIBUTION/AVAILABILITY OF ABSTRACT: ☐ UNCLASSIFIED/UNLIMITED ☐ SAME AS RPT ☒ DTIC USERS

21. ABSTRACT SECURITY CLASSIFICATION: UNCLASSIFIED

22a. NAME OF RESPONSIBLE INDIVIDUAL	22b. TELEPHONE (Include Area Code)	22c. OFFICE SYMBOL
Lt. H. Joseph Storr	(513) 255-6104	AFWAL/FIBEC

DD FORM 1473, 84 MAR — 83 APR edition may be used until exhausted. All other editions are obsolete.

SECURITY CLASSIFICATION OF THIS PAGE

UNCLASSIFIED

19. abstract (cont.)

In Task III laminate structural characterizations of IM6/3100 and IM6/F650 were completed. Tests were performed on coupons that represented configurations found in typical aircraft designs. Specimens were fabricated and tested in notched and unnotched conditions to represent design applications.

In Task IV the better system (IM6/3100) was chosen to fabricate stiffened panels for evaluation of the bismaleimide's durability and damage tolerance in a structural configuration. Static and fatigue tests were performed on panels with and without impact damage.

FOREWORD

The work reported herein was performed by the McDonnell Aircraft Company (MCAIR) of the McDonnell Douglas Corporation (MDC), St. Louis, Missouri, under Air Force Contract F33615-85-C-3212, "Durability and Damage Tolerance of Bismaleimide Composites", for the Air Force Wright Aeronautical Laboratories, Flight Dynamics Laboratory, Wright-Patterson Air Force Base, Ohio. Lt. David L. Graves (AFWAL/FIBEC) and Lt. H. Joseph Storr (AFWAL/FIBEC) were the Air Force Project Engineers. The work described was conducted during the period 13 September 1985 through 15 January 1988.

The work was managed by the MCAIR Structural Research Department with Harold D. Dill as Program Manager and S. Timothy Tyahla as Principal Investigator. Program testing was conducted under the direction of Paul S. McClellan, Jr., MCAIR Nonmetallics and Chemical Processes Laboratory.

TABLE OF CONTENTS

TABLE OF CONTENTS (Concluded)

LIST OF FIGURES

LIST OF FIGURES (Continued)

LIST OF FIGURES (Continued)

LIST OF FIGURES (Continued)

Figures | Page

LIST OF FIGURES (Continued)

LIST OF FIGURES (Continued)

LIST OF FIGURES (Continued)

LIST OF FIGURES (Concluded)

SECTION 1.

INTRODUCTION

The subject of this program is evaluation of the durability and damage tolerance of bismaleimide (BMI) composites. BMI resin systems have been developed for structural applications in 350°F to 450°F environments. This represents an improvement over epoxy resin capability of approximately 100°F. First generation BMI resins achieved the increased temperature capability at the expense of toughness. Figure 1 shows C-scans of low-velocity impact damage in two panels of identical geometry. The first panel is made with 3501-6 epoxy resin and the second one is made with V378A BMI resin. Both panels were impacted with similar energy levels at similar locations. The predominance of damage (indicated by unshaded area) in the BMI panel compared to the damage in the epoxy panel illustrates the inferior toughness of the BMI resin. Second generation BMI resins have been developed to improve toughness while retaining the high temperature capability. The improvement is illustrated in Figure 2 where a decrease in damage is evident in the panel made with second generation BMI 3100 (compared to the panel made with the first generation BMI V378A). In this program we experimentally evaluated two second generation BMI systems.

In Task I of the program we surveyed candidate material systems and chose IM6/3100 and IM6/F650 for evaluation. The IM6 intermediate modulus fiber system was chosen as the common fiber for both material systems. A common fiber was chosen so that differences in performance could be attributed to the BMI resin. The high strength and stiffness of the IM6 fiber are properties that are important for future fighter designs. The resin systems were chosen for their superior toughness/temperature characteristics. The 3100 resin produced by American Cyanamid was credited as having superior toughness. The F650 resin produced by Hexcel was credited as having superior temperature capability. Evaluation of both systems allowed an assessment of the relative importance of the contradictory properties of toughness and temperature capability.

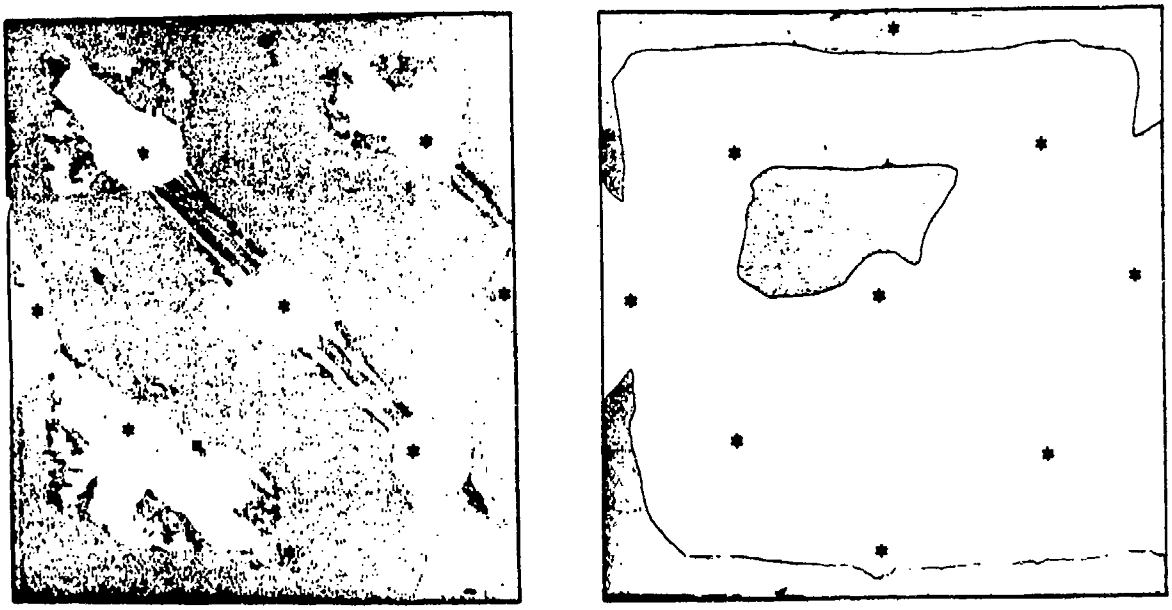

IM6/3501-6 IM6/V378A

GP83-0089-13

Figure 1. First Generation BMI (V378A) Is More Susceptible to Low Velocity Impact Damage Than Epoxy (3501-6)

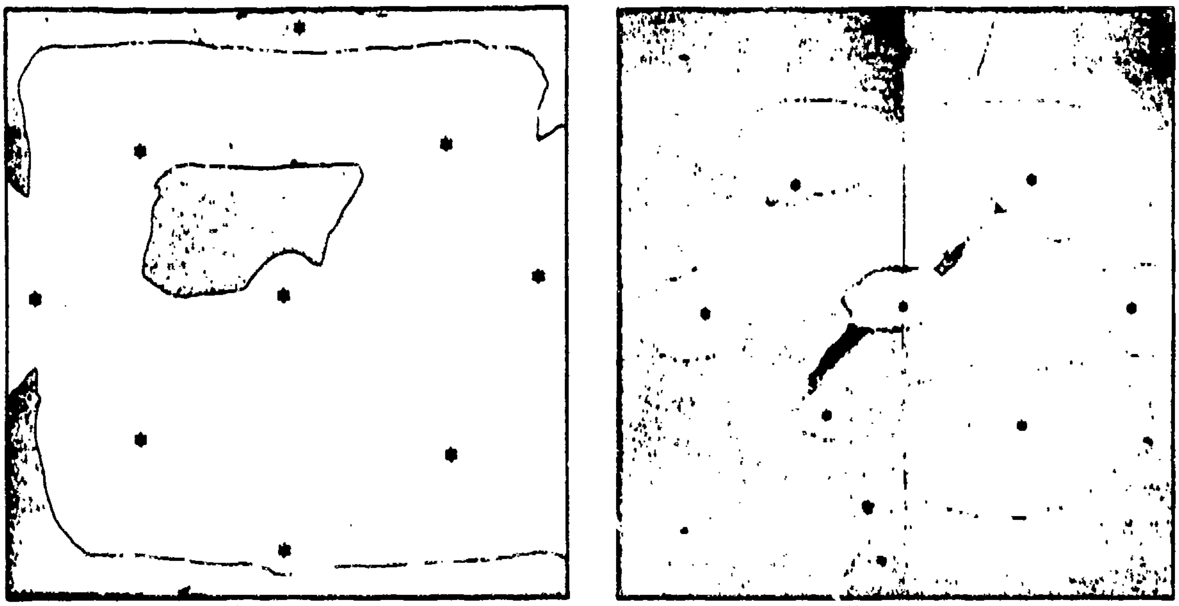

IM6/V378A IM6/3100

GP83-0089-12

Figure 2. Second Generation BMI (3100) Shows Improved Low Velocity Impact Damage Tolerance Compared to First Generation BMI (V378A)

In Task II basic material properties were determined. The data included moisture absorption, glass transition temperature, thermal spike susceptibility, lamina properties, and interlaminar fracture toughness test results. Moisture absorption and glass transition temperature data were used to define elevated temperature/wet conditions for testing that followed. Lamina properties and fracture toughness test data were used to correlate laminate behavior exhibited in Task III.

In Task III laminate structural characterizations of IM6/3100 and IM6/F650 were completed. Tests were performed on coupons that represented configurations found in typical aircraft designs. Figure 3 shows an advanced fighter wingbox design that includes a variety of structural configurations. The mechanically fastened upper skin in the design includes laminates of different thicknesses, different layups, and different notch conditions. To evaluate the performance of the two bismaleimide composite systems, specimens were fabricated and tested in notched and unnotched conditions to represent design applications shown in Figure 4.

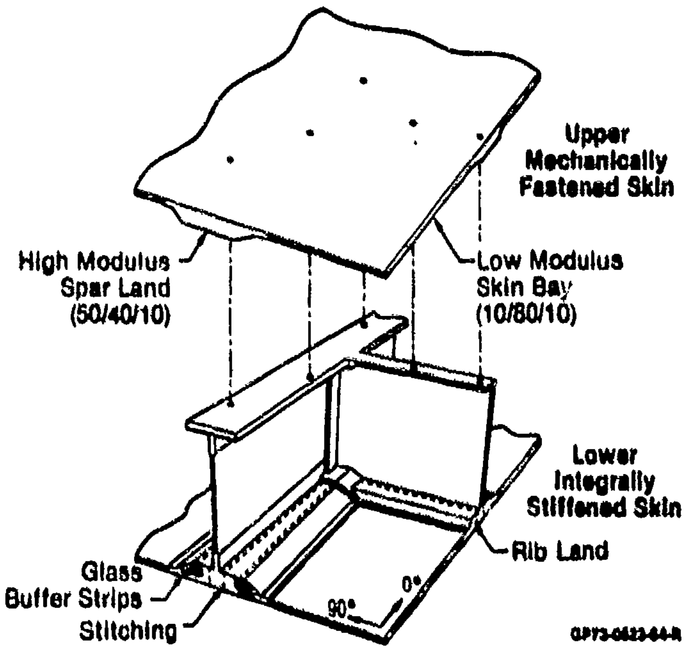

Figure 3. Advanced Fighter Wingbox Design

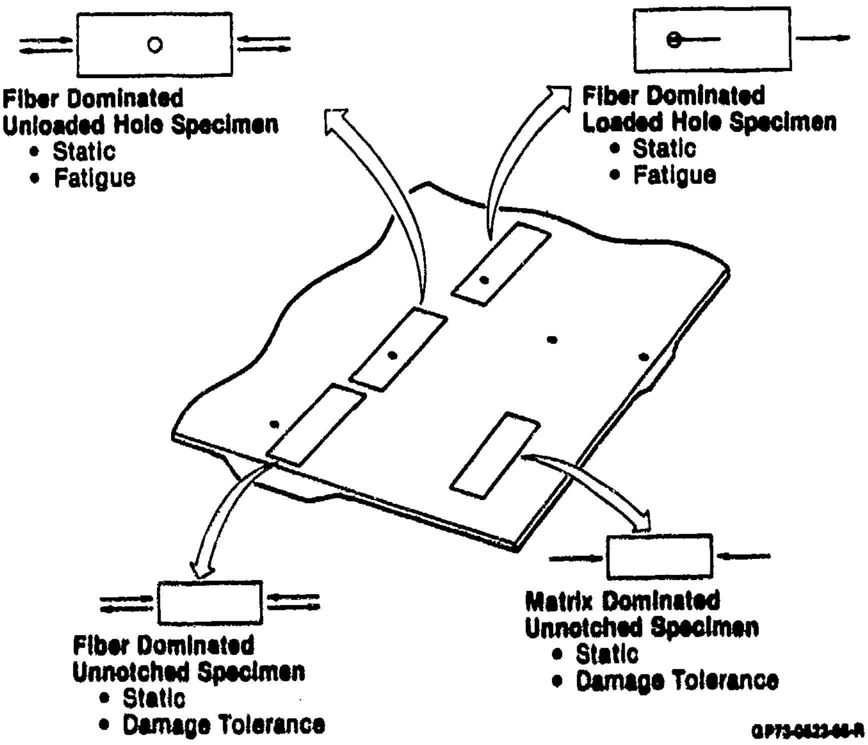

Figure 4. Representative Task III Test Specimens

In Task IV the better system (IM6/3100) was chosen to fabricate stiffened panels for evaluation of the bismaleimide's durability and damage tolerance in a structural configuration. Static and fatigue tests were performed on panels with and without impact damage.

Finally, comments were made as to the applicability of damage tolerance requirements to bismaleimide composites. Also, recommendations were made for future efforts in the area of impact damage analysis development.

SECTION 2.

TASK I: MATERIAL SELECTION

2.1 Assessment Criteria for Carbon/Bismaleimide Properties - Bismaleimide systems were assessed on the basis of both physical and mechanical properties. This assessment included:

(a) production status
(b) manufacturing qualities
(c) handling qualities
(d) resin chemistry
(e) physical and mechanical property data at room and elevated temperature
(f) moisture absorption characteristics
(g) dry and wet glass transition temperatures
(h) solvent resistance
(i) fiber/resin compatibility

The assessment of the physical qualities of the eight resins identified as applicable to this program is shown in Figure 5. Assessment of suppliers' resin data shows that wet glass transition temperatures range from 350°F to 450°F. Since different suppliers use different methods to evaluate wet glass transition temperature there was uncertainty associated with quantitative comparisons of this characteristic. Therefore, this data was used as a qualitative indicator of temperature capabilities of the materials in order to insure that the two resins chosen for the program exhibited characteristics associated with resins from opposite ends of the wet glass transition temperature range.

Assessment of the mechanical properties identified specific fiber and resin combinations which were expected to exhibit improved laminate mechanical properties. These include increased strain capability, and improved damage tolerance (increased toughness) without loss of stiffness or compressive strength over those of earlier carbon/bismaleimide material systems. The baseline material systems used for comparison included T300/V378A carbon/bismaleimide and AS/3501-6 carbon/epoxy.

Criteria	Hitco XV388	Hitco XV398C	Fiberite X86	Cyanamid 3100	Hexcel F650	Ciba-Geigy R6451	Avco 1308	Narmco 5250-2
Production Status	Experimental	Experimental	Experimental	Available	Available	Available	Available	Available
Manufacturing	Acceptable	Acceptable	Acceptable	Acceptable	Acceptable	Acceptable	Acceptable	Unacceptable*
Handleability	Unknown	Unknown	Unknown	Good	Good	Unknown	Moderate	Unknown
Resin Chemistry	Addition	Addition	Addition	Addition	Addition	Addition	Addition	Addition
Moisture Absorption	Unknown	Unknown	Unknown	Epoxy Like	Epoxy Like	Unknown	Unknown	Unknown
Dry Glass Transition Temperature	>650°F	>650°F	>600°F	>600°F	>600°F	>600°F	>600°F	>600°F
Solvent Resistance	Good	Good	Good	Good	Good	Good	Good	Good

*Due to extended post-cure

GP83-0080-4-T

Figure 5. Assessment of Second Generation Bismaleimide Resins

Selection of two carbon fiber/bismaleimide resin system combinations for use in Tasks II through IV was performed using a two step procedure for evaluating constituent fiber and resin properties. The first step of this procedure utilizes basic resin stiffness and strength properties obtained from neat resin tests to predict composite performance. Initial resin modulus, strength, strain to failure and strain energy are key material assessment parameters.

A graphical representation of the resin categorization procedure is shown in Figure 6. Strength and moduli axes are normalized with respect to a baseline material strength, S_o, and modulus E_o, respectively. Four parameters are used to define upper and lower bounds for the region where overall composite structural efficiency improvements can be expected. These parameters are: normalized resin tensile strength, normalized resin strain energy, normalized resin strain to failure, and normalized resin modulus.

These normalized resin-related parameters bound the resin properties which will result in improved laminate transverse strength, transverse modulus, strain energy (toughness) and global matrix (resin) cracking as shown in Figure 6.

Lower bounds for composite material improvement are determined by resin strength, toughness, and strain-to-failure (Figure 6). Increasing the resin strength relative to a baseline ($S > S_o$) is predicted to increase lamina transverse strength and intralaminar shear strength. Increasing the resin strain energy (toughness) increases laminate impact resistance. As compared to a brittle resin, increases in laminate toughness are shown in Figure 6 by a lower bound $S > S_o\sqrt{E/E_o}$.

Global matrix cracking is controlled by resin strain allowables. Cyclic loading for laminates above the matrix cracking strain level has been associated with rapid decrease in fatigue life (Reference 1). Therefore, composite durability is predicted to increase for resin systems in which S/E is greater than S_o/E_o (Figure 6).

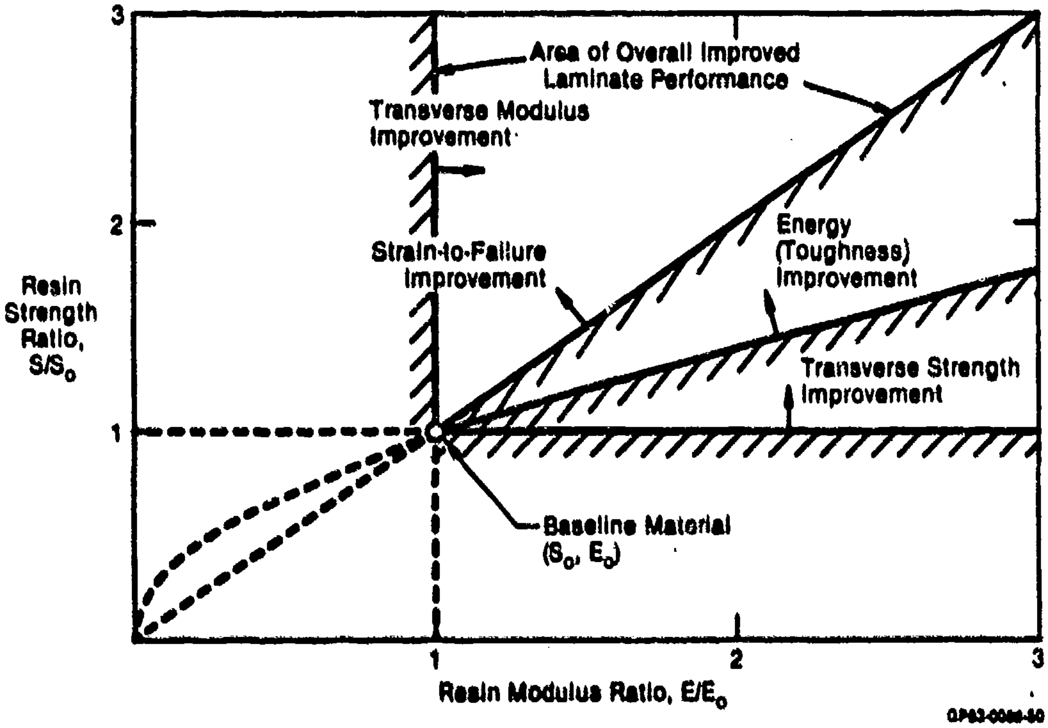

Figure 6. Resin Properties Necessary to Improve Laminate Properties

The upper bound on composite material compressive performance is determined by resin modulus. Longitudinal compression properties are improved with higher resin modulus ($E > E_o$) due to greater fiber stabilization. Potentially large benefits may be gained in toughness through resin formulations, but at the expense of lower resin stiffness. This results in lower longitudinal compression strength compared to the baseline material.

The region where all laminate properties are improved can be expressed by:

$$E > E_o$$

$$S > S_o \frac{E}{E_o}$$

as shown in Figure 6.

The second step of the mechanical property assessment procedure involved evaluation of fiber constituent properties and fiber/resin compatibility. The next generation fighter aircraft will require fibers with greater stiffness than used in current production aircraft. Intermediate modulus carbon fiber properties are compared to current fiber and high strain fibers in Figure 7. Candidate intermediate modulus fibers for evaluation in this program included Hercules IM-6 and IM-7, Union Carbide T-40, and Hitco Hitex 42. The T-40 fiber was not available in production quantities. The IM-7 fiber was a proprietary system not yet commercially available in other manufactures' resin systems.

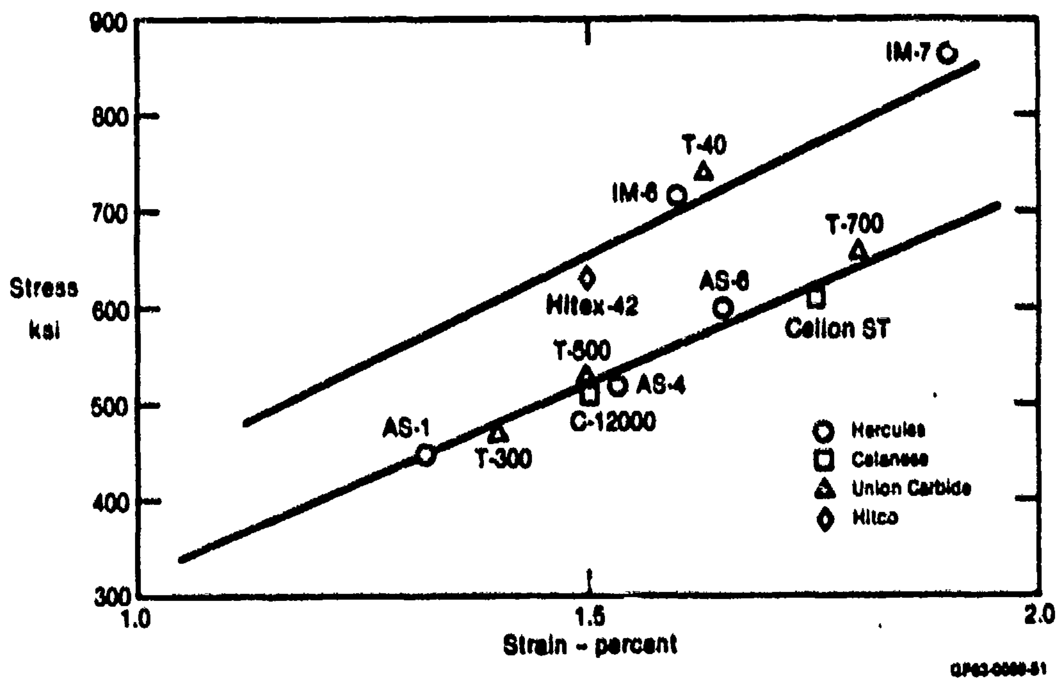

Figure 7. Candidate Carbon Fiber Materials

The mechanical properties of candidate carbon fibers and bismaleimide resins were assessed. Mechanical property data that were available for various fiber/bismaleimide resin combinations for 35 msi and 42 msi modulus fibers are shown in Figures 8 and 9 respectively. Included in these figures are baseline T300/V378A data.

Property			Hitco V-378A T300	Hitco XV388 AS-4	Fiberite X86 T300	Narmco 5250-2 T300	Cyanamid 3100 T300	Hexcel F650 T300	Ciba-Geigy R6451 T300	Avco 1308 T300
0° Tensile Properties										
Strength	(ksi)	R.T.	230	297	227	—	—	251	230	—
		350°F	210	281	—	—	—	—	181	—
Modulus	(msi)	R.T.	20.1	19.5	20.4	—	—	21.5	19.0	—
		350°F	22.1	19.3	—	—	—	—	19.0	—
Failure Strain	(μin./in.)	R.T.	10,500	13,800	10,800	—	—	11,700	—	—
		350°F	9,800	13,500	—	—	—	—	—	—
0° Flexure Properties										
Strength	(ksi)	R.T.	225	—	—	292	242	288	280	272
		350°F	171	—	—	228	208	230	229	266
		350°F Wet	—	—	—	—	149	153	180	166
Modulus	(msi)	R.T.	17.2	—	—	19.0	16.0	18.4	18.0	17.9
		350°F	15.6	—	—	19.1	17.9	17.9	17.0	17.9
		350°F Wet	—	—	—	—	16.1	17.7	17.0	16.7
0° Compressive Properties										
Strength	(ksi)	R.T.	192	229	245	320	—	238	—	—
		350°F	162	174	173[1]	—	—	181	—	—
		350°F Wet	—	—	—	—	—	130	—	—
Modulus	(msi)	R.T.	19.8	—	—	—	—	—	—	—
		350°F	23.4	—	—	—	—	—	—	—
		350°F Wet	—	—	—	—	—	—	—	—
Interlaminar Shear Strength	(ksi)	R.T.	15.0	14.9	19.8	—	19.3	20.2	16.3	16.8
		350°F	10.0	10.4	11.4[1]	—	11.5	12.4	11.6	11.3
		350°F Wet	7.9	6.5	—	—	8.8	8.2	7.8	7.1
Edge Delamination Tension, $[(\pm 25)_2, 90]_s$										
Stress at First Crack	(ksi)	R.T.	15.0	—	—	—	40.9	32.6	—	—

(1) 375°F

GP53-0686-53-T

Figure 8. Low Modulus Carbon Fiber Bismaleimide Composite Property Comparison

Property			Hitco V-378A Hitex 42	Hitco XV388 Hitex 46	Hitco XV398C Hitex 46	Fiberite X86 IM6 (G)	Cyanamid 3100 IM6 (G)	Hexcel F650 IM6 (G)
0° Tensile Properties								
Strength	(ksi)	R.T.	327	407	415	362	370	—
		350°F	—	—	420	—	—	—
Modulus	(msi)	R.T.	22.9	25.8	25.8	24.3	23.1	—
		350°F	—	—	25.5	—	—	—
Failure Strain	(μin./in.)	R.T.	13,100	14,800	15,000	14,600	16,300	—
		350°F	—	—	15,400	—	—	—
0° Flexure Properties								
Strength	(ksi)	R.T.	—	—	273	—	228	—
		350°F	—	—	220	—	196	—
		350°F Wet	—	—	176	—	135	—
Modulus	(msi)	R.T.	—	—	21.5	—	18.6	—
		350°F	—	—	21.5	—	19.2	—
		350°F Wet	—	—	20.9	-	18.3	—
0° Compressive Properties								
Strength	(ksi)	R.T.	—	227	270	225	—	—
		350°F	—	162	170	159(1)	—	—
		350°F Wet	—	—	160	164(1)	—	—
Modulus	(msi)	R.T.	—	—	23.2	—	—	—
		350°F	—	—	23.9	—	—	—
		350°F Wet	—	—	24.2	—	—	—
Interlaminar Shear Strength	(ksi)	R.T.	13.6	15.4	21.9	17.3	16.8	17.1
		350°F	10.5	10.4	15.1	11.3(1)	11.4	12.9
		350°F Wet	7.1	6.3	10.6	7.7(1)	7.7	6.5
Edge Delamination Tension, $[(\pm 25)_2, 90]_s$								
Stress at First Crack	(ksi)	R.T.	17.0	26.0	36.9	—	26.4	23.0

(1) 375°F
(2) 317°F, 83% R.H.

Figure 9. Intermediate Modulus Carbon Fiber Bismaleimide Composite Property Comparison

Based on the resin-related failure data available, these materials were correlated with the resin selection criteria envelope in Figure 10. The properties presented in Figure 10 are normalized to the baseline Hitco V378A resin system. As seen in this figure, all second generation bismaleimides, with the exception of Avco 130, were expected to show an overall improvement in laminate structural and damage tolerance properties. However, none were expected to reach the performance of current epoxy systems.

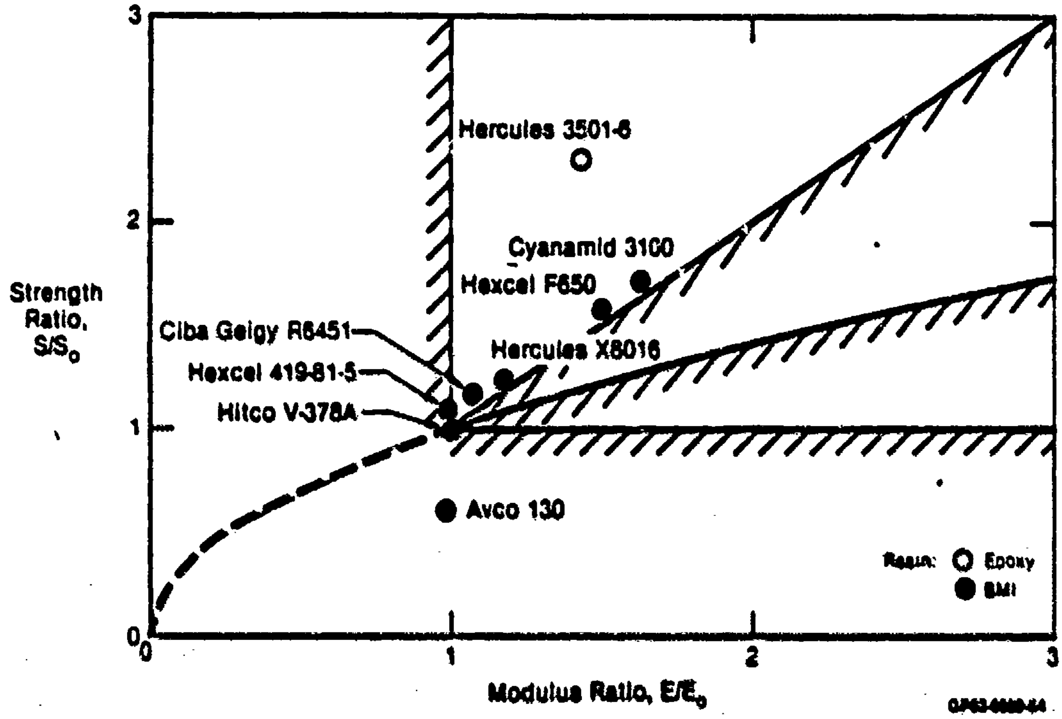

Figure 10. Resin Related Properties of BMI and Epoxy Resins

2.2 Fiber/Bismaleimide Material Selection - The assessment of the available data for bismaleimide resin material systems was used to select two systems for use in Tasks II through IV. These resin systems were American Cyanamid's Cycom 3100 and Hexcel's F650. Selection was based on resin mechanical and physical properties, processibility, availability and compatibility with the Hercules IM6 fiber. The Hercules IM6 fiber was selected for evaluations with these resins because of its high strength and stiffness properties. A common fiber was chosen so that differences in performance could be attributed to the BMI resin.

Both Cycom 3100 and Hexcel F650 have improved interlaminar fracture toughness and improved interlaminar shear strength over the current carbon/bismaleimide system. Both of these systems have excellent handling characteristics, similar to epoxies. The assessment showed these materials should maximize structural performance, including higher strains to failure (reducing microcracking), improved transverse lamina strength, retention of stiffness and unidirectional compression strengths at elevated temperature, and improved toughness.

The Cycom 3100 system has a hot/wet service temperature capability of 350°F while the Hexcel F650 system has a hot/wet service temperature in the 400°F range. The increased service temperature capability of F650 sacrifices some toughness and damage tolerance. Selection of the two bismaleimide resins permitted an assessment of new second generation materials with a range of temperatures and improvements in toughness that may encompass requirements of future aircraft. The two material systems selected for use in this program are summarized in Figure 11.

Material System Fiber/Resin	Fiber Manufacturer	Fiber Strain Capability (μin./in.)	Resin Manufacturer	Resin Description (Hot/Wet Service Temperature)
A) IM6/3100	Hercules	16,000	American Cyanamid	350 - 375
B) IM6/F650	Hercules	16,000	Hexcel	425 - 450

GP63-0080-4-T

Figure 11. Fiber/Resin Materials Selected for the Program

SECTION 3.

TASK II: ENVIRONMENTAL MATERIAL ALLOWABLES

3.1. <u>Summary and Conclusions</u> - IM6/3100 and IM6/F650 specimens were tested to determine moisture absorption characteristics, glass transition temperatures, susceptibility to thermal spiking, lamina mechanical properties, fracture toughness, and crack growth characteristics. These properties were compared to available data for baseline epoxy (AS1/3501-6) and BMI (T300/V378A) material systems.

Moisture absorption tests were performed to determine how much and how fast water is absorbed. The quantity of water that could be absorbed was determined from test results that show IM6/3100 achieved a saturation level of 1.34 percent which is 87 percent of the saturation level of T300/V378A. IM6/F650 achieved a saturation level of 1.28 percent which is 84 percent of the T300/V378A level. The rate at which water is absorbed was determined from diffusivity (D_x) tests that showed IM6/3100 and IM6/F650 bounded by AS1/3501-6 and T300/V378A. At 100°F, the diffusivity of T300/V378A is approximately two times as great as for IM6/F650, two and one-half times as great as for IM6/3100, and ten times as great as for AS1/3501-6.

Glass transition temperature (T_g) tests were performed to determine how moisture affects the T_g of the two material systems. Test results show that the T_g of IM6/3100 decreases linearly with moisture content and that the T_g of IM6/F650 decreases nonlinearly with moisture content. Also, at moisture contents in excess of 1.1 percent, the T_g of IM6/3100 exceeds the T_g of IM6/F650. The T_g test results were used to define the elevated temperature/-wet test conditions for later tasks.

Thermal spike tests were performed to determine the susceptibility of IM6/3100 and IM6/F650 to matrix microcracking or delamination caused by rapid changes in temperature. Tests showed that IM6/3100 did not exhibit micro-cracks or delaminations for either dry or wet laminates. IM6/F650 exhibited microcracking only in wet laminates.

Lamina property test results show that 0° properties of IM6/3100 and IM6/F650 compare favorably with baseline systems AS1/3501-6 and T300/V378A. This quality is attributable to the superiority of the IM6 fiber compared to either AS1 or T300 fibers. In contrast, the 90° properties of IM6/3100 and IM6/F650 were not as good as the 90° properties of the baseline materials. The shear properties of IM6/3100 exceeded those of T300/V378A but fell short of those of AS1/3501-6; while the shear properties of IM6/F650 matched those of T300/V378A and also fell short of those of AS1/3501-6.

Fracture toughness and crack growth testing was performed to determine the Mode I, Mode II, and interaction characteristics. IM6/3100 was found to be tougher than IM6/F650. IM6/3100 showed equal toughness at cold temperature/dry (CTD), room temperature/dry (RTD), or elevated temperature/wet (ETW) conditions. IM6/F650 exhibited degraded toughness at ETW conditions compared to its CTD or RTD toughness. Results show that Mode I fracture toughness increases with crack length. This behavior has been attributed to fiber bridging. Mode II fracture toughness was found to be independent of crack length. It was found that IM6/3100 is generally tougher than AS1/3501-6 and T300/V378A, and IM6/F650 is generally not as tough as the baseline materials.

For both materials the mode with the greatest crack growth rate under CTD and RTD conditions was mixed mode with 83 percent Mode II. Under ETW conditions, crack growth was greatest in Mode I for IM6/3100. IM6/F650 showed significant increases in crack growth for all modes at ETW conditions. The results from Mode II IM6/F650 testing indicate that resin weakened by ETW conditions caused unstable crack growth.

3.2 <u>Testing and Evaluation</u> - The objective of the test program was to define the environmental material allowables for the bismaleimide composites IM6/3100 and IM6/F650. Data was recorded to determine environmental effects, basic lamina material properties, toughness, and crack growth characteristics.

3.2.1 Overview - In this program, 162 static tests and 72 fatigue tests were performed under cold temperature dry (CTD), room temperature dry (RTD), and elevated temperature wet (ETW) conditions. The tests were conducted to determine:

- o moisture absorption properties
- o glass transition temperatures
- o susceptibility to thermal spike damage
- o unidirectional lamina material properties
- o fracture toughness interaction characteristics
- o interlaminar crack growth behavior

according to the matrix in Figure 12.

Test Types	Number of Tests
Moisture Absorption	36
Glass Transition Temperature	24
Thermal Spiking	16
Lamina Mechanical Property	90
Fracture Toughness	144
Total	310

GP73-0343-3

Figure 12. Task II Test Matrix

3.2.2 Moisture Absorption - Figure 13 shows the environmental conditions imposed during the tests. For the first three conditions, the relative humidity (RH) was held constant and temperature was varied in order to determine the diffusivity (D_x) of the material as a function of temperature. The results in Figure 14 show the diffusivities of IM6/3100 and IM6/F650 are bounded by the diffusivities of AS/3501-6 and T300/V378A. At 100° F, the diffusivity of T300/V378A is approximately two times as great as for IM6/F650, two and one-half times as great as for IM6/3100 and ten times as great as for AS1/3501-6.

Absorption Environment		Number of Tests		Total
Temperature (°F)	R.H. (%)	IM6/3100	IM6/F650	
100	75	3	3	6
140	75	3	3	6
180	75	3	3	6
160	50	3	3	6
160	75	3	3	6
160	95	3	3	6
				36

GP73-0343-4

Figure 13. Moisture Absorption Test Matrix

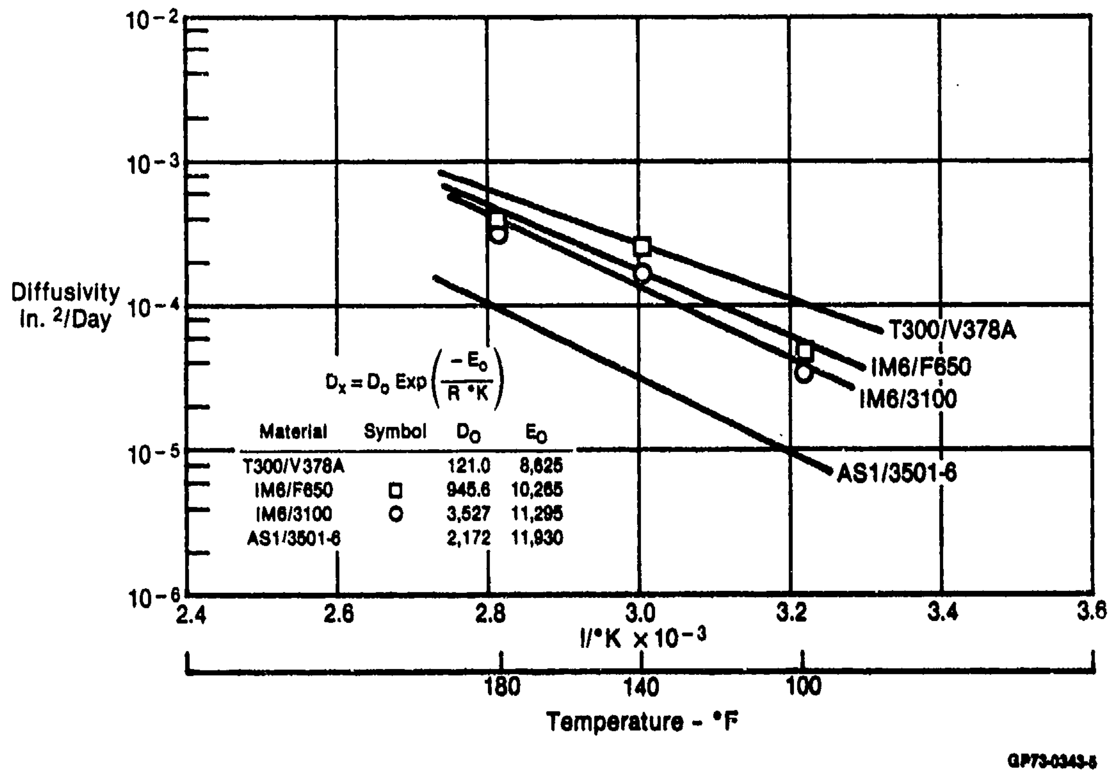

Figure 14. Diffusivity as a Function of Temperature

In the last three conditions of Figure 13, the temperature was held constant and RH varied to determine the moisture content at equilibrium (M_{eq}) as a function of RH. Figure 15 shows a comparison of M_{eq} for T300/V378A, IM6/3100, and IM6/F650 with resin contents (RC) of 30.2 percent, 30.1 percent, and 31.4 percent respectively. The RC of the test laminate is important because M_{eq} is directly proportional to RC as shown in Equation 1.

$$M_{eq} = A * (\%RC/100) * (\%RH/100)^B \tag{1}$$

The M_{eq} of T300/V378A at 100 percent RH is 1.534 percent. For IM6/3100 the M_{eq} at 100 percent RH is 1.341 percent (87 percent of the T300/V378A value) and for IM6/F650 the M_{eq} at 100 percent RH is 1.281 percent (84 percent of the T300/V378A value).

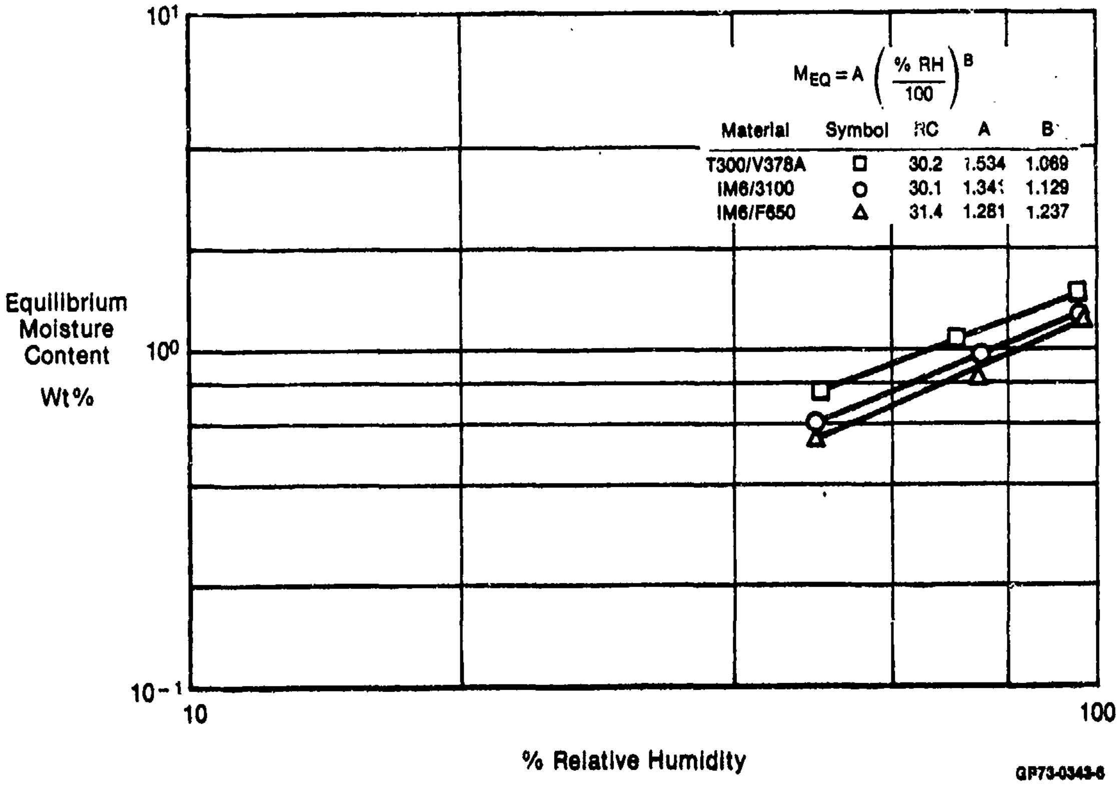

Figure 15. Equilibrium Moisture Content vs Relative Humidity

After the moisture absorption characteristics of both material systems were determined, analyses were performed in order to define an end-of-life moisture content for a representative composite structure exposed to a 20-year basing scenario. Weather data composed of temperatures and relative humidities for various Air Force bases, along with the moisture absorption test results discussed previously, were used as input to a one-dimensional moisture diffusion model called WETLAM. WETLAM was used to model a 1/4 inch thick laminate representing a section of an F-15 wing skin. Weather data for European, American, and Far Eastern basing scenarios were used to determine the most critical exposure. Figure 16 summarizes the results of the investigation. The most critical exposure for both material systems was the European basing scenario resulting in end-of-life moisture contents of 0.712 percent for IM6/3100 and 0.714 percent for IM6/F650. These moisture levels were used later with glass transition temperature test results to determine ETW test conditions for future testing in this program.

20-Year Basing Scenario	% Moisture Content Predicted by WETLAM	
	IM6/3100	IM6/F650
Europe	0.712	0.714
Far East	0.699	0.679
United States	0.644	0.639

GP73-0343-10

Figure 16. End-of-Life Moisture Contents in F-15 Wing Skins After 20-Year Exposures

3.2.3 Glass Transition Temperature - Glass transition temperatures (T_g) limit usage temperatures. Tests were performed on dry and wet laminates to measure T_g, as shown in the test matrix in Figure 17. Thermal Mechanical Analysis (TMA) was used to measure T_g for both bismaleimide systems. The TMA measures thermal expansion dimensional changes as a function of temperature. The T_g of each material is the point on the expansion versus temperature plot where the coefficient of thermal expansion (i.e. slope of expansion versus temperature plot) changes, as shown in Figure 18. The T_g decreases as moisture content increases.

Moisture Content	Number of Tests		Total
	IM6/3100	IM6/F650	
Dry	3	3	6
Level 1	3	3	6
Level 2	3	3	6
Level 3	3	3	6
			24

GP83-0099-63-T

Figure 17. Glass Transition Temperature Test Matrix

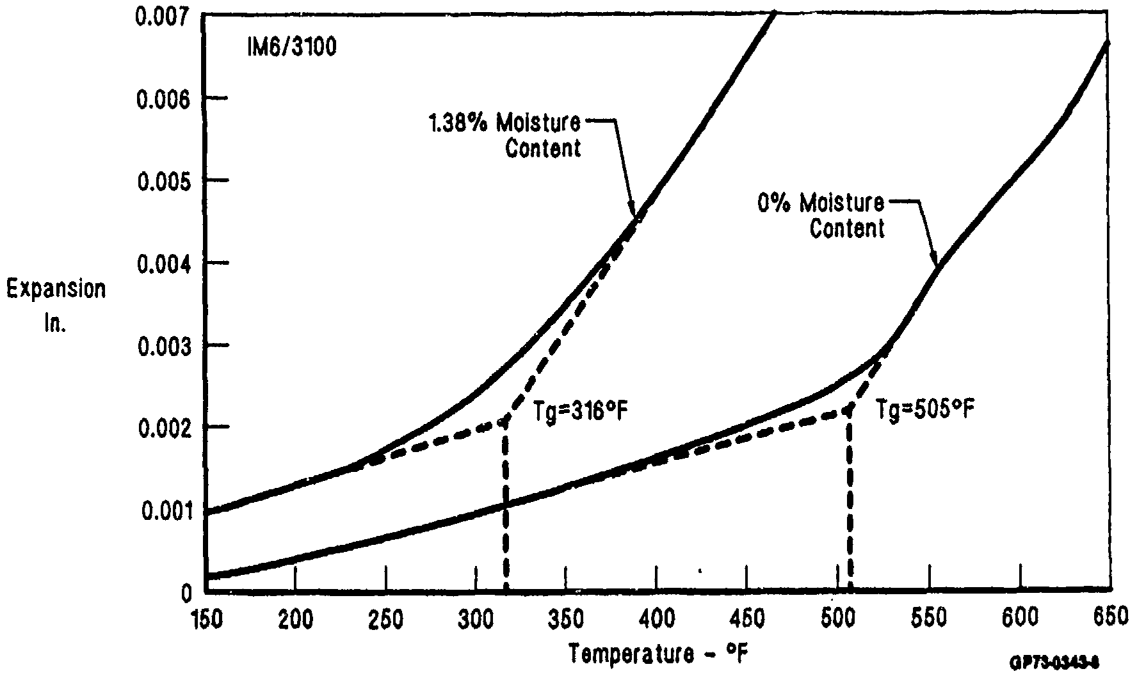

Figure 18. Glass Transition Temperature Determined by Thermal Mechanical Analysis

In Figure 19, T_g as a function of moisture content is shown for both material systems. The T_g of IM6/3100 decreases linearly with increasing moisture content. The T_g of IM6/F650 decreases nonlinearly with increasing moisture content. It is interesting to note that for high moisture contents, the T_g of IM6/F650 is lower than the T_g of IM6/3100.

The T_g vs. moisture content relationships shown in Figure 19 were used with previously determined end-of-life moisture contents to define the upper use temperatures for both BMI systems. For IM6/3100 at a moisture content of 0.712 percent the T_g is predicted to be 408°F. To insure that the degradation associated with the T_g was not encountered, a buffer of approximately 50°F was applied, resulting in an upper use temperature of 360°F for IM6/3100. In a similar manner the upper use temperature for IM6/F650 was defined as 410°F. The ETW test conditions for both materials are shown in Figure 20.

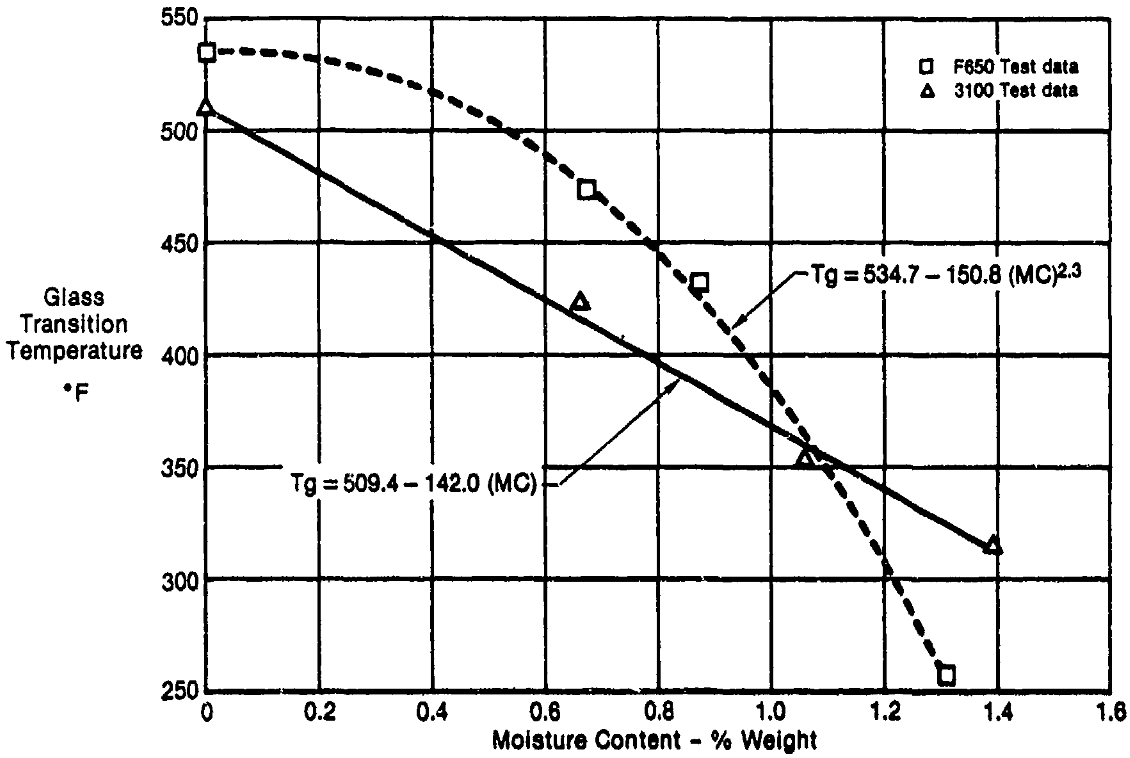

Figure 19. Variation of Glass Transition Temperature With Absorbed Moisture Content

Material	% Moisture Content Predicted by WETLAM	Glass Transition Temperature (°F)	Elevated Test Temperature (°F)
IM6/3100	0.712	408	360
IM6/F650	0.714	465	410

GP73-0343-11

Figure 20. Elevated Temperature/Wet Test Conditions Determined From End-of-Life Moisture Level

3.2.4 Thermal Spike Susceptibility - Thermal spike tests were performed in order to evaluate the susceptibility to matrix microcracking or delamination due to rapid changes in temperature. Each material system was cycled from -65°F to its upper use temperature and back to -65°F, five times, as shown in Figure 21. The rate of temperature change was 1°F/sec, which is representative of the rate with supersonic dash conditions. Both dry and wet specimens were tested as shown in Figure 22. Each test involved a test specimen and a rider specimen. The test specimen was sectioned and polished for micrographic investigation. The rider specimen was instrumented with a thermocouple to monitor the temperature vs. time schedule. Wet laminates were tested to see if entrapped moisture would promote delaminations or microcracking in severe hot or cold environments.

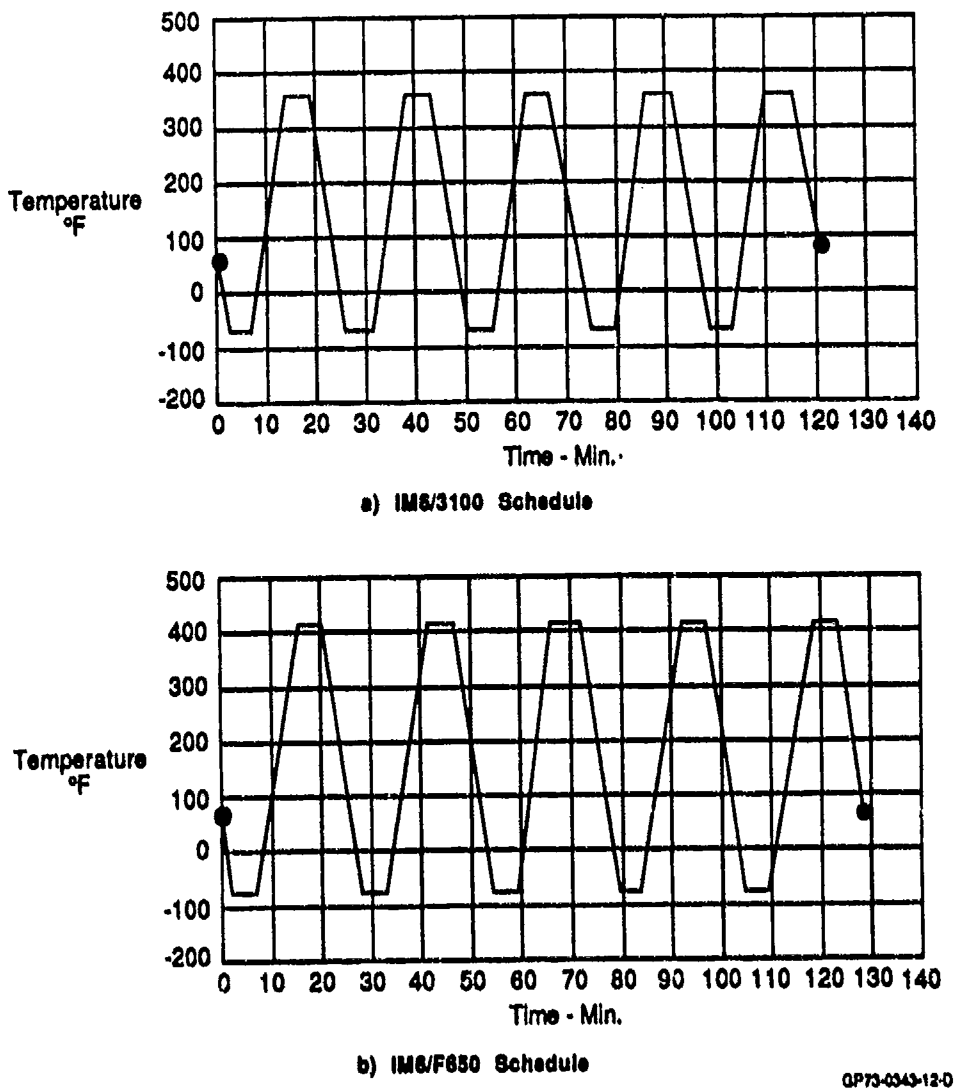

Figure 21. Thermal Spike Temperature and Time Schedules

Spike Range (°F)	Moisture Condition	Number of Tests IM6/3100	IM6/F650	Number of Specimens
$-65 - T_{up}$[a]	Dry	2[b]	2[b]	8
$-65 - T_{up}$[a]	Wet	2[b]	2[b]	8
Total				16

Notes:
a $T_{up} = 360$ for IM6/3100
a $T_{up} = 410$ for IM6/F650
b Each test involved one test specimen and one rider specimen

GP73-0343-16

Figure 22. Thermal Spike Test Matrix

For both dry and wet conditions, IM6/3100 showed no sign of microcracking or delamination. Also, dry IM6/F650 laminates showed no signs of cracking or delamination. In contrast, wet IM6/F650 laminates did exhibit microcracking. The microcracks occurred in the 90° ply that was sandwiched between two 0° plies of a 20-ply 50/40/10 laminate.

3.2.5 Lamina Mechanical Properties - Lamina mechanical property tests were performed as shown in the test matrix, Figure 23.

	IM6/3100 CTD	RTD	ETW	IM6/F650 CTD	RTD	ETW	Number of Tests
0° Tension	3	3	3	3	3	3	18
90° Tension	3	3	3	3	3	3	18
0° Compression	6	6	6	6	6	6	36
± 45° Shear	3	3	3	3	3	3	18
Total							90

GP73-0343-17

Figure 23. Lamina Mechanical Property Test Matrix

3.2.5.1 <u>0° Tension Test Results</u> - The test specimen configuration is shown in Figure 24. Figure 25 shows a typical failed specimen. Test data are tabulated in Figure 26. These test results indicate the ability of the BMI resin to transfer the strain capability of the fiber (16,000 μn/in) to the composite laminate.

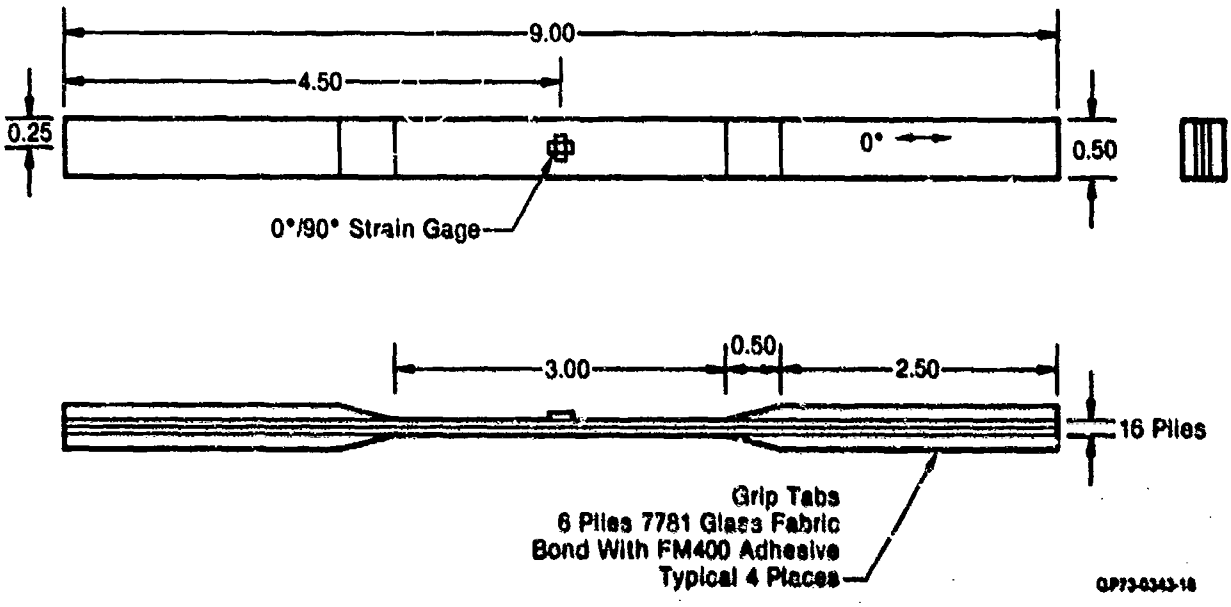

Figure 24. Unidirectional 0° Tension Test Specimen

Figure 25. Failed 0° Tensile Specimen

Material System	Environment	Specimen Number	Thickness (in.)	Width (in.)	Failure Load (lb)	Failure Stress (ksi)		Failure Strain (μin./in.)		Modulus (msi)		Poisson's Ratio
						Ind	Avg	Ind	Avg	Ind	Avg	
		1-4-10	0.088	0.491	15,300	390.5		16,100		23.02		0.317
	CTD	1-4-11	0.089	0.506	16,900	402.2	382.3	15,720	15,347	23.68	23.19	0.319
		1-4-12	0.089	0.507	14,900	354.4		14,220		22.87		0.277
		1-4-13	0.089	0.506	16,860	401.9		—		—		—
IM6/3100	RTD	1-4-14	0.089	0.508	15,750	373.8	382.6	14,840	14,940	22.96	23.02	0.311
		1-4-15	0.089	0.508	15,690	372.2		15,040		23.09		0.299
		1-4-16	0.088	0.510	8,820	208.6		8,570		24.43		0.317
	ETW	1-4-17	0.088	0.508	10,320	245.0	231.2	10,800	10,083	20.95	22.13	0.288
		1-4-18	0.088	0.509	10,140	240.1		10,880		21.01		0.307
		2-4-10	0.088	0.501	14,300	343.9		13,150		23.46		0.270
	CTD	2-4-11	0.087	0.505	13,230	315.6	330.8	13,150	12,833	23.42	23.17	0.322
		2-4-12	0.088	0.503	13,900	332.9		12,200		22.61		0.306
		2-4-13	0.088	0.503	12,330	295.3		11,270		23.53		0.307
IM6/F650	RTD	2-4-14	0.088	0.505	12,390	295.6	280.6	13,600	13,290	23.60	23.38	0.299
		2-4-15	0.088	0.504	10,500	251.0		15,000		23.00		0.309
		2-4-16	0.088	0.506	9,200	219.1		10,130		22.41		0.275
	ETW	2-4-17	0.087	0.509	9,120	215.9	205.3	9,810	9,332	22.37	22.42	0.335
		2-4-18	0.088	0.506	7,600	181.0		8,055		22.50		0.324

Note: Results normalized to 63% fiber volume fraction with a nominal ply thickness of .0052 in.

Figure 28. Unidirectional 0° Tension Test Results

IM6/3100 showed a 40 percent loss in strength under ETW conditions. The CTD and RTD strengths of IM6/3100 were equal.

In the case of IM6/F650, the RTD strength was 15 percent lower than the CTD strength. The IM6/F650 ETW strength was 38 percent lower than the CTD strength. The decrease in strength with increasing temperature is a reflection of a decrease in load/strain transfer capability of the matrix material.

3.2.5.2 90° Tension Test Results - The test specimen configuration is shown in Figure 27. Figure 28 shows a typical failed specimen. Test data are tabulated in Figure 29. These test results indicate the susceptibility of the resins to environmental degradation. IM6/3100 showed gradual strength reduction with increasing temperature. The RTD strength was 5 percent less than the CTD strength. The ETW strength was 70 percent lower than the CTD strength.

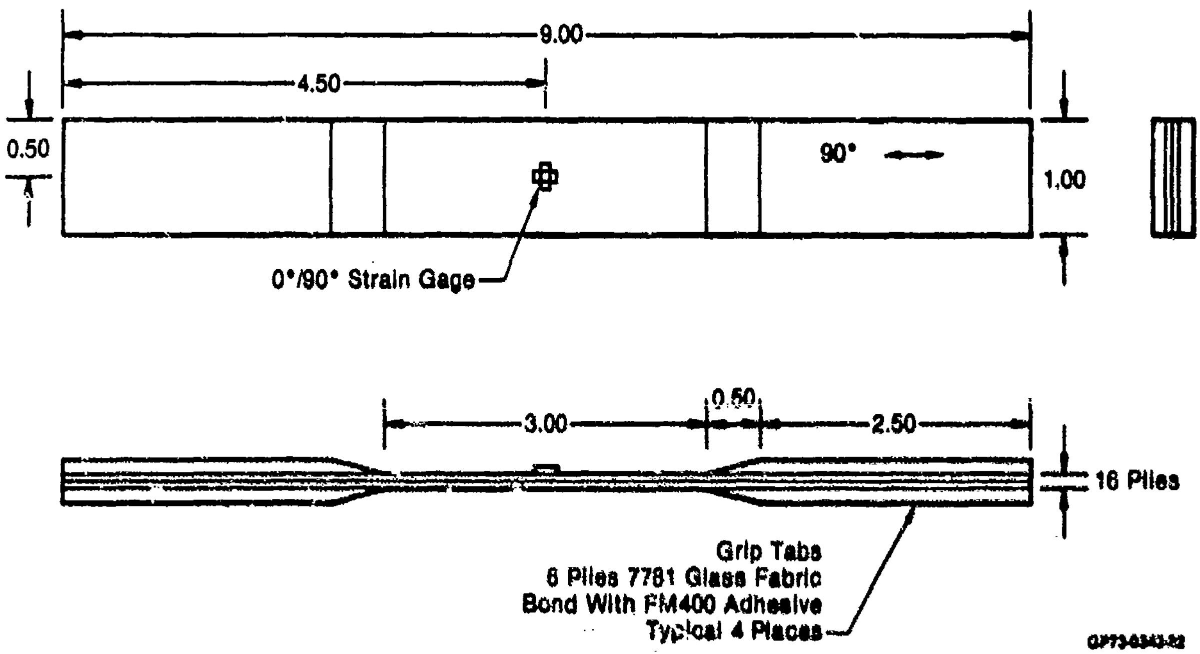

Figure 27. Unidirectional 90° Tension Test Specimen

GP83-0089-24

Figure 28. Failed 90° Tensile Specimen

Material System	Environment	Specimen Number	Thickness (in.)	Width (in.)	Failure Load (lb)	Failure Stress (ksi)		Failure Strain (μ in./in.)		Modulus (msi)		Poisson's Ratio
						Ind	Avg	Ind	Avg	Ind	Avg	
		1-4-1	0.087	1.000	410	4.94		3.400		1.41		0.018
	CTD	1-4-2	0.089	1.001	577	6.95	5.86	4.500	3.853	1.56	1.50	0.019
		1-4-3	0.089	1.002	473	5.69		3.660		1.54		0.016
		1-4-4	0.090	1.002	447	5.37		3.740		1.45		0.020
IM6/3100	RTD	1-4-5	0.089	1.002	476	5.72	5.59	3.980	3.877	1.45	1.46	0.021
		1-4-6	0.089	1.002	471	5.66		3.910		1.48		0.020
		1-4-7	0.088	1.004	—	—		—		—		—
	ETW	1-4-8	0.088	1.003	132	1.59	1.76	2.500	2.930	0.69	0.65	0.052
		1-4-9	0.088	1.004	162	1.94		3.360		0.62		0.041
		2-4-1	0.088	0.998	252	3.04		1.870		1.56		0.019
	CTD	2-4-2	0.088	0.998	452	5.46	4.25	3.610	2.740	1.54	1.55	0.020
		2-4-3	0.088	0.996	—	—		—		—		—
		2-4-4	0.087	1.007	554	6.63		5.100		1.31		0.017
IM6/F650	RTD	2-4-5	0.088	1.004	473	5.68	6.28	4.220	4.673	1.38	1.36	0.020
		2-4-6	0.088	0.994	540	6.55		4.700		1.41		0.018
		2-4-7	0.088	0.995	30	0.36		616		0.59		0.019
	ETW	2-4-8	0.088	1.007	81	0.97	0.74	1.428	1.097	0.68	0.66	0.017
		2-4-9	0.087	1.007	73	0.87		1.248		0.70		0.015

Note: Results normalized to 63% fiber volume fraction with a nominal ply thickness of .0052 in.

GP73-0343-31

Figure 29. Unidirectional 90° Tension Test Results

In contrast to IM6/3100, IM6/F650 showed maximum strength under RTD conditions. The CTD strength was 32 percent lower than the RTD strength. Apparently the CTD condition embrittled the F650 resin resulting in fragile material that was very susceptible to bending loads. One specimen of this group (Spec. 2-4-3) actually broke prior to testing as it was being positioned into the load frame. The ETW strength was 88 percent lower than the RTD strength. This drastic strength reduction in IM6/F650 under ETW conditions correlates with the microcracking that occurred in wet IM6/F650 during thermal spike testing. As the wet laminates were spiked to elevated temperatures, the matrix tension strength diminished and matrix cracks formed.

3.2.5.3 <u>0° Compression Test Results</u> - 0° compression mechanical properties were determined using both unidirectional coupons and unidirectional sandwich beams. The 0° compression coupon test specimen configuration is shown in Figure 30. Two coupon configurations were used to determine stiffness and strength. The configuration without tabs was instrumented to measure modulus and Poisson's ratio. The tabbed specimen was used to determine strength. The unsupported specimen length was chosen so that the buckling strength would exceed compression strength. Due to the short gage length these tabbed specimens could not be instrumented.

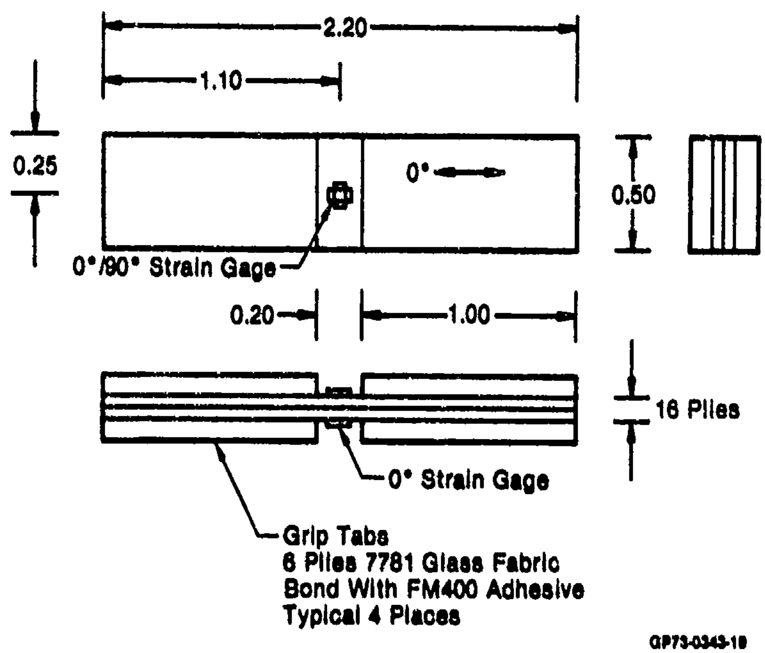

Figure 30. Unidirectional 0° Compression Coupon Test Specimen

Specimens were tested in the loading fixture shown in Figure 31. This test fixture includes two vertical alignment pins assuring loading directly along the axis of the specimen precluding eccentric loading and premature buckling of the specimen. Blocks at the grip ends provided lateral support. Compression loading was introduced on the ends of the specimen.

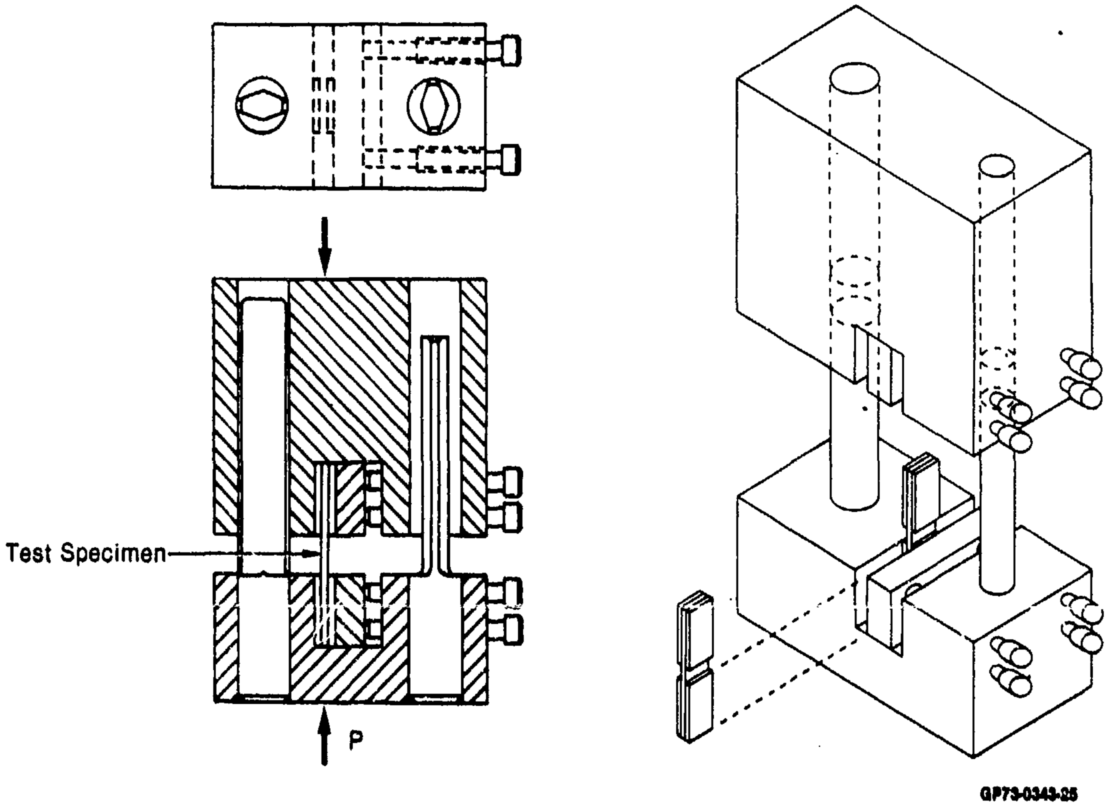

Figure 31. Compression Test Fixture

Test data from 0° compression coupon tests are tabulated in Figure 32. The results include strengths that correspond to a variety of failure modes. In addition to true fiber compression failures, there were through-the-thickness shear failures and end failures. Figure 33 shows a typical 0° compression coupon failure. The shear and end failures were premature, and did not give a true representation of the compressive capability of the BMI systems.

Material System	Environment	Specimen Number	Thickness (in.)	Width (in.)	Failure Load (lb)	Failure Stress (ksi)		Modulus (msi)		Poisson's Ratio
						Ind	Avg	Ind	Avg	
IM6/3100	CTD	1-4-19	0.088	0.503				22.29		0.286
		1-4-20	0.088	0.505				22.31	22.03	—
		1-4-21	0.088	0.506				21.50		0.309
	CTD	1-4-28	0.089	0.507	7,250	172.3				
		1-4-29	0.089	0.507	8,740	207.7	184.3			
		1-4-30	0.089	0.507	7,275	172.9				
	RTD	1-4-22	0.088	0.507				21.24		0.333
		1-4-23	0.089	0.519				21.95	22.32	0.345
		1-4-24	0.088	0.511				23.78		0.332
	RTD	1-4-31	0.090	0.507	8,125	193.1				
		1-4-32	0.089	0.507	8,250	196.1	194.0			
		1-4-33	0.089	0.512	8,190	192.7				
	ETW	1-4-25	0.088	0.506				22.91		0.417
		1-4-26	0.089	0.507				23.77	23.63	0.400
		1-4-27	0.089	0.506				24.20		0.420
	ETW	1-4-34	0.090	0.505	6,130	146.2				
		1-4-35	0.089	0.506	4,750	113.1	137.1			
		1-4-36	0.089	0.506	6,380	151.9				
IM6/F650	CTD	2-4-19	0.088	0.503				23.61		0.385
		2-4-20	0.088	0.503				22.81	23.17	0.381
		2-4-21	0.088	0.502				23.09		0.350
	CTD	2-4-28	0.088	0.500	7,150	172.3				
		2-4-29	0.088	0.508	6,630	157.2	163.5			
		2-4-30	0.087	0.508	6,790	161.0				
	RTD	2-4-22	0.088	0.503				22.66		0.364
		2-4-23	0.088	0.503				23.02	22.89	0.396
		2-4-24	0.088	0.502				22.99		0.389
	RTD	2-4-31	0.088	0.513	7,250	170.3				
		2-4-32	0.087	0.505	8,230	196.3	176.7			
		2-4-33	0.087	0.507	6,880	163.5				
	ETW	2-4-25	0.088	0.503				21.64		0.473
		2-4-26	0.088	0.504				23.28	22.83	—
		2-4-27	0.088	0.503				23.56		0.443
	ETW	2-4-34	0.087	0.492	4,000	98.0				
		2-4-35	0.088	0.489	4,030	99.3	96.7			
		2-4-36	0.088	0.499	3,840	92.7				

Note: Results normalized to 63% fiber volume fraction with a nominal ply thickness of .0052 in.

GP73-0343-33

Figure 32. Unidirectional 0° Compression Coupon Test Results

GP83-0089-25

Figure 33. Failed 0° Compression Coupon

3.2.5.4 <u>0° Compression Sandwich Beam Test Results</u> - In order to determine more representative compression properties, unidirectional sandwich beam tests were performed. The test specimen configuration is shown in Figure 34. Figure 35 shows a typical 0° compression sandwich beam failure. Test data from 0° compression sandwich beam tests are tabulated in Figure 36.

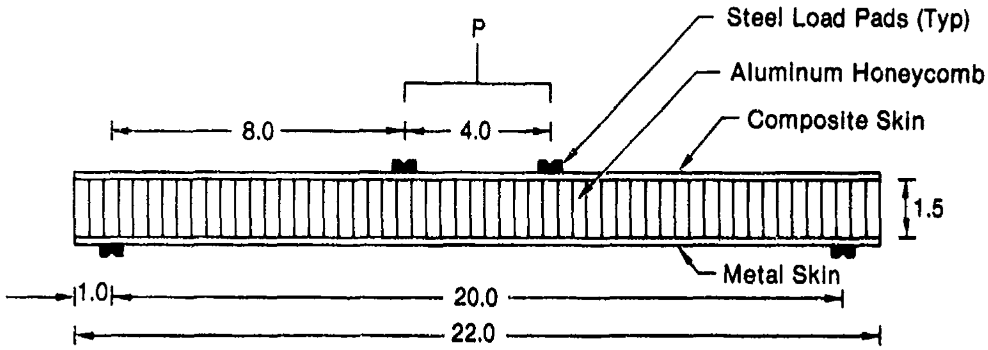

Composite Skin: 1.00 in. Wide; 22.0 in. Long; 6 Plies Thick
Metal Skin: 1.00 in. Wide; 22.0 in. Long; 0.125 in. Thick; 6Al-4V Annealed Titanium
Aluminum Honeycomb: 1.25 in. Wide; 22.0 in. Long; 1.50 in. Thick
Data Reduction:

$$\sigma = \frac{P\,L}{2\,w\,t\,(C + \frac{t+T}{2})}$$

Where: σ = Uniaxial Compression Stress
P = Applied Load
w = Composite Skin Width (1.00 in.)
t = Nominal Composite Skin Thickness (6 Plies)
C = Honeycomb Core Height (1.50 in.)
T = Metal Skin Thickness (0.125 in.)
L = Moment Arm Between Applied Load and Reaction Support (8.0 in.)

GP73-0343-20

Figure 34. Unidirectional 0° Compression Sandwich Beam Test Arrangement

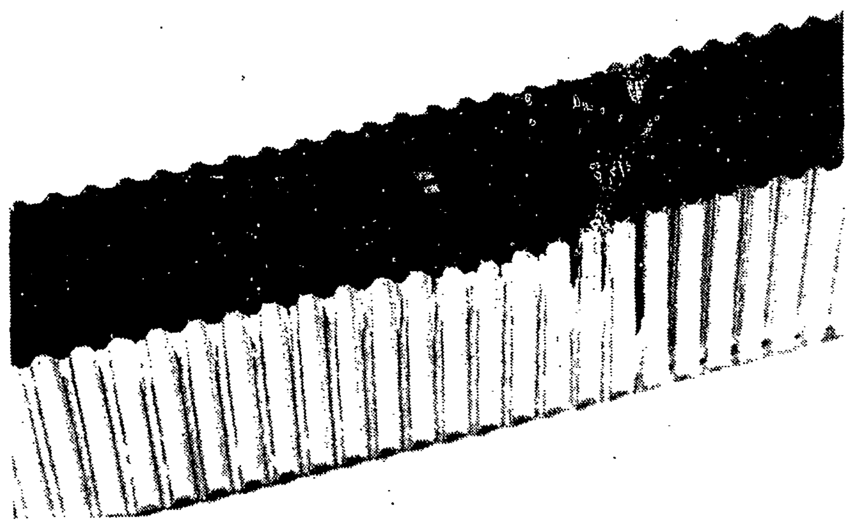

GP83-0089-26

Figure 35. Failed 0° Compression Sandwich Beam Specimen

Material System	Environment	Specimen Number	Thickness (in.)	Width (in.)	Failure Load (lb)	Failure Stress (ksi)		Failure Strain (μ in./in.)		Modulus (msi)	
						Ind	Avg	Ind	Avg	Ind	Avg
		1-0-1	0.035	1.014	3,530	284.7		14,400		23.57	
	CTD	1-0-2	0.036	1.005	3,740	304.3	283.9	15,720	14,327	24.41	24.07
		1-0-3	0.037	1.005	3,230	262.8		12,860		24.22	
		1-0-4	0.037	1.001	2,960	241.8		11,890		22.98	
IM6/3100	RTD	1-0-5	0.037	1.008	2,740	222.3	242.5	10,200	11,790	24.22	23.39
		1-0-6	0.036	1.003	3,230	263.3		13,280		22.96	
		1-0-7	0.038	1.005	1,390	113.1		4,900		24.05	
	ETW	1-0-8	0.037	1.009	1,670	135.3	122.6	6,250	5,540	23.12	23.57
		1-0-9	0.035	1.007	1,470	119.4		5,470		23.54	
		2-0-1	0.033	0.964	3,290	279.1		14,200		23.81	
	CTD	2-0-2	0.034	1,018	3,540	284.3	291.6	14,580	15,110	23.84	23.94
		2-0-3	0.034	0.938	3,800	311.3		16,550		24.18	
		2-0-4*	0.034	0.996	3,540	290.6		15,560		23.72	
IM6/F650	RTD	2-0-5*	0.034	1.002	3,460	282.4	283.0	14,570	14,500	24.09	24.04
		2-0-6	0.034	1.001	3,380	276.1		13,370		24.32	
		2-0-7*	0.034	0.998	1,420	116.3		4,880		24.88	
	ETW	2-0-8*	0.034	0.992	1,470	121.2	118.5	5,450	5,150	24.73	24.97
		2-0-9*	0.034	1.012	1,460	118.0		5,130		25.29	

*Failure occurred outside load introduction points

Note: Results normalized to 63% fiber volume fraction with a nominal ply thickness of .0052 in.

GP73-0343-32

Figure 36. Unidirectional 0° Compression Sandwich Beam Test Results

Results from these tests show that as temperature and moisture content increase, the 0° compression strength decreases. This is due to the decreased fiber support of softened matrix material.

The RTD strength of IM6/3100 was 15 percent lower than its CTD strength. The ETW strength was 57 percent lower than its CTD strength.

The compression strengths of IM6/F650 covered a wider range than the strengths of IM6/3100. IM6/F650 was stronger than IM6/3100 for CTD and RTD conditions and was virtually equal in strength for ETW conditions. The RTD strength of IM6/F650 was 3 percent lower than its CTD strength. The ETW strength was 59 percent lower than its CTD strength.

Five IM6/F650 sandwich beam tests had failures occur outside of the load introduction points where shear load exists in addition to the compression skin load. In the RTD cases where specimen 2-0-6 failed inside the loading points and specimens 2-0-4 and 2-0-5 failed outside the loading points, there is no significant difference in compression strengths. The 0° compression strengths obtained by sandwich beam tests were more representative of the material systems' compression strengths and were used to predict laminate strengths in Task III.

3.2.5.5 <u>Intralaminar Shear Test Results</u> - Intralaminar shear mechanical behavior was evaluated using the ±45° test specimen shown in Figure 37. Figure 38 shows a typical failed ±45° shear specimen. Test results are summarized in Figure 39. Complete shear stress-strain curves for both BMI systems are shown in Figures 40 and 41.

IM6/3100 showed less shear strength environmental degradation than did IM6/F650. The RTD strength of IM6/3100 was slightly less (3 percent) than the CTD strength. The ETW strength was 18 percent lower than the CTD strength. The ETW strength reduction was accompanied by an ETW modulus that was 57 percent lower than the CTD modulus.

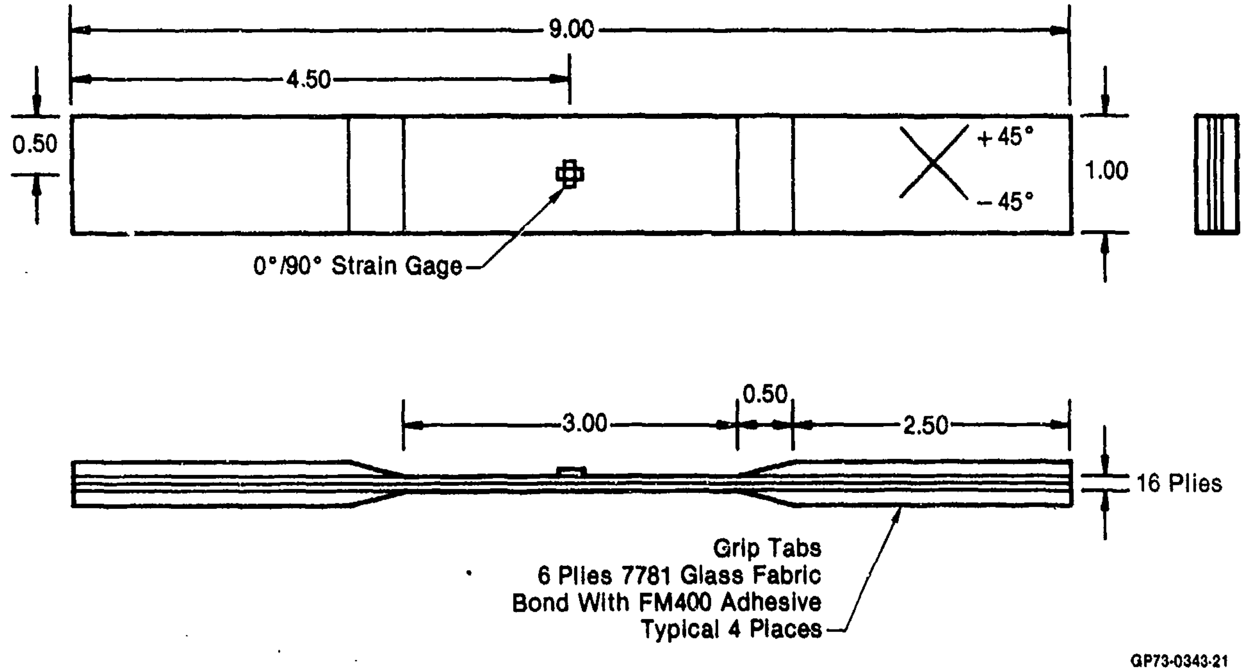

Figure 37. ±45° Intralaminar Shear Test Specimen

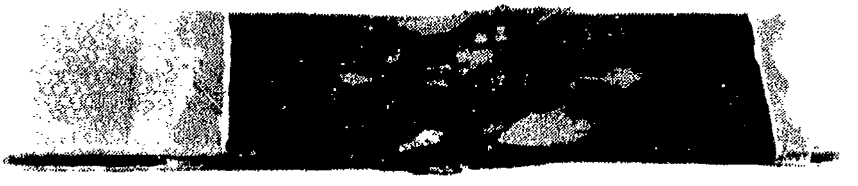

Figure 38. Failed ±45° Shear Specimen

Material System	Environment	Specimen Number	Thickness (in.)	Width (in.)	Failure Shear Stress (psi)		Failure Shear Strain (μ in./in.)	Shear Modulus (msi)	
					Ind	Avg		Ind	Avg
IM6/3100	CTD	1-5-1	0.0893	1.006	13,140		16,950	1.035	
		1-5-2	0.0906	1.005	13,570	13,440	16,500	1.021	1.026
		1-5-3	0.0902	1.007	13,610		17,700	1.021	
	RTD	1-5-4	0.0901	1.008	13,060		22,370	0.837	
		1-5-5	0.0902	1.012	13,020	13,060	30,000	0.770	0.818
		1-5-6	0.0909	1.004	13,110		23,200	0.846	
	ETW	1-5-7	0.0900	1.009	11,470		>32,000	0.524	
		1-5-8	0.0901	1.008	10,680	10,960	>32,000	0.426	0.441
		1-5-9	0.0901	1.009	10,720		>32,000	0.372	
IM6/F650	CTD	2-5-1	0.0870	1.006	10,180		11,480	1.024	
		2-5-2	0.0877	1.006	10,470	10,110	12,160	1.039	1.011
		2-5-3	0.0876	1.006	9,680		11,120	0.969	
	RTD	2-5-4	0.0873	1.007	10,560		15,120	0.865	
		2-5-5	0.0867	1.006	10,390	10,200	15,440	0.864	0.867
		2-5-6	0.0865	1.008	9,660		13,180	0.873	
	ETW	2-5-7	0.0863	1.005	6,100		>32,000	0.375	
		2-5-8	0.861	1.005	6,100	5,950	>32,000	0.325	0.339
		2-5-9	0.0862	1.005	5,650		>32,000	0.316	

Note: Results normalized to 63% fiber volume fraction with a nominal ply thickness of .0052 in.

GP73-0343-35

Figure 39. Intralaminar Shear Test Results

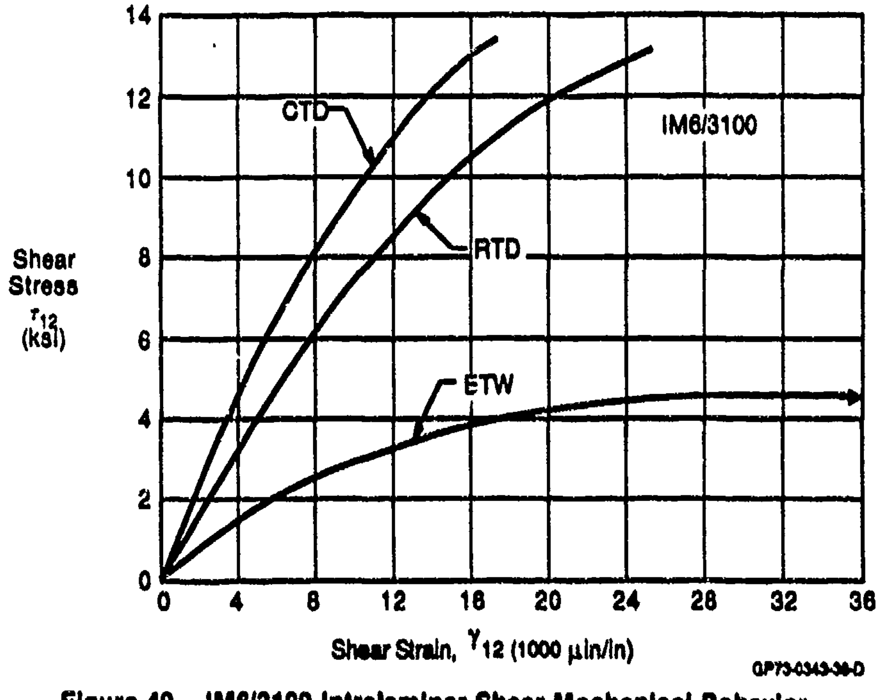

Figure 40. IM6/3100 Intralaminar Shear Mechanical Behavior

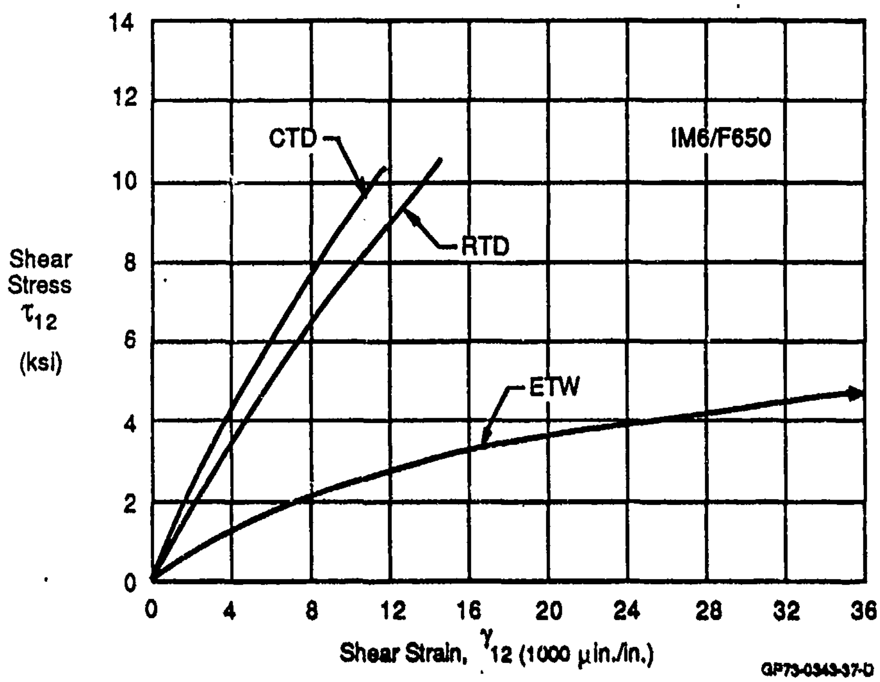

Figure 41. IM6/F650 Intralaminar Shear Mechanical Behavior

The CTD strength and RTD strength of IM6/F650 were virtually equal. The CTD strength was 1 percent lower than the RTD strength. The ETW strength of the IM6/F650 was 42 percent lower than the RTD strength. The ETW strength reduction was accompanied by an ETW modulus that was 66 percent lower than the CTD modulus.

Shear stress-strain mechanical behavior was determined from measurements of load versus longitudinal and transverse strain using the following relations (Reference 2):

$$G_{12} = \sigma_x/2(\varepsilon_x - \varepsilon_y) \tag{2}$$

$$\tau_{12} = \sigma_x/2 \tag{3}$$

$$\gamma_{12} = \varepsilon_x - \varepsilon_y \tag{4}$$

There are two important approximations inherent with this test and data reduction procedure (Reference 3). One approximation is caused by the lack of a pure shear stress or strain state in each ply of the ±45° test specimen. From test results, e.g., Figure 42 it is shown that the laminate Poisson's ratio is not unity. Since the longitudinal strain is not quite equal to the negative of the transverse strain, the strain state in each ply at 45° to the laminate axes is not quite pure shear. If laminate strains are plotted on a Mohr's strain circle, results shown in Figure 43 are obtained. Small tensile strains exist in addition to the relatively large shear strains in the principal directions of the lamina. The tensile strains across the transverse direction of the lamina result in a slightly reduced shear modulus and contribute to laminate failure.

Specimen	Thickness	Width	Step Number	Load	σ_x	E_x	ϵ_x	ϵ_y	ν_{xy}	τ_{12}	γ_{12}	G_{12}
1-5-4	0.0901	1.008	1	300	3,580	2.96	1,209	930	0.769	1,790	2,139	0.837
			2	600	7,150	2.95	2,418	1,860	0.769	3,575	4,278	0.835
			3	900	10,730	2.75	3,720	2,790	0.750	5,365	6,510	0.802
			4	1,200	14,310	2.57	5,115	3,906	0.764	7,155	9,021	0.713
			5	1,500	17,890	2.26	6,696	5,115	0.764	8,945	11,811	0.642
			6	2,190	26,110	1.44	12,415	9,951	0.801	13,055	22,366	0.389

GP73-0343-36

Figure 42. Intralaminar Shear Test Data

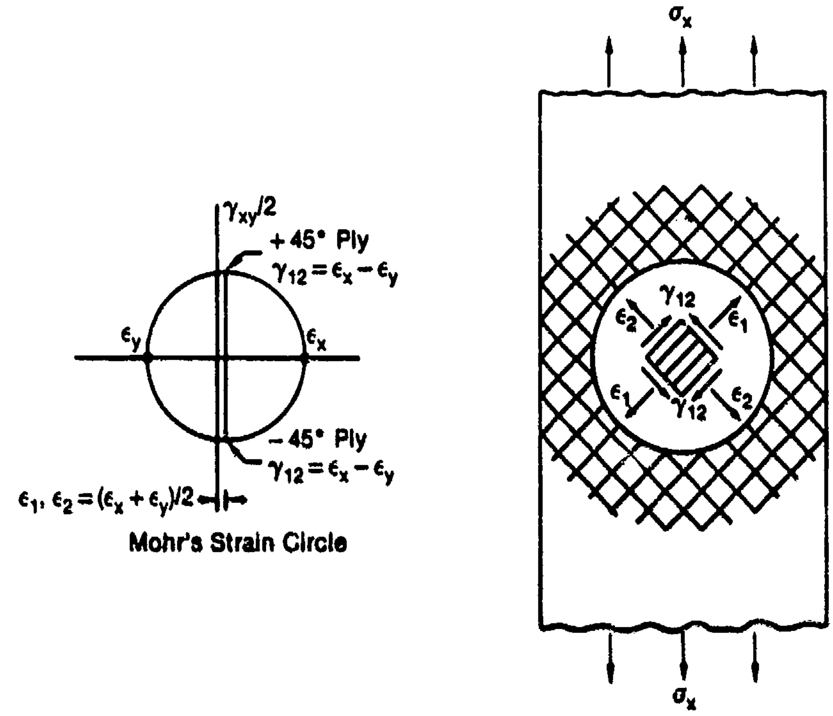

Figure 43. Strain State in ±45° Intralaminar Shear Test Specimen

The second approximation is due to the existence of large free edge stresses in the region near the boundary of the $\pm 45°$ test specimen. Predictions of free edge stresses in $\pm 45°$ laminates have been discussed in the literature (Reference 4). Results are reproduced in Figure 44. Failure of the $\pm 45°$ intralaminar shear test specimen is influenced by damage growth caused by these large free edge stresses. Damage growth is primarily a Mode II fracture due to the interlaminar shear stress state at the laminate free edge. The toughness of the IM6/3100 resin system inhibits growth of this free edge damage and accounts for its high shear strength relative to the IM6/F650 strength, as measured using the $\pm 45°$ test specimen. Recognizing the limitations of the $\pm 45°$ test method for measuring lamina shear mechanical properties, lamina shear strength test results and hence laminate strength predictions will in general be conservative.

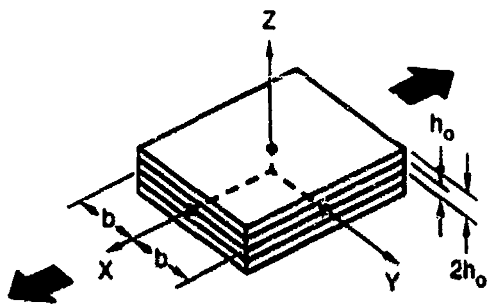

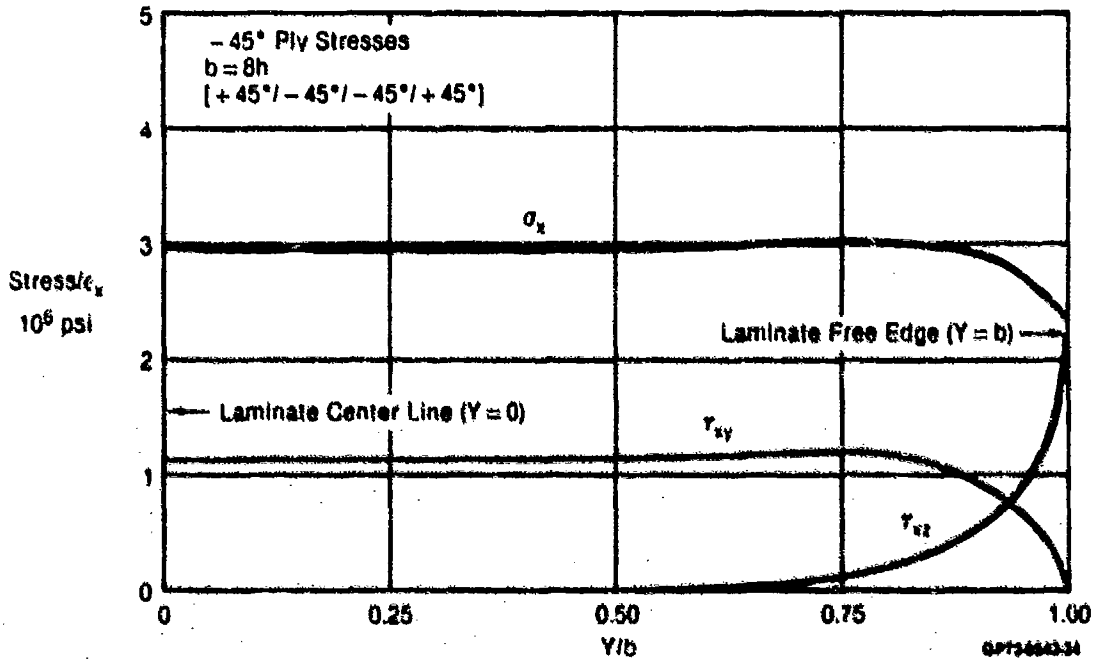

Figure 44. Interfacial Stresses in ±45° Intralaminar Shear Test Specimen

3.2.5.6 Comparison with Baseline Material Systems - Figure 45 summarizes the lamina properties of IM6/3100 and IM6/F650. The baseline material systems' lamina properties are also included.

3.2.6 Interlaminar Fracture Toughness - Fracture toughness tests were performed to determine critical strain energy release rates (from static tests) and crack growth rates (from fatigue tests) as shown in the test matrix in Figure 46.

		AS1/3501-6		T30/V378A			IM6/3100			IM6/F650		
		R.T.	250°F	R.T.	250°F	350°F	−65°F	R.T.	ETW(1)	−65°F	R.T.	ETW(2)
0° Tension	F_1^{tu} (ksi)	274	267	193	217	191	382	383	231	331	281	205
	E_1^t (msi)	20.8	20.3	21.6	19.9	20.4	23.2	23.0	22.1	23.2	23.4	22.4
	ϵ_1^{tu} (μin./in.)	12,440	12,735	9,580	10,480	9,570	15,350	14,940	10,080	12,830	13,290	9,330
90° Tension	F_2^{tu} (ksi)	9.5	9.1	7.8	6.3	5.1	5.9	5.6	1.8	4.2	6.3	0.7
	E_2^t (msi)	1.9	1.6	1.7	1.4	1.3	1.5	1.5	0.6	1.6	1.4	0.7
	ϵ_2^{tu} (μin./in.)	5,380	6,125	4,760	4,870	4,630	3,850	3,880	2,930	2,740	4,670	1,100
0° Compression	F_1^{cu} (ksi)	280	227	142	—	103	284	242	123	292	283	118
	E_1^c (msi)	18.6	18.6	18.6	—	23.5	22.0	22.3	23.6	23.2	22.9	22.8
	ϵ_1^{cu} (μin./in.)	18,180	12,965	8,190	—	4,780	14,330	11,790	5,540	15,110	14,500	5,150
Shear	F_{12}^u (ksi)	17.3	—	10.4	—	8.8	13.4	13.1	11.0	10.1	10.2	6.0
	G_{12} (msi)	0.85	—	0.86	—	0.73	1.03	0.82	0.44	1.01	0.87	0.34
	γ_{12}^u (μin./in.)	69,000	—	18,500	—	32,100	17,050	25,190	>32,000	11,590	14,580	>32,000

Notes (1) ETW - 360°F 0.71% MC
(2) ETW - 410°F, 0.71% MC

GP73-0343-39

Figure 45. Lamina Property Comparison: Baseline Material Systems vs Second Generation BMIs

	IM6/3100 CTD	IM6/3100 RTD	IM6/3100 ETW	IM6/F650 CTD	IM6/F650 RTD	IM6/F650 ETW	Number of Tests
Double Cantilever Beam							
Static	3	3	3	3	3	3	18
Fatigue	3	3	3	3	3	3	18
Cracked Lap Shear (a)							
Static	3	3	3	3	3	3	18
Fatigue	3	3	3	3	3	3	18
Cracked Lap Shear (b)							
Static	3	3	3	3	3	3	18
Fatigue	3	3	3	3	3	3	18
End Notched Flexure							
Static	3	3	3	3	3	3	18
Fatigue	3	3	3	3	3	3	18
						Total	144

GP73-0343-67

Figure 46. Interlaminar Fracture Toughness Test Matrix

3.2.6.1 Specimen Description - Interaction envelopes for strain energy release rates of IM6/3100 and IM6/F650 were developed. The interaction characteristics were determined by testing different specimen configurations that exhibited different mixtures of Mode I and Mode II fracture. Double cantilever beam (DCB) specimens were tested to determine pure Mode I behavior (Figure 47). End notched flexure (ENF) specimens were tested to determine pure Mode II behavior (Figure 48). To determine intermediate points in the interaction envelope, cracked lap shear (CLS) specimens were tested (Figure 49).

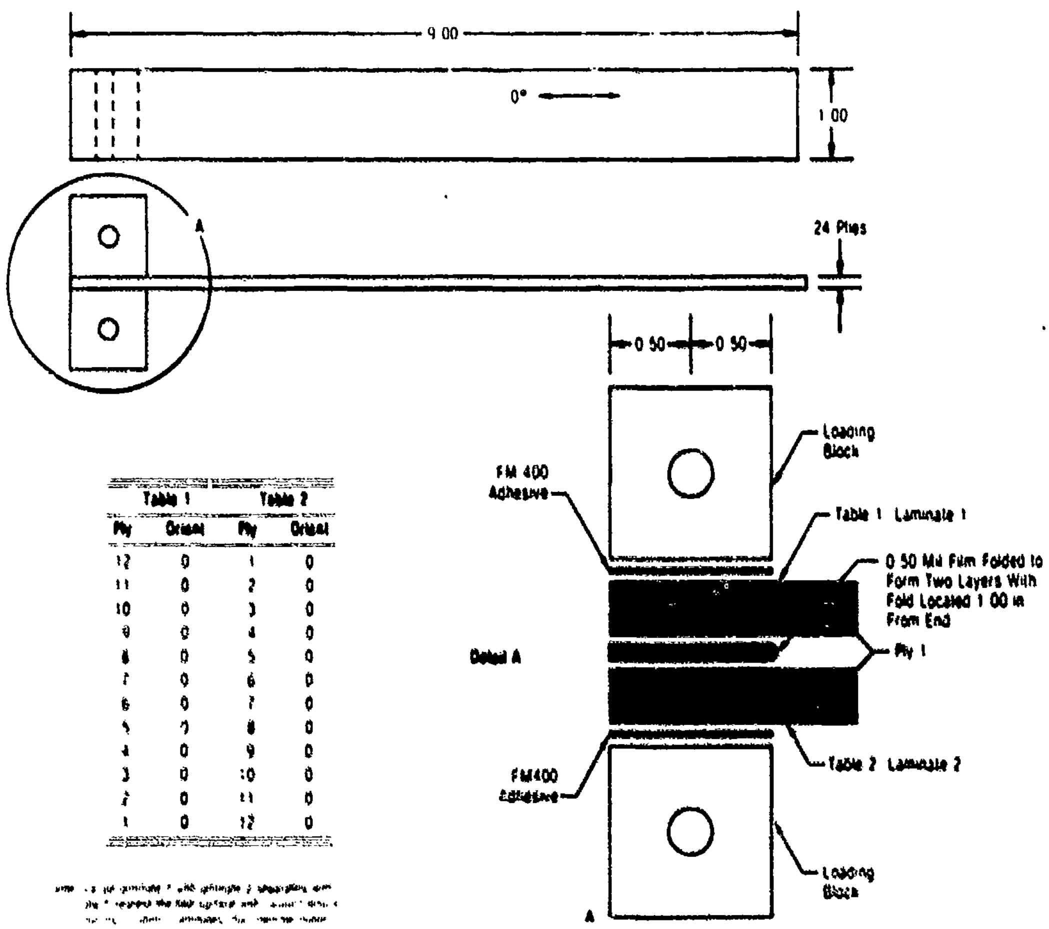

Table 1		Table 2	
Ply	Orient	Ply	Orient
12	0	1	0
11	0	2	0
10	0	3	0
9	0	4	0
8	0	5	0
7	0	6	0
6	0	7	0
5	0	8	0
4	0	9	0
3	0	10	0
2	0	11	0
1	0	12	0

Figure 47. Double Cantilever Beam (Mode I) Fracture Toughness Specimen

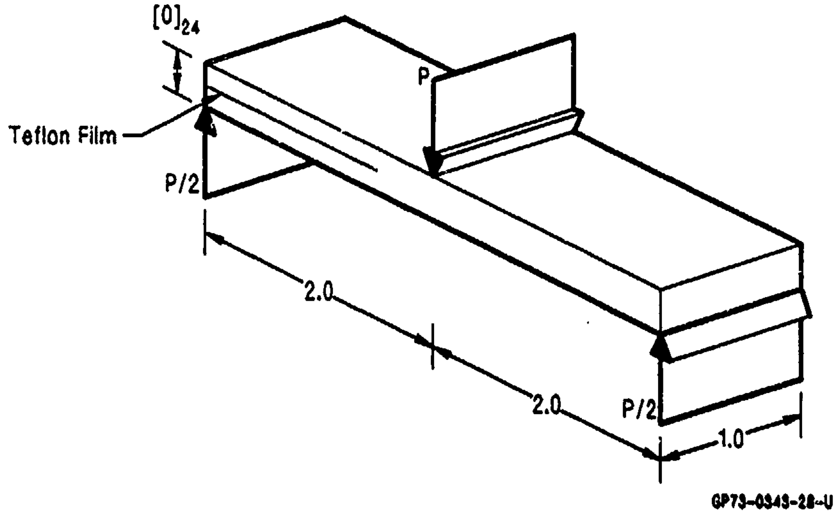

Figure 48. End Notched Flexure (Mode II) Fracture Toughness Specimen

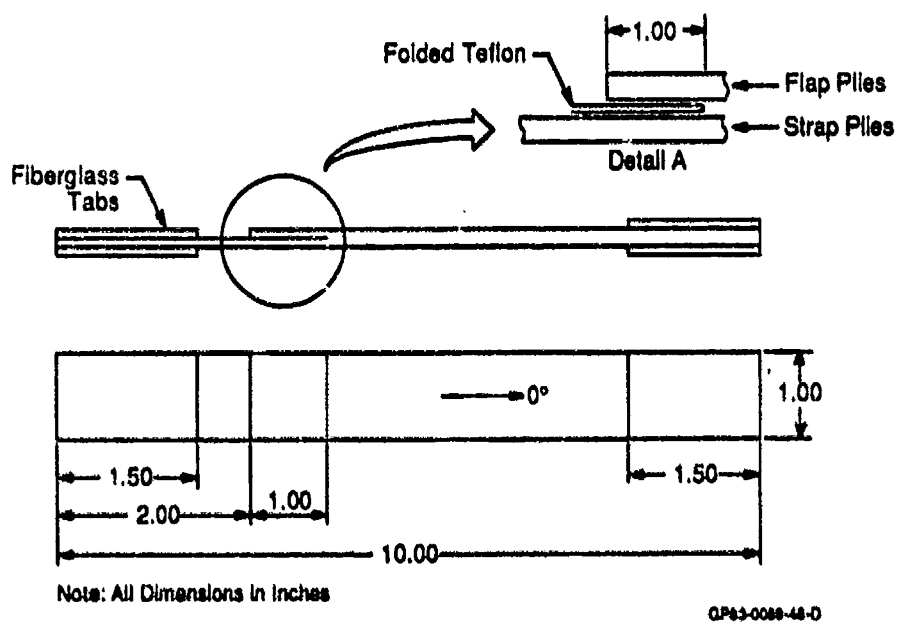

Figure 49. Cracked Lap Shear (Mixed Mode) Fracture Toughness Specimen

By varying the number of continuous and discontinuous plies in the CLS specimen, the proportions of Mode I and Mode II fracture can be changed. The specimen identification scheme used in this program was:

CLS-XY

X ≡ total number of plies

Y ≡ number of continuous plies .

The CLS configurations used in this program were CLS-63 and CLS-82. The CLS-63 specimens exhibited 30 percent Mode I and 70 percent Mode II fracture behavior. The CLS-82 specimens exhibited 17 percent Mode I and 83 percent Mode II fracture behavior. These proportions were determined by finite element analyses in the Navy program, "Delamination Failure Criteria for Composite Structures", (Reference 5). The interaction curves determined by the test results were in the form shown in Figure 50.

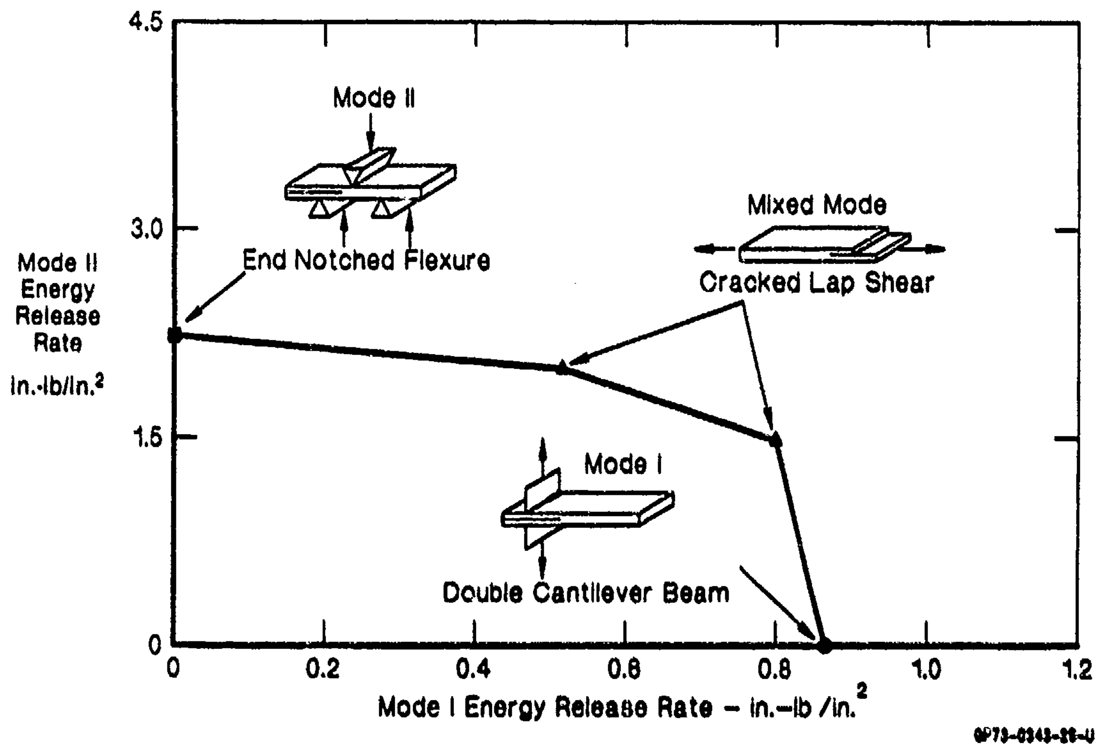

Figure 50. Specimens Required to Determine Fracture Toughness Interaction

3.2.6.2 Strain Energy Release Rate Formulation - Critical strain energy release rates were obtained from measurements of crack length, failure load, deflection, and compliance. The data was used with the following formula to calculate the strain energy release rate of the composite system.

$$G = \frac{P^2}{2W} * \frac{dC}{da} \tag{5}$$

In the formula, P is the failure load, W is the specimen width, and dC/da is the change in specimen compliance with change in crack length.

3.2.6.3 Mode I Data Reduction - Several tests were performed on each DCB specimen. Displacement was applied to initiate crack growth in the starter film and increased until the crack extended some distance from the loading blocks. For each test measurement, displacement was applied to start crack growth, and the displacement was increased until the crack propagated some arbitrary distance along the specimen. Crack length measurements were taken visually on the specimen edge with a traveling microscope.

To compute G_{IC} from test results, the Compliance Calibration Method

$$G_{IC} = 3A_1A_2^2/2W \tag{6}$$

This relationship is obtained by describing C and P_c by the equations,

$$C = \delta/P = A_1a^3 \tag{7}$$

$$P_c = A_2a^{-1} \tag{8}$$

$C \equiv$ compliance

$P_c \equiv$ critical load (to initiate crack growth)

and substitution into Equation (5). The data indicated however, that the compliance was not a cubic function of crack length (a), and critical load was not an inverse function of crack length. Typical data is shown in Figure 51 where compliance varies with crack length to the power of 3.35 and critical load varies with crack length to the power of -0.9695. In the general case Equations (7) and (8) are:

$$C = \delta/P = A_1a^N \tag{9}$$

$$P_c = A_2a^{-M} \tag{10}$$

Substitution of Equations (9) and (10) into Equation (5) gives the general equation:

$$G_{IC} = NA_1 \, A_2^2 a^{N-1-2M}/2W \tag{11}$$

For the conditions described in Figure 51 Equation (11) becomes:

$$G_{IC} = 1.915a^{0.411} \tag{12}$$

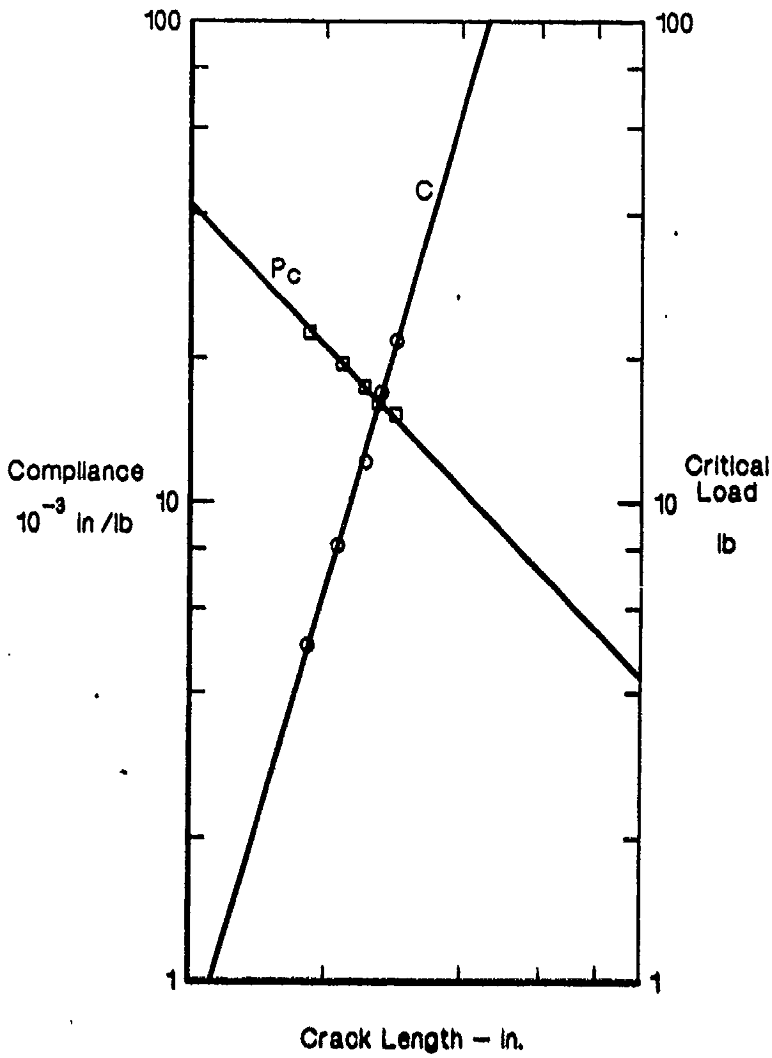

$$C = A_1 a^N = 6.95*(10)^{-4} \, a^{3.35}$$

$$P_c = A_2 a^{-M} = 40.56 \, a^{-0.9695}$$

GP78-0343-48-U

Figure 51. Typical Mode I Test Data

Equation (12) is in terms of the experimental crack length referenced to the applied load axis that is 0.5 inch into the Teflon insert (See Figure 52). To evaluate the effects of crack length on apparent toughness, G_{IC} values were calculated for a = 0.5 inch and 2.5 inch which represent 0.0 inch and 2.0 inch of natural crack length, respectively. The relationship defined by Equation 12 is shown in Figure 53. For natural crack lengths of 0.0 inch (artificial crack length of 0.5 inch) and 2.0 inch the values of G_{IC} are 1.44 and 2.79 respectively. The variation of G_{IC} has been attributed to fiber bridging along the natural crack surface. The effects of fiber bridging have also been seen in mixed mode CLS specimen tests. However, fiber bridging effects have not be observed in Mode II ENF specimen tests. Apparently fiber bridging affects the Mode I component of toughness and not the Mode II component. To indicate the magnitude of fiber bridging effects for various conditions, G_C values are summarized for natural crack lengths of 0.0 inch (i.e. no fiber bridging) and 2.0 inches.

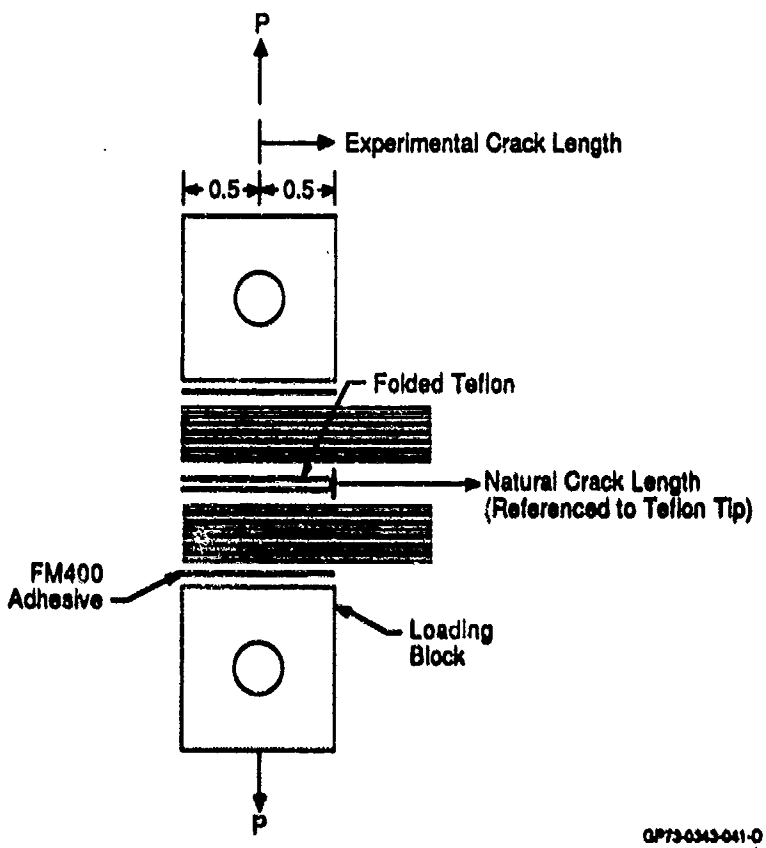

Figure 52. In DCB Specimens the Natural Crack Length is 0.5 Inch Shorter Than the Experimental Crack Length

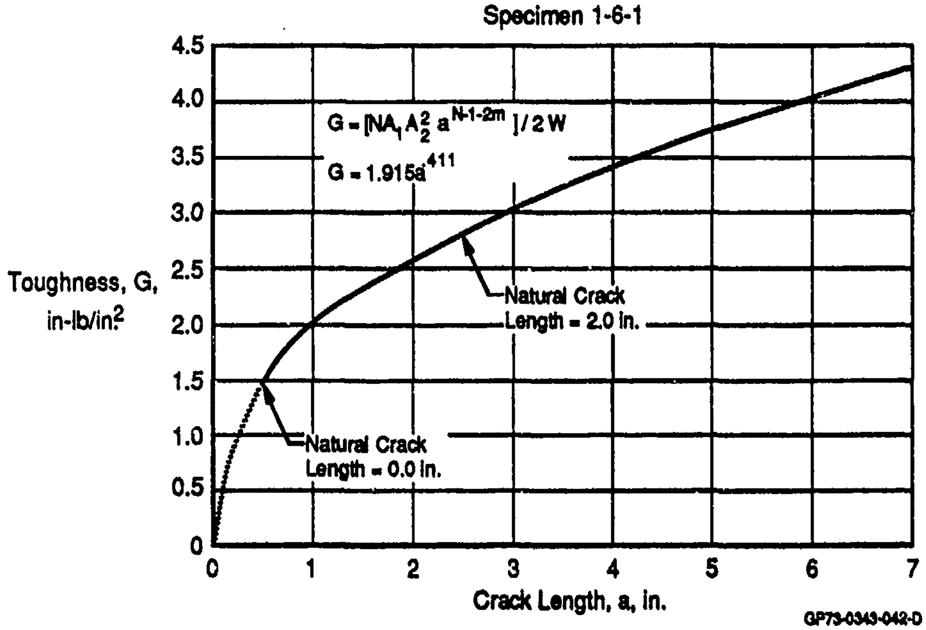

Figure 53. Mode I Toughness Increases With Crack Length

3.2.6.4 <u>Mixed Mode Data Reduction</u> - As with Mode I, the mixed mode toughness varied with crack length. Similar efforts were made to define the variation in terms of natural crack length. Figure 54 shows that for the CLS specimen configuration, the natural crack length is 1.5 inches shorter than the experimental crack length.

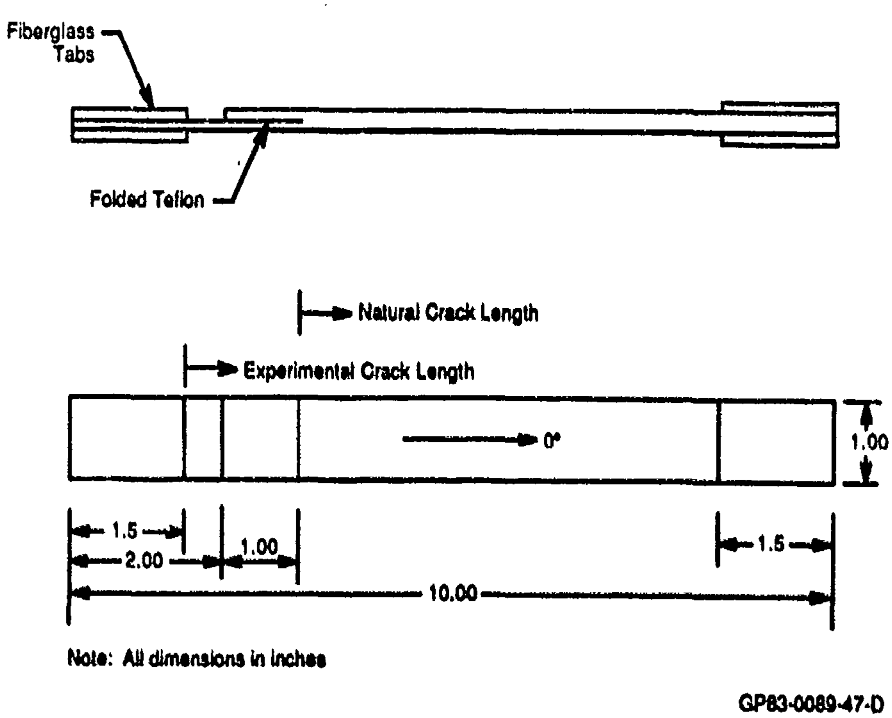

Figure 54. In CLS Specimens The Natural Crack Length Is 1.5 Inches Shorter Than The Experimental Crack Length

Several tests were performed on each CLS specimen. Both critical load and compliance as functions of crack length were determined. Figure 55 shows typical compliance versus crack length data. The data indicates that dC/da (the slope of the plot in Figure 55) is constant. To compute G_C from test results the constant value of dC/da was substituted into Equation (5) resulting in,

$$G_C = \frac{P_c^2}{2W} * 2.094E\text{-}06 \qquad (13)$$

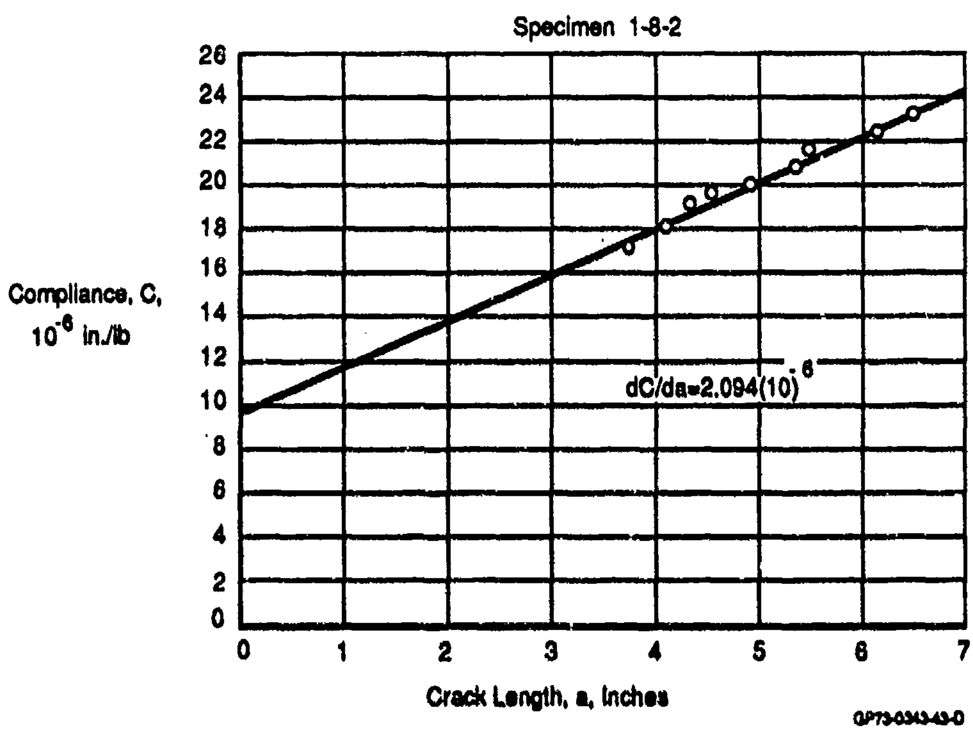

Figure 55. Mixed Mode Compliance Varies Linearly With Crack Length

Figure 56 shows that critical load varied with crack length. Using the critical load vs. crack length data from Figure 56 and Equation (13), G_C as a function of crack length was determined as shown in Figure 57. For natural crack lengths of 0.0 inch (experimental crack length of 1.5 inch) and 2.0 inch the values of G_C are 1.31 and 1.67 respectively. This variation has been attributed to the effects of fiber bridging on the opening mode of CLS specimens.

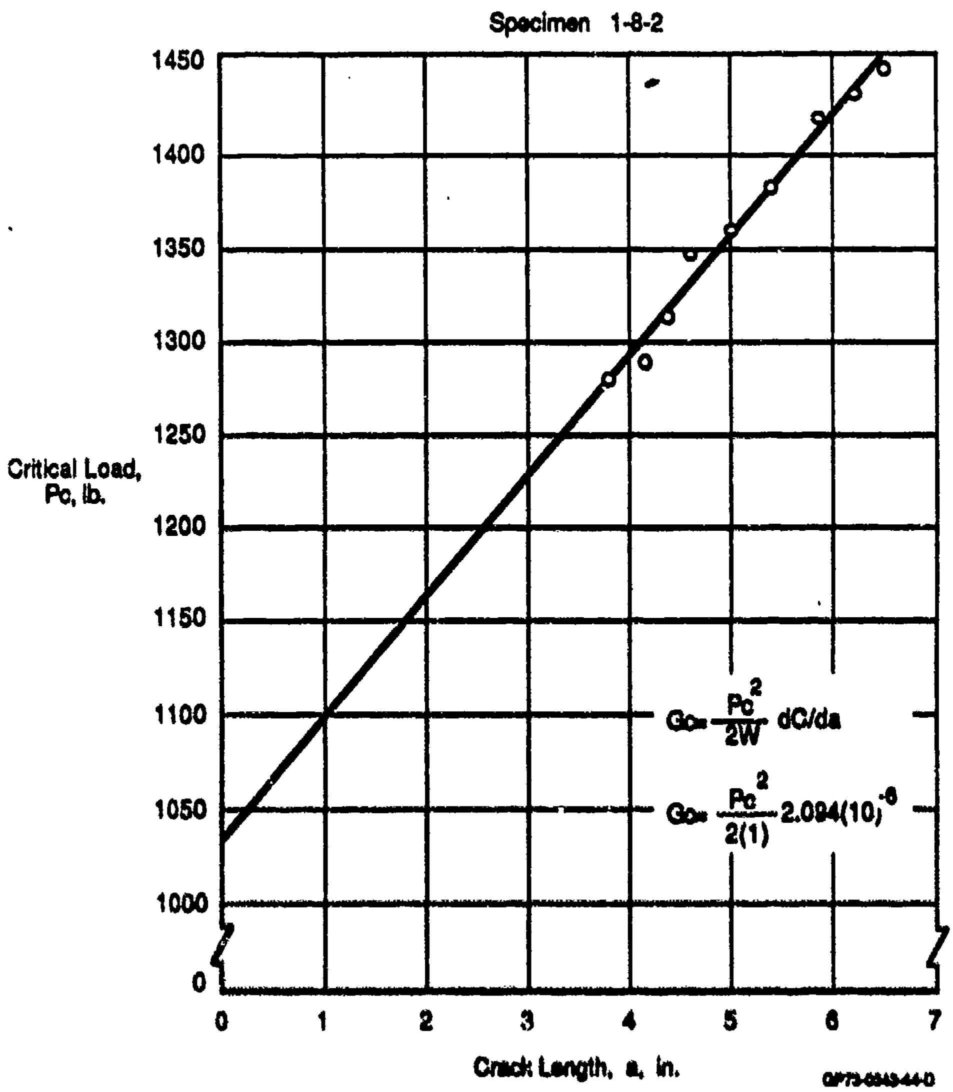

Figure 56. Critical Load of Mixed Mode Specimen Varies With Crack Length

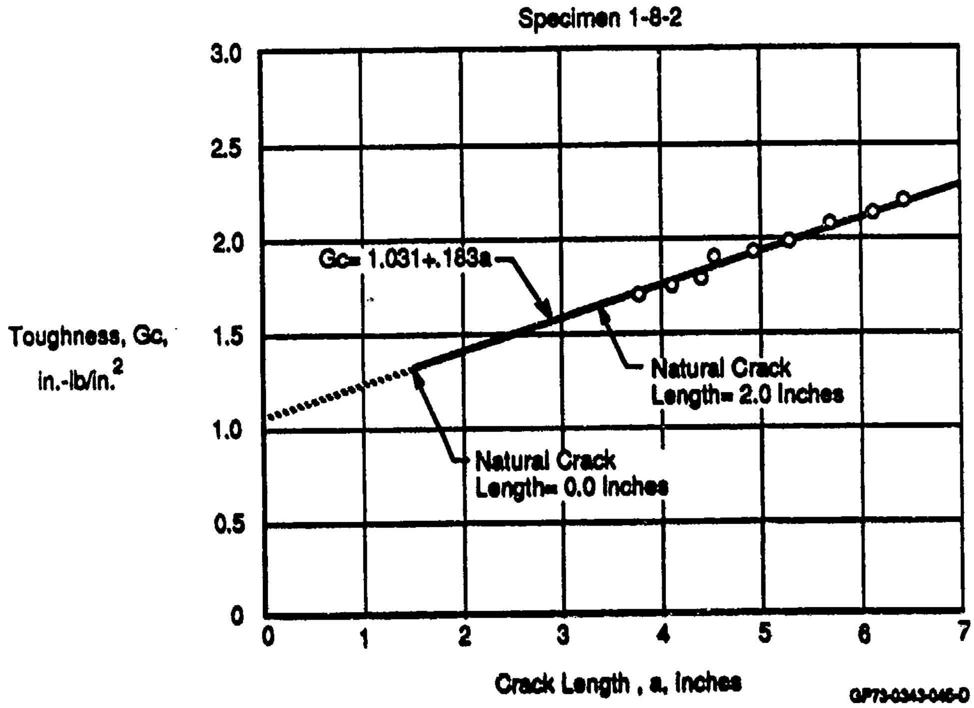

Figure 57. Mixed Mode Toughness Varies With Crack Length

3.2.6.5 Mode II Data Reduction - ENF specimens exhibited no Mode I (opening) behavior which is appropriate for this type of specimen. It was discovered that the lack of opening prevented crack length measurement once the crack started to grow from the Teflon tip. To solve this problem, compliance vs. crack length functions were experimentally determined for each specimen prior to performing several fracture toughness tests on each specimen. The crack (Teflon) tip of the undamaged specimen was visible through microscopic observation. Compliance scans were done by loading the ENF specimen to subcritical levels, unloading the specimen, and repositioning the crack tip (simulated by a Teflon insert) to establish various crack lengths. Crack length could then be defined through compliance measurements.

In contrast to Mode I and Mixed Mode tests, Mode II tests showed that crack length did not affect the measured value of critical strain energy release rate. To calculate G_{IIC} the following formulation was used. The compliance is given by beam theory as:

$$C = \frac{2L^3 + 3a^3}{8Ebh^3} \tag{14}$$

where,

$L \equiv$ half-span (2.0 inch)
$a \equiv$ crack length
$E \equiv$ Modulus
$b \equiv$ width
$h \equiv$ specimen half-thickness

This definition of compliance in turn defines:

$$dC/da = \frac{9a^2}{8Ebh^3} \tag{15}$$

Solving Equation (14) for the quantity $8Ebh^3$, and substituting into Equation (15), gives:

$$dC/da = \frac{9a^2C}{2L^3+3a^3} \tag{16}$$

Substitution of Equation (16) into Equation (5) gives the final formula for G_{IIC} as:

$$G_{IIC} = \frac{9P_c{}^2a^2C}{2b * (2L^3 + 3a^3)} \tag{17}$$

This formulation has been reported previously by Russel and Street (Reference 7).

To determine Mode II fracture toughness, each ENF specimen was loaded in 3-point bending to the critical load level where the crack grew to the midspan location and stopped. During the loading event, compliance data was recorded. The previously determined compliance vs. crack length relationship was then used to determine the crack length corresponding to the measured compliance. The critical load, compliance, crack length, specimen width, and half-span length were then entered in Equation (17) to calculate G_{IIC}. After each loading, the specimen was repositioned with the crack tip away from the midspan location. The loading and repositioning process was repeated several times to obtain multiple fracture toughness values from each specimen. The values were averaged to define the specimen fracture toughness. Typical test results are shown in Figure 58.

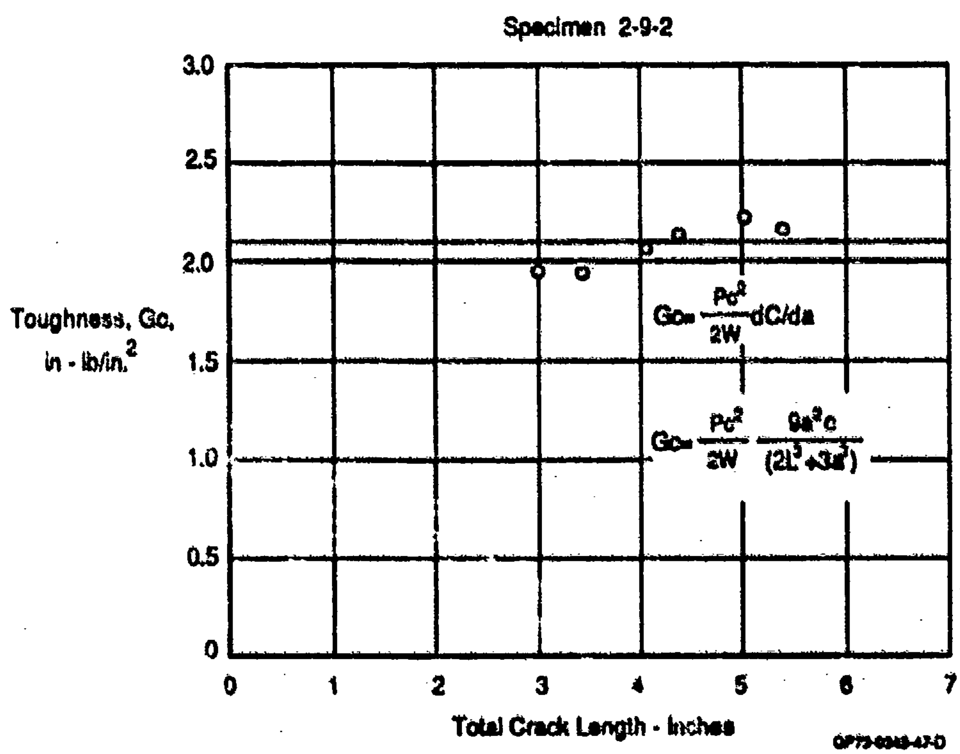

Figure 58. Mode II Toughness is Independent of Crack Length

3.2.6.6 Static Test Summary - The critical strain energy release rate data are tabulated in Figures 59 through 61. The data has been separated by environment. Each table includes data for all four specimen types (DCB, CLS-63, CLS-82, and ENF). Data is reported for natural crack lengths of 0.0 inch and 2.0 inch to indicate the effectiveness of fiber bridging on measured fracture toughness. Note that for ENF specimens the toughness average is a weighted average of specimen averages. The number of tests performed on each ENF specimen is included in parentheses after the data.

Fracture Toughness Test Results
CTD Conditions

Material	Specimen Type	Specimen Number	G_c (a = 0.0 in.) Ind	G_c (a = 0.0 in.) Avg	G_c (a = 2.0 in.) Ind	G_c (a = 2.0 in.) Avg
		1-6-4	1.16		2.25	
IM6/3100	DCB	1-6-5	2.03	1.61	2.44	2.43
		1-6-6	1.65		2.59	
		1-7-4	1.76		3.15	
IM6/3100	CLS-63	1-7-5	—	1.39	—	2.31
		1-7-6	1.02		1.46	
		1-8-4	2.06		2.26	
IM6/3100	CLS-82	1-8-5	1.57	1.79	1.39	2.11
		1-8-6	1.74		2.19	
		1-9-4	3.07(4)		3.07(4)	
IM6/3100	ENF	1-9-5	2.90(4)	2.98*	2.90(4)	2.98*
		1-9-6	2.98(4)		2.98(4)	
		2-6-4	0.79		1.92	
IM6/F650	DCB	2-6-5	1.57	1.14	2.58	2.29
		2-6-6	1.06		2.38	
		2-7-4	1.30		1.71	
IM6/F650	CLS-63	2-7-5	1.67	1.53	1.89	1.85
		2-7-6	1.62		1.96	
		2-8-4	0.88		1.18	
IM6/F650	CLS-82	2-8-5	1.96	1.37	2.26	1.71
		2-8-6	1.27		1.69	
		2-9-4	2.32(5)		2.32(5)	
IM6/F650	ENF	2-9-5	1.86(4)	2.06*	1.86(4)	2.06*
		2-9-6	1.93(4)		1.93(4)	

*Weighted average - Individual values are averages of different numbers of tests indicated in parentheses.

[illegible]

Figure 59. Critical Strain Energy Release Rates for CTD Conditions

Fracture Toughness Test Results
RTD Conditions

Material	Specimen Type	Specimen Number	G_C (a = 0.0 in.) Ind	G_C (a = 0.0 in.) Avg	G_C (a = 2.0 in.) Ind	G_C (a = 2.0 in.) Avg
		1-6-1	1.44		2.79	
IM6/3100	DCB	1-6-2	0.91	1.19	3.09	2.99
		1-6-3	1.23		3.08	
		1-7-1	1.58		3.00	
IM6/3100	CLS-63	1-7-2	1.48	1.46	2.10	2.43
		1-7-3	1.32		2.17	
		1-8-1	1.36		1.79	
IM6/3100	CLS-82	1-8-2	1.31	1.23	1.67	1.65
		1-8-3	1.02		1.47	
		1-9-1	3.53(2)		3.53(2)	
IM6/3100	ENF	1-9-2	3.25(5)	3.15*	3.25(5)	3.15*
		1-9-3	2.95(6)		2.95(6)	
		2-6-1	0.76		1.94	
IM6/F650	DCB	2-6-2	0.58	0.72	2.64	2.23
		2-6-3	0.82		2.12	
		2-7-1	0.80		1.63	
IM6/F650	CLS-63	2-7-2	1.39	0.88	2.12	1.50
		2-7-3	0.46		0.74	
		2-8-1	1.15		2.14	
IM6/F650	CLS-82	2-8-2	1.12	1.22	1.50	1.83
		2-8-3	1.39		1.84	
		2-9-1	2.10(4)		2.10(4)	
IM6/F650	ENF	2-9-2	2.09(6)	2.06*	2.09(6)	2.06*
		2-9-3	2.01(6)		2.01(6)	

*Weighted average - individual values are averages of different numbers of tests indicated in parentheses.

GP73-0343-46

Figure 60. Critical Strain Energy Release Rates for RTD Conditions

Fracture Toughness Test Results
ETW Conditions

Material	Specimen Type	Specimen Number	G_C (a = 0.0 in.) Ind	G_C (a = 0.0 in.) Avg	G_C (a = 2.0 in.) Ind	G_C (a = 2.0 in.) Avg
		1-6-7	2.66		2.49	
IM6/3100	DCB	1-6-8	1.78	2.07	2.81	2.87
		1-6-9	1.78		3.32	
		1-7-7	2.38		2.94	
IM6/3100	CLS-63	1-7-8	1.25	1.92	1.60	2.36
		1-7-9	2.13		2.54	
		1-8-7	1.45		1.81	
IM6/3100	CLS-82	1-8-8	1.89	1.60	2.13	1.90
		1-8-9	1.45		1.75	
		1-9-7	3.30(6)		3.30(6)	
IM6/3100	ENF	1-9-8	3.20(5)	3.19*	3.20(5)	3.19*
		1-9-9	3.06(6)		3.06(6)	
		2-6-7	0.69		1.14	
IM6/F650	DCB	2-6-8	0.35	0.56	1.53	1.26
		2-6-9	0.63		1.11	
		2-7-7	0.97		1.44	
IM6/F650	CLS-63	2-7-8	1.15	0.87	1.65	1.37
		2-7-9	0.48		1.01	
		2-8-7	0.78		1.41	
IM6/F650	CLS-82	2-8-8	0.78	0.74	1.51	1.33
		2-8-9	0.65		1.08	
		2-9-7	1.78(6)		1.78(6)	
IM6/F650	ENF	2-9-8	1.73(6)	1.75*	1.73(6)	1.75*
		2-9-9	1.74(5)		1.74(5)	

*Weighted average - individual values are averages of different numbers of tests indicated in parentheses.

GP73-0343-C0

Figure 61. Critical Strain Energy Release Rates for ETW Conditions

The average values tabulated in Figures 59 through 61 are plotted in Figures 62 through 64. Each figure shows a comparison of both IM6/3100 and IM6/F650 interaction envelopes at a single environment.

The test data indicates that the fracture toughness interaction boundaries are more accurately defined by a function that is linear on stress rather than linear on strain energy release rate. The stress based boundaries are defined as the sum of the square roots of Mode I and Mode II fractional components, set equal to unity (see Eq. (18)).

$$\sqrt{\frac{G_I}{G_{IC}}} + \sqrt{\frac{G_{II}}{G_{IIC}}} = 1 \qquad (18)$$

The test results show that Mode I fracture toughness of both material systems increases with crack length. As mentioned previously, this increase has been attributed to fiber bridging of the fracture surface. As the crack grows, more fracture surface develops and more fiber bridging occurs, raising the load and energy required to grow the crack further. In Figures 62 through 64 the interaction boundaries are shown for initial toughness values (crack length = 0.0 inch) and a subsequent toughness value (crack length = 2.0 inch). In all cases the Mode I components of toughness increase with crack length resulting in an expansion of the interaction boundary. Note that the pure Mode II results were independent of crack length.

Figure 62 shows the interaction boundaries for IM6/3100 and IM6/F650 at CTD conditions. The IM6/3100 is generally tougher than the IM6/F650. The Mode I toughness of IM6/3100 increased by a factor of 1.5 with 2 inches of crack growth and the IM6/F650 Mode I toughness increased by a factor of 2.

Figure 63 shows the interaction boundaries for IM6/3100 and IM6/F650 at RTD conditions. The IM6/3100 is again generally tougher than the IM6/F650. The Mode I toughness of IM6/3100 increased by a factor of 2.5 with 2 inches of crack growth and the IM6/F650 Mode I toughness increased by a factor of 3.

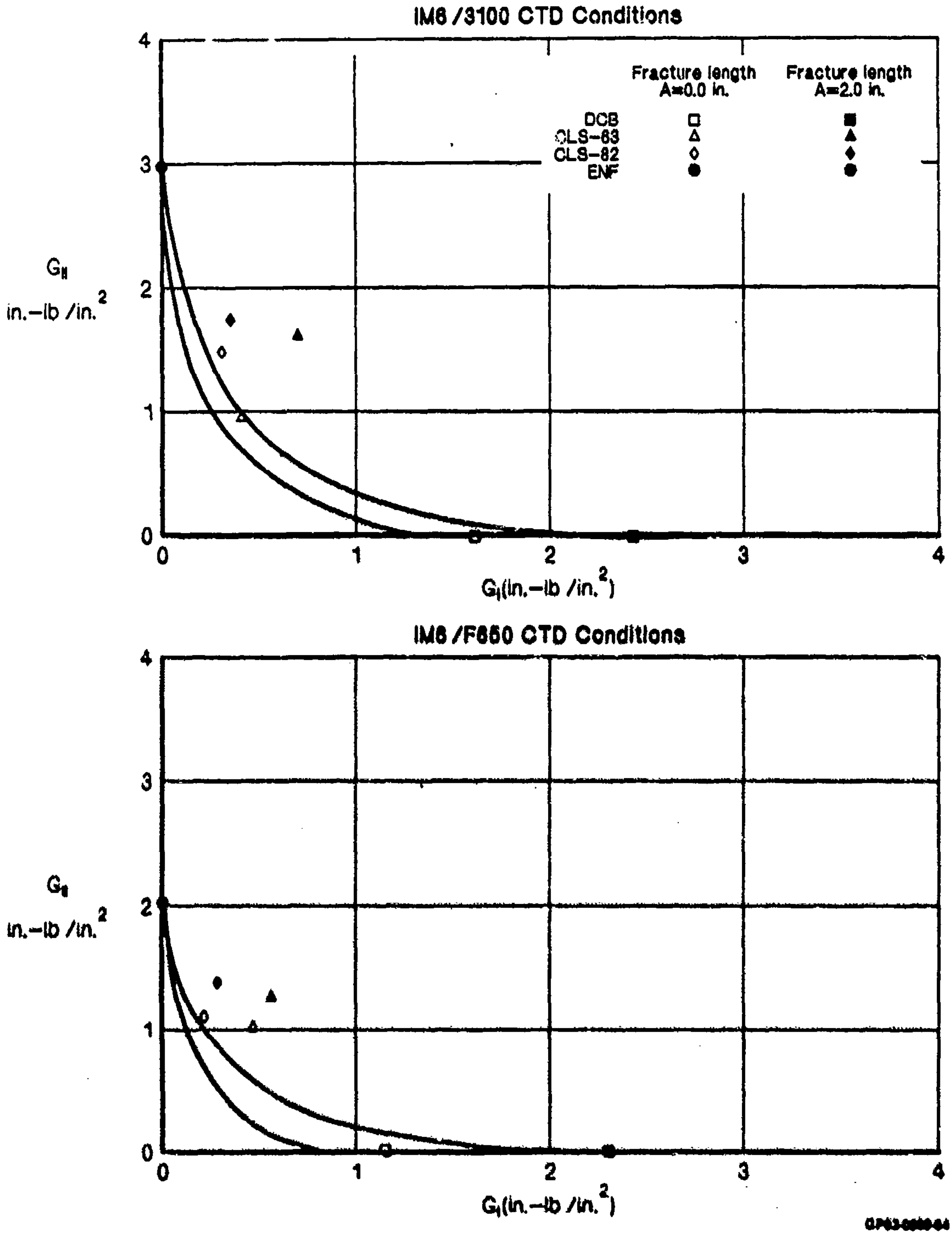

Figure 62. Fracture Toughness Interaction Envelopes for CTD Conditions

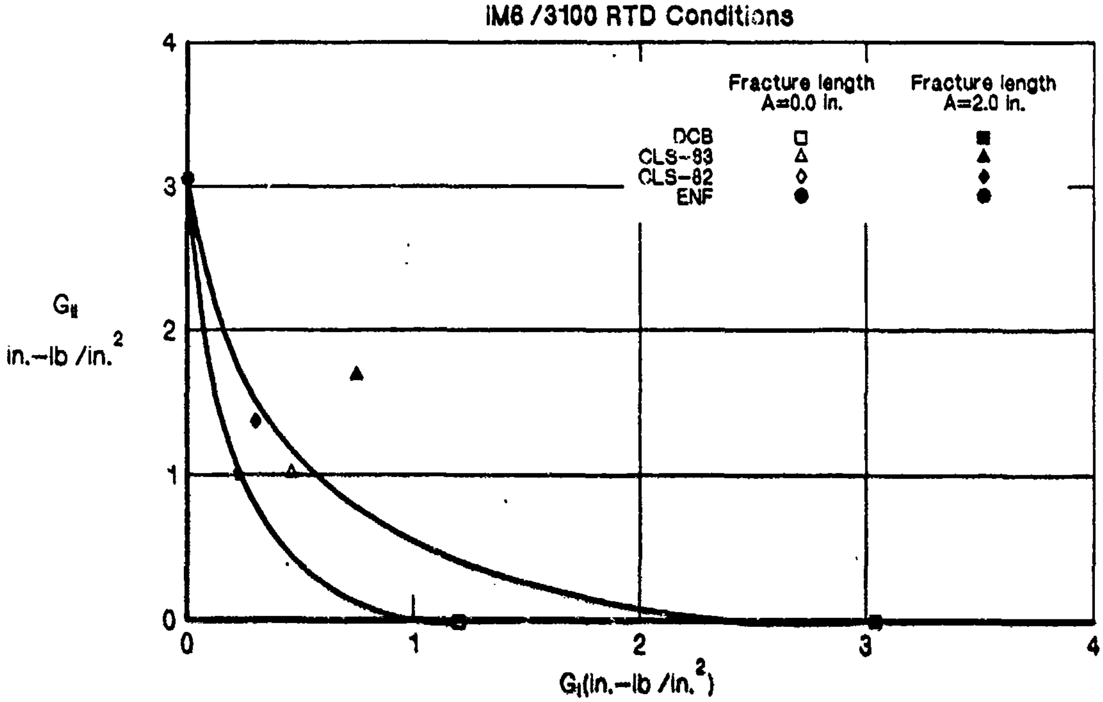

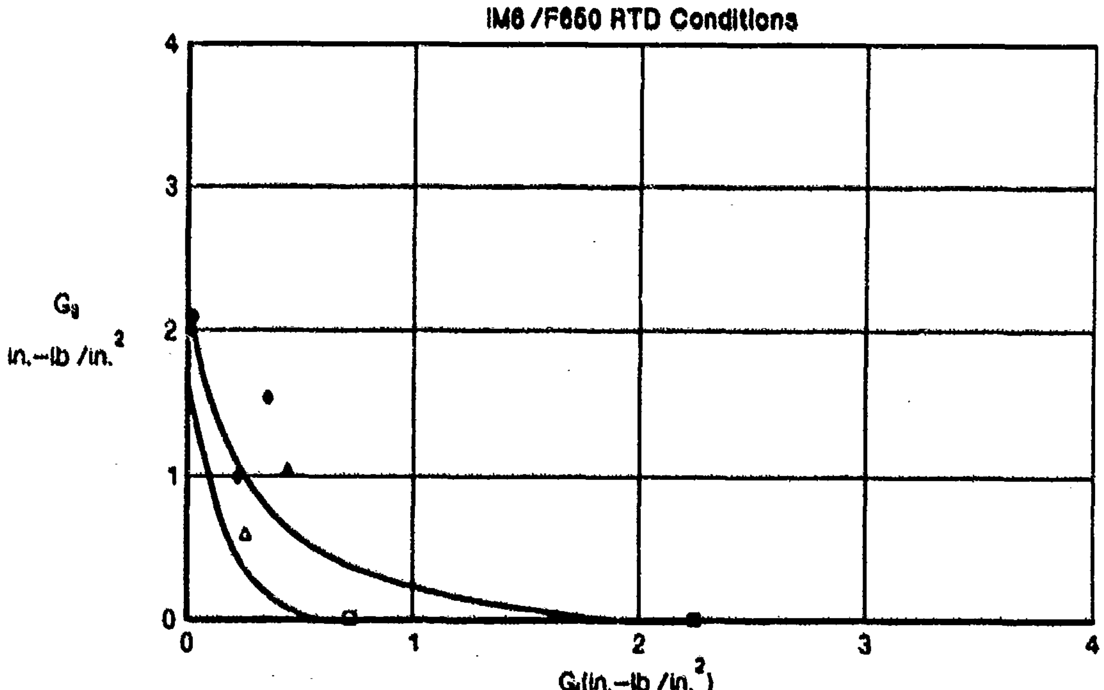

Figure 63. Fracture Toughness Interaction Envelopes for RTD Conditions

Figure 64 shows the interaction boundaries for IM6/3100 and IM6/F650 at ETW conditions. Again the IM6/3100 is generally tougher than the IM6/F650. The data indicates that the IM6/3100 at ETW conditions is just as tough as at RTD conditions and tougher than at CTD conditions. In contrast, the IM6/F650 at ETW conditions is less tough than at either CTD or RTD conditions.

Figure 65 shows a comparison of second generation BMI toughness and baseline material toughness. IM6/3100 is generally tougher than the baseline systems while IM6/F650 is generally not as tough.

3.2.6.7 <u>Fatigue Test Summary</u> - Crack growth characteristics were determined for both material systems at CTD, RTD and ETW conditions. Fatigue tests were performed with compliance measurements recorded between cycle blocks for each specimen. Tests were run under displacement control so that stable crack growth occurred. The minimum and maximum displacements were held constant during fatigue testing, resulting in a decrease in load (and energy) as the crack propagated in the specimen.

Fatigue data is presented as crack growth (da/dn vs. ΔG) plots. Change in crack length (da) was determined by evaluating the compliance of each specimen before and after each block of a specified number (dn) of fatigue cycles. Then compliances were translated into crack lengths through compliance vs. crack length relationships. In cases where it was possible to determine the compliance vs. crack length function for a specimen without affecting its fatigue response, compliance surveys were run on each specimen prior to testing. This was possible for ENF specimens under dry (CTD & RTD) conditions. In all other cases, the compliance vs. crack length functions were determined from static tests of other specimens, under the same environmental conditions. A summary of the compliance vs. crack length relationships is shown in Figure 66. The change in crack length divided by dn fatigue cycles in that block gives the crack growth rate, da/dn.

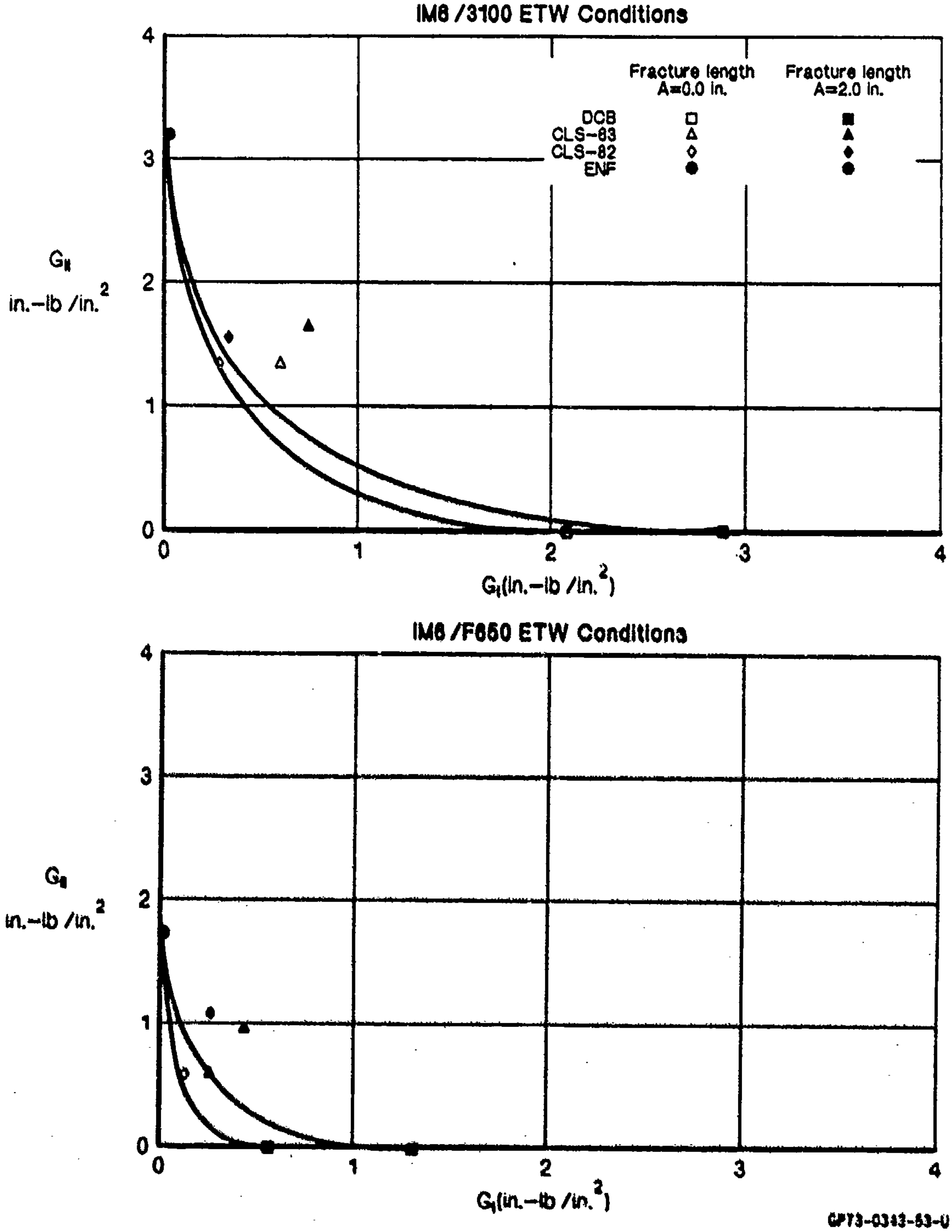

Figure 64. Fracture Toughness Interaction Envelopes for ETW Conditions

	AS1/3501-6	T300/V378A	IM6/3100	IM6/F650
Cold Temperature/Dry				
G_{IC}	0.70*	0.77*	1.61	1.14
G_{IIC}	3.17**	—	2.98	2.06
Room Temperature/Dry				
G_{IC}	0.75*	0.85*	1.19	0.72
G_{IIC}	2.58**	—	3.15	2.06

*Reference 6
**Reference 7

GP83-0089-65-T

Figure 65. Fracture Toughness Comparison: Baseline Material System vs Second Generation BMIs

		CTD		RTD		ETW	
		IM6/3100	IM6/F650	IM6/3100	IM6/F650	IM6/3100	IM6/F650
DCB $C = Aa^B$	A	4.46E-04	1.14E-03	4.35E-04	1.03E-03	1.67E-03	1.40E-03
	B	3.65	2.89	3.75	3.10	2.54	2.59
CLS-63 $C = C_0 + dc/da\ a$	C_0	1.02E-05	1.11E-05	1.03E-05	1.13E-05	1.12E-05	1.09E-05
	dc/da	1.23E-06	1.36E-06	1.12E-06	1.09E-06	9.80E-07	1.05E-06
CLS-82 $C = C_0 + dc/da\ a$	C_0	1.02E-05	8.33E-06	1.12E-05	7.05E-06	7.70E-06	9.91E-06
	dc/da	2.19E-06	2.50E-06	2.00E-06	2.91E-06	2.53E-06	2.02E-06
ENF $C = C_0 + Aa^B$	C_0	3.93E-04	3.63E-04	4.20E-04	4.29E-04	4.03E-04	3.72E-04
	A	6.83E-05	6.57E-05	7.03E-05	8.02E-05	7.47E-05	9.09E-05
	B	3.00	2.89	2.90	2.89	2.95	2.86

GP73-0343-66

Figure 66. Compliance vs Crack Length Parameters

The variation in strain energy release rate (ΔG) during cycling was calculated with the equation:

$$\Delta G = \frac{P_{mean}^2}{2W} * (1 - R^2) * \frac{\Delta C}{\Delta a} \tag{19}$$

where,

Pmean ≡ average of initial and final maximum cyclic loads for each block

W ≡ specimen width (1.0 inch)

R ≡ fatigue ratio (0.1)

ΔC ≡ difference in compliance before and after each block

Δa ≡ difference in crack lengths corresponding to compliances that determine ΔC

Each block of fatigue cycling then produced a da/dn and ΔG data pair. The data for each specimen was then plotted on log-log scales to determine a crack growth curve in the form,

$$da/dn = D * (\Delta G)^K \tag{20}$$

for each specimen. A summary of the D and K parameters for each test condition is shown in Figure 67. Each test condition included a replication of three specimens. The values of D and K (shown in Figure 67) are averages of the three replications and were used to plot a crack growth curve through all the data generated by the three specimens at each condition. The plots for each of 24 test conditions (i. e. combinations of 2 materials * 4 specimen types * 3 environments) are shown in the Appendix volume of this report.

Crack Growth Data
$da/dn = D\,(\Delta G)^K$

	CTD		RTD		ETW	
	D	K	D	K	D	K
DCB	4.175E-09	19.50	2.014E-08	19.00	2.919E-03	3.37
CLS-63	1.780E-06	15.10	2.403E-05	8.27	5.845E-04	5.92
CLS-82	2.346E-04	7.37	2.535E-04	9.69	5.653E-04	6.88
ENF	1.679E-09	15.00	1.682E-07	9.53	1.124E-05	6.47
			IM6/3100			
	CTD		RTD		ETW	
	D	K	D	K	D	K
DCB	7.078E-07	14.30	8.253E-07	16.40	7.876E-02	5.32
CLS-63	9.078E-05	15.80	2.147E-04	10.60	2.703E-03	8.65
CLS-82	6.558E-04	12.40	2.134E-04	8.86	2.917E-02	10.10
ENF	1.590E-06	12.20	1.957E-06	16.50	—	—(1)
			IM6/F650			

Note: (1) Critical value of $\Delta G = 1.47$ in.-lb/in.^{2}
No growth for $\Delta G < 1.47$, unstable growth at $\Delta G = 1.47$.

GP83-0008-47-T

Figure 67. Crack Growth Parameters

Interpretation of the crack growth curves involves observation of two characteristics of each curve. The first is the location of the lower end (i.e. low crack growth rates) of each curve. Threshold strain energy release rate increases as the lower end of the curve moves to the right, to higher energy conditions. Systems with higher thresholds resist crack growth until relatively high strain energy release rates are developed. Another way of identifying the relative locations of the lower end of various curves is to observe the intercept value of each curve. The intercept value (the D parameter in Equation (26)) defines the crack growth rate of each condition for a ΔG value equal to 1. Tougher systems will have lower intercept crack growth rate values.

The second characteristic to be observed is the slope of the curve (the K parameter in Equation (20)). As the slope of the curve decreases, the ductility increases. A relatively shallow slope indicates a gradual increase in crack growth rate with an increase in strain energy release rate. In contrast, a steep slope represents a more rapid increase in crack growth rate as strain energy release rate increases. In the limiting case of a vertical da/dn vs. ΔG curve, the system would exhibit no crack growth until the critical energy level was established. At that level, failure would occur instantaneously without warning, in terms of crack initiation and growth.

Figure 67 shows the crack growth parameters for both systems. IM6/3100 was generally tougher than IM6/F650. The superior toughness of IM6/3100 was previously shown in static fracture toughness test results.

Under RTD and CTD conditions, mixed mode crack growth rate intercept values are two to three orders of magnitude higher than Mode I or Mode II intercepts as evidenced by the values reported in Figure 67. Of the two mixed mode configurations tested, the mixture exhibiting the greater Mode II component (CLS-82) generally exhibited the higher crack growth rate intercept value. The critical mode of crack growth, for RTD and CTD conditions, was the mixed mode with 83 percent Mode II, behavior as compared to the mixed mode with 70 percent Mode II behavior.

In contrast, under ETW conditions, Mode I crack growth appears to be the critical mode for IM6/3100. Whereas the mixed mode intercept values were greatest under CTD and RTD conditions, the Mode I intercept was greatest under ETW conditions. IM6/F650 showed significant degradation for all configurations tested at ETW conditions.

Another interesting result of ETW crack growth testing is the behavior of IM6/F650 during Mode II testing. During these tests it was found that the da/dn vs. ΔG curve was vertical. Under ETW conditions the F650 resin was weakened resulting in unstable crack growth at the critical ΔG level. The critical value of ΔG (1.47 in-lbs/in^2) was included as a note in Figure 67.

3.2.6.8 Fractographic Investigation - The fracture surfaces of static and fatigue fracture toughness specimens were investigated to determine environmental and fracture mode effects on the failure process. Results from the investigation have been compared with results from similar investigations of the baseline materials (AS1/3501-6 and T300/V378A). The baseline materials were investigated by Law and Wilkins (Reference 5). These observations might be used to qualitatively evaluate the type of fracture that occurred in a failed structure.

As temperature and moisture content increased, the matrix material weakened. The weakened material provided less fiber support, allowing fibers to be pulled out of the surface and broken. In addition, the weakened matrix exhibited more ductility, resulting in a rougher fracture surface than in the case of colder, drier conditions. Both broken fibers and roughness due to ductility cause the surfaces to be more dull. This effect is shown in Figure 68 where the dullness of the Mode I static specimen surfaces increases as conditions vary from CTD to ETW. Figure 68 also shows that under all three environmental conditions the IM6/F650 specimens experienced more fiber pullout than the IM6/3100 specimens, and therefore are more dull. This variation in surface appearance with environment has also been documented for AS1/3501-6 and T300/V378A (Reference 5).

The effects of crack growth rate have also been recorded. Figure 69 shows mixed mode (CLS-63) RTD fracture surfaces for both systems at two crack growth rates. For IM6/3100, increasing the crack growth rate decreases the density of surface features. In contrast, for IM6/F650 the crack growth rate does not appear to affect the density of surface features.

The fracture mode effects can be seen in Figures 70 and 71. In Figure 70 the variation in the IM6/3100 fracture surface is shown as the proportion of Mode II fracture increases. The DCB specimen exhibits broken fibers that are expected from pullout during out-of-plane loading. The surface of the CLS-63 specimen (70 percent Mode II) shows hackles and ridges formed by resolved tension stresses in shear strain fields created in mixed mode and Mode II specimens (Reference 5). The surface of the CLS-82 specimen (83 percent Mode II) and the ENF specimen (100 percent Mode II) also show ridges and hackles, but not to the extent shown in the CLS-63 surface.

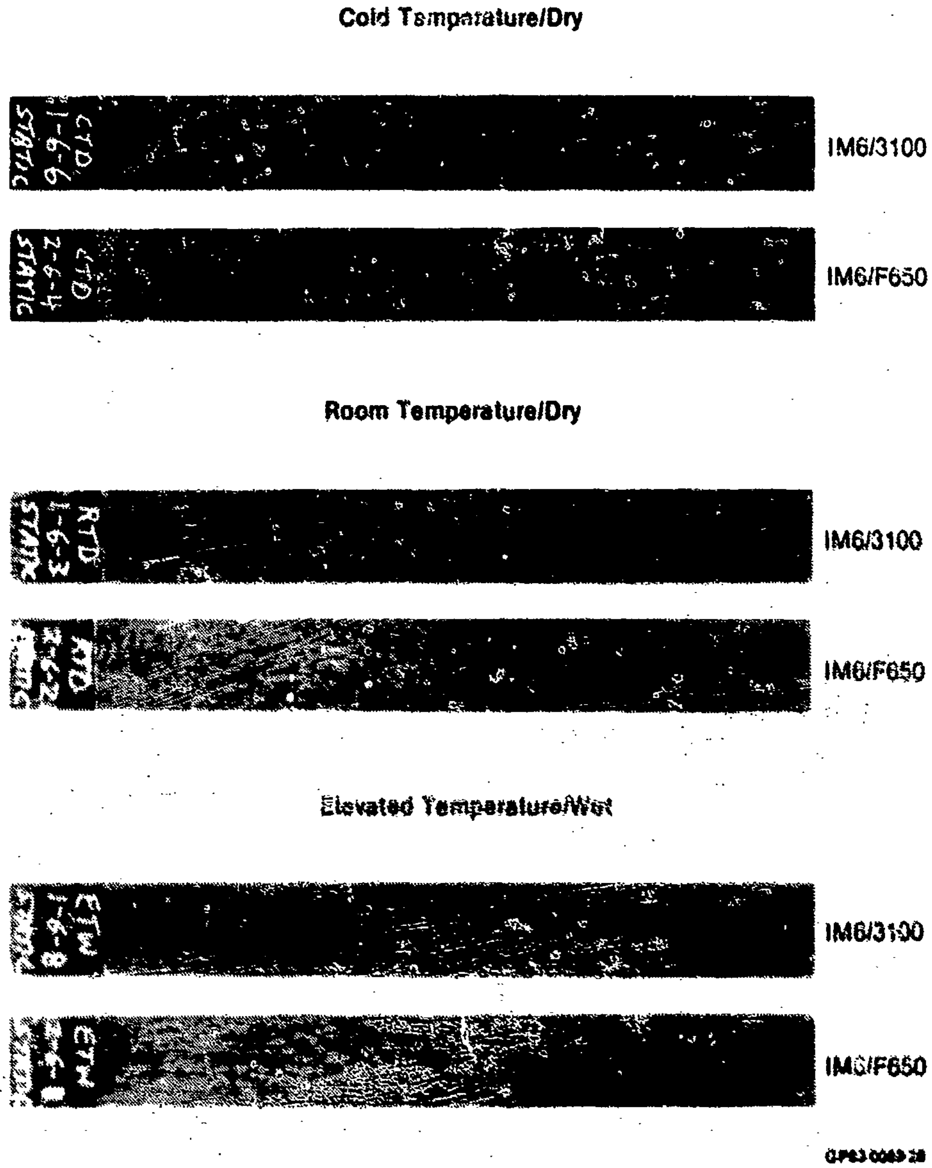

Figure 68. Mode I Static Fracture Surfaces for Three Environments

da/dn = 10^{-5} in/cycle
(CLS - 63, RTD)

IM6/3100

da/dn = 10^{-3} in/cycle
(CLS - 63, RTD)

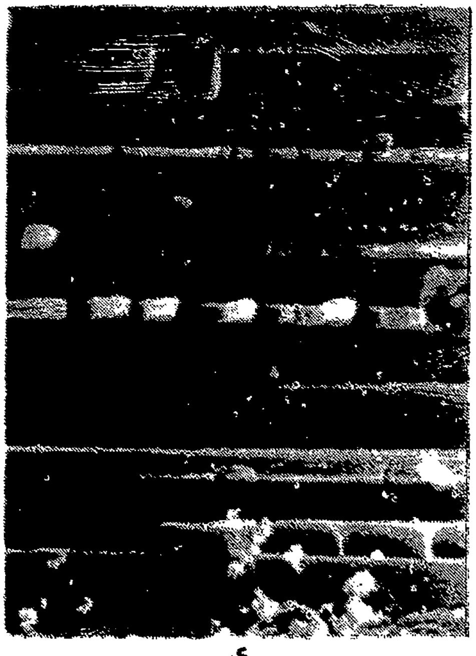

da/dn = 10^{-5} in/cycle
(CLS - 63, RTD)

IM6/F650

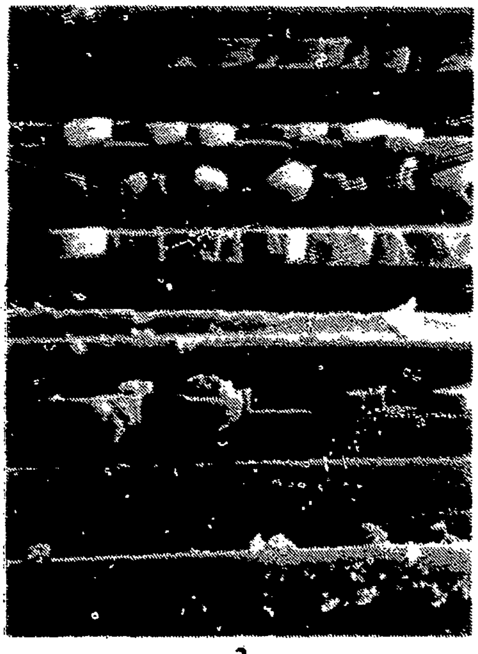

da/dn = 10^{-3} in/cycle
(CLS - 63, RTD)

G/P83-0086-23

Figure 69. Effects of Crack Growth Rate on Surface Appearance

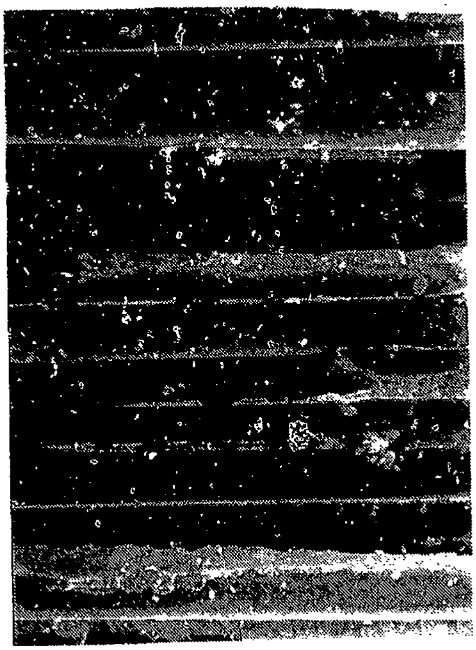

DCB
(RTD, Fatigue)

CLS-63
(RTD, Fatigue)

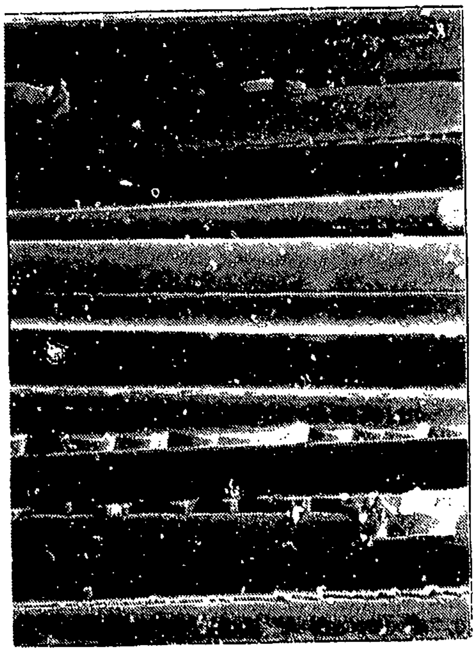

CLS-82
(RTD, Fatigue)

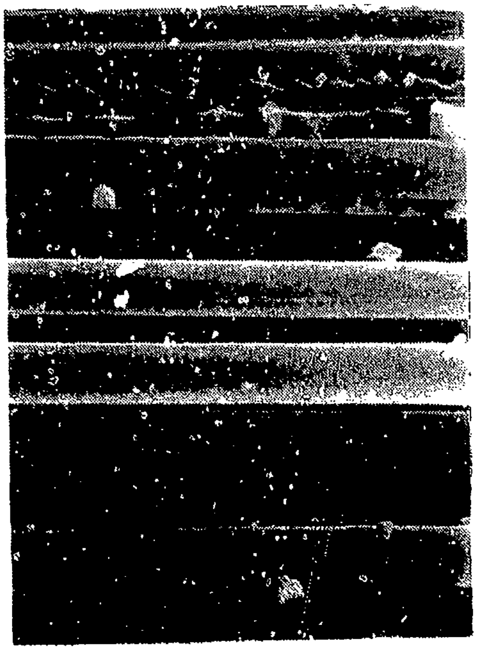

ENF
(RTD, Fatigue)

GP83-0089-34

Figure 70. Variation In IM6/3100 Fracture Surface Due to Variation In Fracture Mode

In Figure 71 the variation in the IM6/F650 fracture surface is shown. In contrast to IM6/3100, which showed the most roughness in the CLS-63 configuration, IM6/F650 surfaces gradually increase in roughness as the proportion of Mode II fracture increases. Beginning with the DCB configuration, missing fibers due to fiber pullout are apparent. Progressing to the CLS-63 surface, hackles and ridges are exhibited. Finally the CLS-82 and ENF surfaces exhibit the most roughness.

The susceptibility to fiber/resin interfacial failure is seen in Figure 72. The fractographs are from CLS-82 specimens, which produce only 17 percent Mode I behavior. Even this relatively small amount of pullout behavior causes clean fiber/resin separation in IM6/F650 when conditions are changed from RTD to ETW. In contrast, the IM6/3100 did not show this tendency as obviously as did IM6/F650.

DCB
(RTD, Fatigue)

CLS-63
(RTD, Fatigue)

CLS-82
(RTD, Fatigue)

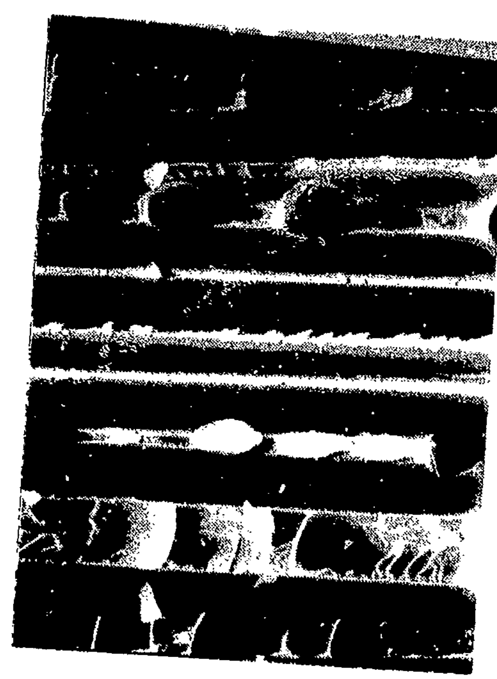

ENF
(RTD, Fatigue)

GP83-0089-35

Figure 71. Variation In IM6/F650 Fracture Surface Due to Variation In Fracture Mode

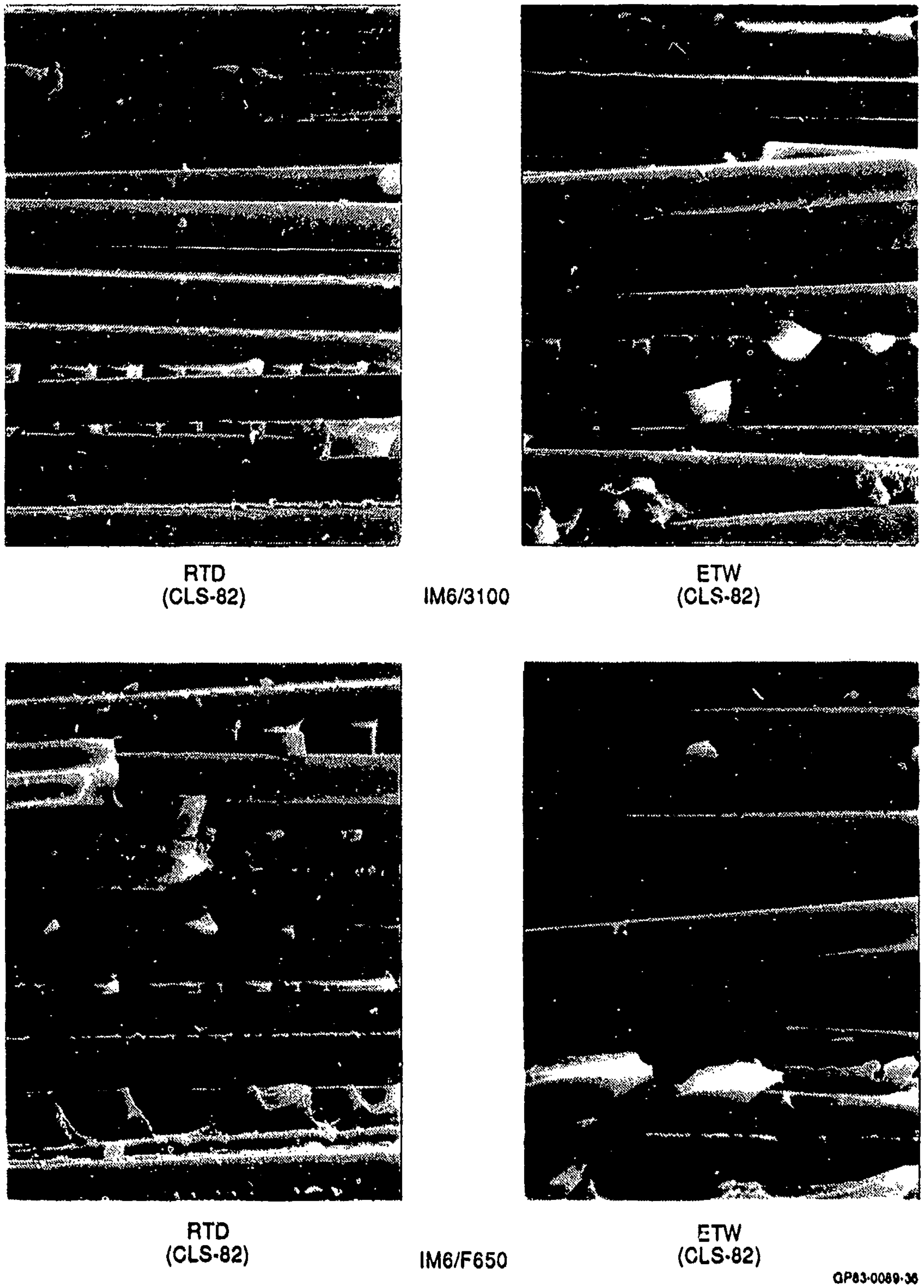

Figure 72. ETW Conditions Produce Cleaner Fiber Pullout In IM6/F650 Than In IM6/3100

SECTION 4.

TASK III: LAMINATE STRUCTURAL CHARACTERIZATION

4.1 Summary and Conclusions - IM6/3100 and IM6/F650 were tested to determine unnotched laminate strengths, notched strengths and fatigue lives, loaded hole (bearing) strengths and fatigue lives, and low-velocity impact damage tolerance. Low-velocity impact tests were performed to evaluate the non-visible damage threshold, thin laminate damage behavior, and visible damage energy levels of both systems.

Unnotched laminate tests showed that IM6/3100 had the greatest properties under CTD conditions. IM6/F650, on the other hand, showed the greatest properties under RTD conditions. Classical lamination theory accurately predicted laminate moduli. Laminate strength predictions for 50/40/10 layups were made using Tsai-Hill and maximum stress failure criteria. Tsai-Hill predictions were generally conservative while maximum stress predictions were generally unconservative. Strength predictions of 10/80/10 laminates were generally conservative. This was attributed to the conservative shear strength values determined in Task II lamina property tests.

Unloaded hole static strength tests showed that the notched tensile strength degradation (from unnotched strengths) of IM6/3100 was approximately 40 percent and that of IM6/F650 was approximately 30 percent. The notched compression strengths of both materials showed 30 percent to 40 percent degradation at CTD and RTD conditions. Under ETW conditions, the notched compression strengths of both systems were less than half the unnotched compression strengths.

Unloaded hole fatigue testing showed that for IM6/3100 compression-only (R = 10) cycling produced longer fatigue lives than reversed (R = -1) cycling. It was hypothesized that IM6/3100 fatigue behavior is controlled by matrix cracking. IM6/F650 showed no R ratio effect. It was hypothesized that IM6/F650 fatigue behavior is controlled by delamination growth. ETW fatigue test results indicated that the specimens dried due to the relatively

high diffusivity of BMIs (compared to epoxies). The data showed large scatter because as specimens dried, they were strengthened and lasted longer, increasing the opportunity for further drying and even further life extension.

Loaded hole static (bearing) strength test results showed that the bearing strength of both systems gradually decreased with increasing temperature and moisture content. The ETW bearing strength of IM6/3100 was 62 percent of its CTD strength. The ETW bearing strength of IM6/F650 was 49 percent of its CTD strength.

Loaded hole fatigue testing was performed to determine the fatigue life to 0.02 inch hole elongation. The systems were compared on the basis of the stress level corresponding to a fatigue life of 10,000 cycles. Under ETW conditions, IM6/3100 must be cycled at 79 percent (55 ksi vs 70 ksi) of the stress level required for a 10,000 cycle life at RTD conditions. The corresponding value for IM6/F650 was 75 percent (45 ksi vs 60 ksi).

Low-velocity impact tests determined that the maximum non-visible damage energy threshold of IM6/F650 was consistently lower than that of IM6/3100. The residual compression strength of IM6/F650 in the non-visible damage condition was also consistently lower than that of IM6/3100.

Visible impact damage tests showed that the impact energy/dent depth relationships of IM6/3100 and IM6/F650 were similar. Residual compression strength data showed that after visible damage was produced, IM6/3100 was stronger than IM6/F650.

Thin laminate impact damage testing also showed that the residual compression strength of IM6/3100 was greater than that of IM6/F650.

4.2 Testing and Evaluation - The objective of the test program was to characterize the laminate structural performance of IM6/3100 and IM6/F650.

4.2.1 Overview - In this program, 318 static tests and 186 fatigue tests were performed under cold temperature dry (CTD), room temperature dry

(RTD), and elevated temperature wet (ETW) conditions. The tests were conducted to determine:

- unnotched laminate strength
- unloaded hole static strength
- unloaded hole fatigue life
- loaded hole static strength
- loaded hole fatigue life
- threshold energy for non-visible impact damage
- thin laminate impact response
- energy level for visible (0.1 inch dent) impact damage
- residual compression strength after impact

as summarized in Figure 73.

Test Types	Number of Tests
Unnotched	48
Unloaded Hole (Static)	36
Unloaded Hole (Fatigue)	130
Loaded Hole (Static)	18
Loaded Hole (Fatigue)	56
Non-Visible Impact Damage Threshold	72
Thin Laminate Impact Damage	72
Visible Impact Damage	72
Total	504

GP73-0833-44

Figure 73. Task III Test Matrix

Both fiber and matrix dominated layups were used in Task III testing. Laminate stacking sequences were:

$$50/40/10 \quad [+45/0/-45/0/90/0/+45/0/-45/0]_{ns}$$
$$10/80/10 \quad [+45/-45/+45/-45/90/+45/-45/0/+45/-45]_{ns}$$

where the integer n takes the values of 1, 2, or 4 depending on the thickness of the laminate.

For thin laminate impact tests the stacking sequences were:

0/100/0 $[+45/-45]_{ns}$
50/0/50 $[0/90]_{ns}$

where the integer n takes the value of 1, 2, or 3 depending on the thickness of the laminate.

The following sections describe test results and correlation of analytical predictions with test results.

4.2.2 Unnotched Laminate Static Testing - Unnotched laminate mechanical property tests were performed to determine the undamaged strength and stiffness of fiber dominated and matrix dominated BMI laminates. Tension and compression tests were performed in CTD, RTD, and ETW environments as shown in the test matrix in Figure 74. The cold temperature for CTD testing was -65°F. For IM6/3100 the ETW conditions were 360°F and 0.71 percent (by weight) moisture content. For IM6/F650 the ETW conditions were 410°F and 0.71 percent moisture content.

Specimen Type	Layup	Loading	Environment			Number of Tests Per Material
		Static (1)	CTD	RTD	ETW	
Unnotched	50/40/10	T	✓			3
		T		✓		3
		T			✓	3
		C	✓			3
		C		✓		3
		C			✓	3
	10/80/10	C		✓		3
		C			✓	3

Notes.
(1) T - Tension
C - Compression

GP73-0623-69-R

Figure 74. Unnotched Laminate Static Test Matrix

4.2.2.1 Test Results - The test specimen configurations are shown in Figure 75. Figure 76 shows a typical failed tension specimen. A failed compression specimen is shown in Figure 77. The data for unnotched laminate tension and compression tests are tabulated in Figures 78 and 79 respectively.

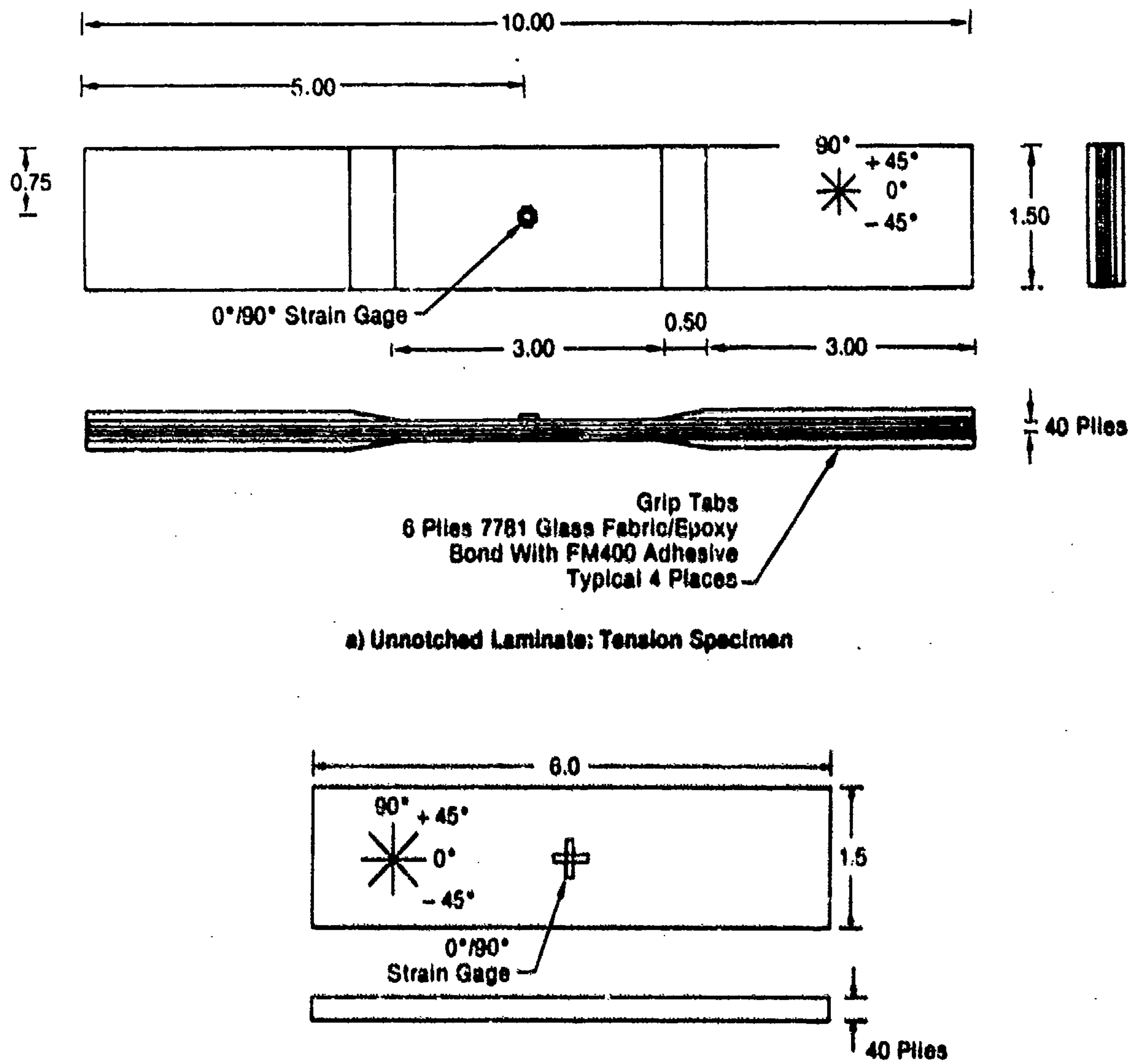

a) Unnotched Laminate: Tension Specimen

b) Unnotched Laminate: Compression Specimen

Note: All dimensions are in inches.

Figure 75. Unnotched Static Test Specimens

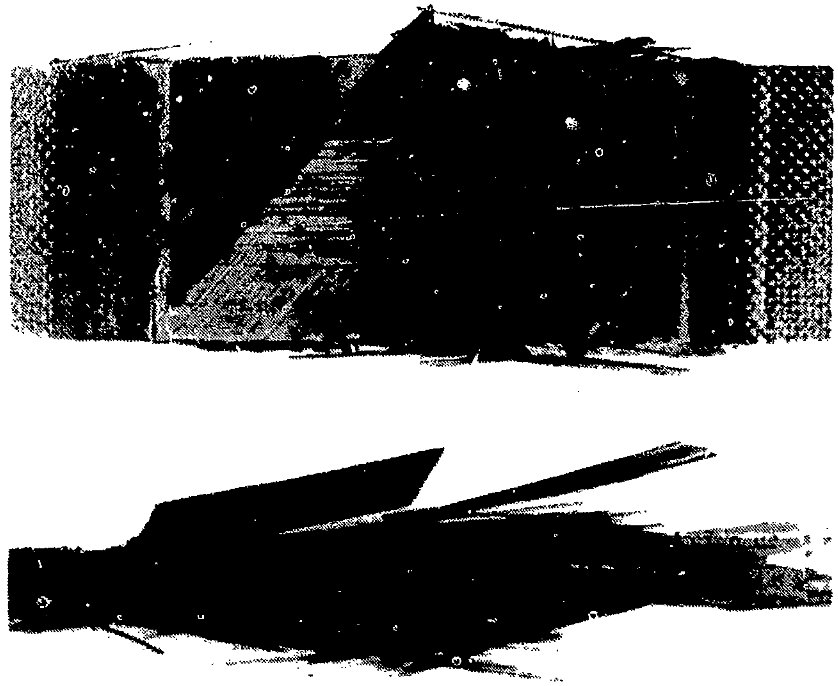

GP83-0039-14

Figure 76. Failed Unnotched Tension Specimen

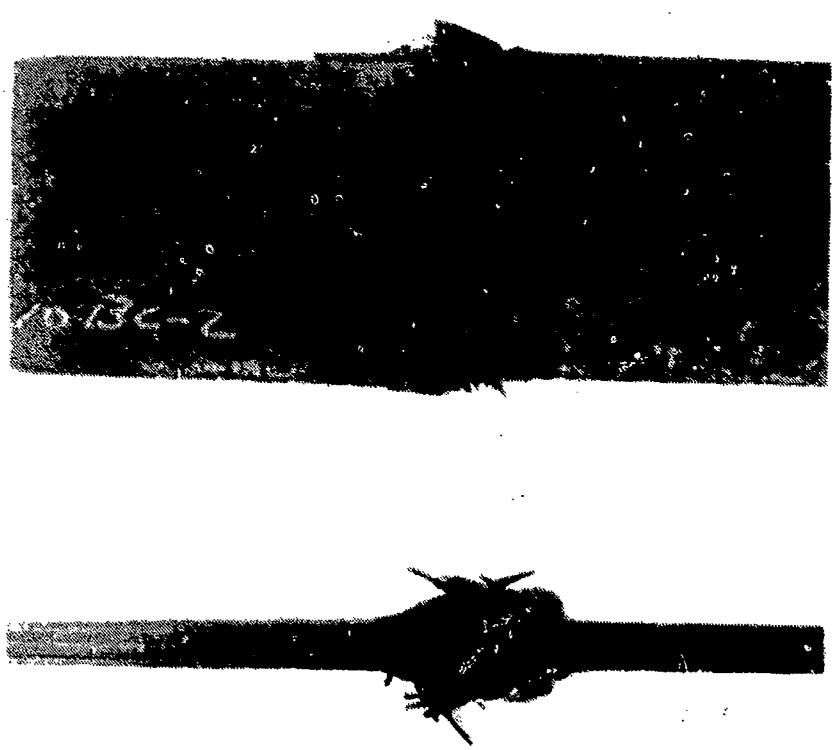

GP83-0039-15

Figure 77. Failed Unnotched Compression Specimen

Material System	Layup	Specimen Number	Thickness (in.)	Width (in.)	Failure Load (lb)	Failure Stress (ksi)		Failure Strain (μin./in.)		Modulus (msi)		Poisson's Ratio
						Ind	Average	Ind	Average	Ind	Average	
Cold Temperature Dry												
		1-10A-4	0.2216	1.510	61,400	195.5		14,640		13.31		0.379
IM6/3100	50/40/10	1-10A-5	0.2224	1.509	65,000	207.1	207.8	14,520	15,000	13.57	13.55	0.383
		1-10A-6	0.2247	1.509	69,300	220.8		15,840		13.77		0.423
		2-10A-4	0.2198	1.510	59,000	187.9		13,200		13.66		0.389
IM6/F650	50/40/10	2-10A-5	0.2186	1.510	56,900	181.2	184.0	13,500	13,600	13.08	13.34	0.399
		2-10A-6	0.2179	1.509	57,400	182.9		14,100		13.28		0.400
Room Temperature Dry												
		1-10A-1	0.2239	1.509	60,500	192.8		13,920		13.36		0.406
IM6/3100	50/40/10	1-10A-2	0.2252	1.510	64,000	203.8	201.0	14,300	14,270	13.74	13.73	0.440
		1-10A-3	0.2244	1.508	64,700	206.3		14,580		14.05		0.416
		2-10A-1	0.2169	1.509	57,700	183.8		13,500		13.57		0.409
IM6/F650	50/40/10	2-10A-2	0.2188	1.509	59,400	189.2	192.2	12,240	13,220	13.75	13.83	0.403
		2-10A-3	0.2194	1.509	63,900	203.6		13,920		14.16		0.418
Elevated Temperature Wet												
		1-10A-7	0.2257	1.510	—	—		—		13.84		0.501
IM6/3100	50/40/10	1-10A-8	0.2233	1.509	53,800	171.4	176.6	14,310	13,790	12.62	13.04	0.488
		1-10A-9	0.2235	1.510	57,100	181.8		13,260		12.67		0.500
		2-10A-7	0.2177	1.508	57,400	183.0		13,920		12.50		0.463
IM6/F650	50/40/10	2-10A-8	0.2189	1.508	60,400	192.6	190.1	14,220	14,080	13.39	13.04	0.455
		2-10A-9	0.2163	1.509	61,100	194.7		14,100		13.22		0.481

GP73-0523-40

Figure 78. Unnotched Laminate Tension Strength Data

Material System	Layup	Specimen Number	Thickness (in.)	Width (in.)	Failure Load (lb)	Failure Stress (ksi) Ind	Failure Stress (ksi) Average	Failure Strain (μin./in.) Ind	Failure Strain (μin./in.) Average	Modulus (msi) Ind	Modulus (msi) Average	Poisson's Ratio
Cold Temperature Dry												
		1-108-4	0.2268	1.506	43,050	137.4		12,300		13.03		—
IM6/3100	50/40/10	1-108-5	0.2261	1.505	48,320	154.4	143.7	13,900	12,700	13.42	13.29	—
		1-108-6	0.2274	1.500	43,490	139.4		11,900		13.41		—
		2-108-4	0.2213	1.524	30,830	97.3		9,850		12.88		0.273
IM6/F650	50/40/10	2-108-5	0.2209	1.526	31,040	97.8	111.1	8,250	10,330	13.35	13.12	0.258
		2-108-6	0.2205	1.512	43,480	138.3		12,900		13.14		0.293
Room Temperature Dry												
		1-108-1	0.2266	1.507	35,570	113.5		10,020		12.27		0.394
IM6/3100	50/40/10	1-108-2	0.2278	1.508	41,830	133.4	123.4	11,400	10,770	12.33	12.40	0.360
		1-108-3	0.2285	1.507	38,640	123.3		10,900		12.61		0.365
		1-11-1	0.2242	1.480	21,410	69.5		15,720		5.27		0.552
IM6/3100	10/80/10	1-11-2	0.2253	1.471	21,380	69.9	70.3	15,690	16,010	5.33	5.27	0.538
		1-11-3	0.2241	1.491	22,[illegible]	71.6		16,420		5.21		0.521
		2-108-1	0.2206	1.506	43,380	138.5		13,580		12.13		0.340
IM6/F650	50/40/10	2-108-2	0.2210	1.503	42,180	134.9	137.1	12,950	13,110	12.42	12.39	0.354
		2-108-3	0.2221	1.305	43,160	137.9		12,810		12.61		0.398
		2-11-1	0.2149	1.504	18,660	59.6		13,440		5.17		0.522
IM6/F650	10/80/10	2-11-2	0.2153	1.503	19,870	63.6	61.1	14,630	13,880	5.16	5.16	0.499
		2-11-3	0.2157	1.506	18,780	60.0		13,580		5.16		0.498
Elevated Temperature Wet												
		1-108-7	0.2268	1.496	30,780	98.9		—		13.39		0.417
IM6/3100	50/40/10	1-108-8	0.2258	1.506	36,800	117.5	107.3	10,400	9,660	13.39	13.31	0.448
		1-108-9	0.2253	1.504	33,010	105.5		8,910		13.15		0.417
		1-11-4	0.2231	1.497	15,050	48.3		12,015		4.91		0.530
IM6/3100	10/80/10	1-11-5	0.2237	1.497	21,090	67.7	54.2	14,085	12,950	5.21	5.16	0.508
		1-11-6	0.2245	1.500	14,570	46.7		12,760		5.36		0.559
		2-108-7	0.2215	1.510	—	—		—		—		—
IM6/F650	50/40/10	2-108-8	0.2210	1.509	31,590	100.6	103.6	8,640	8,820	13.11	13.10	0.386
		2-108-9	0.2208	1.506	33,390	106.6		9,000		13.08		0.394
		2-11-4	0.2156	1.506	14,880	47.5		11,200		4.84		0.532
IM6/F650	10/80/10	2-11-5	0.2152	1.504	14,860	47.5	45.9	—	11,400	4.87	4.88	0.522
		2-11-6	0.2160	1.504	13,320	42.6		11,610		4.94		0.536

GP73-0623-47

Figure 79. Unnotched Laminate Compression Strength Data

The tension strengths of 50/40/10 laminates are summarized in Figure 80. The strength of IM6/3100 gradually decreased with increasing temperature and moisture content. The ETW strength was 85 percent of the CTD strength.

Figure 80 also shows that the tension strength of IM6/F650 50/40/10 laminates is not as significantly affected by environment as the strength of IM6/3100. The range of IM6/F650 tensile strengths was only 4 percent compared to 15 percent for IM6/3100.

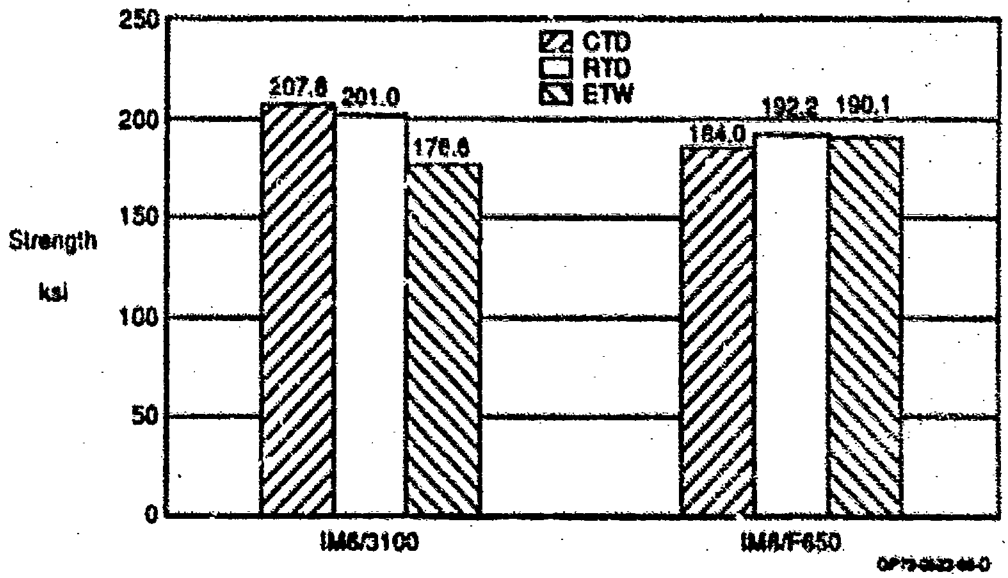

Figure 80. Unnotched 50/40/10 Laminate Tension Strength Test Results

The compression strengths of 50/40/10 laminates are summarized in Figure 81. Again, increasing temperature and moisture content resulted in gradual degradation of IM6/3100 strength. The ETW strength was 75 percent of the CTD strength.

In contrast to IM6/3100, the greatest IM6/F650 compression strength occurred under RTD conditions. The ETW strength was 76 percent of the RTD strength.

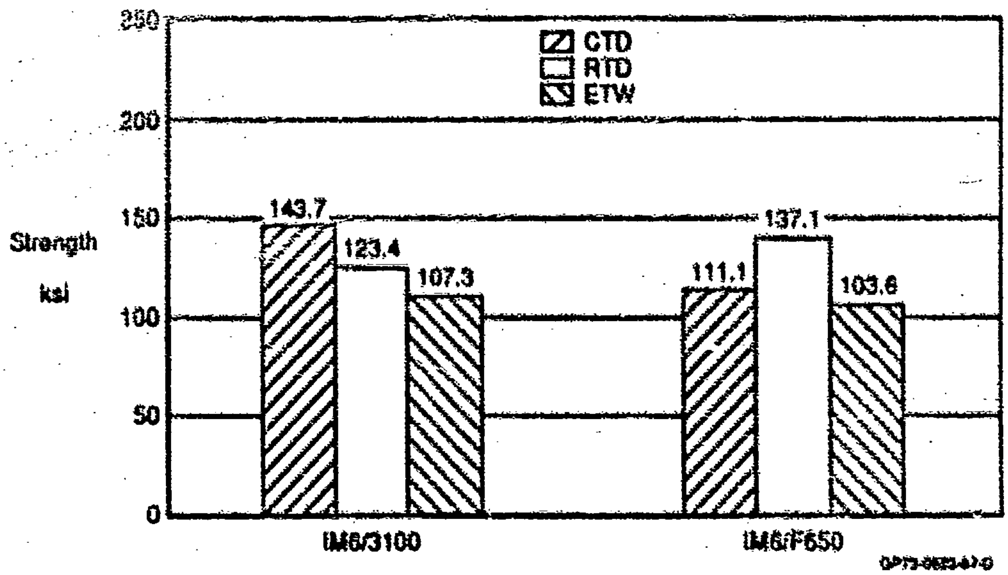

Figure 81. Unnotched 50/40/10 Laminate Compression Strength Test Results

Figure 82 summarizes the compression strengths of 10/80/10 laminates. The ETW compression strength of IM6/3100 was 77 percent of the RTD compression strength. For IM6/F650 the ETW strength was 75 percent of the RTD strength. These strengths were used as baseline values for comparisons with residual compression strengths after low-velocity impact.

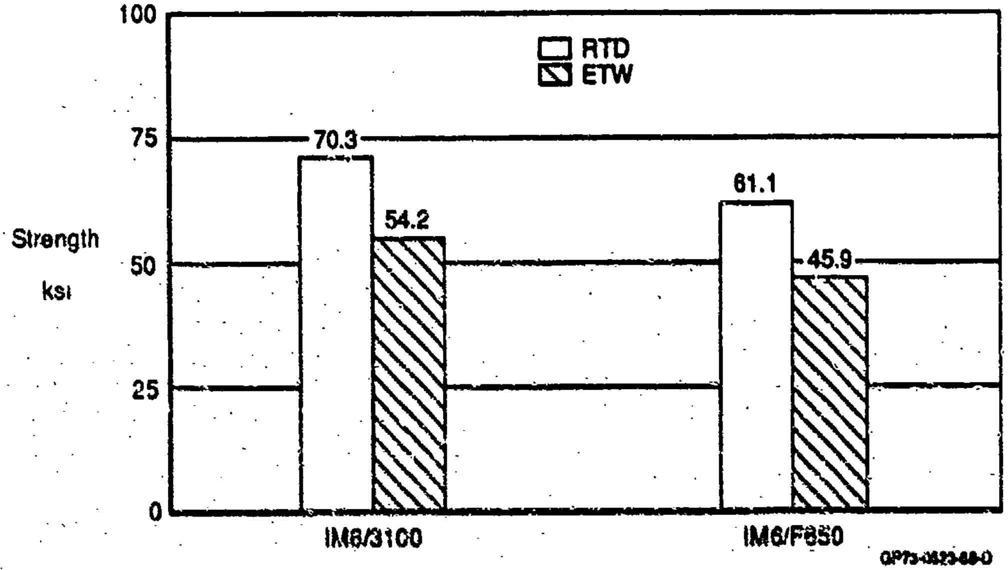

Figure 82. Unnotched 10/80/10 Laminate Compression Strength Test Results

4.2.2.2 Analysis - Classical lamination theory was used to predict the moduli of 50/40/10 and 10/80/10 laminates. Figures 83 through 85 show the correlation of predicted moduli with test data. Predicted values are generally within 6 percent of the test values.

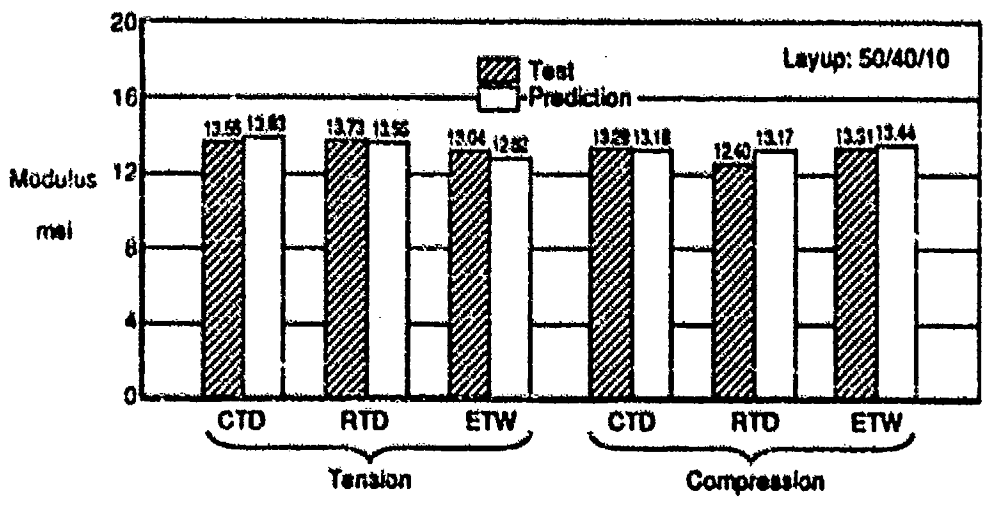

Figure 83. IM6/3100 Laminate Moduli

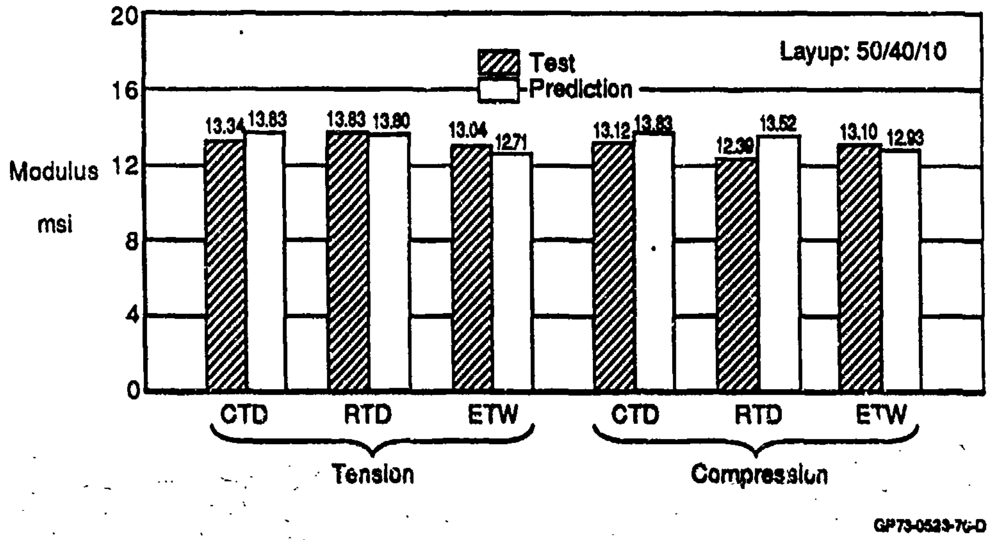

Figure 84. IM6/F650 Laminate Moduli

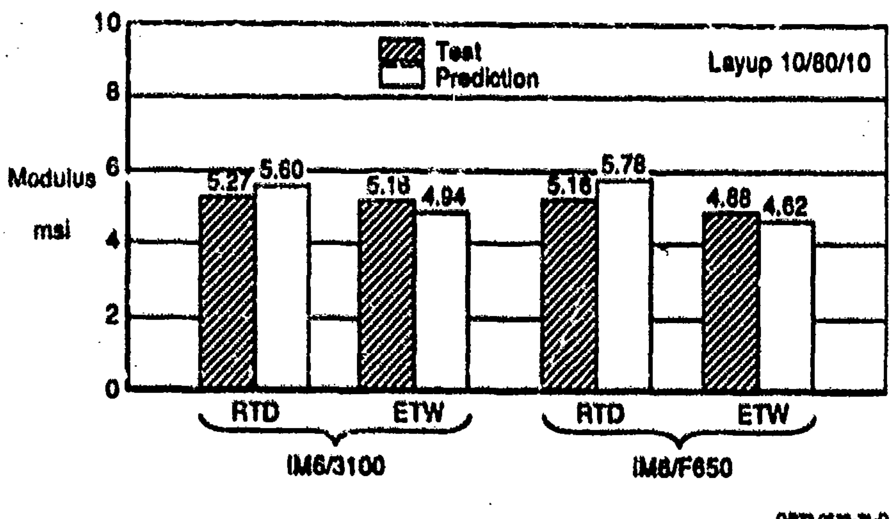

Figure 85. Laminate Compression Moduli

Unnotched laminate stresses were also computed with classical lamination theory. Laminate failure was predicted by comparing elastic stresses with material failure criteria on a ply-by-ply basis. The maximum stress and Tsai-Hill failure criteria were evaluated in correlating predicted strength with test results. The maximum stress failure criteria evaluates three stress components independently:

$$\frac{\sigma_1}{F_1} = 1, \qquad \frac{\sigma_2}{F_2} = 1, \qquad \frac{\tau_{12}}{F_{12}} = 1$$

When any of these ratios reach unity, failure is predicted. The Tsai-Hill failure criteria evaluates the stress components interactively:

$$\frac{\sigma_1{}^2}{F_1} + \frac{\sigma_2{}^2}{F_2} + \frac{\tau_{12}{}^2}{F_{12}} - \frac{\sigma_1\sigma_2}{F_1{}^2} = 1$$

Prediction of laminate strength was done on a last ply failure basis. Figure 86 shows an example of predictions, by the Tsai-Hill and maximum stress criteria, of the series of ply failures leading to ultimate failure. The 90° plies are predicted to fail first due to weak transverse (matrix) strength. The ± 45° plies then experience shear failure. Finally, fibers in the 0° plies fail.

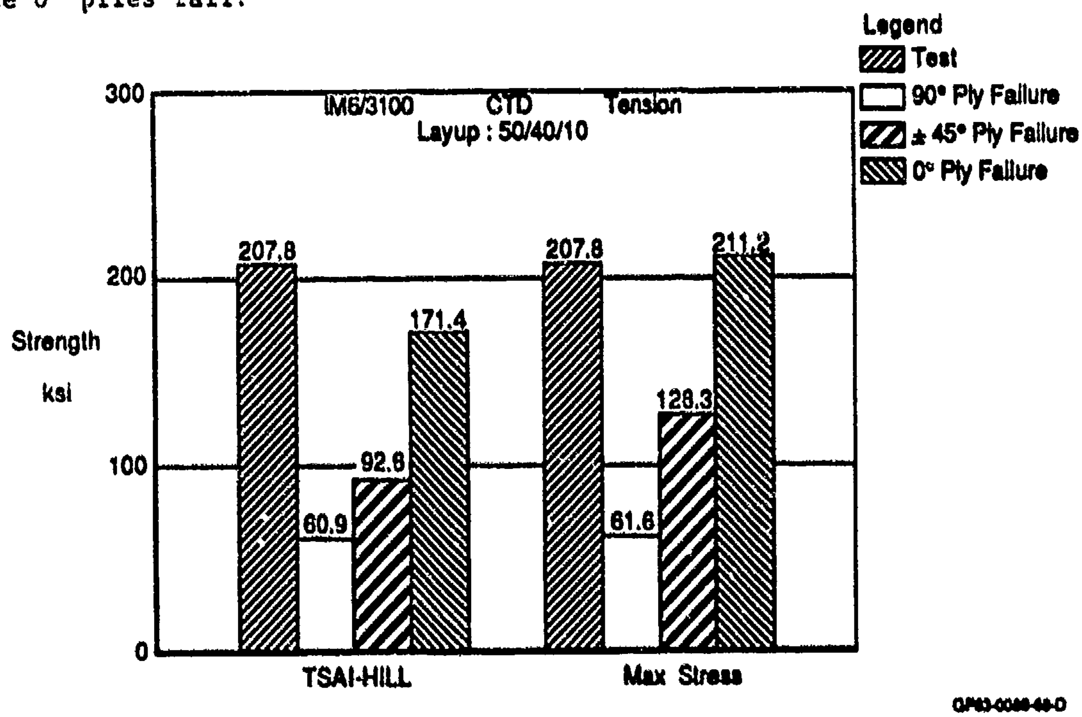

Figure 86. Prediction of Laminate Ply Failure Sequence

Correlation of unnotched laminate tension and compression strength test results with predicted last ply failure is shown in Figures 87 through 89. In general, predictions made with the Tsai-Hill failure criteria were conservative and those made with the maximum stress criteria were higher and unconservative. This difference is an indication of the interactive nature of the Tsai-Hill criteria and the noninteractive nature of the maximum stress criteria.

All predictions for 10/80/10 laminate strengths were conservative. This is due to the conservative shear strengths determined in lamina property testing, in Task II (Reference 8). Since the 10/80/10 laminates contained a higher percentage of ± 45° plies than the 50/40/10 laminates, the conservative lamina shear properties are more apparent.

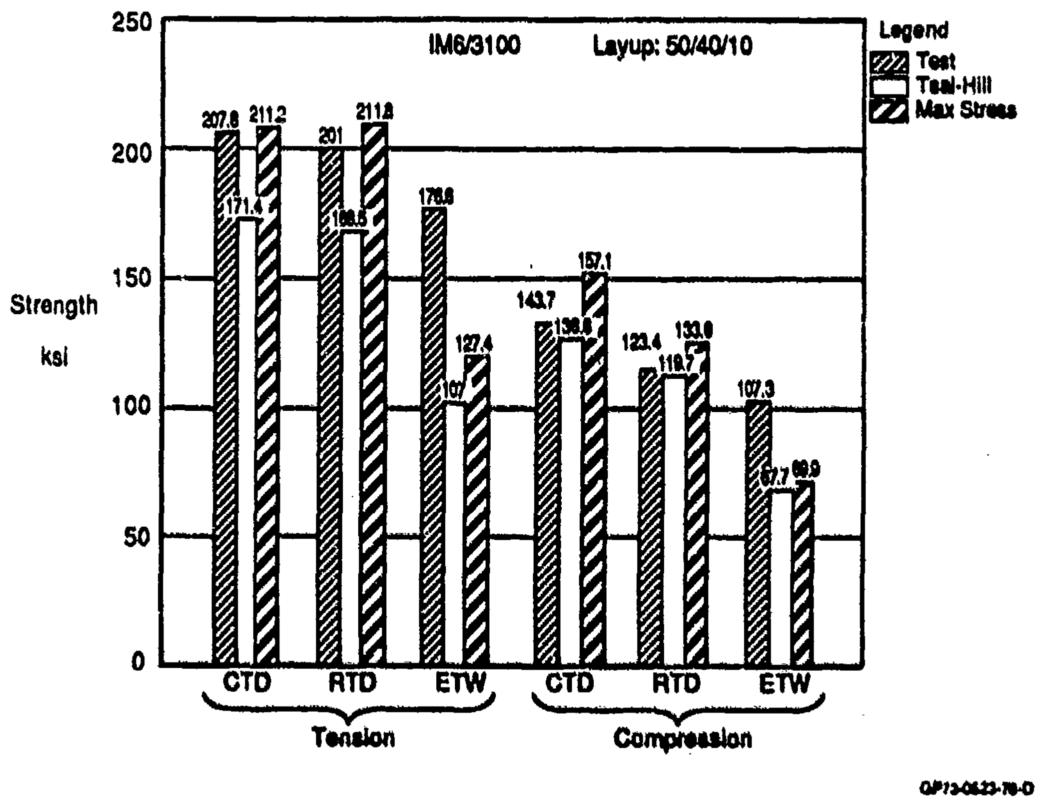

Figure 87. Prediction of IM6/3100 50/40/10 Laminate Strengths

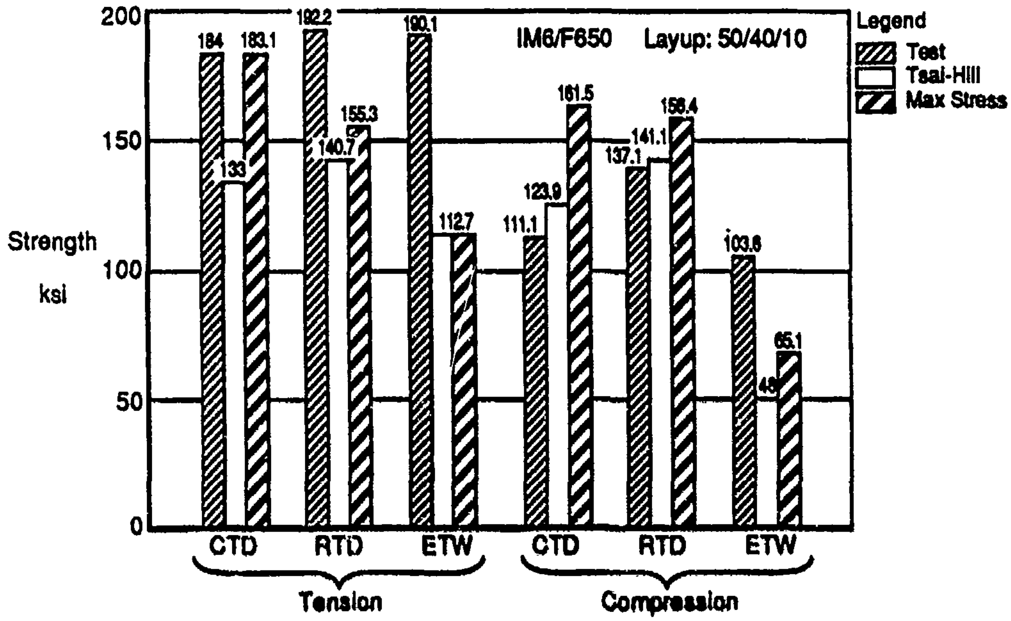

Figure 88. Prediction of IM6/F650 50/40/10 Laminate Strengths

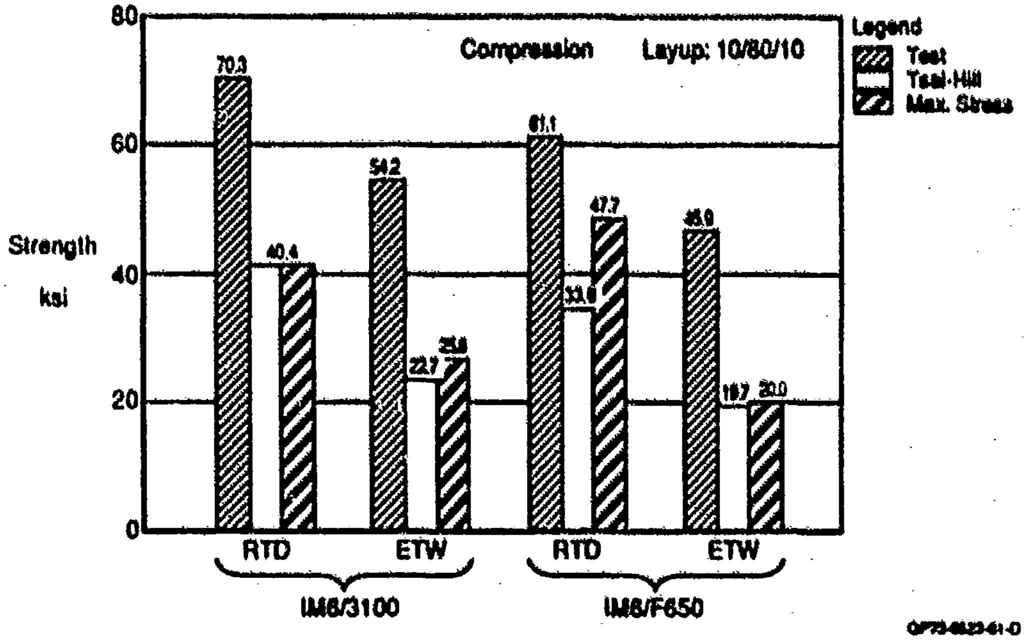

Figure 89. Prediction of 10/80/10 Laminate Compression Strengths

4.2.3 Unloaded Hole Static Strength - Unloaded hole static strength tests were performed to determine the notch sensitivity of the two BMI systems. Fiber dominated 50/40/10 laminates were tested in tension and compression at three environmental conditions as shown in Figure 90.

Specimen Type	Layup	Loading Static (1)	Environment CTD	RTD	ETW	Number of Tests Per Material
Unloaded Hole	50/40/10	T	✓			3
		T		✓		3
		T			✓	3
		C	✓			3
		C		✓		3
		C			✓	3

Notes:
(1) T - Tension
C - Compression

Figure 90. Unloaded Hole Static Test Matrix

4.2.3.1 Test Results - The unloaded hole test specimen configuration is shown in Figure 91. Typical tension and compression specimen failures are shown in Figures 92 and 93. The data for unloaded hole tension and compression static tests are tabulated in Figure 94 and 95 respectively.

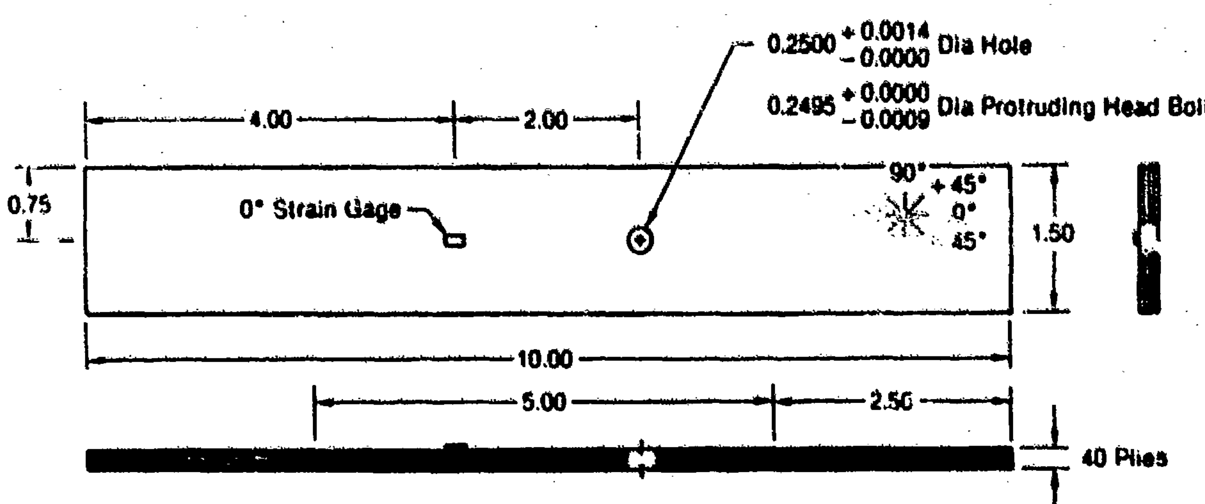

Figure 91. Unloaded Hole Tension and Compression Static Test Specimen

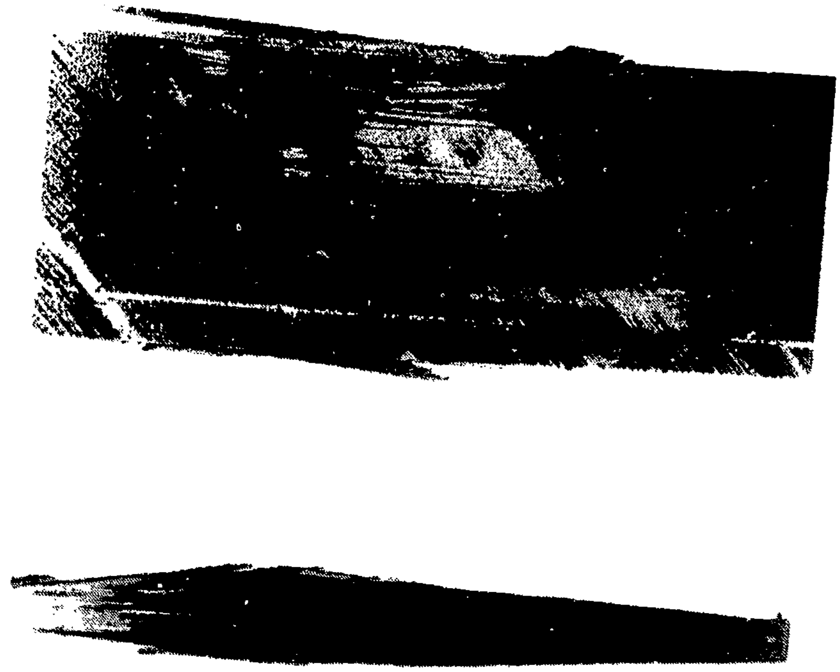

GP83 0089-16

Figure 92. Failed Unloaded Hole Static Tension Specimen

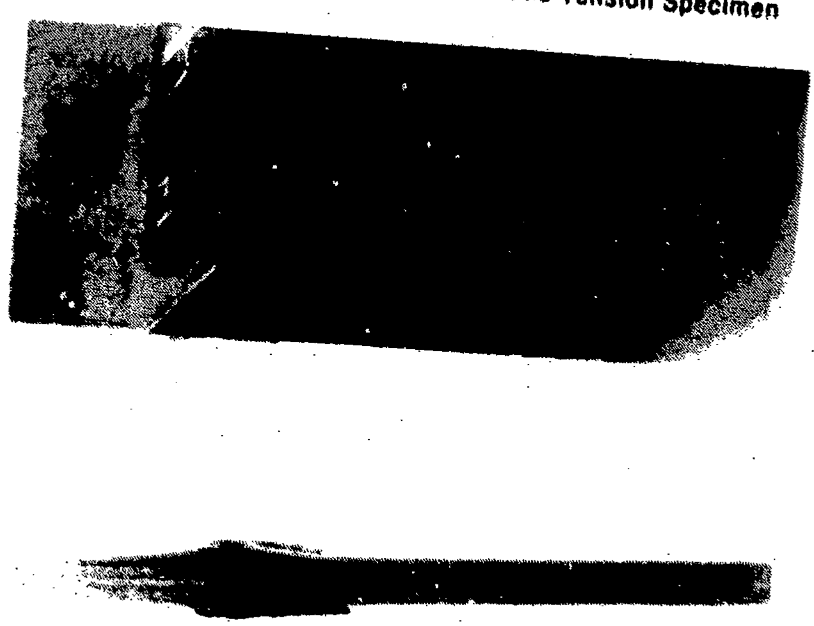

GP83 0089-17

Figure 93. Failed Unloaded Hole Static Compression Specimen

Material System	Environment	Specimen Number	Thickness (in.)	Width (in.)	Hole Diameter (in.)	Failure Load (lb)	Failure Stress (ksi) Ind	Failure Stress (ksi) Average	Failure Strain (μin./in.) Ind	Failure Strain (μin./in.) Average	Modulus (msi)
		1-10A-13	0.2246	1.510	0.25	38,500	122.6		8,320		13.61
IM6/3100	CTD	1-10A-14	0.2249	1.509	0.25	39,850	127.0	123.6	8,360	8,240	13.56
		1-10A-15	0.2231	1.509	0.25	38,000	121.1		8,040		14.42
		2-10A-13	0.2176	1.507	0.25	42,900	136.9		9,360		13.63
IM6/F650	CTD	2-10A-14	0.2165	1.510	0.25	37,050	118.0	125.3	8,480	8,800	12.98
		2-10A-15	0.2162	1.510	0.25	38,050	121.1		8,560		13.32
		1-10A-10	0.2243	1.510	0.25	36,350	115.7		7,830		13.72
IM6/3100	RTD	1-10A-11	0.2243	1.510	0.25	37,850	120.5	114.8	8,340	7,930	13.61
		1-10A-12	0.2233	1.510	0.25	34,000	108.3		7,620		13.40
		2-10A-10	0.2193	1.508	0.25	44,050	140.4		9,300		14.76
IM6/F650	RTD	2-10A-11	0.2201	1.506	0.25	42,500	135.7	136.0	9,260	9,090	13.71
		2-10A-12	0.2196	1.507	0.25	41,300	131.8		8,700		14.99
		1-10A-16	0.2217	1.509	0.25	33,500	106.7		7,385		13.79
IM6/3100	ETW	1-10A-17	0.2149	1.510	0.25	35,400	112.7	114.2	7,245	7,640	14.73
		1-10A-18	0.2231	1.499	0.25	38,400	123.2		8,295		14.10
		2-10A-16	0.2170	1.509	0.25	41,200	131.3		8,595		13.05
IM6/F650	ETW	2-10A-17	0.2163	1.508	0.25	41,600	132.6	131.5	8,260	8,480	14.34
		2-10A-18	0.2157	1.508	0.25	41,000	130.7		8,580		13.37

GP73-0623-46

Figure 94. Unloaded Hole Tension Test Data
Layup 50/40/10

Material System	Environment	Specimen Number	Thickness (in.)	Width (in.)	Hole Diameter (in.)	Failure Load (lb)	Failure Stress (ksi) Ind	Failure Stress (ksi) Average	Failure Strain (μin./in.) Ind	Failure Strain (μin./in.) Average	Modulus (msi)
		1-10A-22	0.2226	1.497	0.25	24,900	80.0		6,000		13.78
IM6/3100	CTD	1-10A-23	0.2223	1.495	0.25	25,700	82.6	84.8	5,190	6,340	14.23
		1-10A-24	0.2244	1.503	0.25	28,700	91.8		7,830		14.15
		2-10A-22	0.2184	1.510	0.25	26,500	84.4		6,210		13.32
IM6/F650	CTD	2-10A-23	0.2183	1.510	0.25	28,550	90.9	80.0	6,750	6,080	13.84
		2-10A-24	0.2180	1.510	0.25	20,350	64.8		5,280		13.61
		1-10A-19	0.2238	1.498	0.25	23,900	76.7		6,690		13.66
IM6/3100	RTD	1-10A-20	0.2245	1.496	0.25	22,700	73.0	75.6	6,120	6,500	13.85
		1-10A-21	0.2245	1.496	0.25	24,000	77.1		6,690		13.65
		2-10A-19	0.2177	1.508	0.25	20,650	65.8		5,310		13.68
IM6/F650	RTD	2-10A-20	0.2187	1.509	0.25	22,550	71.8	69.6	4,830	5,010	13.73
		2-10A-21	0.2196	1.510	0.25	22,350	71.2		4,900		13.96
		1-10A-25	0.2236	1.506	0.25	13,350	42.6		3,220		13.39
IM6/3100	ETW	1-10A-26	0.2217	1.499	0.25	14,140	45.4	45.2	3,000	3,320	14.25
		1-10A-27	0.2226	1.503	0.25	14,920	47.7		3,725		13.29
		2-10A-25	0.2190	1.509	0.25	14,900	47.5		3,660		13.41
IM6/F650	ETW	2-10A-26	0.2189	1.510	0.25	14,200	45.2	46.4	3,600	3,630	13.13
		2-10A-27	0.2198	1.508	0.25	14,550	46.4		3,615		13.61

GP73-0623-40

Figure 95. Unloaded Hole Compression Test Data
Layup 50/40/10

Figure 96 summarizes the tensile strength reduction caused by the fastener hole in both IM6/3100 and IM6/F650 laminates. The notched tensile strength of IM6/3100 was approximately 40 percent less than the unnotched strength. The notched tensile strength of IM6/F650 was approximately 30 percent less than the unnotched strength.

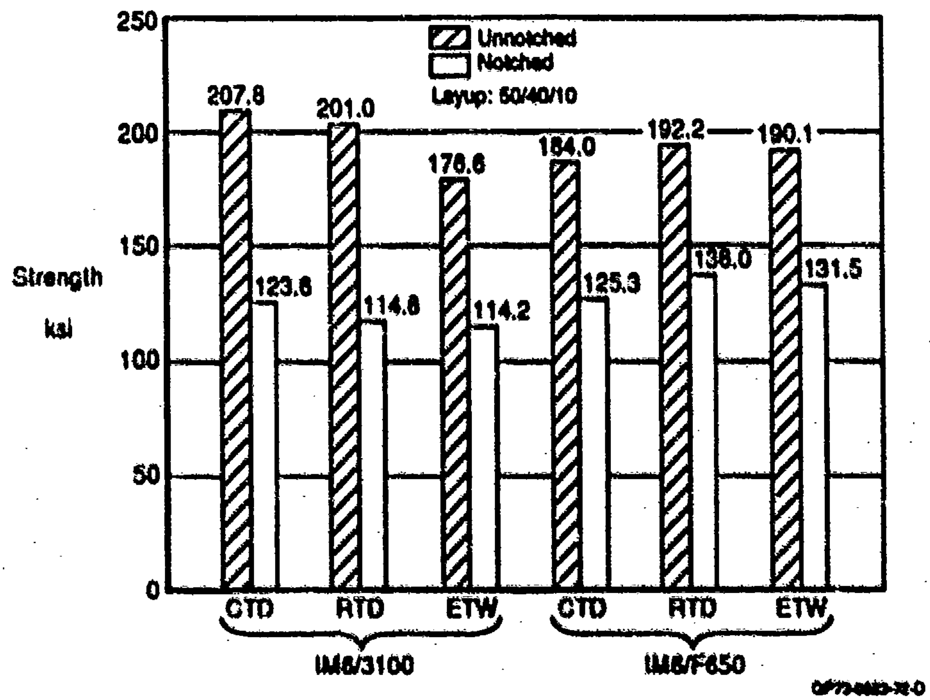

Figure 96. Notched Laminate Tensile Strength Reduction

Similarly, Figure 97 summarizes the compression strength reduction caused by the fastener hole. The notched compression strength of IM6/3100 and IM6/F650 at CTD and RTD conditions was generally 30 percent to 40 percent less than the unnotched compression strengths. At ETW conditions, the notched compression strengths of IM6/3100 and IM6/F650 were less than half (approximately 43 percent) of the unnotched strengths.

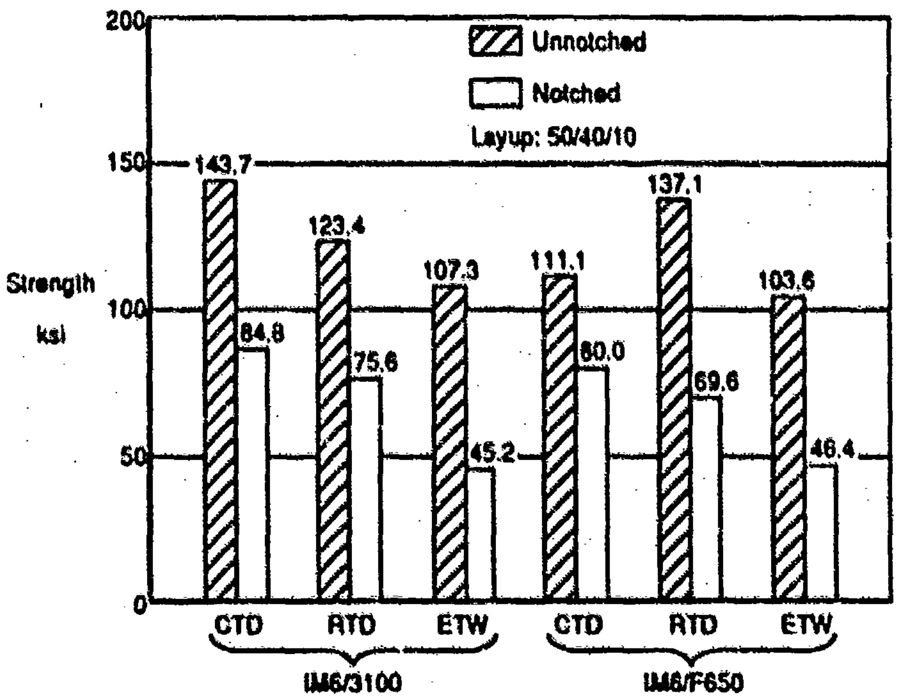

Figure 97. Notched Laminate Compression Strength Reduction

4.2.3.2 Analysis - Unloaded hole strength predictions were performed using the "Bolted Joint Stress Field Model" (BJSFM) (Reference 9), outlined in Figure 98. This methodology is based upon classical lamination plate theory and anisotropic theory of elasticity to obtain laminate stress and strain distributions, and a characteristic dimension (R_c) failure hypothesis. Unidirectional (lamina) stiffness and strength data were used with an empirical value of R_c to predict stress distributions, critical plies, failure location, and failure load.

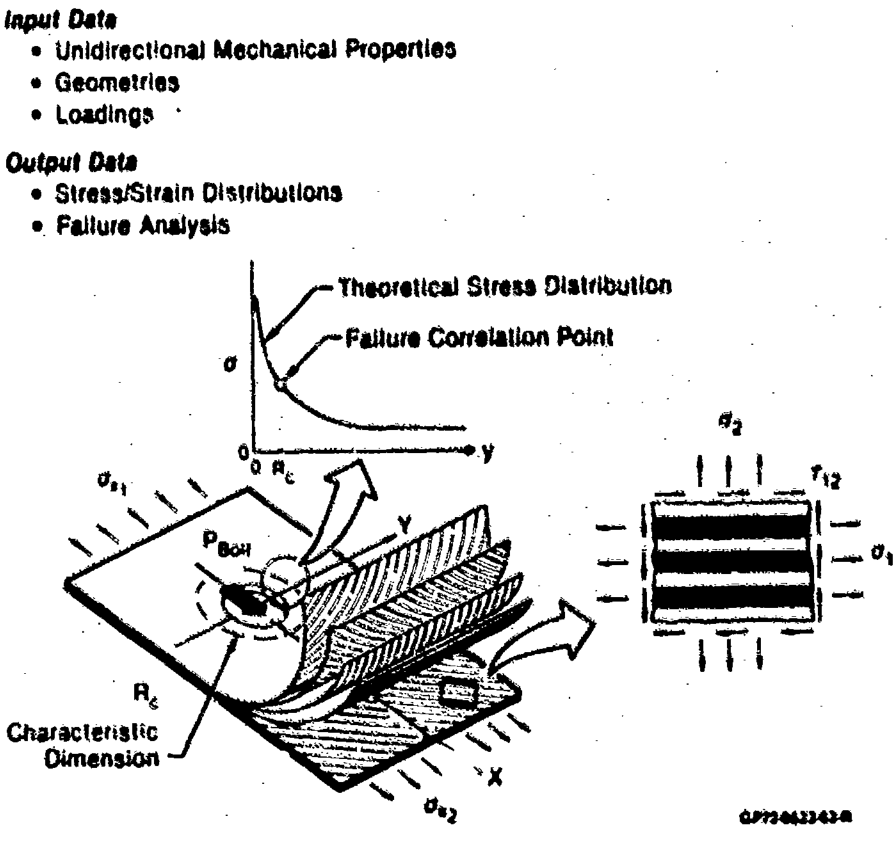

Figure 98. Bolted Joint Stress Field Model

Both the Tsai-Hill and maximum stress failure criteria were used to predict unloaded hole strengths. The strengths were predicted with the last ply failure analysis, as previously used to predict unnotched strengths. As plies were predicted to fail due to matrix tension or shear, the modulus corresponding to the failure mode was reduced by a factor of 1000 to represent the lack of load carrying capability. The analysis was continued, until finally the 0° fibers were predicted to fail near the side of the hole. The Tsai-Hill and maximum stress failure criteria predicted equal ultimate strengths and similar failure modes. This was due to the analytic removal of matrix and shear load capability that would have distinguished the interactive Tsai-Hill predictions from the noninteractive maximum stress predictions.

Figure 99 illustrates the variation of predicted notched strength with R_c value. Under CTD conditions, the R_c value of 0.036 inch correctly predicts the notched tension strength of 124 ksi. To correctly predict the notched compression strength of 85 ksi, the R_c value of 0.029 inch must be used.

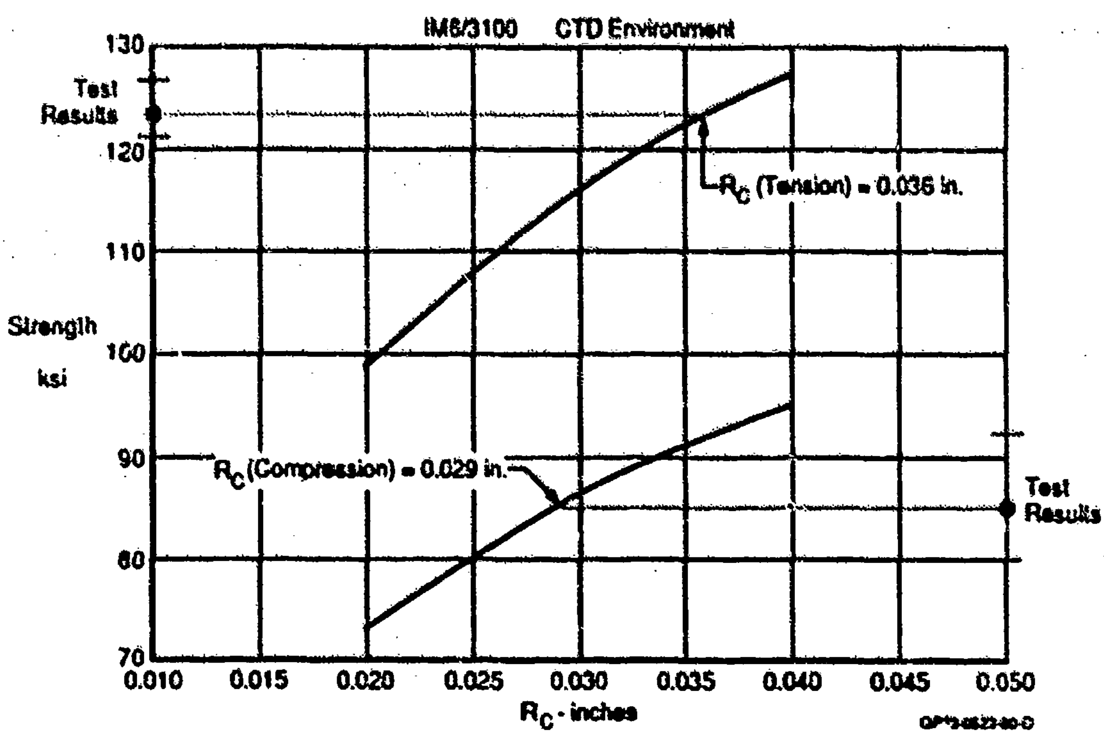

Figure 99. Determination of R_C Values for Unloaded Hole Strength Prediction

Figure 100 summarizes the results for IM6/3100 and IM6/F650 at three environments. Under RTD conditions no reasonably small value of R_c correlated with the IM6/F650 tension strength of 136 ksi. The R_c value of 0.28 inch is too large to consider the failure correlation point as being close to the edge of a 0.25 inch hole. Under ETW conditions, tension strengths for IM6/3100 and IM6/F650 were not predicted for any value of R_c.

			IM6/3100			IM6/F650		
			CTD	RTD	ETW	CTD	RTD	ETW
Tension	R_c	(in.)	0.036	0.029	Large	0.072	0.280	Large
	F^{tu}	(ksi)	123.6	114.8	114.2	125.3	136.0	131.5
Compression	R_c	(in.)	0.029	0.032	0.063	0.023	0.018	0.087
	F^{cu}	(ksi)	84.8	75.6	45.2	80.0	69.6	46.4

GP73-0823-77-R

Figure 100. R_c Values Used to Predict Unloaded Hole Laminate Strengths

4.2.4 Unloaded Hole Fatigue Life - Unloaded hole fatigue tests were performed to determine the durability of the two BMI systems. Fiber dominated 50/40/10 laminates were tested in compression-compression (R = 10) and reversed loading (R = -1) fatigue cycling at three environmental conditions as shown in Figure 101.

Specimen Type	Layup	Loading: Fatigue: Stress Ratio	Loading: Fatigue: Stress Level	Environment: CTD	Environment: RTD	Environment: ETW	Number of Tests Per Material
Unloaded Hole	50/40/10	−1.0	L_1	✓			5 + 1[(1)]
		−1.0	L_1		✓		5 + 2[(1)]
		−1.0	L_1			✓	5 + 1[(1)]
		−1.0	L_2	✓			5
		−1.0	L_2		✓		5
		−1.0	L_2			✓	5
		10.0	L_1	✓			5
		10.0	L_1		✓		5 + 1[(1)]
		10.0	L_1			✓	5
		10.0	L_2	✓			5
		10.0	L_2		✓		5
		10.0	L_2			✓	5

Note: (1) TBE enhanced x-rays to be taken at ¼, ½, ¾ total life.

GP73-0823-61-R

Figure 101. Unloaded Hole Fatigue Test Matrix

4.2.4.1 Test Results - The unloaded hole fatigue test specimen configuration is shown in Figure 102. A typical failure is depicted in Figure 103. Figure 104 shows the progression of damage that precedes unloaded hole fatigue failure. The enhanced X-rays show that matrix cracking initially occurs along fibers, as evidenced by vertical and ±45° lines near the hole edge. Next the cracks coalesce into delaminations which show up as white cloudy areas. The delaminations occur both at the hole edge and at the outer edges of the specimen. The unloaded hole fatigue life data are tabulated in Figures 105 through 107. The data are plotted in Figures 108 through 110. Each plot shows the static compression strength plotted at a life of 1 cycle.

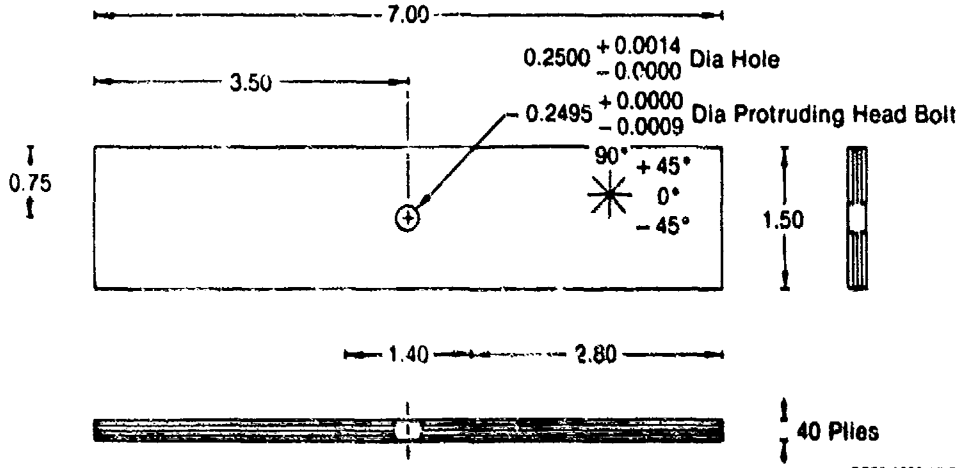

Figure 102. Unloaded Hole Fatigue Test Specimen

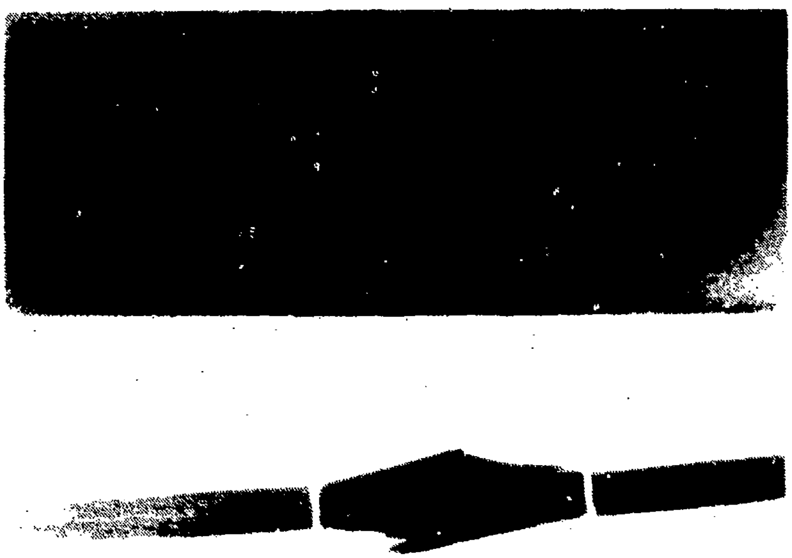

GP83 0069 18

Figure 103. Failed Unloaded Hole Fatigue Specimen

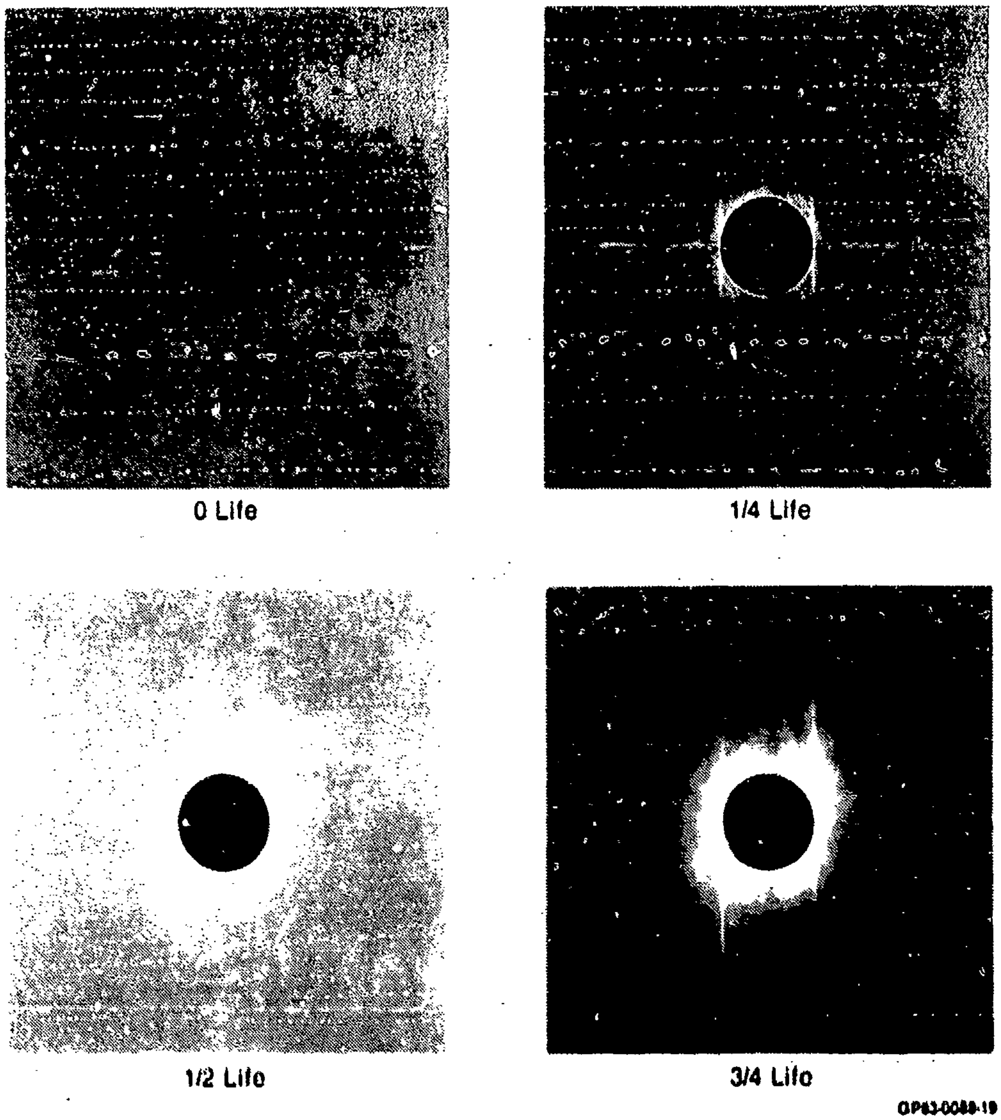

Figure 104. Progression of Unloaded Hole Fatigue Damage (Enhanced X-Rays)

Material System	Specimen Number	Stress Ratio	Load Level (kips)	Stress Level (ksi)	Thickness (in.)	Width (in.)	Hole Diameter (in.)	Life (Cycles)	Log Mean Life (Cycles)
	1-10A-44U				0.225	1.510	0.250	200	
	1-10A-45U				0.225	1.509	0.250	301	
IM6/3100	1-10A-46U	10.0	23.8	76.3	0.224	1.510	0.250	91	250
	1-10A-47U				0.225	1.511	0.250	46	
	1-10A-48U				0.225	1.509	0.250	3,910	
	1-10B-8U				0.227	1.503	0.250	77,400	
	1-10B-9U				0.226	1.501	0.250	73,764	
IM6/3100	1-10B-10U	10.0	20.4	65.4	0.226	1.509	0.250	7,741	40,134
	1-10B-11U				0.225	1.510	0.250	210,000+	
	1-10B-12U				0.226	1.509	0.250	11,219	
	1-10A-11U				0.225	1.508	0.250	1,222	
	1-10A-12U				0.223	1.508	0.250	97	
IM6/3100	1-10A-13U	−1.0	22.6	72.5	0.223	1.507	0.250	1,559	1,281
	1-10A-14U				0.225	1.506	0.250	6,595	
	1-10A-15U				0.225	1.509	0.250	2,829	
	1-10A-25U				0.225	1.501	0.250	34,554	
	1-10A-26U				0.222	1.503	0.250	12,740	
IM6/3100	1-10A-27U	−1.0	20.4	65.4	0.223	1.504	0.250	9,752	15,567
	1-10A-28U				0.225	1.501	0.250	50,508	
	1-10A-29U				0.224	1.510	0.250	4,216	
	2-10A-41U				0.217	1.509	0.250	190	
	2-10A-42U				0.219	1.510	0.250	1,352	
IM6/F650	2-10A-43U	10.0	20.4	65.4	0.219	1.509	0.250	522	591
	2-10A-44U				0.220	1.507	0.250	271	
	2-10A-45U				0.221	1.508	0.250	1,984	
	2-10B-5U				0.220	1.506	0.250	49,032	
	2-10B-6U				0.220	1.506	0.250	17,294	
IM6/F650	2-10B-7U	10.0	19.3	62.0	0.221	1.505	0.250	7,273	9,180
	2-10B-8U				0.221	[illegible]	0.250	9,145	
	2-10B-9U				0.221	1.510	0.250	1,156	
	2-10A-9U				0.219	1.509	0.250	7,124	
	2-10A-10U				0.220	1.508	0.250	449	
IM6/F650	2-10A-11U	−1.0	20.4	65.4	0.220	1.509	0.250	3,909	1,677
	2-10A-12U				0.220	1.509	0.250	493	
	2-10A-13U				0.219	[illegible]	0.250	2,151	
	2-10A-25U				0.219	1.507	0.250	21,340	
	2-10A-26U				0.219	1.507	0.250	10,333	
IM6/F650	2-10A-27U	−1.0	19.3	62.0	0.219	1.507	0.250	1,789	2,376
	2-10A-28U				0.221	1.506	0.250	2,868	
	2-10A-29U				0.220	1.507	0.250	67	

GP73-0622-60-R

Figure 105. Unloaded Hole Fatigue Data for C1D Conditions

Material System	Specimen Number	Stress Ratio	Load Level (kips)	Stress Level (ksi)	Thickness (in.)	Width (in.)	Hole Diameter (in.)	Life (Cycles)	Log Mean Life (Cycles)
	1-10A-41U				0.225	1.508	0.250	4,954	
	1-10A-42U				0.225	1.511	0.250	8,860	
IM6/3100	1-10B-21U	10.0	21.2	68.0	0.227	1.513	0.250	13,476	6,295
	1-10A-43U				0.223	1.512	0.250	10,226	
	1-10B-4U				0.227	1.503	0.250	1,634	
	1-10A-1U				0.223	1.508	0.250	12,578	
	1-10A-2U				0.223	1.510	0.250	4,581	
IM6/3100	1-10A-3U	10.0	20.4	65.4	0.225	1.512	0.250	9,931	16,998
	1-10B-5U				0.227	1.502	0.250	34,508	
	1-10B-6U				0.226	1.502	0.250	272,890	
	1-10B-7U				0.226	1.504	0.250	4,477	
	1-10A-4U				0.225	1.512	0.250	3,724	
	1-10A-5U				0.223	1.511	0.250	6,753	
IM6/3100	1-10A-6U	−1.0	21.2	68.0	0.224	1.511	0.250	906	2,391
	1-10A-7U				0.225	1.510	0.250	1,493	
	1-10A-8U				0.225	1.510	0.250	2,296	
	1-10A-20U				0.225	1.503	0.250	58,788	
	1-10A-21U				0.225	1.488	0.250	20,256	
IM6/3100	1-10A-22U	−1.0	19.3	62.0	0.222	1.501	0.250	2,569	12,870
	1-10A-23U				0.223	1.503	0.250	28,869	
	1-10A-24U				0.226	1.500	0.250	3,998	
	2-10A-38U				0.219	1.485	0.250	1,111	
IM6/F650	2-10A-40U	10.0	20.4	65.4	0.217	1.509	0.250	1,019	845
	2-10B-21U				0.221	1.525	0.250	859	
	2-10B-22U				0.220	1.525	0.250	525	
	2-10A-51U				0.215	1.507	0.250	352	
	2-10B-1U				0.218	1.508	0.250	583	
IM6/F650	2-10B-2U	10.0	19.3	62.0	0.220	1.505	0.250	1,029	1,014
	2-10B-3U				0.220	1.506	0.250	964	
	2-10B-4U				0.220	1.507	0.250	5,268	
	2-10A-1U				0.216	1.503	0.250	833	
	2-10A-2U				0.218	1.508	0.250	1,675	
IM6/F650	2-10A-3U	−1.0	20.4	65.4	0.219	1.509	0.250	4,258	1,323
	2-10A-4U				0.220	1.508	0.250	199	
	2-10A-5U				0.219	1.507	0.250	4,947	
	2-10A-20U				0.219	1.506	0.250	18,088	
	2-10A-21U				0.220	1.508	0.250	8,493	
IM6/F650	2-10A-22U	−1.0	19.3	62.0	0.218	1.508	0.250	7,584	7,257
	2-10A-23U				0.218	1.506	0.250	4,519	
	2-10A-24U				0.218	1.507	0.250	3,824	

GP73-0622-61-R

Figure 106. Unloaded Hole Fatigue Data for RTD Conditions

Material System	Specimen Number	Stress Ratio	Load Level (kips)	Stress Level (ksi)	Thickness (in.)	Width (in.)	Hole Diameter (in.)	Life (Cycles)
IM6/3100	1-10B-1U	10.0	14.3	45.8	0.223	1.504	0.250	68,440
	1-10B-2U		14.3	45.8	0.226	1.499	0.250	1
IM6/3100	1-10A-49U	10.0	14.2	45.5	0.224	1.510	0.250	10
	1-10A-50U		14.2	45.5	0.222	1.510	0.250	170
	1-10A-51U		14.2	45.5	0.221	1.508	0.250	3,860
IM6/3100	1-10B-13U	10.0	14.0	44.9	0.226	1.507	0.250	5,980
	1-10B-14U		14.0	44.9	0.226	1.507	0.250	756,000+
	1-10A-33U		14.0	44.9	0.223	1.509	0.250	19,890
	1-10A-34U		14.0	44.9	0.220	1.508	0.250	90
IM6/3100	1-10A-32U	−1.0	12.4	39.7	0.225	1.510	0.250	5,880
	1-10B-15U		12.4	39.7	0.227	1.506	0.250	8,610
	1-10B-16U		12.4	39.7	0.228	1.505	0.250	10,750
	1-10B-17U		12.4	39.7	0.225	1.506	0.250	2,070
IM6/3100	1-10A-17U	−1.0	11.1	35.6	0.221	1.511	0.250	108,040
	1-10A-18U		11.1	35.6	0.223	1.499	0.250	410,000+
IM6/3100	1-10A-29U	−1.0	10.5	33.7	0.224	1.510	0.250	40
IM6/3100	1-10A-30U	−1.0	10.0	32.1	0.224	1.509	0.250	3,080
	1-10A-31U		10.0	32.1	0.225	1.509	0.250	238,170
IM6/F650	2-10A-47U	10.0	14.5	46.5	0.219	1.506	0.250	150
	2-10A-48U		14.5	46.5	0.217	1.504	0.250	120
	2-10A-49U		14.5	46.5	0.216	1.504	0.250	10
	2-10A-50U		14.5	46.5	0.217	1.504	0.250	7,700
IM6/F650	2-10B-13U	10.0	14.3	45.8	0.221	1.508	0.250	86,180
	2-10B-14U		14.3	45.8	0.218	1.524	0.250	858,000+
	2-10A-46U		14.3	45.8	0.221	1.506	0.250	430,250
IM6/F650	2-10A-14U	10.0	13.9	44.6	0.217	1.509	0.250	7,670
	2-10A-34U		13.9	44.6	0.217	1.508	0.250	67,090
	2-10B-10U		13.9	44.6	0.221	1.507	0.250	148,280
	2-10B-11U		13.9	44.6	0.221	1.508	0.250	710,200+
	2-10B-12U		13.9	44.6	0.222	1.508	0.250	748,240+
IM6/F650	2-10A-33U	10.0	13.8	44.2	0.218	1.507	0.250	700,000+
IM6/F650	2-10A-15U	10.0	13.5	43.3	0.218	1.509	0.250	705,000+
IM6/F650	2-10A-30U	−1.0	14.4	46.2	0.219	1.506	0.250	1,000
	2-10A-31U		14.4	46.2	0.218	1.508	0.250	210
	2-10A-32U		14.4	46.2	0.219	1.503	0.250	1,870
	2-10B-30U		14.4	46.2	0.220	1.505	0.250	25,270
	2-10B-31U		14.4	46.2	0.219	1.508	0.250	250
IM6/F650	2-10A-28U	−1.0	14.0	44.9	0.221	1.506	0.250	3,060
	2-10A-29U		14.0	44.9	0.220	1.507	0.250	567,990+
	2-10B-32U		14.0	44.9	0.219	1.503	0.250	2,010
	2-10B-33U		14.0	44.9	0.218	1.507	0.250	14,810
	2-10B-34U		14.0	44.9	0.217	1.508	0.250	12,920

GP73-0523-63-R

Figure 107. Unloaded Hole Fatigue Data for ETW Conditions

The CTD and RTD fatigue data in Figures 108 and 109 are plotted in terms of the log mean life centered in its 90 percent confidence interval. Each figure includes two fatigue data plots. The first plot shows data for R = 10 and the second shows data for R = -1. Comparing the plots in each figure indicates that IM6/3100 experienced longer lives during compression-only (R = 10) cycling than reversed (R = -1) cycling. One explanation for this behavior is that IM6/3100 is matrix crack dominated in fatigue. Under compression-only conditions, matrix cracks will not reduce life, whereas under reversed loading, matrix cracks grow due to tensile loading thus reducing life.

In contrast to the behavior of IM6/3100, IM6/F650 showed no extension of life during compression-only cycling compared to reversed cycling. IM6/F650 sustained equal peak compression loads for both R = 10 and R = -1 cycling. Perhaps, life was controlled by delamination growth with compression loading. Failure would then occur when delaminations driven by peak compression loading grew to a critical size.

In Figure 110 the ETW fatigue data are plotted as individual points because of the large life scatter that occurred. The increased scatter is attributed to the loss of moisture in the specimens during elevated temperature testing. The high diffusivity of the BMI materials resulted in rapid desiccation of the specimens. Specimens that did not fail early (in less than 4000 cycles) survived longer-than-appropriate lives because of the increased strength in the dry condition.

4.2.4.2 Analysis - The fatigue data for CTD and RTD conditions was analyzed to determine the log mean life and its 90 percent confidence interval for each stress level. A statistical analysis was performed on the fatigue data to determine the 90 percent confidence interval for each set of data. There is 90 percent probability that the mean life of specimens tested at the indicated stress level will be within the range defined by the 90 percent confidence interval.

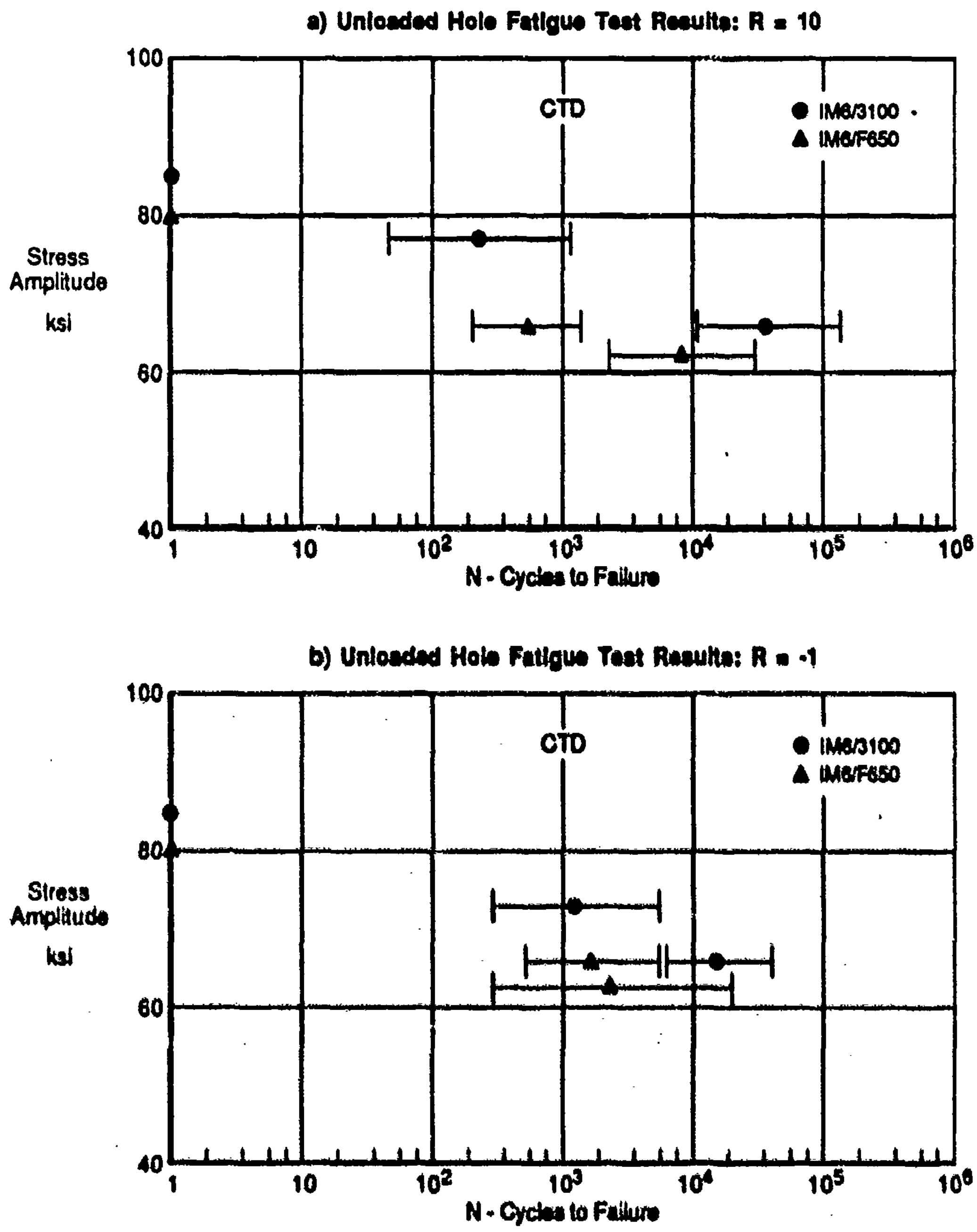

Figure 108. Unloaded Hole Fatigue Test Results for CTD Conditions

a) Unloaded Hole Fatigue Test Results: R = 10

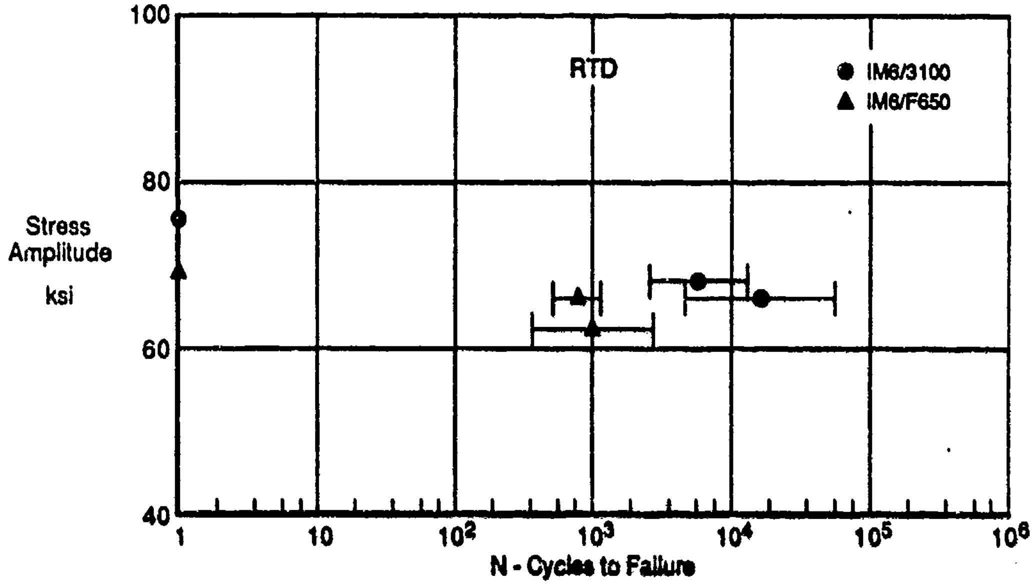

b) Unloaded Hole Fatigue Test Results: R = -1

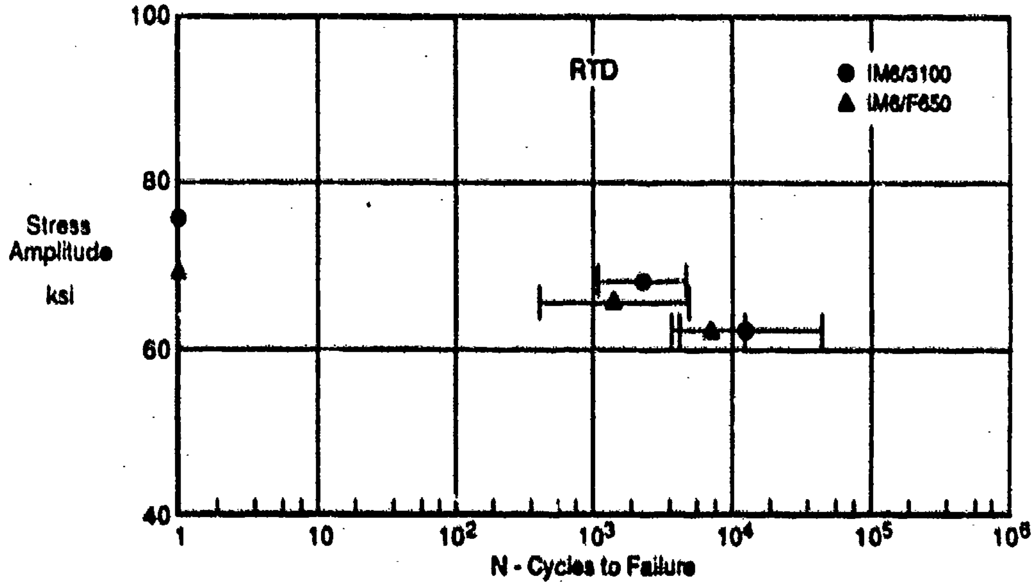

GP73-0523-76-D

Figure 109. Unloaded Hole Fatigue Test Results for RTD Conditions

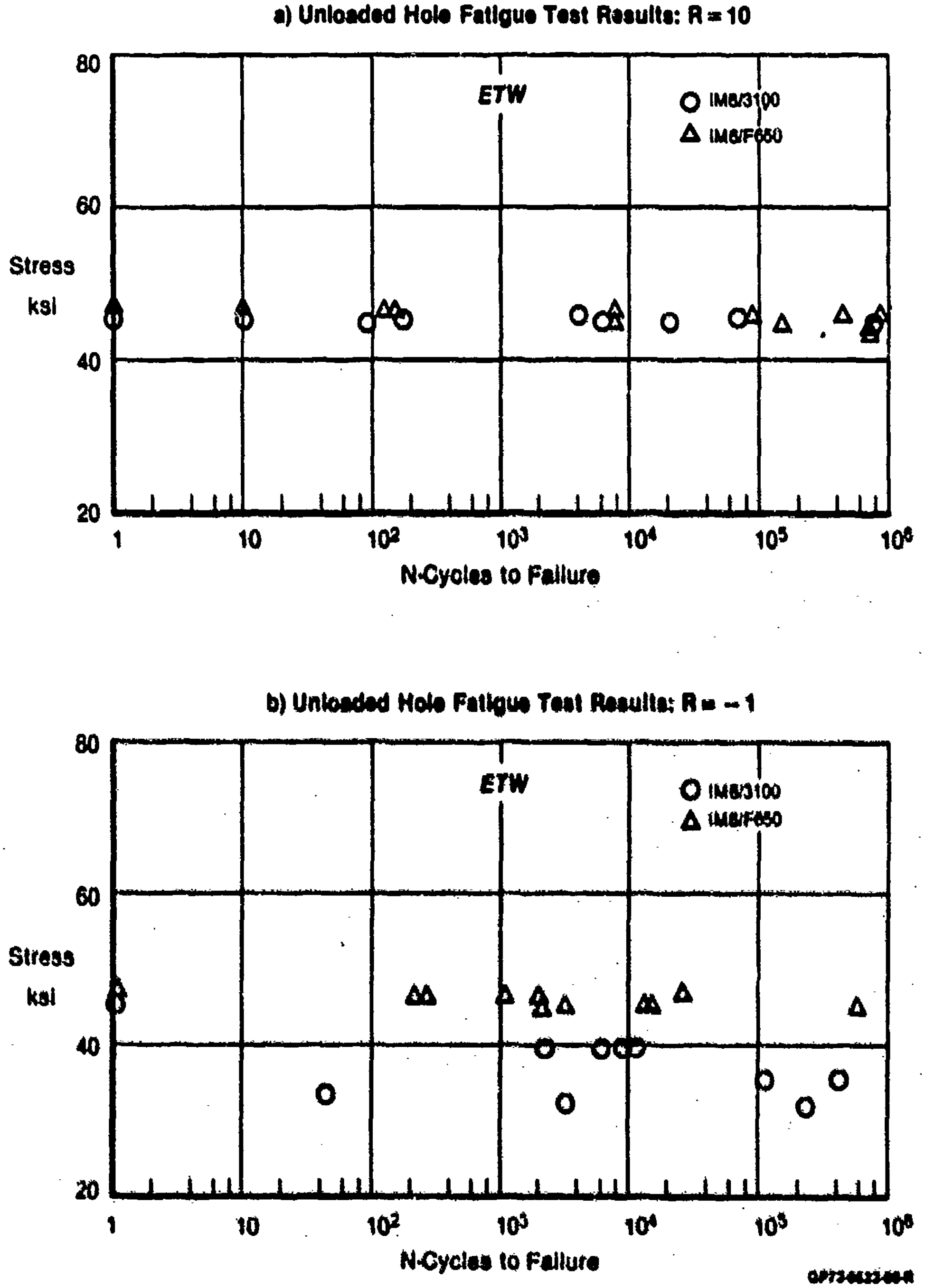

Figure 110. Unloaded Hole Fatigue Test Results for ETW Conditions

4.2.5 Loaded Hole Static Strength - Loaded hole static strength tests were performed to determine the fastener bearing strength of the BMI systems. Fiber dominated 50/40/10 laminates were tested at three environmental conditions as shown in Figure 111.

4.2.5.1 Test Results - The loaded hole test specimen is shown in Figure 112. The loaded hole test setup is shown in Figure 113. With this setup, the bearing load is introduced in double shear to obtain uniform bearing stress through the thickness of the laminate. A typical failed specimen is shown in Figure 114. Test data for loaded hole static tests are tabulated in Figure 115.

Specimen Type	Layup	Loading Static (1)	Environment CTD	Environment RTD	Environment ETW	Number of Tests Per Material
Loaded Hole	50/40/10	T	✓			3
		T		✓		3
		T			✓	3

Notes:
(1) T - Tension
C - Compression

GP73-0623-83-R

Figure 111. Loaded Hole Static Test Matrix

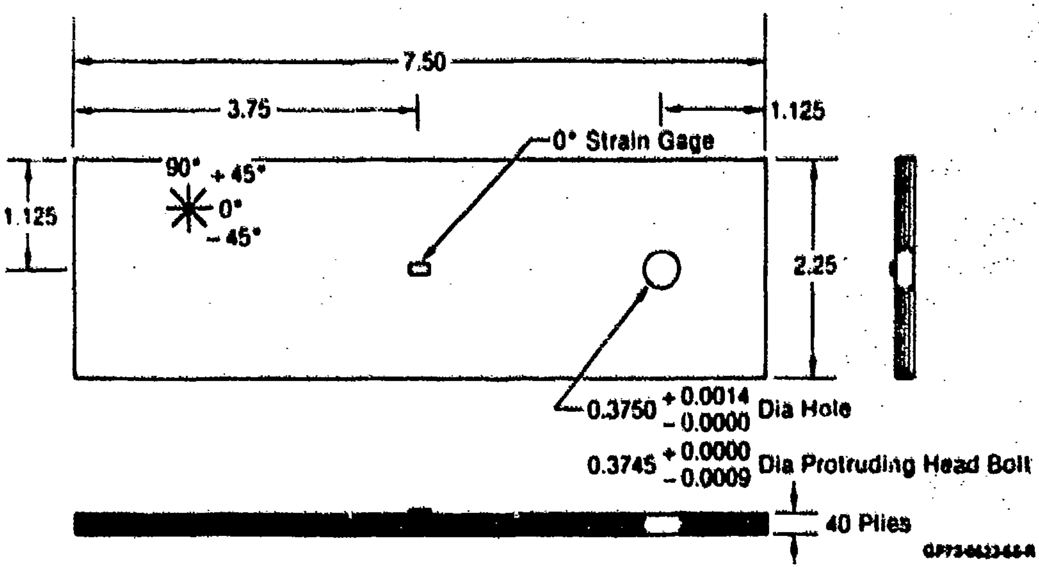

Figure 112. Loaded Hole Static Test Specimen

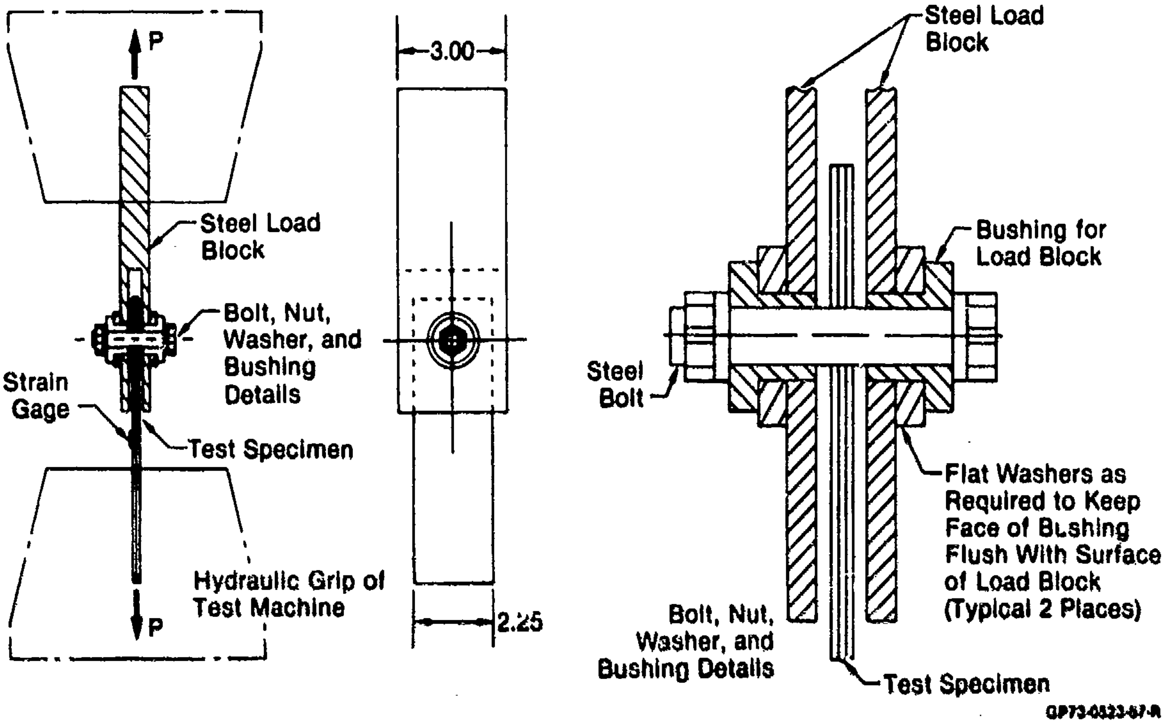

Figure 113. Loaded Hole Test Setup

Figure 114. Failed Loaded Hole Static Specimen

Material System	Environment	Specimen Number	Thickness (in.)	Width (in.)	Hole Diameter (in.)	Failure Load (lb)	Gross Failure Stress (ksi) Ind	Gross Failure Stress (ksi) Avg	Failure Stress, P/dt (ksi) Ind	Failure Stress, P/dt (ksi) Avg	Failure Strain (μin./in.) Ind	Failure Strain (μin./in.) Avg
		1-10B-4L	0.2284	2.255	0.375	9,450	20.1		121.2		1,380	
IM6/3100	CTD	1-10B-5L	0.2287	2.255	0.375	9,260	19.7	19.7	118.7	118.8	1,404	1,376
		1-10B-6L	0.2282	2.255	0.375	9,090	19.4		116.5		1,344	
		2-10B-4L	0.2205	2.253	0.375	8,650	18.5		110.9		1,236	
IM6/F650	CTD	2-10B-5L	0.2209	2.254	0.375	7,670	16.4	17.2	98.3	103.3	1,164	1,200
		2-10B-6L	0.2215	2.252	0.375	7,850	16.8		100.6		1,200	
		1-10B-1L	0.2268	2.255	0.375	7,800	16.6		100.0		1,164	
IM6/3100	RTD	1-10B-2L	0.2273	2.256	0.375	9,140	19.5	18.4	117.2	110.7	1,440	1,324
		1-10B-3L	0.2284	2.256	0.375	8,960	19.1		114.9		1,368	
		2-10B-1L	0.2183	2.249	0.375	7,380	15.8		94.6		1,188	
IM6/F650	RTD	2-10B-2L	0.2201	2.253	0.375	7,700	16.4	16.5	98.7	99.3	1,212	1,236
		2-10B-3L	0.2205	2.255	0.375	8,160	17.4		104.6		1,308	
		1-10B-7L	0.2270	2.251	0.375	5,700	12.2		73.1		870	
IM6/3100	ETW	1-10B-8L	0.2295	2.252	0.375	5,970	12.7	12.3	76.5	73.8	852	838
		1-10B-9L	0.2288	2.244	0.375	5,600	12.0		71.8		792	
		2-10B-7L	0.2209	2.254	0.375	2,930	6.25		37.6		372	
IM6/F650	ETW	2-10B-8L	0.2205	2.254	0.375	4,730	10.1	8.35	60.6	50.2	696	540
		2-10B-9L	0.2209	2.254	0.375	4,080	8.70		52.3		552	

GP73-0623-63-R

Figure 115. Loaded Hole Static Test Data
Pure Bearing Test Results
Layup: 50/40/10

The bearing strengths of both systems are summarized in Figure 116. Bearing strength gradually decreased with increasing temperature and moisture content. The RTD bearing strength of IM6/3100 was 93 percent of the CTD bearing strength. Under ETW conditions the bearing strength of IM6/3100 was 62 percent of the CTD strength. The RTD and ETW bearing strengths of IM6/F650 were 96 percent and 49 percent of the CTD strength, respectively.

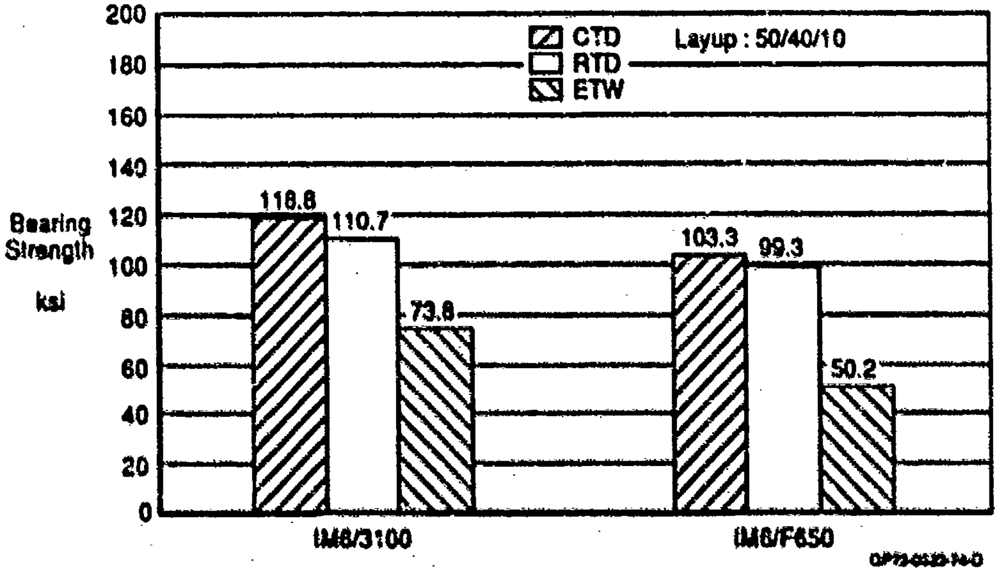

Figure 116. Loaded Hole (Bearing) Strength Test Results

4.2.5.2 Analysis - Loaded hole strength predictions were made using BJSFM. The analyses predicted that initially the laminate experienced matrix compression and shear failures of all plies. Ultimately, the loaded hole laminate was predicted to experience fiber compression failure of ±45° plies at locations 40° from the load line.

Figure 117 summarizes the R_c values used to predict the loaded hole strengths. The data is included along with the unloaded hole R_c values already reported. In general, the R_c value for predicting loaded hole strength is greater than the R_c value for predicting unloaded hole strength.

		IM6/3100			IM6/F650		
		CTD	RTD	ETW	CTD	RTD	ETW
Tension	R_c (in.)	0.036	0.029	Large	0.072	0.280	Large
	F^{tu} (ksi)	123.6	114.8	114.2	125.3	136.0	131.5
Compression	R_c (in.)	0.029	0.032	0.063	0.023	0.018	0.087
	F^{cu} (ksi)	84.8	75.6	45.2	80.0	69.6	46.4
Bearing	R_c (in.)	0.075	0.089	0.134	0.048	0.047	0.078
	F^{bru}	118.8	110.7	73.8	103.3	99.3	50.2

GP73-0623-83-R

Figure 117. R_c Values Used to Predict Unloaded and Loaded Hole Laminate Strengths

4.2.6 Loaded Hole Fatigue Life (Hole Wear) - Loaded hole fatigue tests were performed to determine the hole wear characteristics of the two BMI systems. Fiber dominated 50/40/10 laminates were tested in compression-only (R = 10) and reversed loading (R = -1) fatigue cycling at two environmental conditions as shown in Figure 118.

Specimen Type	Layup	Loading: Fatigue: Stress Ratio	Stress Level	Environment: CTD	RTD	ETW	Number of Tests Per Material
Loaded Hole	50/40/10	-1.0	L_1		✓		3 + 2[1]
		-1.0	L_1			✓	3 + 1[1]
		-1.0	L_2		✓		3
		-1.0	L_2			✓	3
		10.0	L_1		✓		3 + 1[1]
		10.0	L_1			✓	3
		10.0	L_2		✓		3
		10.0	L_2			✓	3

Note: (1) TBE enhanced x-rays to be taken at ¼, ½, ¾ total life.

GP73-0623-80-R

Figure 118. Loaded Hole Fatigue Test Matrix

4.2.6.1 Data Reduction - Loaded hole fatigue failure was defined as the accumulation of 0.02 inch hole elongation. Stiffness and deflection was monitored periodically during each test. Hole elongation measurements were obtained using the data reduction procedure shown in Figure 119. Typical accumulation of hole elongation with fatigue cycling is shown in Figure 120. For much of the specimen life, little or no hole elongation was observed, until there was a rapid increase near the end of life.

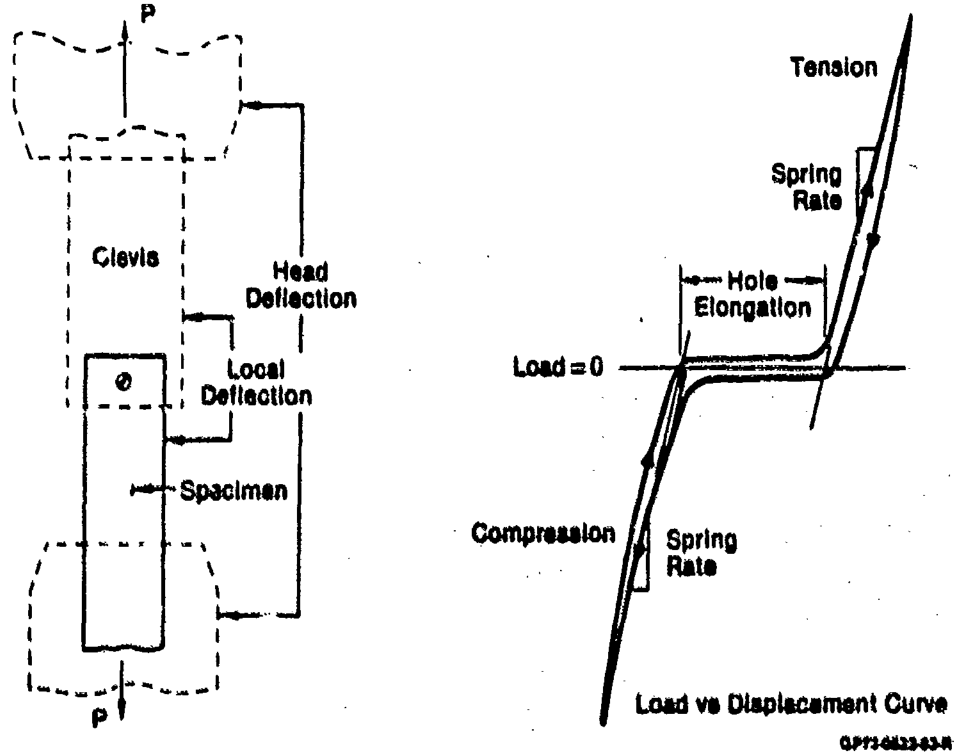

Figure 119. Hole Elongation Determined by Shift in Load Displacement Curve

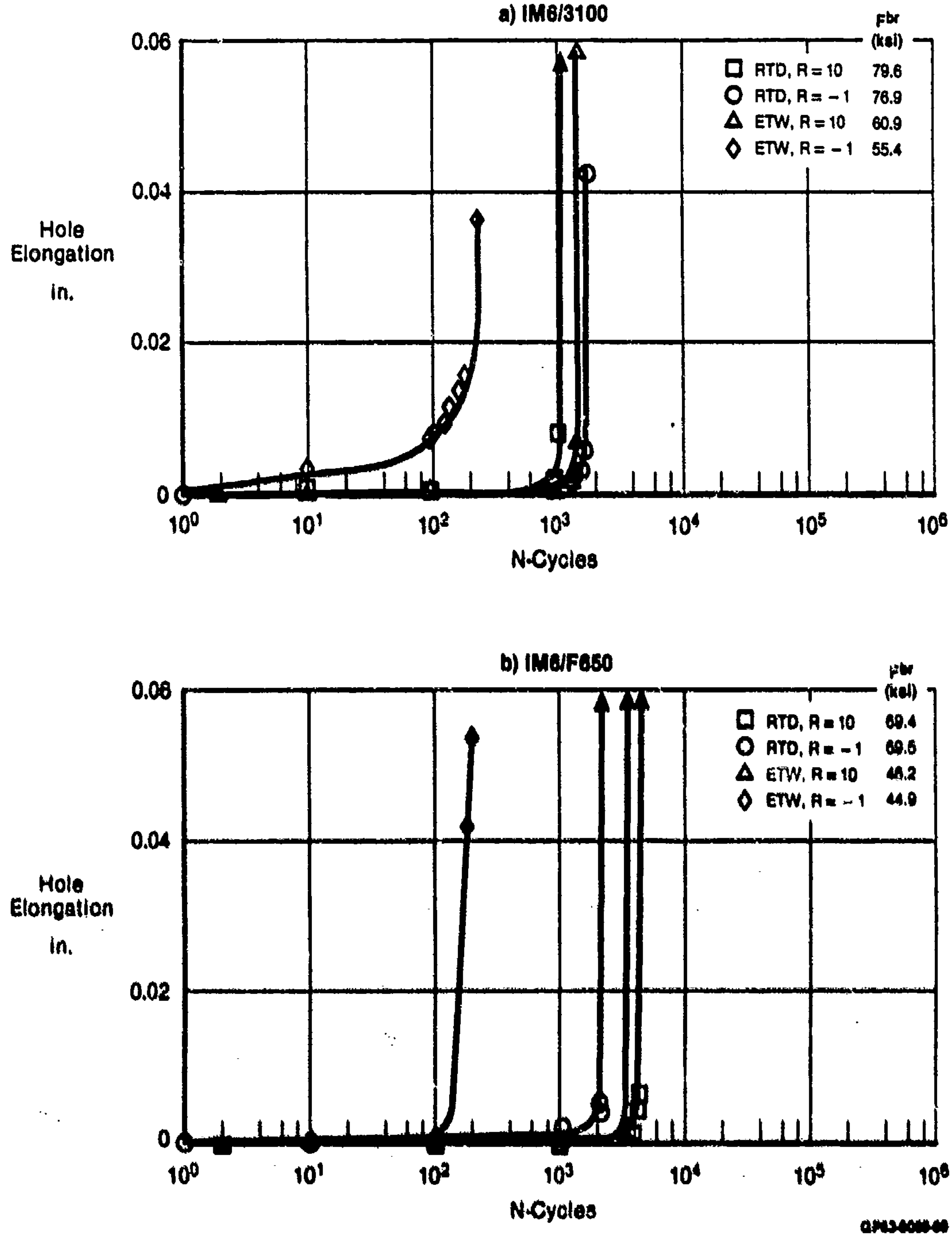

Figure 120. Loaded Hole Elongation Measurements Show Rapid Increase Near End of Life

4.2.6.2 Test Results - The same specimen configuration that was used in static tests was used in fatigue tests (Figure 121). Typical failed specimens are shown in Figure 122. For RTD conditions, stress ratio effects were not apparent. Compression- only (R = 10) cycling and reversed (R = -1) cycling produced failures only on one side of the hole, like that shown in Figure 122a. Under ETW conditions, however, stress ratio effects were evident where R = 10 cycling produced one-sided hole wear and R = -1 cycling produced two-sided hole wear as shown in Figure 122b. Figure 123 shows the progression of damage that leads to loaded hole fatigue failure. Loaded hole fatigue failure is preceded by local matrix crushing at the bearing surfaces of the hole. The X-rays show that the area of crushed matrix gradually grows until the hole wears out (0.02 inch elongation). Data for the loaded hole fatigue tests are tabulated in Figures 124 and 125. The data are plotted in Figures 126 and 127. Each plot shows the static bearing strength plotted at a life of one cycle.

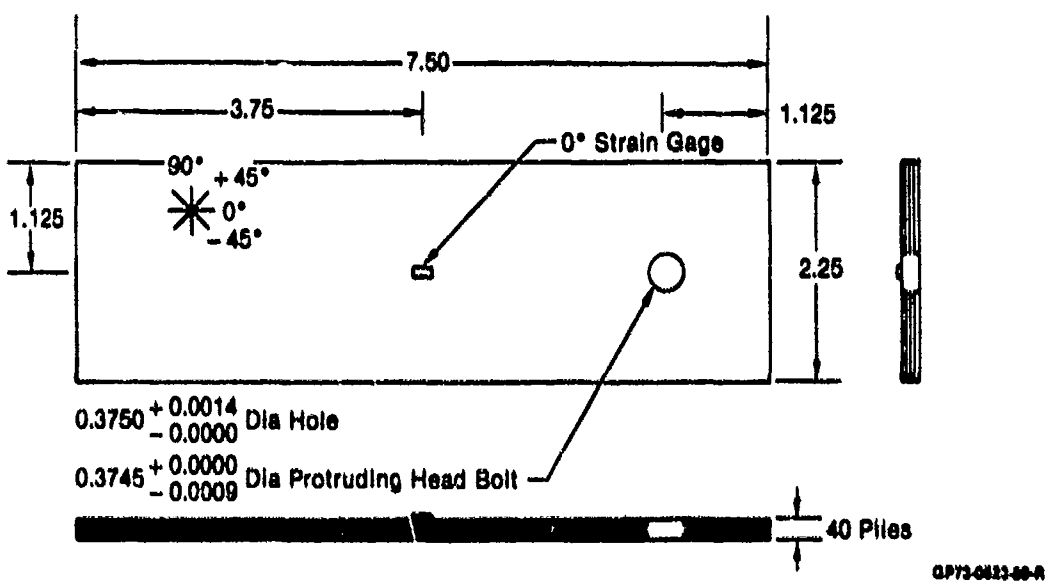

Figure 121. Loaded Hole Fatigue Test Specimen

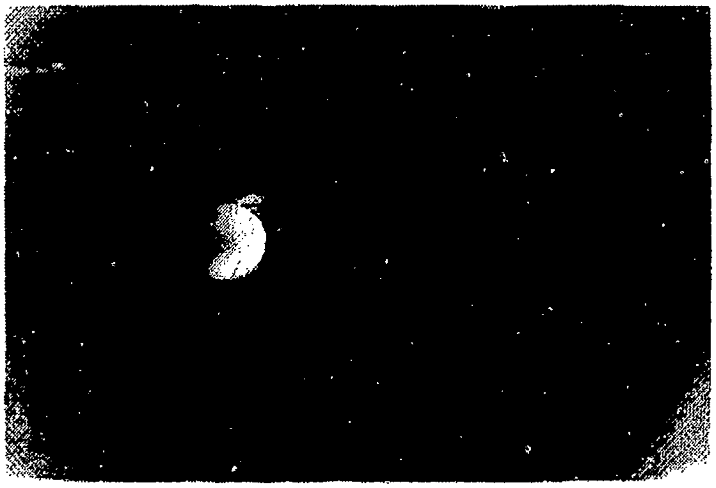

a) RTD

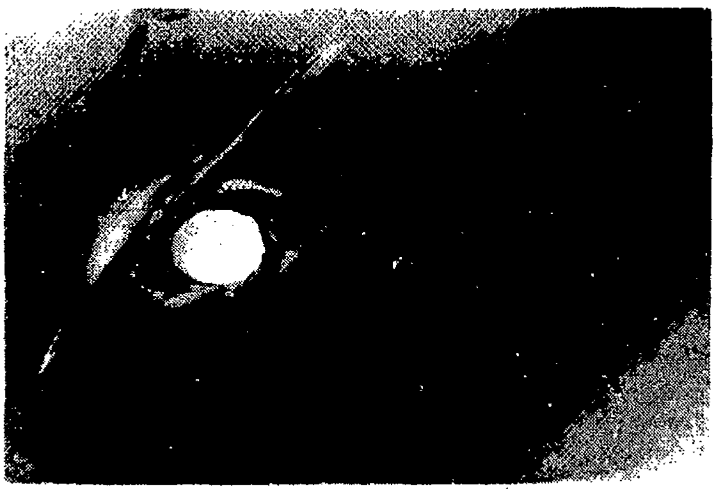

b) ETW

GP83-0089-21

Figure 122. Failed Loaded Hole Fatigue Specimens

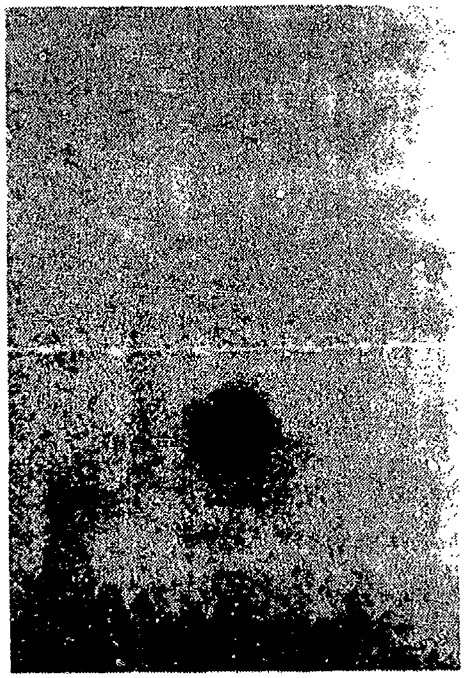

0 Life

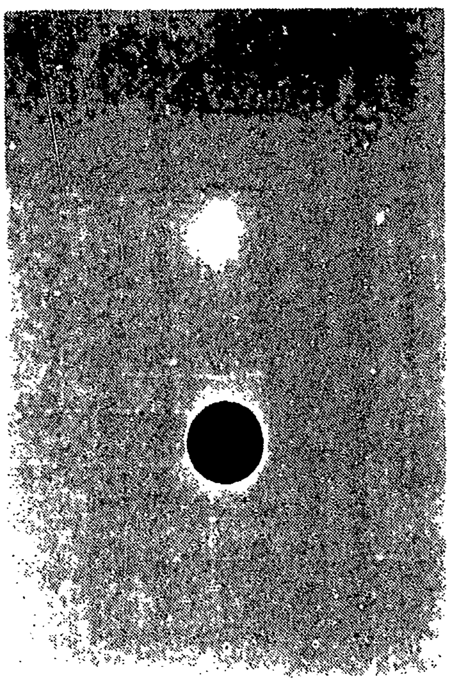

1/4 Life

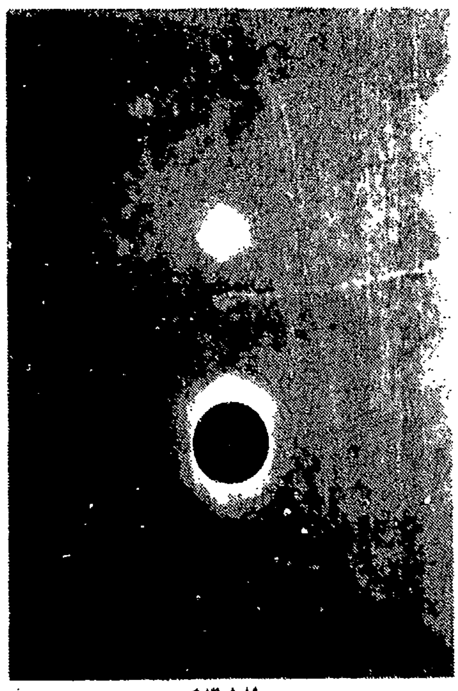

1/2 Life

GP83-0049-22

Figure 123. Progression of Loaded Hole Fatigue Damage (Enhanced X-Rays)

Material System	Specimen Number	Stress Ratio	Load Level (lb)	Bearing Stress Level (ksi)	Thickness (in.)	Width (in.)	Hole Diameter (in.)	Life (Cycles) (1)	Log Mean Life (Cycles)
	1-10B-32				0.224	2.254	0.375	8,600	
IM6/3100	1-10B-33	10	5,530	70.9	0.227	2.255	0.375	8,380	7,550
	1-10B-34				0.227	2.248	0.375	5,960	
	1-10B-25				0.226	2.255	0.375	1,070	
IM6/3100	1-10B-26	10	6,210	79.6	0.226	2.256	0.375	3.920	2,160
	1-10B-27				0.228	2.255	0.375	2,390	
	1-10B-19				0.228	2.254	0.375	4,940	
IM6/3100	1-10B-20	−1	5,620	72.1	0.228	2.252	0.375	4,990	4,550
	1-10B-21				0.228	2.252	0.375	3,830	
	1-10B-10				0.228	2.254	0.375	1,490	
IM6/3100	1-10B-11	−1	6,000	76.9	0.229	2.254	0.375	1,690	1,750
	1-10B-12				0.228	2.253	0.375	2,120	
	2-10B-32				0.222	2.258	0.375	9,600	
IM6/F650	2-10B-33	10	4,790	61.4	0.221	2.258	0.375	11,320	11,300
	2-10B-34				0.221	2.252	0.375	13,260	
	2-10B-25				0.221	2.255	0.375	4,230	
IM6/F650	2-10B-26	10	5,410	69.4	0.222	2.256	0.375	1,500	2,830
	2-10B-27				0.223	2.257	0.375	3,570	
	2-10B-13				0.220	2.254	0.375	19,999	
IM6/F650	2-10B-14	−1	4,520	57.9	0.220	2.254	0.375	21,830	17,180
	2-10B-21				0.221	2.253	0.375	11,610	
	2-10B-10				0.221	2.248	0.375	2,090	
IM6/F650	2-10B-11	−1	5,420	69.5	0.222	2.245	0.375	3,000	1,850
	2-10B-12				0.219	2.253	0.375	1,010	

Note. (1) Life to 0.02 in. of hole elongation

GP83-0088-70-R

Figure 124. Loaded Hole Fatigue Test Data for RTD Conditions

Material System	Specimen Number	Stress Ratio	Load Level (lb)	Bearing Stress Level (ksi)	Thickness (in.)	Width (in.)	Hole Diameter (in.)	Life (Cycles) (1)
	1-10B-35		4,750	60.9	0.228	2.256	0.375	1,470
IM6/3100	1-10B-36	10	4,200	53.8	0.228	2.258	0.375	33,200
	1-10B-37		4,200	53.8	0.226	2.255	0.375	4,650
	1-10B-29		5,000	64.1	0.226	2.254	0.375	990
IM6/3100	1-10B-30	10	5,200	66.7	0.227	2.255	0.375	620
	1-10B-31		5,200	66.7	0.226	2.254	0.375	100
	1-10B-22		3,800	48.7	0.228	2.252	0.375	139,000+
IM6/3100	1-10B-23	−1	4,100	52.6	0.226	2.253	0.375	30,000+
	1-10B-24		4,250	54.5	0.226	2.252	0.375	7,430
	1-10B-15		4,320	55.4	0.227	2.251	0.375	190
IM6/3100	1-10B-16	−1	4,320	55.4	0.227	2.252	0.375	260
	1-10B-17		4.320	55.4	0.226	2.251	0.375	3,650
	2-10B-29		3,600	46.2	0.222	2.257	0.375	3,880
IM6/F650	2-10B-30	10	3,600	46.2	0.222	2.257	0.375	7,600
	2-10B-31		3,600	46.2	0.222	2.257	0.375	77,000+
	2-10B-35		4,000	51.3	0.222	2.257	0.375	3,330
IM6/F650	2-10B-36	10	3,200	41.0	0.221	2.257	0.375	5,230
	2-10B-37		3,200	41.0	0.222	2.256	0.375	69,700+
	2-10B-24		2,730	35.0	0.220	2.254	0.375	82,100
IM6/F650	2-10B-S10	−1	2,900	37.2	0.220	2.258	0.375	272,500+
	2-10B-S11		3,100	39.7	0.221	2.256	0.375	107,200
	2-10B-16		3,520	45.1	0.222	2.253	0.375	60
IM6/F650	2-10B-S12	−1	3,500	44.9	0.219	2.257	0.375	250
	2-10B-S13		3,500	44.9	0.222	2.259	0.375	170

Note: (1) Life to 0.02 in. of hole elongation.

GP83-0089-71-R

Figure 125. Loaded Hole Fatigue Test Data for ETW Conditions

The data in Figure 126 is for RTD testing. The data is plotted in terms of the log mean life surrounded by its 90 percent confidence interval determined for each data set. The data show that under RTD conditions there is no stress ratio (R) effect on fatigue life. Compression-only (R = 10) and reversed (R = -1) cycling resulted in similar lives for both materials. An explanation for this behavior is that the failure mode was dominated by localized matrix crushing due to bearing loads. Once hole wear initiated in the brittle matrix, damage progressed rapidly. The sense of the loading, whether it was tension or compression, was irrelevant.

a) Loaded Hole Fatigue Test Results: R = 10

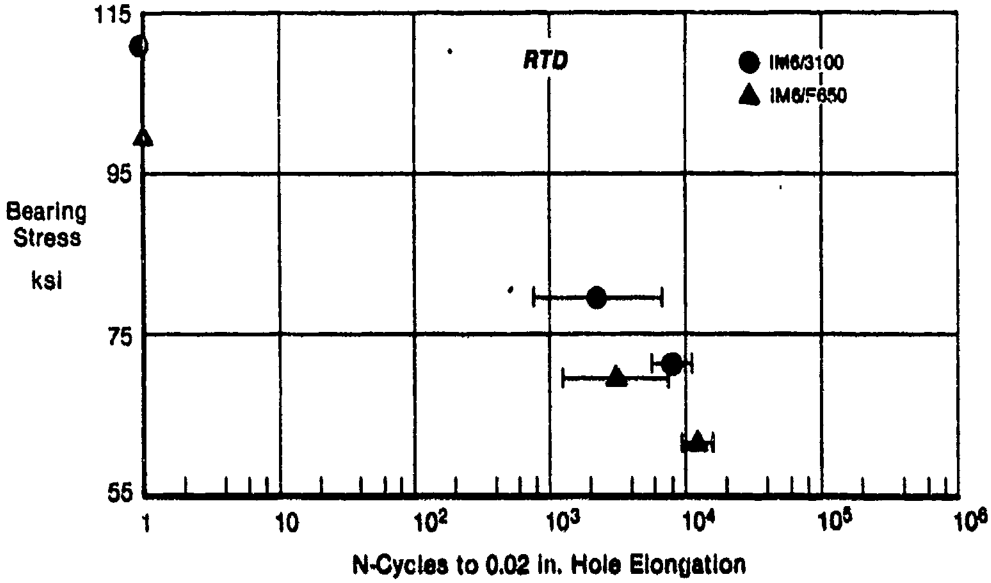

b) Loaded Hole Fatigue Test Results: R = −1

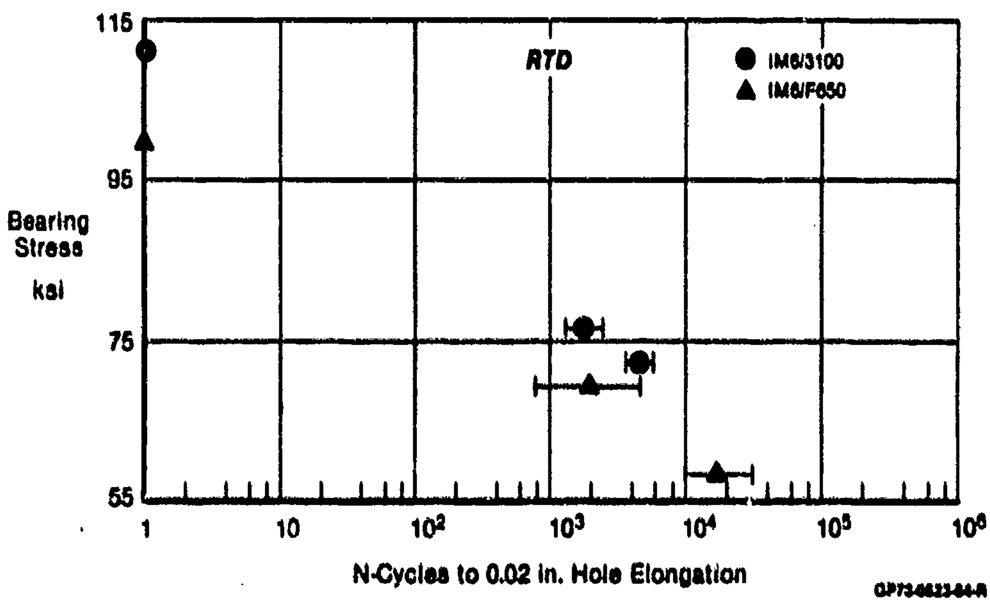

GP73-0623-64-R

Figure 126. Loaded Hole Fatigue Test Results for RTD Conditions

The data in Figure 127 is plotted as individual points. Under ETW conditions, the loaded hole fatigue specimens dried out, resulting in large life scatter. The data show that for a loaded hole fatigue life of 10,000 cycles, the permissible bearing stress level for IM6/3100 is 79 percent (55 ksi vs 70 ksi) of the stress level for RTD conditions. The value for IM6/F650 is 75 percent (45 ksi vs 60 ksi).

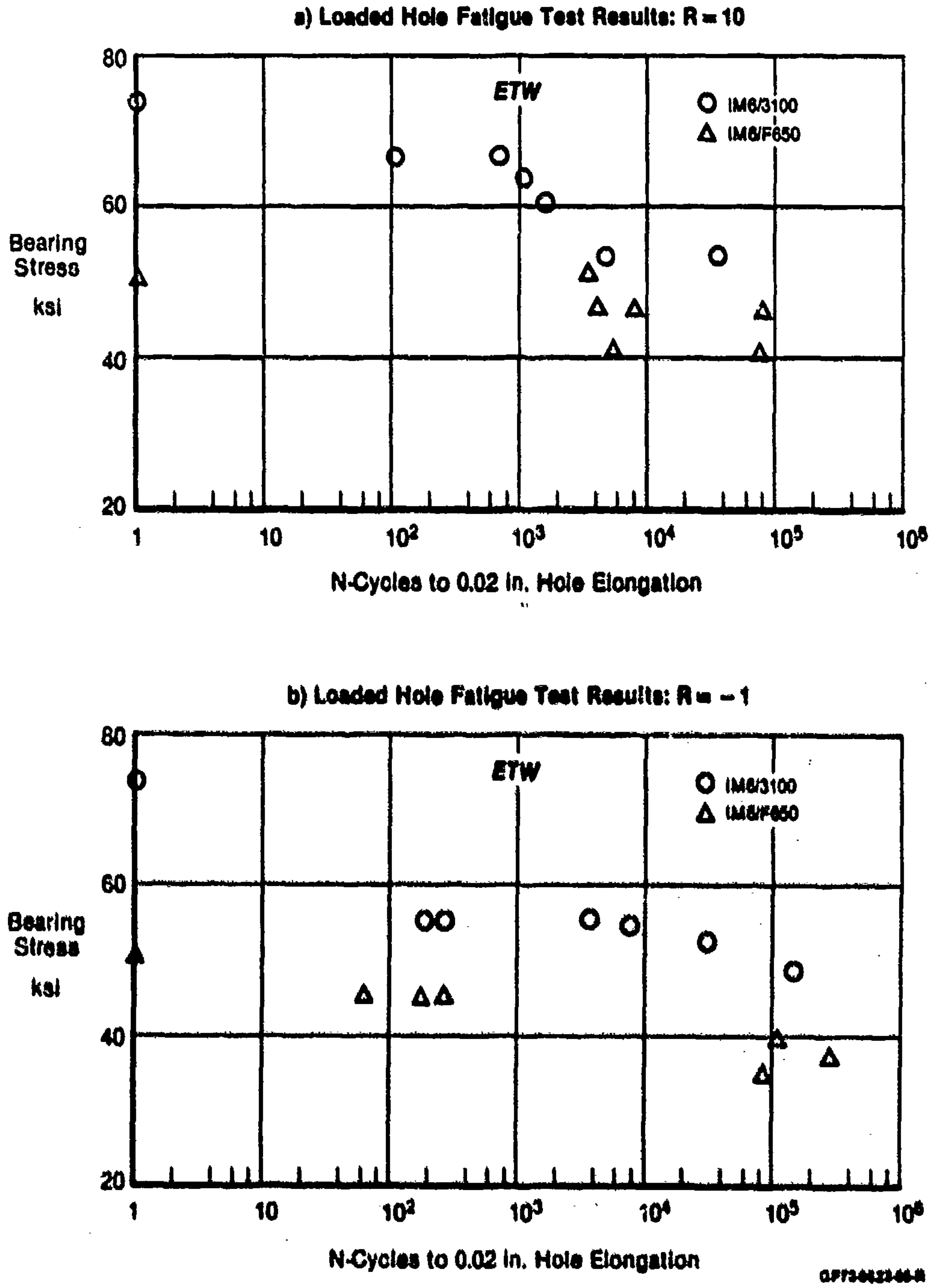

Figure 127. Loaded Hole Fatigue Test Results for ETW Conditions

4.2.7 Low-Velocity Impact Damage/Residual Compression Strength - Low-velocity impact tests were performed to determine the strength of damaged bismaleimide panels. The test program is outlined in Figure 128. Impact tests were performed to determine the maximum energy level that a panel could sustain without showing signs of surface damage. Tests were performed on thin panels, less than 0.080 inch thick, to investigate the impact response of very thin skins. Visible damage tests were performed on thicker panels to determine the strength degradation due to impacts with energies (not to exceed 100 ft-lbs.) sufficient to create a 0.1 inch dent.

4.2.7.1 Test Results - The impact specimen configuration is shown in Figure 129. The 7 inch by 11 inch panels were constrained such that there was a 5 inch by 5 inch unsupported area as shown in Figure 130. All panels were impacted with 1 inch diameter impactor. Prior to impact, the specimen was instrumented with a strain gage on the back side directly under the impact site. This gage was used to monitor panel response during impact. After impact, the panel was instrumented with five strain gages as shown in Figure 129. Back-to-back pair 1,2 was located adjacent to surface damage. Two back-to-back pairs (1,2 and 3,4) were used to monitor delamination buckling response during residual compression strength testing. The single gage (5) was used to monitor far field panel response.

In addition to strain gaging, instrumentation was provided to measure acceleration (and hence loads) during impact. Approach and rebound velocities were measured with optical sensors. Data summarized in Figures 131 through 136 include impact energy, dent depth, and residual compression strength for the 216 impact tests. More data is presented in the Appendix volume of this report.

Maximum non-visible damage was defined as a dent depth of approximately 0.01 inch. This damage was discernible under close inspection, but was not severe enough to be detected during a walk-around inspection of an aircraft. The data in Figures 131 and 132 show that the energy threshold for non-visible damage in fiber dominated 50/40/10 laminates is generally one and one-half to two times as great as the energy threshold for comparable matrix

dominated 10/80/10 laminates. IM6/3100 had higher energy thresholds for non-visible damage than IM6/F650. Residual compression strengths of IM6/3100 were also higher than those of IM6/F650.

Damage Type	Layup	Nominal Thickness	Environment		Number of Residual Strength Compression Tests Per Material
			RTD	ETW	
Maximum Non-Visible Damage	10/80/10	0.104	✓		3
				✓	3
		0.208	✓		3
				✓	3
		0.416	✓		3
				✓	3
	50/40/10	0.104	✓		3
				✓	3
		0.208	✓		3
				✓	3
		0.416	✓		3
				✓	3
Thin Laminate Damage	0/100/0	0.021	✓		3
				✓	3
		0.042	✓		3
				✓	3
		0.062	✓		3
				✓	3
	50/0/50	0.021	✓		3
				✓	3
		0.042	✓		3
				✓	3
		0.062	✓		3
				✓	3
Visible Damage (0.1 in. Dent)	10/80/10	0.104	✓		3
				✓	3
		0.208	✓		3
				✓	3
		0.416	✓		3
				✓	3
	50/40/10	0.104	✓		3
				✓	3
		0.208	✓		3
				✓	3
		0.416	✓		3
				✓	3
Total Number of Tests Per Material					108
Total Tests (2 Materials)					216

Figure 128. Low-Velocity Impact Test Matrix

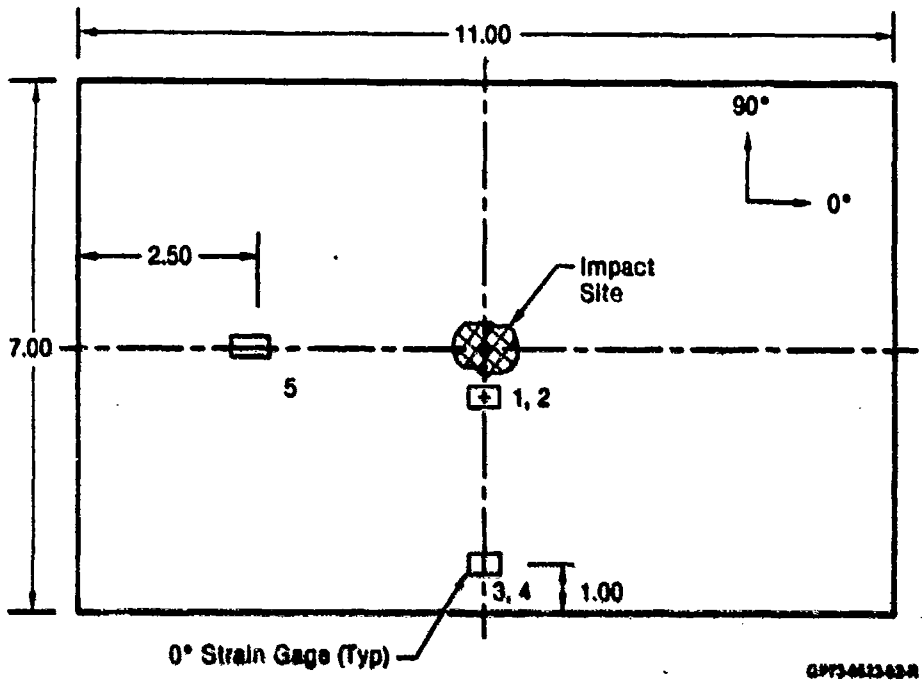

Figure 129. Low-Velocity Impact Test Specimen Instrumented for Residual Compression Strength Testing

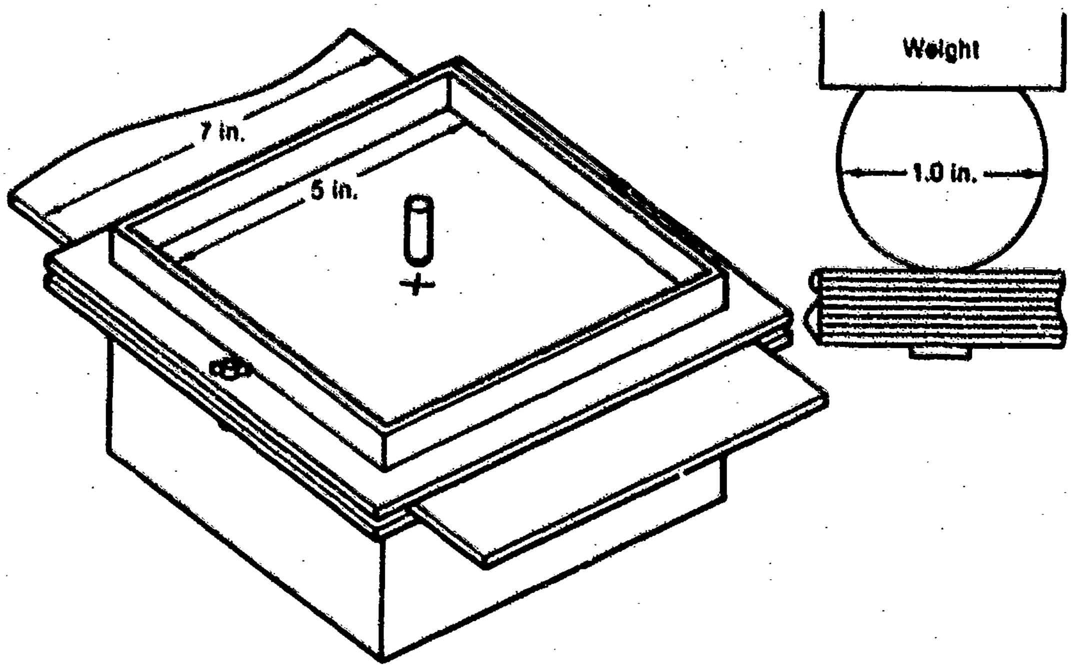

Figure 130. Low-Velocity Impact Damage Test Setup

Material	Specimen Number	Layup	Thickness (in.)	Impact Energy (ft-lb)	Dent Depth (in.)	Residual Compression Strength (ksi) Ind	Residual Compression Strength (ksi) Avg
	1-12-1		0.114	8	0.005	31.7	
IM6/3100	1-12-2	10/80/10	0.114	8	0.005	32.1	31.4
	1-12-3		0.114	8	0.005	30.4	
	1-11-1		0.223	14	0.008	27.7	
IM6/3100	1-11-2	10/80/10	0.221	14	0.009	26.8	27.1
	1-11-3		0.222	14	0.009	26.8	
	1-13-1		0.451	17.5/23	0.004/0.008	29.2	
IM6/3100	1-13-2	10/80/10	0.452	17.5/23	0.001/0.007	34.5	30.2
	1-13-3		0.450	17.5/23	0.005/0.010	27.0	
	1-14-1		0.109	14	0.006	37.1	
IM6/3100	1-14-2	50/40/10	0.110	14	0.006	38.5	36.6
	1-14-3		0.109	14	0.006	34.3	
	1-20-1		0.224	23	0.010	32.7	
IM6/3100	1-20-2	50/40/10	0.224	23	0.011	30.8	31.4
	1-20-3		0.223	23	0.012	30.7	
	1-15-1		0.455	42	0.012	36.2	
IM6/3100	1-15-2	50/40/10	0.453	42	0.012	36.2	36.0
	1-15-3		0.451	42	0.011	35.6	
	2-12-1		0.107	6	0.007	23.0	
IM6/F650	2-12-2	10/80/10	0.106	6	0.007	21.4	22.2
	2-12-3		0.108	6	0.007	22.2	
	2-11-1		0.215	7	0.009	22.1	
IM6/F650	2-11-2	10/80/10	0.218	7	0.011	22.1	21.8
	2-11-3		0.218	7	0.010	21.2	
	2-13-1		0.436	20	0.012	22.5	
IM6/F650	2-13-2	10/80/10	0.438	20	0.010	22.6	22.3
	2-13-3		0.440	20	0.013	21.8	
	2-14-1		0.111	14	0.007	32.0	
IM6/F650	2-14-2	50/40/10	0.112	14	0.006	28.4	29.4
	2-14-3		0.111	14	0.007	27.8	
	2-20-1		0.218	10	0.012	26.7	
IM6/F650	2-20-2	50/40/10	0.219	10	0.012	28.1	27.0
	2-20-3		0.219	10	0.009	26.2	
	2-15-1		0.433	35	0.017	26.3	
IM6/F650	2-15-2	50/40/10	0.443	35	0.017	26.5	26.4
	2-15-3		0.440	35	0.015	26.4	

Figure 131. Maximum Non-Visible Damage Data for RTD Conditions

Material	Specimen Number	Layup	Thickness (in.)	Impact Energy (ft-lb)	Dent Depth (in.)	Residual Compression Strength (ksi)	
						Ind	Avg
	1-12-4		0.114	8	0.005	22.9	
IM6/3100	1-12-5	10/80/10	0.114	8	0.005	22.0	22.7
	1-12-6		0.114	8	0.005	23.3	
	1-11-4		0.222	14	0.009	23.7	
IM6/3100	1-11-5	10/80/10	0.222	14	0.009	21.2	23.1
	1-11-6		0.223	14	0.009	24.4	
	1-13-4		0.449	23	0.006	24.8	
IM6/3100	1-13-5	10/80/10	0.454	23	0.004	24.6	25.4
	1-13-6		0.454	23	0.006	26.8	
	1-14-4		0.110	14	0.005	32.6	
IM6/3100	1-14-5	50/40/10	0.110	14	0.006	33.0	31.8
	1-14-6		0.110	14	0.006	29.9	
	1-20-4		0.225	23	0.008	25.4	
IM6/3100	1-20-5	50/40/10	0.223	23	0.012	25.2	25.5
	1-20-6		0.223	23	0.012	25.9	
	1-15-4		0.451	17.5/23	0.006/0.010	28.5	
IM6/3100	1-15-5	50/40/10	0.445	17.5/23	0.008/0.010	33.0	28.9
	1-15-6		0.448	17.5/23	0.007/0.011	25.2	
	2-12-4		0.107	6	0.006	17.9	
IM6/F650	2-12-5	10/80/10	0.106	6	0.007	17.5	17.4
	2-12-6		0.106	6	0.006	16.7	
	2-11-4		0.216	7	0.011	18.5	
IM6/F650	2-11-5	10/80/10	0.216	7	0.011	17.2	17.7
	2-11-6		0.216	7	0.011	17.5	
	2-13-4		0.438	20	0.012	16.5	
IM6/F650	2-13-5	10/80/10	0.436	15	0.010	17.1	—
	2-13-6		0.438	15	0.011	17.5	
	2-14-4		0.112	14	0.007	24.2	
IM6/F650	2-14-5	50/40/10	0.111	14	0.006	23.5	23.2
	2-14-6		0.112	14	0.006	22.0	
	2-20-4		0.219	10	0.012	21.6	
IM6/F650	2-20-5	50/40/10	0.217	10	0.012	19.1	20.8
	2-20-6		0.218	10	0.011	21.7	
	2-15-4		0.441	35	0.016	18.9	
IM6/F650	2-15-5	50/40/10	0.440	35	0.016	17.8	18.8
	2-15-6		0.442	35	0.017	19.7	

GP63-0080-45-T

Figure 132. Maximum Non-Visible Damage Data for ETW Conditions

Impact tests were performed on thin (less than 0.080 inch thick) laminates to obtain data that would be representative of thin skin structure. All thin laminate tests were performed with impact energies of 5 ft-lbs. The data in Figures 133 and 134 show that IM6/3100 retained higher residual compression strengths than IM6/F650.

Material	Specimen Number	Layup	Thickness (In.)	Impact Energy (ft-lb)	Dent Depth (In.)	Residual Compression Strength (ksi)	
						Ind	Avg
	1-16-1		0.024	5	0.002	10.9	
IM6/3100	1-16-2	0/100/0	0.024	5	0.001	11.5	11.3
	1-16-3		0.024	5	0.001	11.5	
	1-12A-1		0.045	5	0.004	17.0	
IM6/3100	1-12A-2	0/100/0	0.045	5	0.005	17.9	17.2
	1-12A-3		0.045	5	0.004	16.6	
	1-17-1		0.068	5	0.004	20.7	
IM6/3100	1-17-2	0/100/0	0.068	5	0.004	20.8	21.0
	1-17-3		0.069	5	0.004	21.5	
	1-18-1		0.025	5	0.025	15.5	
IM6/3100	1-18-2	50/0/50	0.025	5	0.030	17.1	17.0
	1-18-3		0.025	5	<0.001	18.5	
	1-14A-1		0.046	5	0.004	23.4	
IM6/3100	1-14A-2	50/0/50	0.047	5	0.004	23.5	23.5
	1-14A-3		0.046	5	0.004	23.5	
	1-19-1		0.065	5	0.004	24.1	
IM6/3100	1-19-2	50/0/50	0.065	5	0.004	28.6	27.2
	1-19-3		0.065	5	0.004	28.9	
	2-16-1		0.022	5	0.011	9.1	
IM6/F650	2-16-2	0/100/0	0.022	5	0.001	9.4	9.2
	2-16-3		0.021	5	0.001	9.0	
	2-12A-1		0.044	5	0.005	13.7	
IM6/F650	2-12A-2	0/100/0	0.044	5	0.005	14.6	13.7
	2-12A-3		0.043	5	0.004	12.8	
	2-17-1		0.064	5	0.004	15.8	
IM6/F650	2-17-2	0/100/0	0.064	5	0.005	16.5	16.5
	2-17-3		0.064	5	0.005	17.3	
	2-18-1		0.023	5	<0.001	11.3	
IM6/F650	2-18-2	50/0/50	0.023	5	<0.001	11.0	11.3
	2-18-3		0.022	5	<0.001	11.5	
	2-14A-1		0.043	5	0.005	20.3	
IM6/F650	2-14A-2	50/0/50	0.044	5	0.004	20.7	20.6
	2-14A-3		0.044	5	0.005	20.7	
	2-19-1		0.063	5	0.004	18.2	
IM6/F650	2-19-2	50/0/50	0.064	5	0.005	19.2	20.7
	2-19-3		0.064	5	0.005	24.6	

GP83-0000-88-T

Figure 133. Thin Laminate Damage Data for RTD Conditions

Material	Specimen Number	Layup	Thickness (in.)	Impact Energy (ft-lb)	Dent Depth (in.)	Residual Compression Strength (ksi)	
						Ind	Avg
	1-16-4		0.024	5	<0.001	8.9	
IM6/3100	1-16-5	0/100/0	0.025	5	<0.001	9.3	9.0
	1-16-6		0.024	5	0.001	8.8	
	1-12A-4		0.044	5	0.004	12.3	
IM6/3100	1-12A-5	0/100/0	0.045	5	0.004	12.5	12.1
	1-12A-6		0.045	5	0.003	11.6	
	1-17-4		0.069	5	0.004	13.3	
IM6/3100	1-17-5	0/100/0	0.069	5	0.004	12.1	12.2
	1-17-6		0.069	5	0.004	11.2	
	1-18-4		0.025	5	0.020	16.3	
IM6/3100	1-18-5	50/0/50	0.025	5	<0.001	20.5	18.8
	1-18-6		0.025	5	0.002	19.6	
	1-14A-4		0.046	5	0.004	27.2	
IM6/3100	1-14A-5	50/0/50	0.047	5	0.003	24.5	23.5
	1-14A-6		0.046	5	0.004	26.4	
	1-19-4		0.066	5	0.004	20.5	
IM6/3100	1-19-5	50/0/50	0.065	5	0.004	18.7	17.6
	1-19-6		0.066	5	0.004	13.7	
	2-16-4		0.021	5	0.001	6.1	
IM6/F650	2-16-5	0/100/0	0.022	5	0.001	6.1	6.8
	2-16-6		0.021	5	0.001	8.1	
	2-12A-4		0.043	5	0.004	9.3	
IM6/F650	2-12A-5	0/100/0	0.044	5	0.004	9.1	9.4
	2-12A-6		0.043	5	0.004	9.9	
	2-17-4		0.063	5	0.005	9.2	
IM6/F650	2-17-5	0/100/0	0.065	5	0.005	10.3	9.7
	2-17-6		0.064	5	0.005	9.7	
	2-18-4		0.022	5	0.015	10.6	
IM6/F650	2-18-5	50/0/50	0.022	5	0.015	11.7	11.6
	2-18-6		0.022	5	0.010	12.5	
	2-14A-4		0.044	5	0.005	18.9	
IM6/F650	2-14A-5	50/0/50	0.044	5	0.004	20.0	20.2
	2-14A-6		0.043	5	0.005	21.7	
	2-19-4		0.062	5	0.004	16.0	
IM6/F650	2-19-5	50/0/50	0.062	5	0.004	14.4	15.7
	2-19-6		0.062	5	0.004	16.6	

GP83-0089-61-T

Figure 134. Thin Laminate Damage Data for ETW Conditions

The final category of impact testing was visible damage. In this set of tests, panels were impacted with energy sufficient to cause a 0.1 inch dent, but not exceeding 100 ft-lbs. The data in Figures 135 and 136 show that under similar impact conditions both IM6/3100 and IM6/F650 exhibited similar dent depths. The residual compression strength of IM6/3100 was superior to IM6/F650 for all cases.

Material	Specimen Number	Layup	Thickness (in.)	Impact Energy (ft-lb)	Dent Depth (in.)	Residual Compression Strength (ksi)	
						Ind	Avg
	1-12-7		0.115	60	0.145	17.4	
IM6/3100	1-12-8	10/80/10	0.113	60	0.200	20.1	—
	1-12-9		0.115	45	0.112	19.6	
	1-11-7		0.223	100	0.080	15.4	
IM6/3100	1-11-8	10/80/10	0.222	100	0.083	16.3	16.0
	1-11-9		0.223	100	0.091	16.4	
	1-13-7		0.450	100	0.016	19.4	
IM6/3100	1-13-8	10/80/10	0.448	100	0.017	20.2	20.0
	1-13-9		0.451	100	0.018	20.3	
	1-14-7		0.110	45	0.120	27.3	
IM6/3100	1-14-8	50/40/10	0.110	45	0.100	29.8	28.4
	1-14-9		0.110	45	0.118	28.1	
	1-20-7		0.223	100	0.087	21.8	
IM6/3100	1-20-8	50/40/10	0.224	100	0.103	23.0	22.3
	1-20-9		0.224	100	0.110	22.1	
	1-15-7		0.453	100	0.020	28.6	
IM6/3100	1-15-8	50/40/10	0.452	100	0.018	27.3	27.9
	1-15-9		0.449	100	0.021	27.9	
	2-12-7		0.107	55	0.110	10.8	
IM6/F650	2-12-8	10/80/10	0.106	55	0.095	11.2	10.6
	2-12-9		0.107	55	0.096	9.9	
	2-11-7		0.216	100	0.049	9.8	
IM6/F650	2-11-8	10/80/10	0.216	100	0.078	10.3	10.7
	2-11-9		0.216	100	0.072	12.0	
	2-13-7		0.436	100	0.028	13.9	
IM6/F650	2-13-8	10/80/10	0.437	100	0.030	14.0	14.1
	2-13-9		0.440	100	0.021	14.4	
	2-14-7		0.111	45	0.105	19.9	
IM6/F650	2-14-8	50/40/10	0.112	45	0.090	18.8	20.7
	2-14-9		0.112	45	0.085	23.4	
	2-20-7		0.218	100	0.049	16.9	
IM6/F650	2-20-8	50/40/10	0.219	100	0.040	18.0	17.4
	2-20-9		0.220	100	0.087	17.3	
	2-15-7		0.441	100	0.027	20.0	
IM6/F650	2-15-8	50/40/10	0.439	100	0.030	19.8	20.1
	2-15-9		0.440	100	0.030	20.4	

GP73-0623-100-R

Figure 135. Visible Damage Data for RTD Conditions

Material	Specimen Number	Layup	Thickness (in.)	Impact Energy (ft-lb)	Dent Depth (in.)	Residual Compression Strength (ksi)	
						Ind	Avg
	1-12-10		0.114	100	Hole	14.2	
IM6/3100	1-12-11	10/80/10	0.114	60	0.130	14.5	—
	1-12-12		0.114	60	0.130	14.4	
	1-11-10		0.222	100	0.093	13.6	
IM6/3100	1-11-11	10/80/10	0.223	100	0.096	15.0	14.4
	1-11-12		0.223	100	0.091	14.7	
	1-13-10		0.452	100	0.019	15.5	
IM6/3100	1-13-11	10/80/10	0.452	100	0.015	15.8	15.4
	1-13-12		0.452	100	0.017	14.9	
	1-14-10		0.109	45	0.101	20.9	
IM6/3100	1-14-11	50/40/10	0.109	45	0.120	21.8	23.0
	1-14-12		0.109	45	0.122	26.3	
	1-20-10		0.222	100	0.094	22.4	
IM6/3100	1-20-11	50/40/10	0.225	100	0.090	18.1	18.9
	1-20-12		0.224	100	0.086	16.2	
	1-15-10		0.454	100	0.020	22.2	
IM6/3100	1-15-11	50/40/10	0.452	100	0.020	21.7	22.7
	1-15-12		0.448	100	0.021	24.3	
	2-12-10		0.107	100	Hole	10.2	
IM6/F650	2-12-11	10/80/10	0.106	45/45	0.067/0.110	9.2	—
	2-12-12		0.106	45/45	0.080/0.130	11.0	
	2-11-10		0.215	100	0.047	10.1	
IM6/F650	2-11-11	10/80/10	0.217	100	0.045	9.4	9.1
	2-11-12		0.216	100	0.065	7.9	
	2-13-10		0.437	100	0.026	10.9	
IM6/F650	2-13-11	10/80/10	0.431	100	0.027	11.8	11.2
	2-13-12		0.438	100	0.029	11.0	
	2-14-10		0.111	45	0.085	18.7	
IM6/F650	2-14-11	50/40/10	0.110	45	0.086	17.3	17.1
	2-14-12		0.110	45	0.083	15.3	
	2-20-10		0.218	100	0.045	15.1	
IM6/F650	2-20-11	50/40/10	0.217	100	0.077	14.1	14.5
	2-20-12		0.216	100	0.052	14.2	
	2-15-10		0.440	100	0.027	15.6	
IM6/F650	2-15-11	50/40/10	0.436	100	0.028	15.5	15.7
	2-15-12		0.436	100	0.027	16.1	

GP63-0669-62-T

Figure 138. Visible Damage Data for ETW Conditions

Figures 137 and 138 summarize the residual compression strengths of both material systems. In each figure, the maximum strength shown is the RTD unnotched strength. For 10/80/10 and 50/40/10 laminates the impact damage degradation is greater than environmental (ETW) degradation. Figure 138 shows that both non-visible and visible impact damage degradation is greater than the combination of environmental (ETW) and notched degradation; notched data was available from testing in this program only for 50/40/10 laminates.

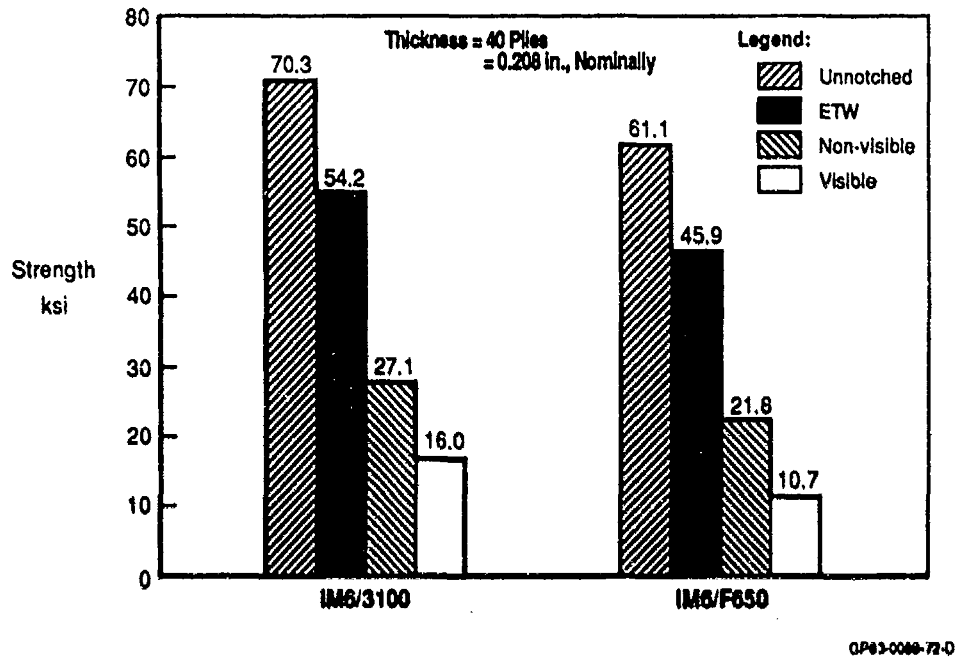

Figure 137. Residual Compression Strength in 10/80/10 Laminates

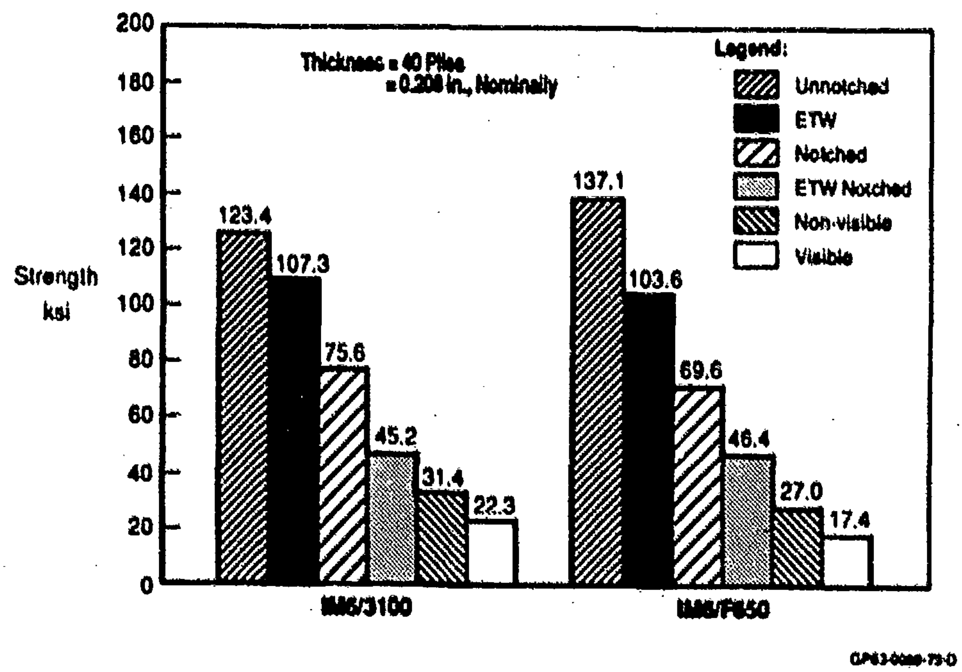

Figure 138. Residual Compression Strength in 50/40/10 Laminates

SECTION 5.

TASK IV: STRUCTURAL ELEMENT DESIGN AND TESTING

5.1 Summary and Conclusions - In the earlier Tasks, the better bismaleimide composite was determined to be IM6/3100. This material was used to fabricate eight stiffened panels for static and fatigue testing. Four of the eight panels were impacted in three locations. Impact energies were sufficient to cause non-visible damage with surface dent depths of less than 0.01 inch.

Static test results showed that the non-visible impact damage reduced RTD compression strength to 74 percent of the undamaged RTD compression strength. Exposing a wet (0.71 percent moisture content) undamaged panel to elevated temperature (360°F) reduced the compression strength to 72 percent of the undamaged RTD compression strength. Impacting a panel, moisturizing it to 0.71 percent moisture content and testing it at 360°F reduced the compression strength to 56 percent of the undamaged RTD compression strength.

Fatigue test results showed that the non-visible impact damage did not grow significantly during fatigue cycling. This was illustrated by A-scans of damage area and strain gage data recorded between fatigue blocks. The lack of significant growth during fatigue cycles correlated with the crack growth data collected during Task II fracture toughness fatigue testing. That data showed that crack growth curves for IM6/3100 Mode I, mixed mode, and Mode II testing were steep. The threshold energy level was nearly equal to the critical energy level, indicating that delamination growth would not occur until critical energy levels were developed. This behavior was apparent as damaged fatigue panels failed during increases in maximum fatigue loads, during strain surveys between fatigue cycle blocks.

5.2 Bismaleimide Material Selection - Based on test results from Task II and III, IM6/3100 was selected as the material for panel fabrication and testing in Task IV. Moisture absorption and glass transition temperature testing indicated that IM6/F650 would have 50°F more hot/wet temperature capability than IM6/3100. Testing both materials under this assumption has shown that IM6/3100 is superior to IM6/F650. The advantage of higher temperature capability attributed to IM6/F650 was not realized.

The resistance to microcracking due to thermal spiking was greater for IM6/3100 than for IM6/F650. Dry laminates for both material systems showed no resin microcracks after thermal spiking. Wet IM6/3100 laminates also showed no resin microcracks. In contrast, wet IM6/F650 laminates did show microcracks after thermal spiking.

Lamina mechanical properties of IM6/3100 at room temperature dry (RTD) and cold temperature dry (CTD) conditions were generally superior to IM6/F650. Under elevated temperature wet (ETW) conditions the IM6/3100 material system suffered less degradation than the IM6/F650 system. The IM6/3100 retained 51 percent of RTD 0° compression strength and IM6/F650 retained only 42 percent. The IM6/3100 retained 84 percent of RTD intra-laminar shear strength and IM6/F650 retained only 59 percent.

The fracture toughness of IM6/3100 was superior to IM6/F650. Under CTD and RTD conditions IM6/3100 was approximately 1.5 times as tough as IM6/F650. Under ETW conditions the IM6/3100 toughness increased and the IM6/F650 toughness decreased resulting in an IM6/3100 toughness that was more than 2 times greater than IM6/F650.

Laminate property tests have shown that the superiority of IM6/3100 lamina properties has translated into superior laminate properties. The CTD unnotched tension strength of fiber dominated IM6/3100 laminates was 13 percent greater than that of IM6/F650. The RTD unnotched tension strength of IM6/3100 was 5 percent greater than that of IM6/F650.

The CTD unloaded hole compression strength of fiber dominated IM6/3100 laminates was 6 percent greater than that of IM6/F650. The RTD unloaded hole compression strength of IM6/3100 was 9 percent greater than that of IM6/F650. The superiority of IM6/3100 in this case has translated into improved fatigue capability and durability which has been observed during unloaded hole fatigue tests.

Low-velocity impact damage test results also showed the superiority of IM6/3100 to IM6/F650. Data from non-visible, thin laminate, and visible damage tests of fiber dominated laminates and matrix dominated laminates

showed that the residual compression strength of IM6/3100 was between 30 percent and 50 percent higher than that of IM6/F650.

5.3 Testing and Evaluation - Eight tests to evaluate the effect of low velocity impact damage were performed. Four static tests determined residual compression strength of impacted panels. Four fatigue tests determined residual life of impacted panels.

5.3.1 Panel Fabrication - The eight panels fabricated for Task IV testing were multibay and incorporated both longitudinal and transverse integral stiffeners as shown in Figure 139. Longitudinal stiffening simulating fuselage longerons was provided by integral hat stiffeners layed up as shown in Figure 140, at 6.5 inch centers. Transverse stiffening representing fuselage frames was provided by blade stiffeners layed up as shown in Figure 141, with 16 inch spacing. The skin bays were matrix dominated with a layup of (+45, -45, 0, 90, 0, -45, +45). The outer two +45° plies were cloth and the inner five plies were tape.

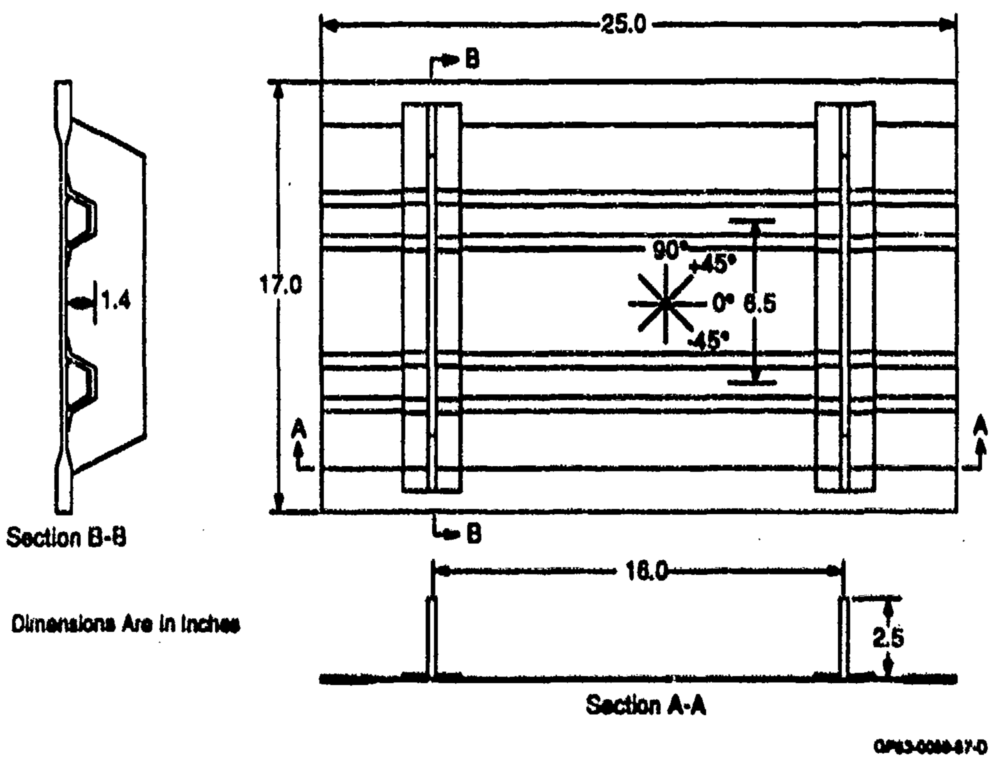

Figure 139. Test Panel Configuration

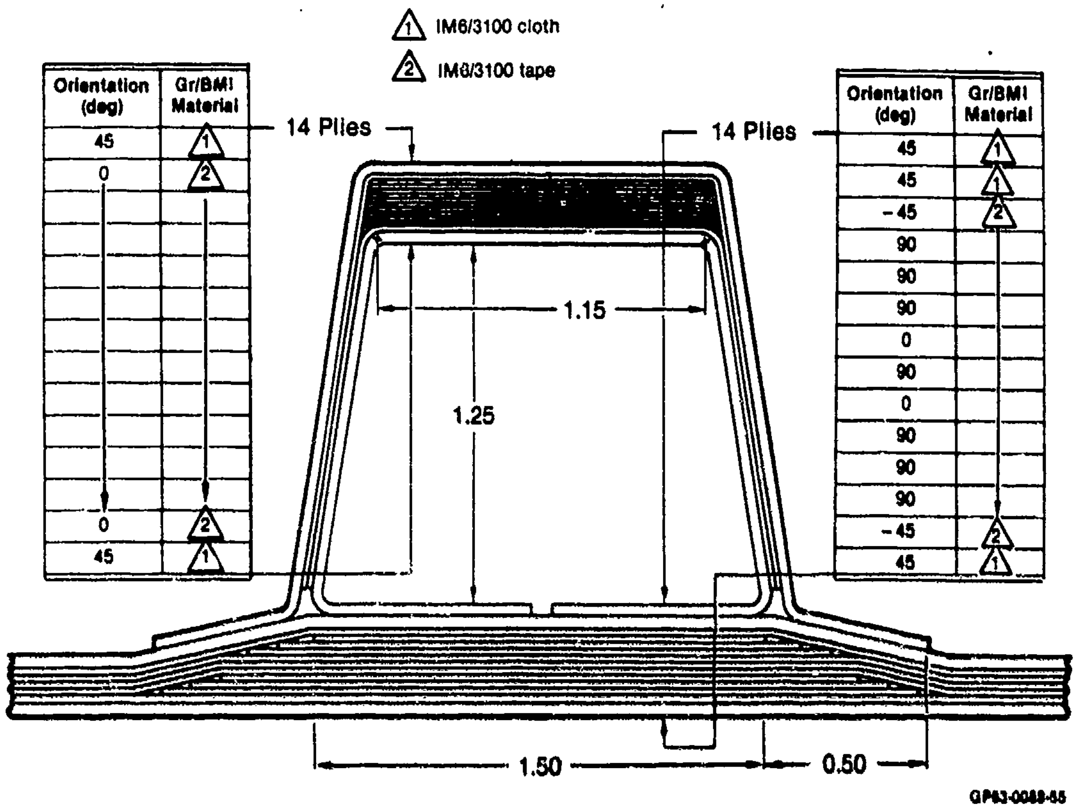

Orientation (deg)	Gr/BMI Material
45	1
0	2
0	2
45	1

Orientation (deg)	Gr/BMI Material
45	1
45	1
-45	2
90	
90	
90	
0	
90	
0	
90	
90	
90	
-45	2
45	1

Figure 140. Hat Stiffener Cross-Section

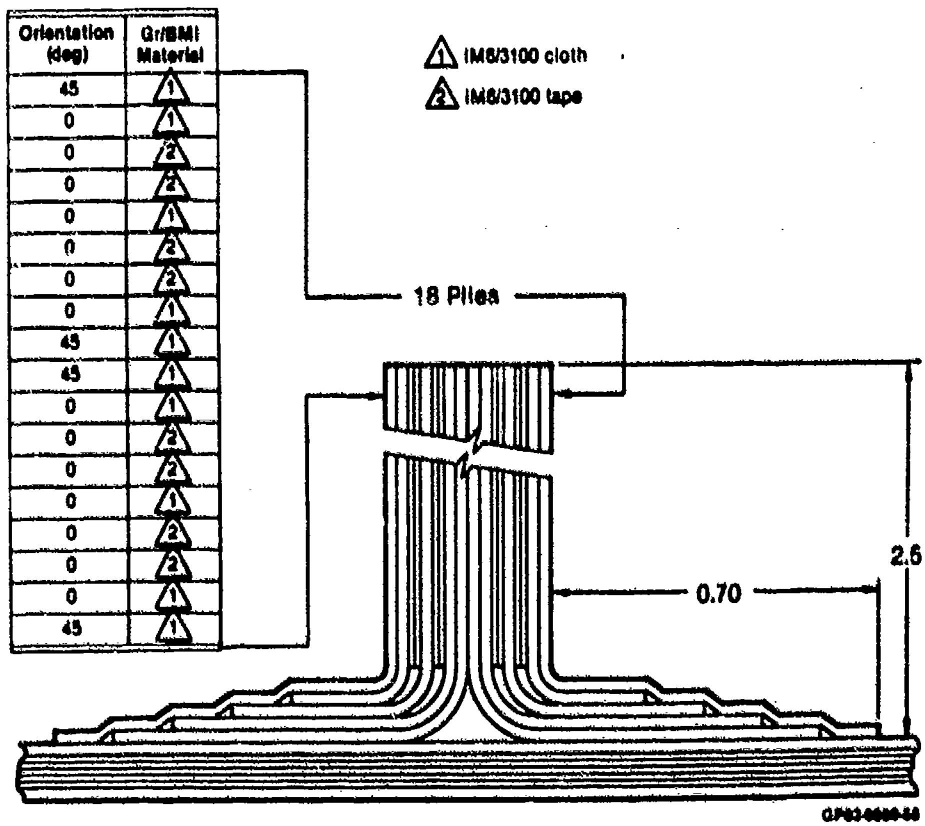

Orientation (deg)	Gr/BMI Material
45	1
0	1
0	2
0	2
0	1
0	2
0	2
0	1
45	1
45	1
0	1
0	2
0	2
0	1
0	2
0	2
0	1
45	1

Figure 141. Blade Stiffener Cross-Section

To stabilize the panels during longitudinal compression loading, the panels had end plates bonded onto the loading ends prior to testing.

5.3.2 Test Matrix - Eight panels were tested according to the test matrix in Figure 142. Static compression testing was conducted at two environmental conditions, RTD and ETW. One undamaged and one damaged panel was tested in each of the two environments to determine the strength reduction due to low velocity impact damage. Static testing was performed in a 100,000 lb. MTS machine. The test set up is shown in Figure 143.

Fatigue tests were conducted under constant amplitude (R = 10) compression loading at RTD conditions. Two undamaged and two damaged panels were tested to determine the life reduction due to low velocity impact damage. Each fatigue test was performed in blocks of 1,250 cycles with each block run at an increased load level to insure failure in the range of 1,000 to 10,000 cycles. The fatigue block load levels are summarized in Figure 144. The schedule in Figure 144 was determined by considering initial buckling of the undamaged static specimen, ultimate failure of the undamaged static specimen, and ultimate failure of the damaged static specimen. Initial buckling occurred at approximately 50 percent of the undamaged ultimate load. Failure of the damaged panel occurred at 74 percent of the undamaged ultimate load. After each block of cycling, A-scans of impact damaged areas were performed to document impact damage growth. Fatigue testing was also performed in a 100,000 lb. MTS machine.

Panel Number	Loading		Environment		Damage Condition
	Static	Fatigue	RTD	ETW	
7	X		X		Undamaged
6	X		X		Damaged
5	X			X	Undamaged
1	X			X	Damaged
2 and 4		X	X		Undamaged
3 and 8		X	X		Damaged

GP03-0000-4-T

Figure 142. Task IV Test Matrix

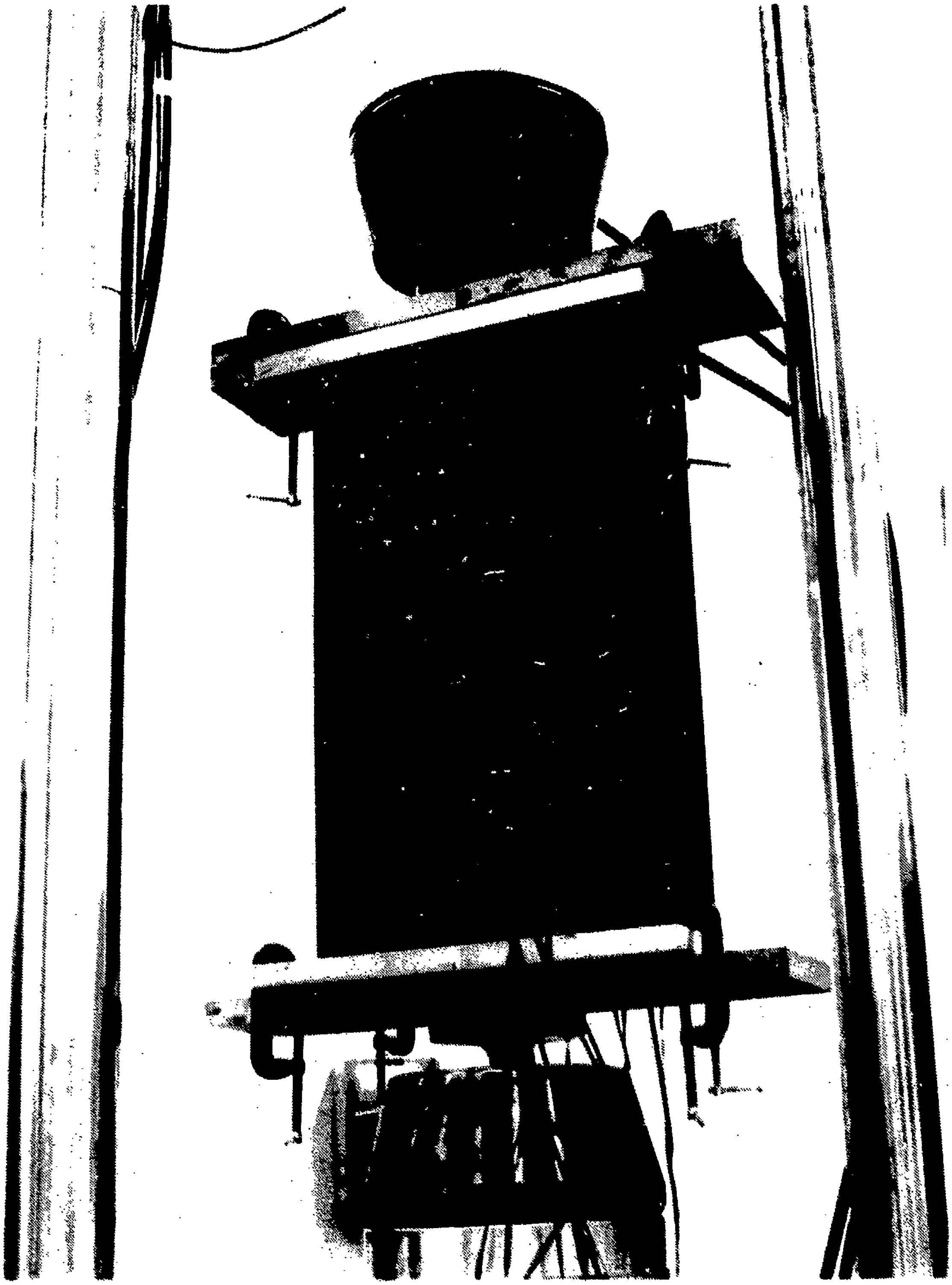

Figure 143. Panel Test Setup

Block Number	Cycles	P_{max} (kips)	% Static Undamaged Strength
1	1,250	16.1	45
2	1,250	19.6	55
3	1,250	23.2	65
4	1,250	26.8	75
5	1,250	32.1	90

Load ratio, $R = \frac{P_{max}}{P_{min}} = 10$ (compression only)

Cycle frequency = 1 Hz

Static undamaged ultimate load = 35.7 kips

Static damaged ultimate load = 26.5 kips

GP63-0669-7-T

Figure 144. RTD Fatigue Test Schedule

5.3.3 Environmental Conditioning - Panels tested at the ETW condition were preconditioned to a moisture content of 0.71 percent by weight. The moisture level was predicted in Task II to be the end-of-life moisture content of an F-15 wing skin exposed to a 20 year basing scenario.

In Task II, glass transition temperature (T_g) tests determined that an IM6/3100 laminate with a moisture content of 0.71 percent had a T_g of 408°F. With a buffer of 50°F, the temperature for IM6/3100 ETW tests was 360°F. For environmental tests, an enclosing manifold was placed around the panel so that a controlled temperature was maintained during the test. The test setup with environmental chamber is shown in Figure 145.

5.3.4 Introduction of Impact Damage - Low velocity impact damage was induced on the outer mold line of four panels at three critical locations as shown in Figure 146. These locations were selected in order to investigate impact damage effects on thick structure (stiffener land) thin structure (skin bay), and transitional structure (stiffener-to-skin taper). The energy levels used for introducing impact damage into the panels were sufficient to create nonvisible damage (approximately 0.01 inch surface dent). This test program simulated the scenario in which fuselage structure is subjected to damage from debris kicked up during takeoff and landing but the damage is not severe enough to be visible during walk-around inspection.

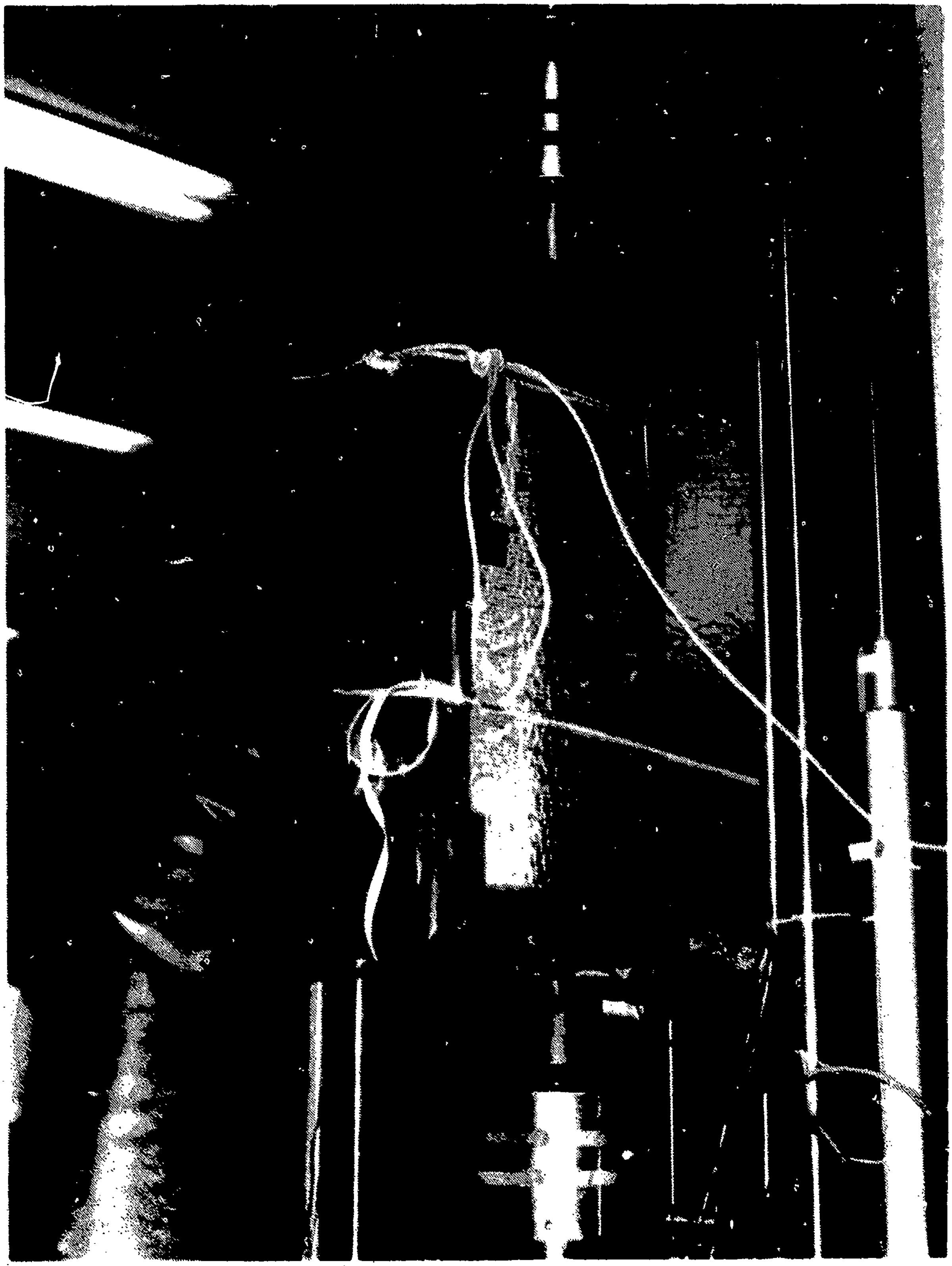

GP83-0680-49

Figure 145. Environmental Chamber for ETW Tests

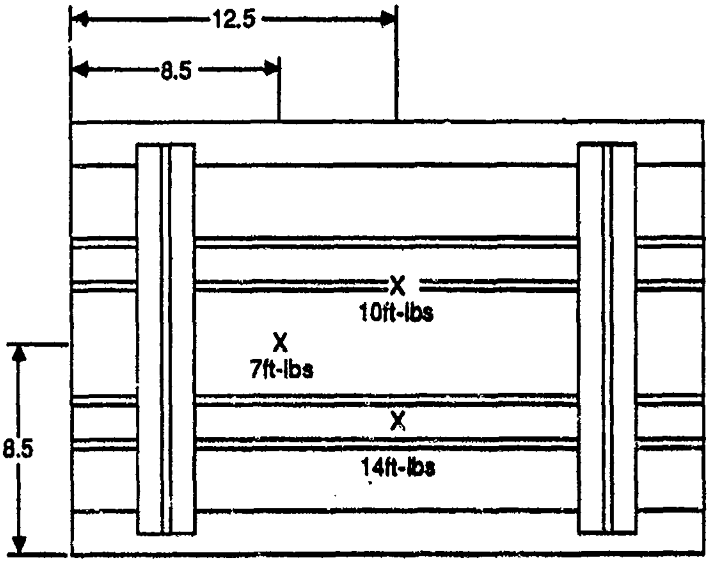

Figure 146. Outer Mold Line Impact Locations and Energy Levels

5.3.5 Data Analysis (Static) - The panel design includes longitudinal stiffeners that were sized to carry a majority of the compression loading. As a result, the failure mode of the panels was stiffener crippling accompanied by stiffener separation as shown in Figure 147. Ultimate loads for the four static tests are summarized in Figure 148. In order to predict panel compression strength, the hat stiffener crippling strength was calculated. Because the slenderness ratio, L'/ρ, of the stiffener section was greater than 20, column behavior was accounted for and a correction to the predicted crippling strength was made using the Johnson-Euler equation. The damaged panel compression strength was predicted by accounting for the degree of delamination of the stiffener from the skin. In the case of impact damaged panels, A-scans of damage area determined the degree of stiffener delamination.

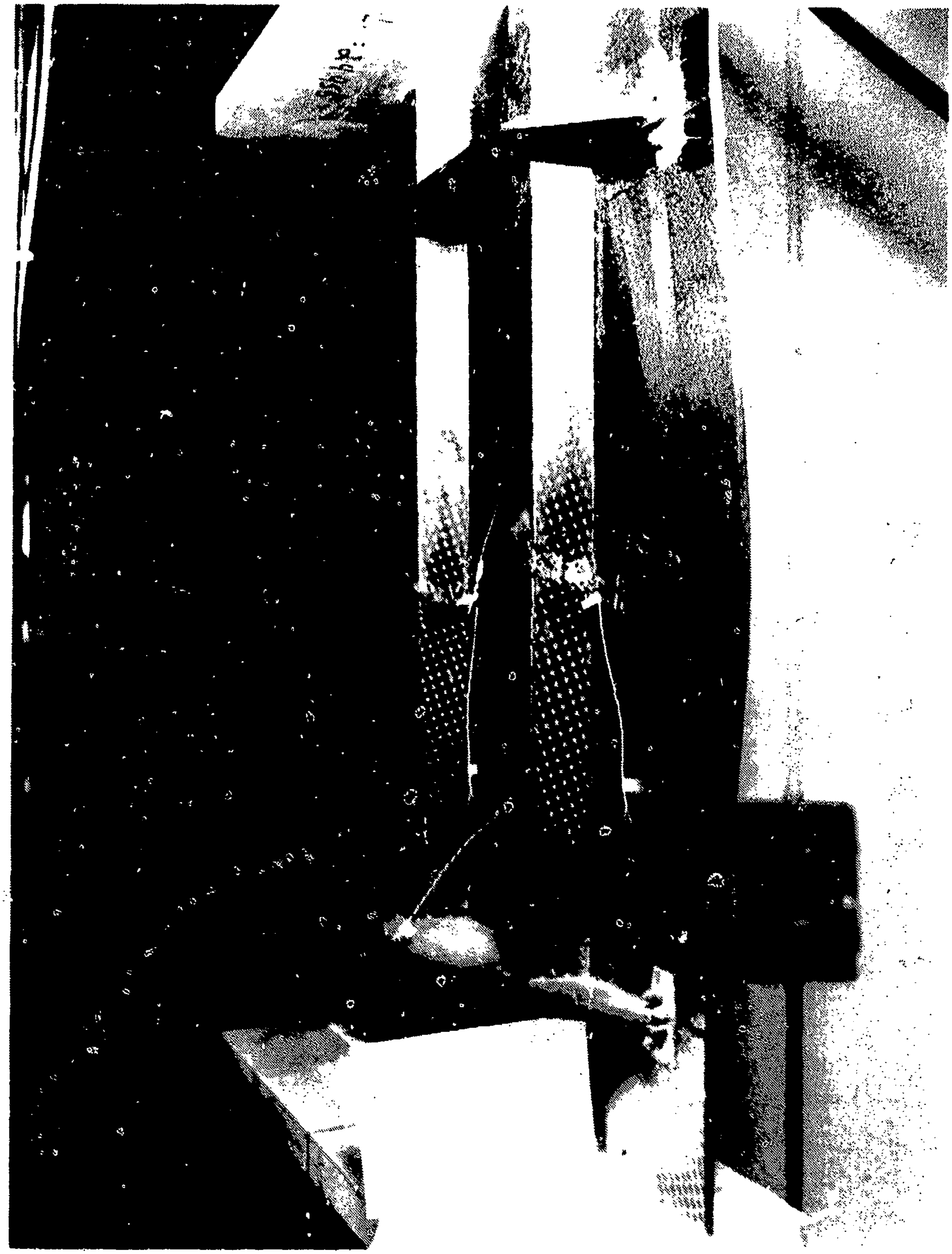

GP83 0049 58

Figure 147. Stiffened Panel Failure Including Stiffener Crippling and Separation

Panel Number	Environment	Impact Damage Condition	Ultimate Load (kips)	% RTD Undamaged Ultimate Load
7	RTD	Undamaged	35.7	100
6	RTD	Damaged	26.5	74
5	ETW	Undamaged	25.7	72
1	ETW	Damaged	20.1	56

GP83-0089-6-T

Figure 148. Ultimate Loads for Static Panel Tests

The hat stiffener crippling strength was calculated using a technique developed at MCAIR. The calculation involves the summation of crippling strengths of elements contributing to the total stiffener crippling strength. The summation equation has the form,

$$F^{cc} = \frac{\sum_{i=1}^{n} F_i^{cc} \; A_i}{\sum_{i=1}^{n} A_i}$$

where F^{cc} = section crippling strength

F_i^{cc} = element crippling strength

n = number of elements

A_i = element area

Element crippling strengths were determined from crippling curves shown in Figure 149. The curves are for no-edge-free and one-edge-free elements. The crippling calculations are tabulated in Figure 150 for RTD and ETW conditions. In both cases, the hat stiffener was modeled with 6 elements. Laminate properties (E_x^c, E_y^c, and F_x^{cu}) were calculated using lamina properties determined in Task II. $\bar{E}$ was determined by the equation:

$$\bar{E} = \frac{12\,(1 - \nu_{xy}\,\nu_{yx})\,D_{11}}{t^3}$$

where

ν_{xy}, ν_{yx} = laminate Poisson's ratios

D_{11} = flexibility term from laminate "ABD" matrix

t = laminate thickness

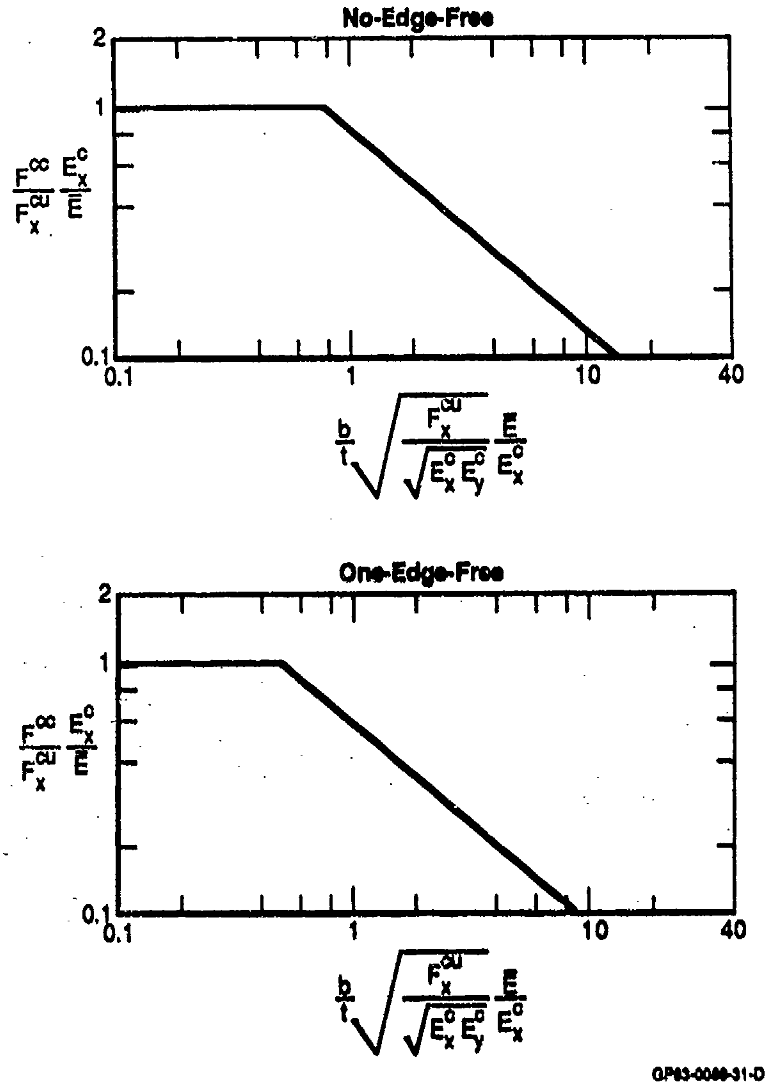

Figure 149. Nondimensional Crippling Curves for No-Edge-Free and One-Edge-Free Elements

RTD Crippling Analysis

Element	b (in.)	t (in.)	F_x^{cu} (ksi)	E_x^c (msi)	E_y^c (msi)	$\bar{E}$ (msi)	$\frac{b}{t}\sqrt{\frac{F_x^{cu}}{\sqrt{E_x^c E_y^c}}}\frac{\bar{E}}{E_x^c}$	$\frac{F^{cc}}{F_x^{cu}}\frac{E_x^c}{\bar{E}}$	F^{cc} (ksi)	P^{cc} (lb)
1	0.50	0.0836	66.5	6.14	7.98	6.04	0.57	0.88	57.6	2,410
2	1.50	0.0992	62.9	5.80	10.66	5.78	1.35	0.64	40.1	5,970
3	0.50	0.0836	66.5	6.14	7.98	6.04	0.57	0.88	57.6	2,410
4	1.26	0.0384	88.8	8.23	4.07	5.39	2.66	0.37	21.5	1,040
5	1.26	0.0384	88.8	8.23	4.07	5.39	2.66	0.37	21.5	1,040
6	1.15	0.0904	177.7	16.44	3.00	11.26	1.38	0.62	75.5	7,850
Total Area = 0.433 in.^{2}										Total = 20,720

ETW Crippling Analysis

Element	b (in.)	t (in.)	F_x^{cu} (ksi)	E_x^c (msi)	E_y^c (msi)	$\bar{E}$ (msi)	$\frac{b}{t}\sqrt{\frac{F_x^{cu}}{\sqrt{E_x^c E_y^c}}}\frac{\bar{E}}{E_x^c}$	$\frac{F^{cc}}{F_x^{cu}}\frac{E_x^c}{\bar{E}}$	F^{cc} (ksi)	P^{cc} (lb)
1	0.50	0.0836	29.3	5.61	7.66	5.43	0.39	1.00	28.4	1,190
2	1.50	0.0992	27.8	5.34	10.64	5.29	0.91	0.88	24.2	3,600
3	0.50	0.0836	29.3	5.61	7.66	5.43	0.39	1.00	28.4	1,190
4	1.26	0.0384	39.7	7.64	3.39	4.72	1.79	0.51	12.5	600
5	1.26	0.0384	39.7	7.64	3.39	4.72	1.79	0.51	12.5	600
6	1.15	0.0904	87.9	16.91	2.26	11.23	1.01	0.81	47.3	4,920
Total Area = 0.433 in.^{2}										Total = 12,100

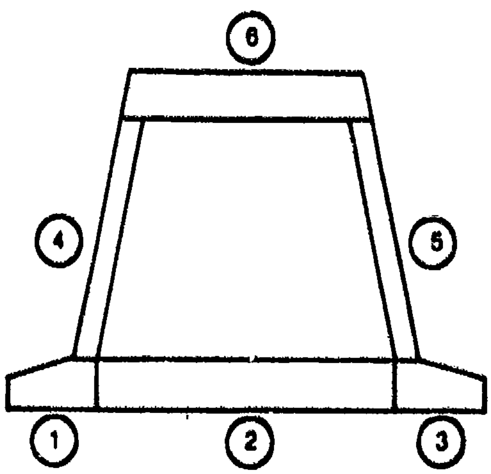

Figure 150. RTD and ETW Crippling Analyses of Hat Stiffener Modeled With 6 Elements

Corrections for column behavior were calculated with the Johnson-Euler Equation:

$$F^c = F^{cc} - \frac{(F^{cc})^2}{4\pi^2 E} (L'/\rho)^2$$

where

F^c = stiffener failing strength

F^{cc} = stiffener crippling strength

E = average stiffener modulus

L' = L/1.5 = effective stiffener length (assuming fixity (1.5) is half way between simply supported (1) and clamped (2)).

ρ = radius of gyration

L'/ρ = slenderness ratio

The results of the calculations are tabulated in Figure 151 for RTD and ETW conditions.

	F^{cc} (ksi)	E (msi)	L'/ρ	F^c (ksi)	P^c (kips)
RTD	47.8	8.23	26.3	42.9	18.6
ETW	27.9	7.64	26.2	26.1	11.3
Total Area = 0.433 in.^{2}					

$F^c = F^{cc} - [(F^{cc})^2/4\,\pi^2 E]\,(L'/\rho)^2$

GP83-0000-74-R

Figure 151. Column Strength Correction Results

Under RTD conditions, the undamaged stiffener failing load was predicted to be 18,580 lbs. The total failing load for 2 stiffeners is 37,160 lbs. This prediction was 4 percent higher than the actual failing load of 35,700 lbs. The damaged panel failing load was predicted to be 23,970 lbs. by assuming elements 1, 2, and 3 of one stiffener and element 1 of the other stiffener did not contribute to the strength. This assumption was made based on A-scans of impact damage prior to compression testing. Figure 152 shows the damage area that was located across the width (flange-to-flange) of the left hat stiffener and over only one flange of the right hat stiffener. This prediction was 10 percent lower than the actual failing load of 26,500 lbs.

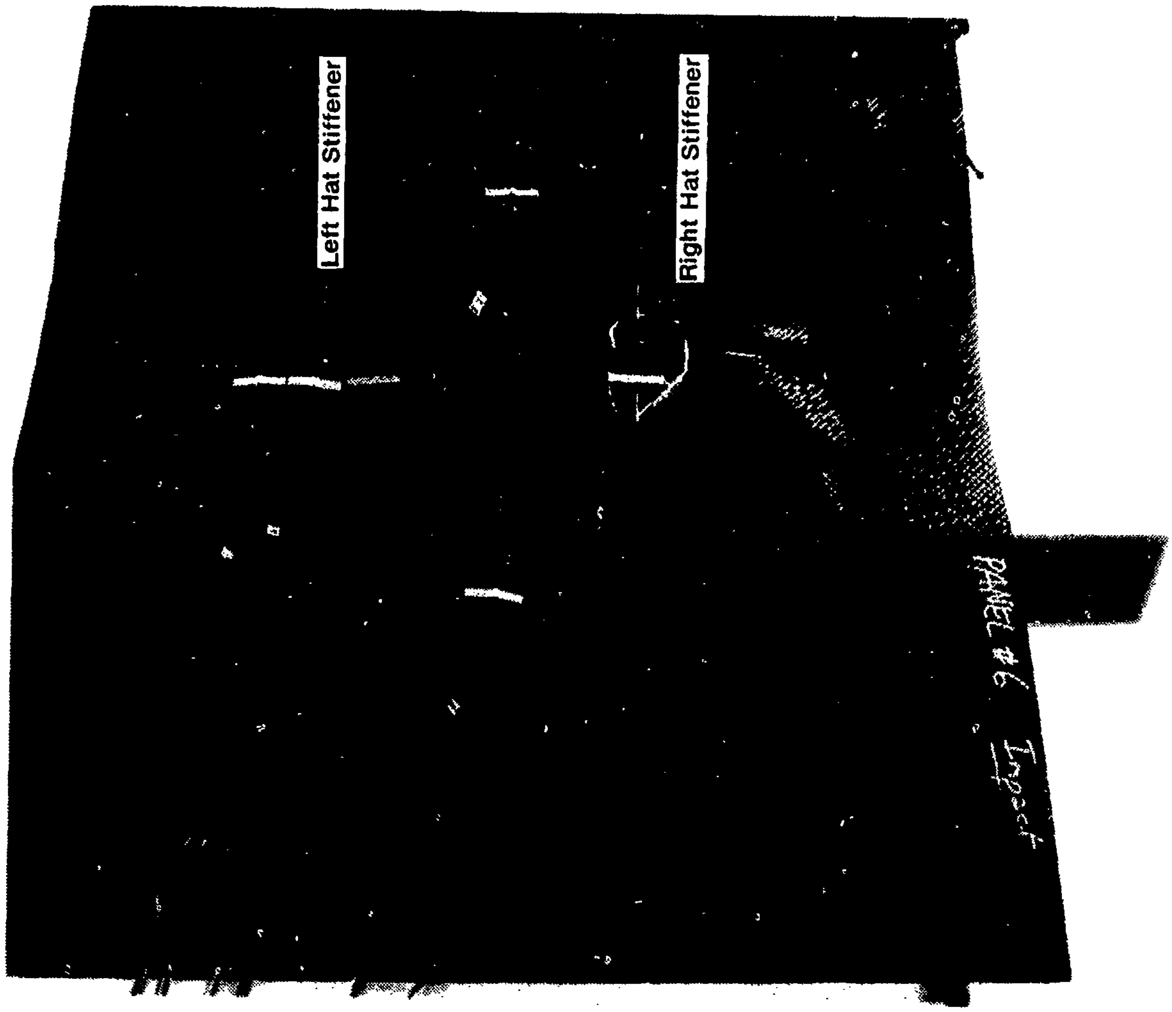

GP83-0088-11

Figure 152. Impact Damage Referenced to Longitudinal Hat Stiffeners

Similar calculations were made for ETW tests of damaged and undamaged panels. The undamaged panel ultimate load prediction of 22,610 lbs. was 12 percent lower than the actual failing load of 25,700 lbs. The predicted damaged panel failing load of 15,440 lbs. was 23 percent lower than the actual failing load of 20,100 lbs. These results are summarized in Figure 153.

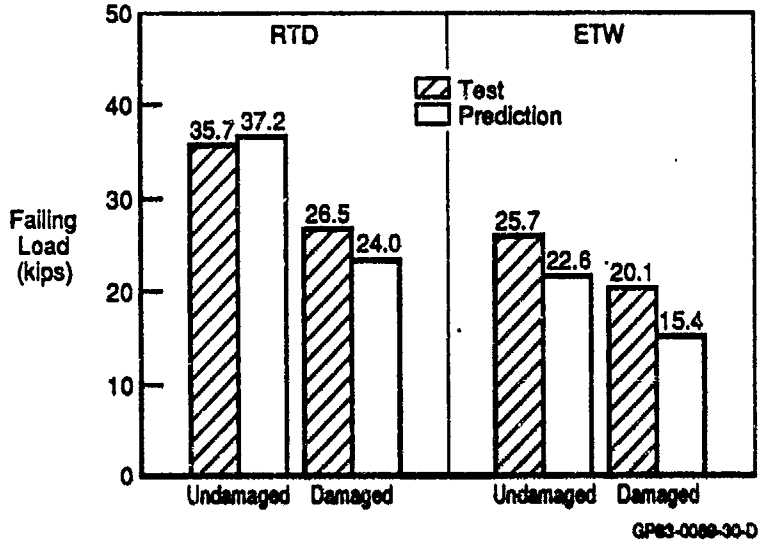

Figure 153. Crippling Load Predictions for Undamaged and Damaged Panels

5.3.6 Data Analysis (Fatigue) - As shown in Figure 144, fatigue testing was performed in blocks of 1,250 cycles. The first fatigue block was run at 45 percent of the undamaged ultimate load. The next three blocks were run at increasing increments of 10 percent up to 75 percent of the undamaged ultimate load. In the case of panel #4, a fifth block was started at 90 percent of the undamaged ultimate load. Fatigue lives for the four fatigue panels are summarized in Figure 154.

Panel Number	Impact Damage Condition	Cycles to Failure	Comment
2	Undamaged	3,426	Failed 926 cycles Into 3rd Fatigue Block With Maximum Load of 23.2 kips (65% of Ultimate)
4	Undamaged	5,174	Failed 174 cycles Into 5th Fatigue Block With Maximum Load of 32.1 kips (90% of Ultimate)
3	Damaged	3,750	Failed at 25.3 kips During the 4th Strain Survey to 26.8 kips (75% of Ultimate)
8	Damaged	2,500	Failed at 22.8 kips During the 3rd Strain Survey to 23.2 kips (65% of Ultimate)

GP83-0069-37-T

Figure 154. Panel Fatigue Test Results

Between cycle blocks, all the panels were strain surveyed in order to monitor changes in panel response due to fatigue. Gages were mounted on the panels as shown in Figure 155. All odd numbered gages were located on the outer mold line. All even numbered gages were located on the inner mold line.

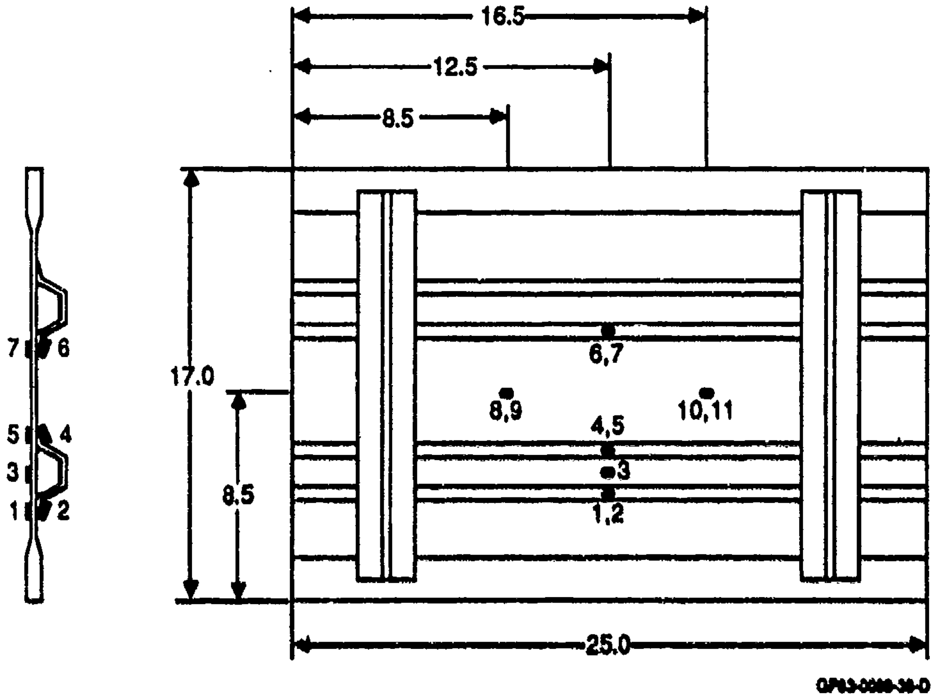

Figure 155. Strain Gage Locations

In addition to being strain surveyed, impact damaged panels (Numbers 3 and 8) were A-scanned between cycle blocks to determine impact damage growth due to fatigue. Figures 156 and 157 show damage histories for Panel 3 and 8 respectively. Figures 156 and 157 show that the impact damage was located such that back-to-back gage pairs 1,2 and 4,5 were on or near delamination edges. Back-to-back gages 6,7 were closer to the center of a delamination. The figures also show that there was very little damage growth in Panel 3 and no damage growth in Panel 8 prior to failure. This behavior correlates with crack growth data from Task II. That data showed that the crack growth curves for both bismaleimides were steep, with the growth threshold nearly equal to the critical strain energy release rate.

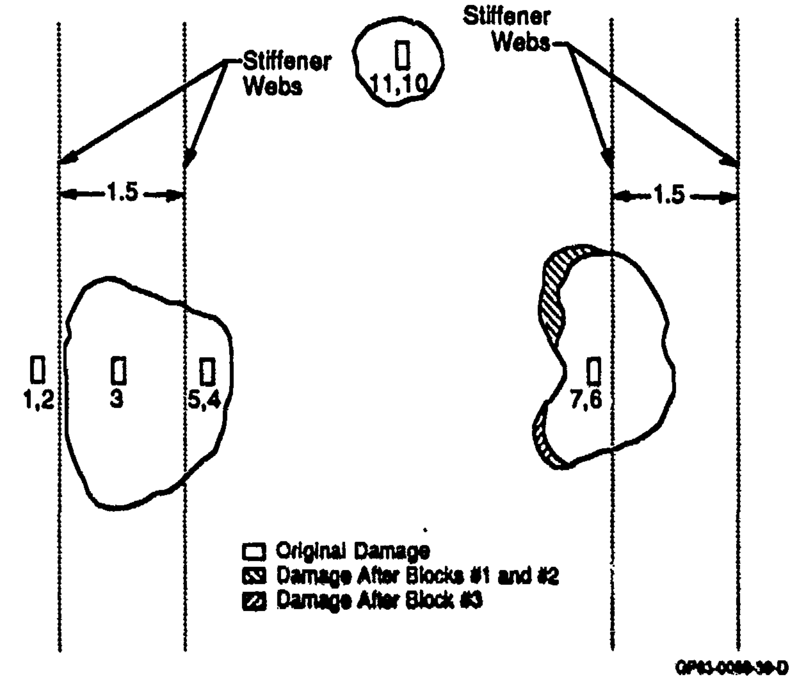

Figure 156. Damage as Viewed From Outer Mold Line of Panel #3

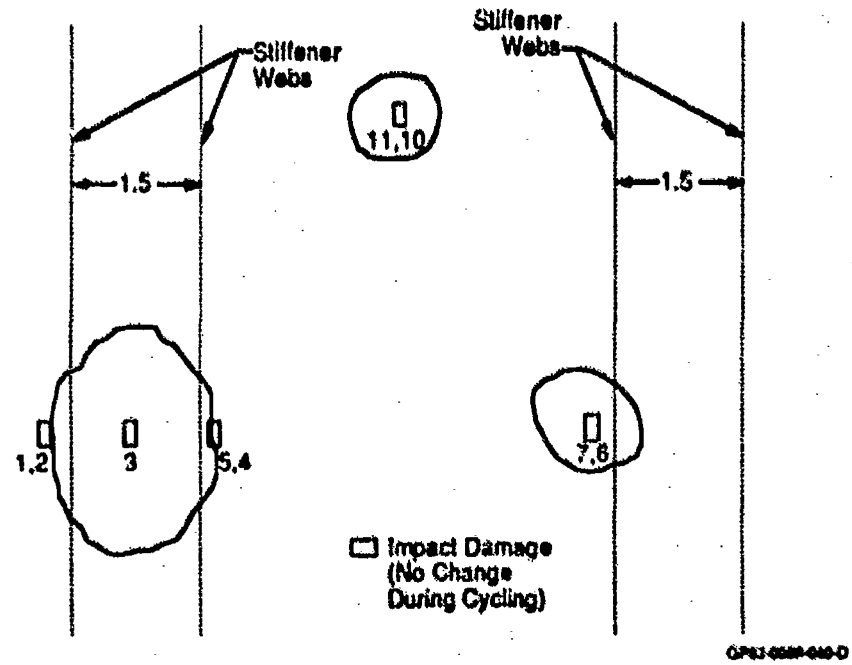

Figure 157. Damage as Viewed From Outer Mold Line of Panel #6

Strain survey data also indicated that there was little change in the panel damage state prior to failure. Figures 158 through 160 show the strain surveys for each of the three back-to-back gage pairs (1,2 4,5 6,7) on Panel 3. The strain response of the panels was consistent from survey to survey. Slight deviations were evident for final surveys in which failure did occur. Note that the surveys in Figures 158 and 159 show less divergence than that in Figure 160. This can be explained by the fact that gages 6 and 7 (data in Figure 160) were located in the middle of a delamination where local buckling occurred and gage pairs 1,2 and 4,5 (data in Figures 158 and 159) were located at a delamination edge where buckling did not occur.

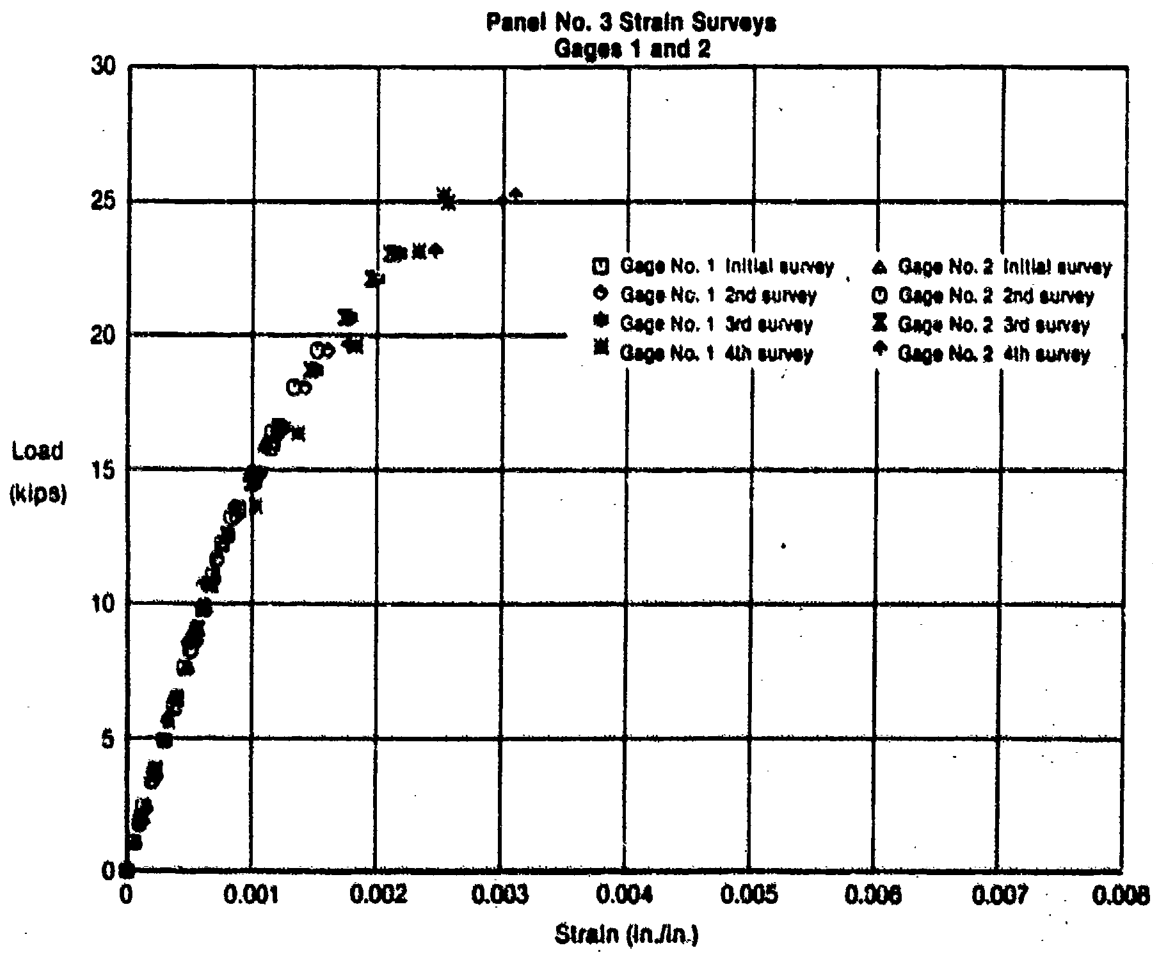

Figure 158. Strain Surveys of Strain Gages 1 and 2 of Panel No. 3

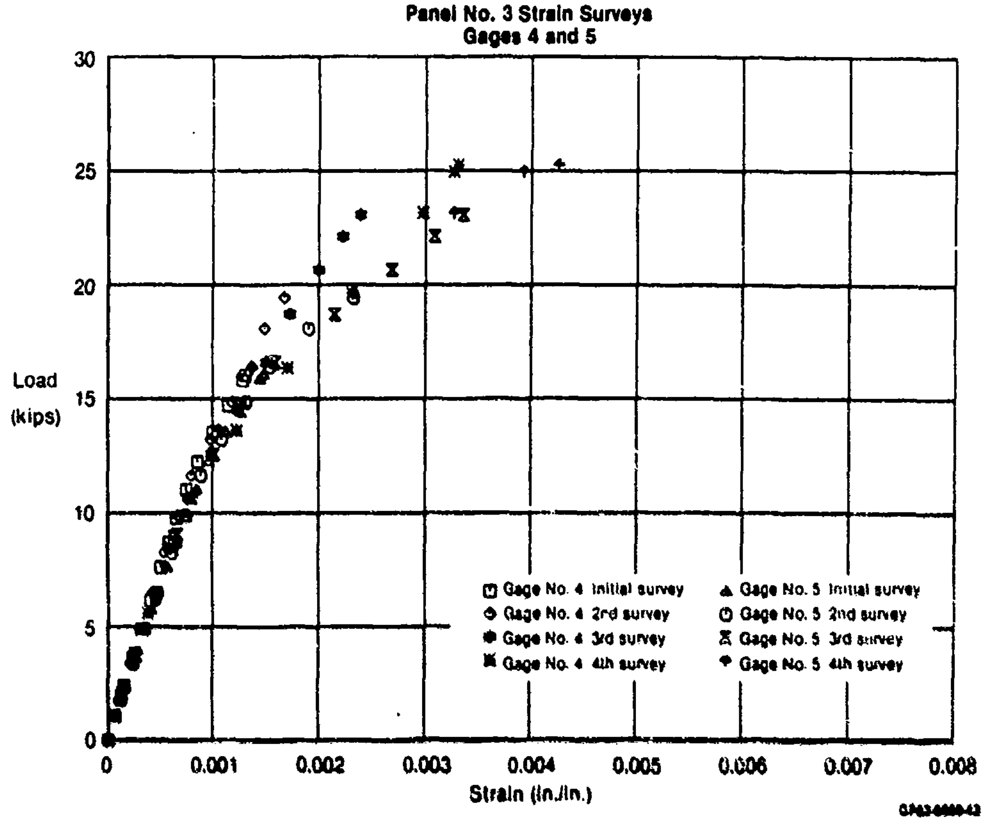

Figure 159. Strain Surveys of Strain Gages 4 and 5 of Panel No. 3

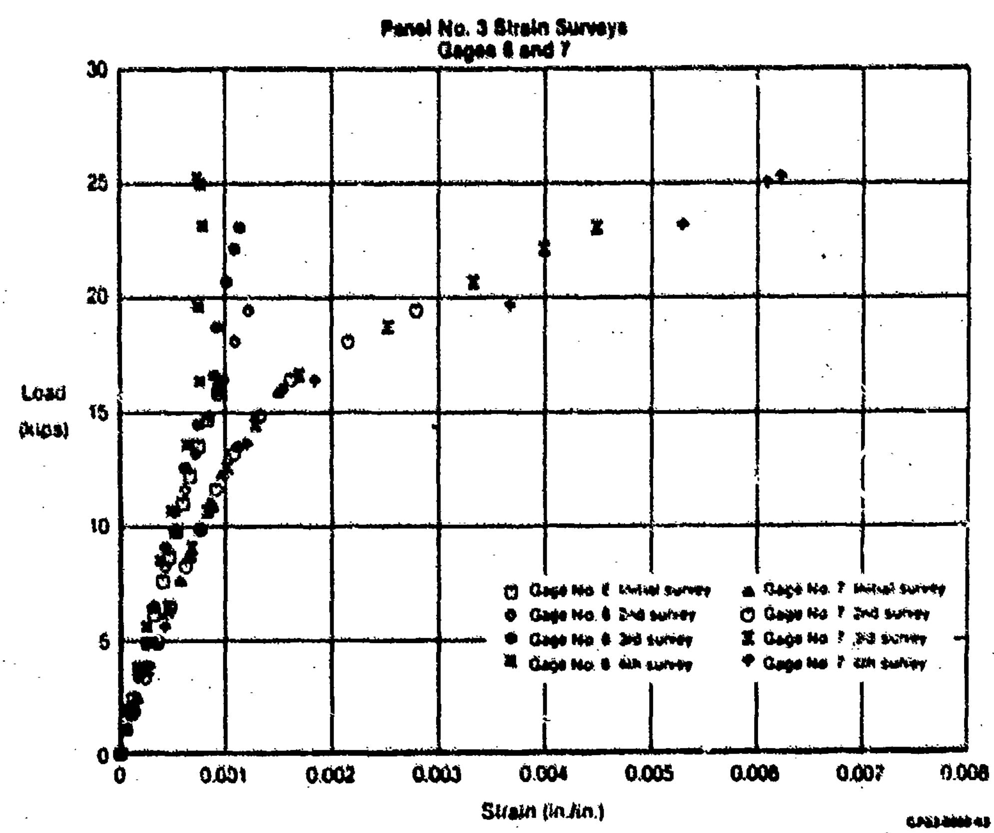

Figure 160. Strain Surveys of Strain Gages 6 and 7 of Panel No. 3

Panel 8 exhibited similar behavior. Figures 161 through 163 show the strain surveys for back-to-back pairs 1,2 4,5 and 6,7 on Panel 8. Again the surveys illustrate consistent behavior until slight deviations occur during the final survey. Also, buckling behavior was exhibited at gage pair 6,7 and not at pairs 1,2 and 4,5.

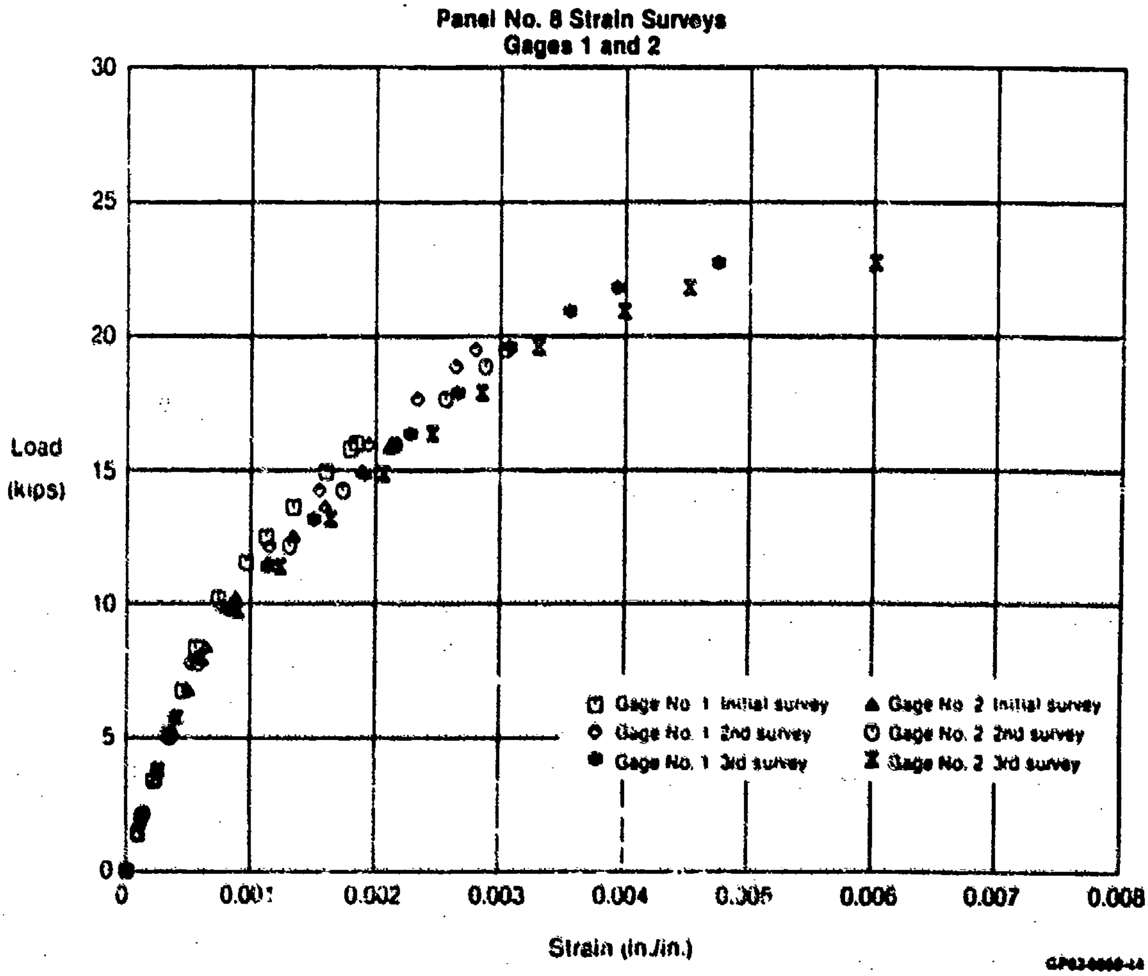

Figure 161. Strain Surveys of Strain Gages 1 and 2 of Panel No. 8

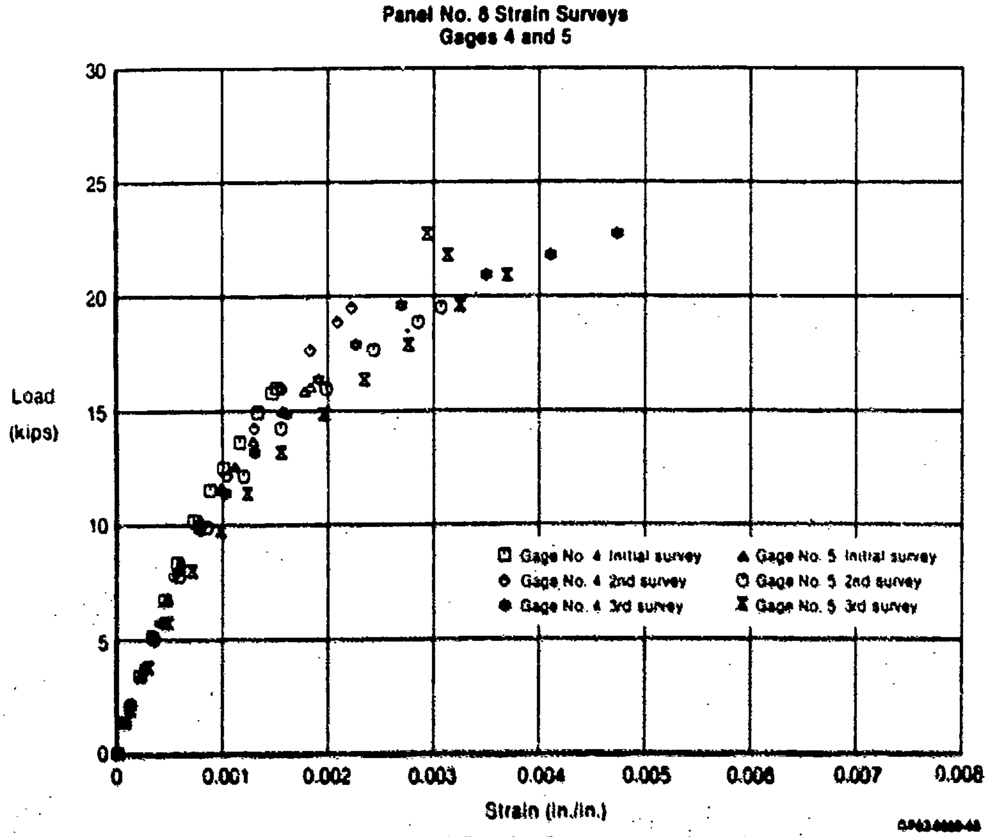

Figure 162. Strain Surveys of Strain Gages 4 and 5 of Panel No. 8

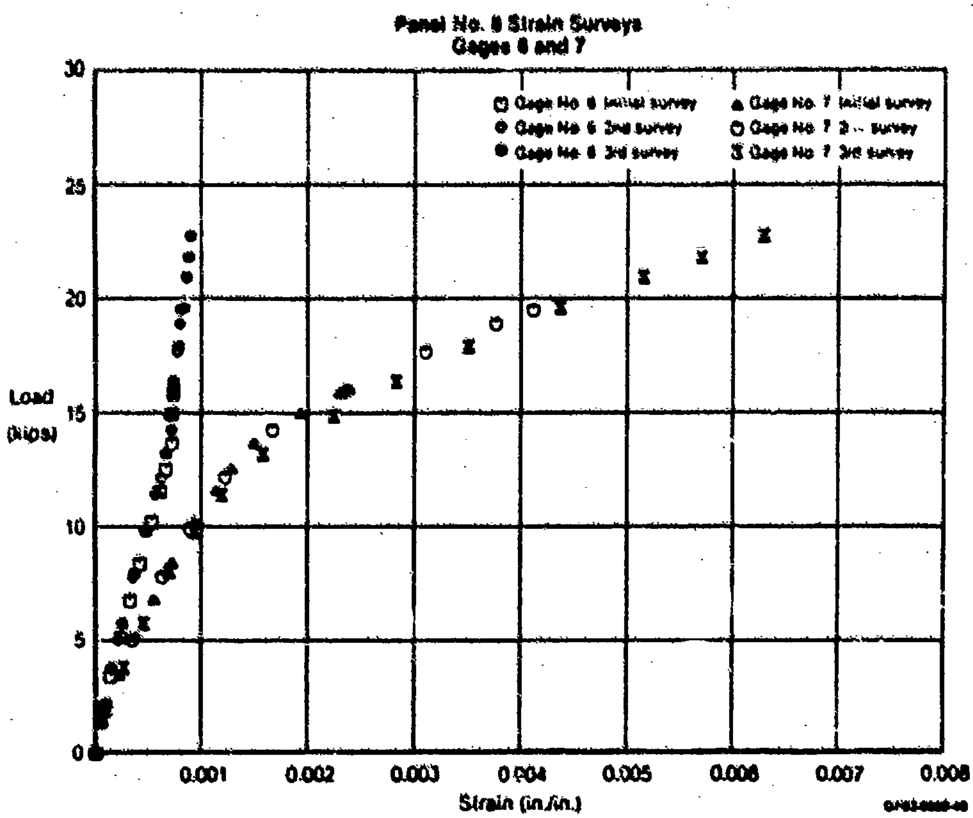

Figure 163. Strain Surveys of Strain Gages 6 and 7 of Panel No. 8

5.3.7 Discussion of Results - Static and fatigue test results are summarized in Figure 164. Static results show that the crippling/column analyses produced conservative predictions for all cases except the undamaged RTD test, where the analysis was unconservative by 4 percent. When either damage or ETW conditions were involved, the analysis was conservative by approximately 10 percent. When both damage and ETW conditions were involved the analysis was conservative by approximately 30 percent. The analysis was reasonably accurate except in the damage/ETW case. Apparently the crippling/column analysis was not rigorous enough to correctly account for both impact damage and ETW conditions.

Static Results

Damage	Environment	Ultimate Load (kips)		$\Delta\%$, Test-Predicted
		Predicted	Test	Prediction
No	RTD	37.2	35.7	−4
Yes	RTD	24.0	26.5	+10
No	ETW	22.6	25.7	+14
Yes	ETW	15.4	20.1	+31

Fatigue Results

Damage	Peak Load at Failure (kips)	% of Ultimate (Ultimate = 35.7 kips)	
No	23.2	65	
No	32.1	90	
Yes	26.8	75	(100% Damaged Ultimate)
Yes	23.2	65	(87% Damaged Ultimate)

GP83-0089-78-T

Figure 164. Summary of Static and Fatigue Results

Fatigue results show that, except for one case, the panels survived until peak loads were increased to approximately 90 percent of the undamaged ultimate load (or 90 percent of the damaged ultimate load in the case of damaged panels). The exception where an undamaged panel failed at peak loads of 65 percent of the ultimate load was noteworthy. The behavior reinforces questions of the reliability of cocured structure. The failure at 65 percent of ultimate may be a result of imperfect bonding of cocured stiffeners. Before cocured structures can be effective, more work must be done to develop effective analyses to determine the translaminar capability of composite laminates with cocured elements.

SECTION 6.

CONCLUSIONS AND RECOMMENDATIONS

In this program a large data base of material properties was developed for two second generation bismaleimide composite systems. The test program sufficiently defined the materials, and existing analytical techniques proved to be as effective for bismaleimide matrix composites as they were for epoxy matrix composites.

IM6/3100 was found to be tougher than IM6/F650. IM6/3100 exhibited toughness as great as the toughness of the baseline epoxy system AS1/3501-6. Under similar conditions, impact damage in panels made with 3100 resin has been shown to be similar to damage in panels made with 3501-6 resin. While the test procedures used to determine toughness and impact damage response were effective, there is still a need for an effective analytical tool with which to predict impact damage response. It is expected that the toughness and instrumented impact data presented in this program will serve as a basis for the development of empirical and, eventually, analytical methods in the future.

The similarity in impact damage characteristics of epoxy and the second generation bismaleimide IM6/3100 indicates that damage tolerance requirements applicable to epoxy systems would also be applicable to IM6/3100. The similarity in impact damage performance is a reflection of the improvements in toughness that have been made in second generation bismaleimides compared to first generation bismaleimides such as V378A. At the start of this program, American Cyanamid's 3100 BMI resin was the toughest, most readily available candidate for evaluation. Since then, further improvements have been made in both BMIs and epoxies resulting in tougher systems than 3100 or 3501-6. As systems continue to evolve, the applicability of the draft Air Force durability and damage tolerance design requirements for composite aircraft structures must be investigated.

REFERENCES

1. Badaliance, R., and Dill, H. D., "Effects of Fighter Attack Spectrum on Composite Fatigue Life," AFWAL-TR-81-3001, March 1981.

2. Rosen, B. W., A Simple Procedure for Experimental Determination of the Longitudinal Shear Modulus of Unidirectional Composites, J. Composite Materials, Vol. 6, October 1972, p. 552.

3. Petit, P. H., A Simplified Method of Determining the Inplane Shear Stress-Strain Response of Unidirectional Composites, Composite Materials: Testing and Design, ASTM STP 460, American Society for Testing and Materials, 1969, pp 83-93.

4. Pipes, R. B. and Pagano, N. J., Intralaminar Stresses in Composite Laminates Under Uniform Axial Extension, J. Composite Materials, October 1970, pp 538-548.

5. Law, G. E., and Wilkins, D. J., "Delamination Failure Criteria for Composite Structures," Report No. NAV-GD-0053, May 1984.

6. Wilkins, D. J., "A Comparison of the Delamination and Environmental Resistance of a Graphite-Epoxy and a Graphite-Bismaleimide," Report No. NAV-GD-0037, September 1981.

7. Russell, A. J., and Street, K. N., "Factors Affecting the Interlaminar Fracture Energy of Graphite/Epoxy Laminates," Proceedings of the Fourth International Conference on Composite Materials, Tokyo, Japan, October 1982.

8. Task II Interim Technical Report, "Durability and Damage Tolerance of Bismaleimide Composites," Contract No. 33615-85-C-3212, July 31, 1987.

9. Garbo, S.P. and Ogonowski, J.M. "Effect of Variances and Manufacturing Tolerances on the Design Strength and Life of Mechanically Fastened Composite Joints," AFWAL-TR-81-3041, Volumes 1, 2 and 3, April 1981.